Altered Calcium Flux Drives VSMC Matrix Rigidity Response

Finn Wostear

Thesis submitted for the degree of Doctor of Philosophy

University of East Anglia
School of Chemistry, Pharmacy and Pharmacology

September 2025

Abstract

Arterial stiffening is a key component of cardiovascular disease and ageing. This stiffening is primarily driven by remodelling of the extracellular matrix and the subsequent response of vascular smooth muscle cells (VSMCs). The stiffening of VSMCs in response to enhanced vessel rigidity is termed 'vascular smooth muscle cell stiffness syndrome (VSMCSS)' and is regarded as a core component of vessel stiffening. However, the signalling and mechanistic pathways that induce VSMCSS are not well understood. The work in this thesis aims to elucidate the pathways that drive VSMC dysfunction.

I use primary human aortic VSMCs and polyacrylamide hydrogels of tuneable stiffness to mimic the rigidity of the VSMC extracellular environment in health and disease. This assay is used in combination with targeted pharmacological inhibition/activation of key VSMC signalling pathways. Microscopy techniques, such as confocal immuno-fluorescence microscopy and live-cell video time-lapse microscopy, are used to identify stiffness-dependent responses.

I find that inhibition of key signalling pathways modulates VSMC morphology response to enhanced matrix rigidity. I specifically identify aquaporins as key regulators of the VSMC morphology response to enhanced matrix rigidity. I additionally identify microtubule stability and Ca^{2+} signalling machinery as vital components in this response. I use the Fluo-4 calcium indicator and live cell time-lapse microscopy to highlight increased Ca^{2+} flux on rigid matrices. I find that this increased flux can be modulated by targeted inhibition of mechanosensitive ion channels and promotion of microtubule stability. These novel findings highlight the role of Ca^{2+} as a central integrator of the VSMC response to enhanced matrix rigidity. I additionally examine downstream effectors of VSMC stiffness response to enhanced matrix rigidity and confinement. I highlight the diverse responses of VSMCs through traction stress generation and area/volume regulation.

My findings develop our understanding of VSMCSS and provide novel targets for pharmacological treatment of stiffness-induced VSMC dysfunction.

Acknowledgements

This thesis wouldn't have been possible without the support of so many people, and I am deeply grateful for their help. I would especially like to thank:

My supervisor, Dr. Derek Warren, for his unwavering support and guidance throughout my postgraduate career. From the earliest days of my master's degree, I knew the Warren lab was where I wanted to begin my career as a scientist. Your commitment to the success and well-being of all your students is evident to everyone who has the privilege of working in the Warren group, and I feel incredibly grateful to have spent the last 5 years working with you. I would also like to thank the other members of UEA academic staff who have guided me, including Dr. Julie Sanderson, Dr. Stefan Bidula, and Dr. James McColl.

My fantastic friends and colleagues in the Warren group. Firstly, Dr. Rob Johnson for teaching me most of what I know about doing lab science. Your expertise, patience, and friendship during the early days of my PhD were invaluable. This thesis would be significantly weaker without the foundation you helped put down. Also, thanks for helping me over that fence! Dr. Reesha Solanki, for your steadfast friendship through the ups and downs of our PhDs. The games of shoe-ball, mushroom hunts, DIY, job hunting, and aimless wandering kept me going during the tougher days of this journey. I cannot imagine the last 4 years without your friendship. Alice Bradford for being the best housemate and personal chef anyone could ask for. I'm amazed we got anything done between "going crazy mode" and liver-destroying Tuesday nights. I feel so fortunate to have made a friend like you during my PhD. Shall we have a strange tea? Finally, Ollie Steward and George Smy. I can't imagine two better people to have joined the group over the last few years. Thank you for keeping me company in the lab, and I can't wait to see where your work takes you. Science is a collaborative effort, and I couldn't have asked for better collaborators and friends. Thank you all!

My friends, both near and far, for reminding me about life outside of the PhD bubble. I would especially like to thank Cameron Nicholls, Sam Speak, Emily Smith, Alex Merchan,

and Esme Peers. Thank you for all the nights at the pub, nights in, board games, Aldi trips, camping holidays, meals, climbing sessions, house parties, cats, waterfront nights, episodes of Criminal Minds watched, time spent talking about the gym rather than going to the gym, and hikes.

My brother James, for being my oldest friend, and my sister Charlotte, for keeping me young. Finally, my parents, thank you for your constant support and for your unwavering belief in me – this thesis belongs to you as much as it does to me.

Contents

List of Figures

List of Tables

Publications

The work in this thesis has contributed to two published papers:

Robert T. Johnson*, Reesha Solanki*, Finn Wostear, Sultan Ahmed, James C. K. Taylor, Jasmine Rees, Geraad Abel, James McColl, Helle F. Jørgensen, Chris J. Morris, Stefan Bidula, Derek T. Warren. **Piezo1- mediated regulation of smooth muscle cell volume in response to enhanced extracellular matrix rigidity.** British Journal of Pharmacology, 2023.

Robert T. Johnson*, Finn Wostear*, Reesha Solanki*, Oliver Steward, Alice Bradford, Christopher Morris, Stefan Bidula, Derek T. Warren. **A microtubule stability switch alters isolated vascular smooth muscle Ca^{2+} flux in response to matrix rigidity.** Journal of Cell Science, 2024.

*Joint first author.

Glossary of Acronyms

α-SMA:	Alpha-smooth muscle actin
AFM:	Atomic force microscopy
Ang II:	Angiotensin II
APES:	(3-Aminopropyl)triethoxysilane
APS:	Ammonium persulfate
AQP:	Aquaporin
AT1:	Angiotensin II receptor type 1
AUC:	Area under the curve
AVN:	Atrioventricular node
BSA:	Bovine serum albumin
Ca^{2+}:	Calcium ion
CVD:	Cardiovascular disease
DAG:	Diacylglycerol
DAPI:	Diamidino-2-Pheylindoledihydrochloride
dH_2O:	Distilled water
DMSO:	Dimethyl sulfoxide
DNA:	Deoxyribonucleic acid
DGPC:	Dystrophin–glycoprotein complex
ECM:	Extracellular matrix
FA:	Focal adhesion
F-actin:	Filamentous actin
FGF:	Fibroblast growth factor
GPCR:	G protein-coupled receptor
GSK3:	Glycogen synthase kinase 3
HDAC:	Histone deacetylase (general)
IC_{50}:	Half maximal inhibitory concentration
IP_3:	Inositol 1,4,5-trisphosphate
IP_3R:	IP_3 receptor
kPa:	Kilopascal
MAP:	Microtubule-associated protein
MAPK:	Mitogen-activated protein kinase
MMP:	Matrix metalloproteinase
MLC:	Myosin light chain
MLCK:	Myosin light chain kinase
MLCP:	Myosin light chain phosphatase
MT:	Microtubule
NKCC:	Na–K–Cl cotransporter
NO:	Nitric oxide
Pa:	Pascal
PAH:	Polyacrylamide hydrogel
PARP1:	Poly [ADP-ribose] polymerase 1
PBS:	Phosphate-buffered saline
PDGF:	Platelet-derived growth factor
PFA:	Paraformaldehyde
PIP2:	Phosphatidylinositol 4,5-bisphosphate
PKC:	Protein kinase C
PLC:	Phospholipase C
ROI:	Region of interest (in context of image analysis)
RyR:	Ryanodine receptor
RT:	Room temperature
SAC:	Stretch-activated ion channel
SAN:	Sinoatrial node
SEM:	Standard error of the mean
SR:	Sarcoplasmic reticulum
TEMED:	Tetramethylethylenediamine
TFM:	Traction force microscopy
TGF-β:	Transforming growth factor beta
TIMP:	Tissue inhibitors of metalloproteinases
TNF:	Tumour necrosis factor
TRPC:	Transient receptor potential channel
TRPV:	Transient receptor potential vanilloid
UV:	Ultraviolet
VSMC:	Vascular smooth muscle cell
VSMCSS:	Vascular smooth muscle cell stiffness syndrome
VGCC:	Voltage-gated calcium channel
Wnk:	Lysine-deficient protein kinase

Chapter 1: Introduction

1.1 Background to the Project

Cardiovascular disease (CVD) represents the most significant cause of mortality and reduced quality-adjusted life years in the developed world. The global prevalence of CVD has roughly doubled over the last 30 years to an estimated 523 million cases in 2019, with approximately 18.6 million deaths recorded in the same year[1]. In addition to the human cost, endemic CVD is a significant contributor to the economic burden of global health, with the cost of CVD treatment predicted to exceed $250 billion in the US alone by 2030[2]. CVD is an all-encompassing term for disease of the cardiovascular system and includes coronary heart disease, cerebrovascular disease (including stroke), peripheral arterial disease and aortic disease. Almost all CVDs have common risk factors, including hypertension, obesity, age, and diabetes, which are provoked by lifestyle factors such as diet, smoking and inactivity. Genetic factors such as race and gender can also play a role in both prevalence and outcomes of CVD. Treatment of CVD primarily involves prophylactic measures such as education and promotion of healthy lifestyle choices in addition to the pharmacological use of aspirin, beta-blockers, statins and angiotensin-converting enzyme inhibitors[3]. While these pharmaceutical compounds are effective in preventing CVD onset, we currently have very few compounds to effectively target and treat pathophysiological conditions in established CVD.

One of the least understood elements of CVDs is arterial stiffening. Stiffening plays a role in a range of cardiovascular diseases and is one of the primary drivers of hypertension. Blood vessel stiffening is primarily driven by remodelling of the extracellular matrix (ECM). Specifically, the increased synthesis of rigid structural proteins such as collagen and increased breakdown of flexible and stretch resistant proteins such as elastin. These ECM changes are mediated by the cell populations that reside within blood vessels. In the muscular arteries, such as the aorta, these cells include endothelial cells, and a large population of vascular smooth muscle cells (VSMCs). Recent work has shown that changes in VSMC phenotype, contractility and biomechanics play a vital role in pathological stiffening of the arteries. This project aims to further elucidate the role VSMCs play in arterial stiffening in the context of ageing and disease.

1.2 The Cardiovascular System

The cardiovascular system is a complex organ system that consists of the heart, blood vessels, and blood. Its primary function is to deliver oxygen and nutrients to the body's tissues and facilitate the removal of waste products. This function is achieved through the circulation of blood within the blood vessels, in a process driven by the cyclical contraction and relaxation of the ventricles[4].

1.2.1 The Heart and the Cardiac Cycle

The heart is the pump that drives blood around the body; to facilitate this function, it is split vertically into the left and right atria and ventricles. At the beginning of the cardiac cycle, deoxygenated blood is received into the right atrium from the vena cava and then forced into the right ventricle during atrial systole. This process is regulated by the sinoatrial node (SAN), a specialised myocardial structure that generates the electrical impulses required for depolarisation and contraction of cardiomyocytes in the atria[5]. Following this, blood is pumped into the pulmonary artery during ventricular systole; much like atrial systole, this process is controlled by a specialised structure similar to the SAN called the atrio-ventricular node (AVN). Once blood is in the pulmonary artery, it is pumped to the lungs, where gaseous exchange takes place before returning to the heart as oxygenated blood[5].

Oxygenated blood enters the left atria through the pulmonary vein. Once in the heart, the previously described cycle of atrial and ventricular systole pumps the blood into the aorta and then around the body via a network of progressively smaller arteries, arterioles, and capillaries that eventually reconverge into the venules and veins, which return deoxygenated blood to the heart[6]. Each of these blood vessels possess unique structural specialisation depending on their function.

1.2.2 Aortic Structure in Health and Disease

The aorta is the largest blood vessel in the body. During ventricular systole, blood is pumped into the aorta. This sudden influx of blood creates a significant spike in hydrostatic pressure. The requirement to modulate this spike in pressure is the

predominant function of arterial wall structure. Like all arteries, the aortic wall is split into three distinct layers: the tunica intima, tunica media, and tunica adventitia (Figure 1). The tunica intima is the inner most layer, which consists of an endothelial monolayer and its supporting basement membrane. Acting as an interface between the vessel wall and the lumen, the tunica intima plays important roles in cell signalling, cell migration (e.g. immune cell transmigration), and angiogenesis[7].

The middle layer is the tunica media. This layer is by far the largest and consists of vascular smooth muscle cells (VSMCs) and their supporting elastic and structural tissues. The tunica media is involved in the most important element of aortic wall physiology: its ability to act as an elastic buffering chamber. This unique biomechanical function derives from the elastic tissues in the tunica media and involves the cyclical stretching and recoiling of the arterial wall to modulate the pressures generated by ventricular systole. During peak systolic pressure, the aortic wall stretches to approximately half the total stroke volume before recoiling during ventricular diastole. This process is known as the Windkessel function and prevents damage to the aortic wall while contributing to efficient circulation[8].

The outer most layer is the tunica adventitia which is comprised entirely of connective tissues such as collagen[9]. This layer is important in preventing overexpansion of the aorta as well as anchoring the blood vessel to the surrounding tissue (Figure 1.1).

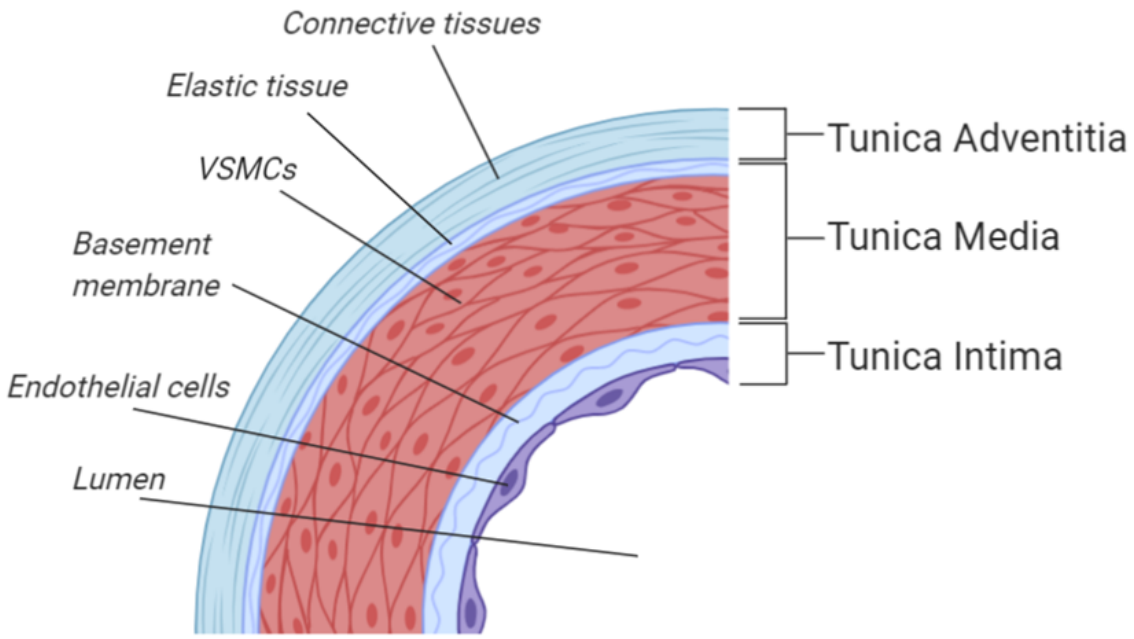

Figure 1.1. Cross-sectional structure of an arterial wall. *The arterial wall consists of three distinct layers. The tunica adventitia is the outermost layer and consists primarily of connective tissues. The tunica media is the middle and largest layer and consists of the VSMCs and elastic tissues. The inner layer is the tunica intima and is made up of endothelial cells and their supporting basement membrane. (Figure generated using biorender: https://biorender.com)*

The large smooth muscle layer and the balance between structural and elastic ECM components confer arteries with their specialised ability to withstand substantial hydrostatic pressures. However, during ageing and cardiovascular disease, this balance can become disrupted, resulting in the loss of aortic compliance (Figure 1.2). Reduced arterial pliability – the loss of the artery's ability to stretch and recoil - has a significant impact on pulse wave velocity and is associated with hypertension, increased shear stress, and organ damage, all key predictors of cardiovascular events[10]. Historically, aortic stiffening has been attributed to ECM remodelling, specifically the aberrant degradation of elastic ECM components such as elastin and increased deposition of structurally rigid elements such as collagen and fibronectin[11]. A key driver of ECM remodelling is the balance between ECM degrading enzymes such as matrix metalloproteases (MMPs) and their inhibitors[12]. In the vasculature, the collagenase MMP-2 has been found to be constitutively expressed by both endothelial and smooth muscle cells and is understood to play an important physiological role in ECM turnover[13]. In healthy aortae, the activity of MMP-2 is tightly regulated by the inhibitory action of TIMP-1 and -2[13]. In diseased conditions, however, the activity of MMP-2 is significantly

increased, as is the activity of elastase MMP-9[14,15]. This ultimately leads to increased degradation of elastin and reduced arterial compliance.

The dysregulation of this protease network is primarily driven by changes in gene expression and increased enzymatic activation through MMP-MMP interactions.

Additional remodelling of the ECM is mediated through low-level inflammatory responses induced by chronic hypertension and activation of the renin-angiotensin pathway. These processes induce endothelial and smooth muscle dysfunction, which further promote collagen deposition, elastin degradation, increased levels of glycation end-products, and increased production of reactive oxygen species[16]. The renin-angiotensin pathway has also been shown to induce VSMC proliferation[11].

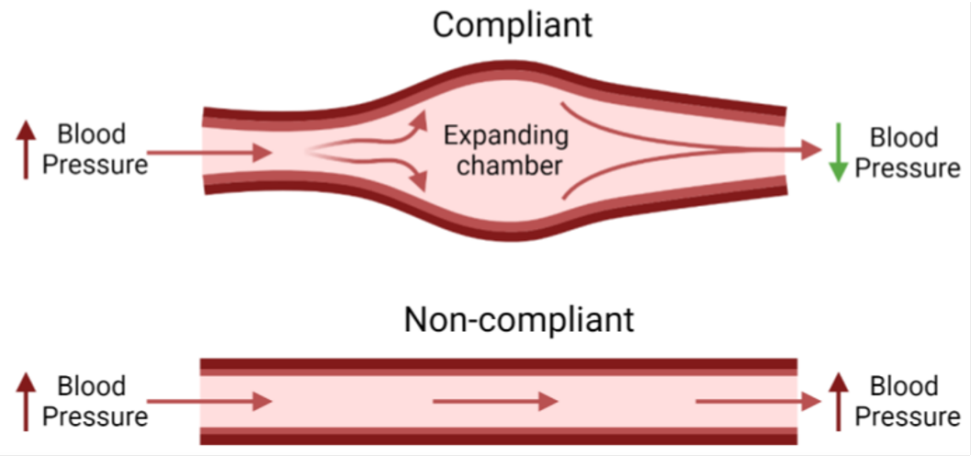

Figure 1.2. A schematic representation of a compliant vs non-compliant aorta. *In the healthy, compliant aorta, the vessel walls stretch to modulate the increased hydrostatic pressure, preventing damage to the blood vessel and smoothening out blood flow. In the diseased, non-compliant aorta the vessel walls are unable to stretch, leading to hypertension and increased risk of cardiovascular events such as stroke or aortic aneurism. (Figure generated using biorender: https://biorender.com)*

The described mechanism of arterial stiffening and its relationship to CVDs is well understood. However, over the last decade *in vitro* studies have revealed the significant role of the cellular component in arterial stiffening. Specifically, attention has now turned towards the mechanosensitive and contractile activity of VSMCs.

1.2.3 Disease of the Arteries

Cardiovascular disease is a broad term that covers a range of pathological conditions. These conditions are often multifactorial and include both acquired and congenital

diseases. The most common form of CVD is atherosclerosis, an acquired disease where the main pathology is inflammation of the large arteries and lipid accumulation. Atherosclerosis is known to be slow progressing and is associated with a range of serious clinical events such as stroke and myocardial infarction[17]. It occurs primarily in older individuals and those who maintain a sedentary lifestyle. Atherosclerosis is characterised by the presence of atherosclerotic lesions - areas of abnormal material accumulation within the intimal and medial layers of the arterial wall. These lesions consist of large aggregations of low-density lipoproteins, immune cells (such as leukocytes and macrophages), smooth muscle cells, and cell debris. Over time, these lesions can grow to obscure >50% of the arterial lumen, leading to angina and hypertension and substantially reducing the flow of oxygenated blood to tissues of the body. In advanced atherosclerosis, lesions can rupture, resulting in clot formation that can completely obstruct the coronary arteries, leading to myocardial infarction, or travel to the brain, where the subsequent risk of stroke is high[17].

Another common cardiovascular pathology is aortic aneurism. An aortic aneurism is a dilation of the aorta where the normal vessel diameter is exceeded by 50%. The four classifications of aortic aneurysm are aortic root, thoracic aortic, abdominal aortic, and thoracoabdominal aortic aneurisms, with abdominal aortic aneurisms being by far the most common[18]. The aetiology of aortic aneurisms is still unclear. However, it is understood that they represent a distinct, degenerative pathology of the aortic wall characterised by remodelling of the vascular ECM, infiltration by immune cells, and thinning of the tunica media[19]. Aortic aneurisms are often asymptomatic until they rupture, a usually lethal event with a mortality rate of 85-90%.

It is important to consider the multifactorial nature of cardiovascular disease when discussing its aetiology and placing it within the context of ageing and lifestyle. For example, hypertension has been shown to be the most significant risk factor for coronary heart disease and stroke[20], but is itself a symptom of arterial stiffening and vascular wall remodelling. This demonstrates the complex interplay between the structure and function of the vascular ECM, the cell component (smooth muscle, endothelial, and

immune cells), blood pressure, and inflammation, which are kept in homeostatic balance in health, but which become dysfunctional in disease.

1.3 The Vascular Smooth Muscle Cell in Health & Disease

1.3.1 Smooth Muscle & Molecular Regulators of Vascular Tone

Smooth muscle is non-striated, involuntary muscle tissue found in the walls of the hollow organs. In the arteries, smooth muscle is found in the tunica media where it acts as a coordinated syncytia to regulate vascular tone and resistance. Vascular tone refers to the extent to which blood vessels are dilated or constricted and is essential to the healthy functioning of the vasculature and the regulation of haemodynamics. This process is regulated by both endogenous and exogenous factors which work synergistically to maintain homeostasis.

Endogenous regulation of vascular tone is primarily driven by the endothelium, which produces various vasoactive factors in response to mechanical stimuli such as blood pressure and shear stress. These factors can be vasodilatory, such as nitric oxide (NO), or vasoconstrictive, such as endothelin-1. Nitric oxide is a gaseous signalling molecule produced by endothelial cells in response to increased shear stress. Under high shear stress conditions, Ca^{2+} diffuses across the endothelial cell membrane through specialised Ca^{2+} activated K^{+} channels. Increased intracellular Ca^{2+} causes the enzyme nitric oxide synthase (NOS) to detach from caveolin, its membrane-bound scaffold protein, and become activated[21]. Activated NOS subsequently converts the amino acid $_{L}$-arginine into NO. Once synthesised, NO diffuses out of the endothelium and into the adjacent smooth muscle where it binds to cytosolic guanylyl cyclase, causing it to become activated, and increasing the production of cGMP from GTP. cGMP inhibits the release of Ca^{2+} from the sarcoplasmic reticulum, reducing the rate of actomyosin cross-bridge cycling and preventing contraction[22]. NO is also a key regulator of vasoconstrictive Endothelin-1 expression.

Endothelin-1 is the primary vasoconstrictive factor released by the endothelium. Levels of endothelin-1 are regulated primarily at the level of transcription, with endothelin

precursor peptide, preproendothelin, expression modulated by several transcription factors, including AP-1, NF-KB and FOXO1. This precursor protein is then cleaved by furin and ECE proteases to generate functional endothelin-1[23]. The endothelin peptide is released from the endothelium through exocytosis and binds to the ubiquitously expressed ET_A and ET_B GPCRs. In smooth muscle cells, the binding of endothelin to ET_A induces contraction through $G\alpha_{q/11}$ activation of phospholipase C (PLC) and the subsequent inositol triphosphate (IP3) mediated release of Ca^{2+} from intracellular stores[24].

Exogenous regulation of vascular tone involves systemic changes to vascular homeostasis driven by circulating hormones and innervation of the vasculature by the autonomic nervous system. Many of the neurohormonal factors involved in regulating vascular tone can be both vasoconstrictive and vasodilatory. For example, the catecholamine neurotransmitters (norepinephrine and epinephrine) have been shown to be vasoconstrictive in the arteries but vasodilatory in the liver and skeletal muscle due to the differential expression of adrenergic receptors[25]. In the vascular smooth muscle, norepinephrine binding to α1-adrenergic receptors induces contraction through downstream activation of PLC and its secondary messenger IP3[26].

One of the most important molecules involved in regulating vascular tone is angiotensin II (Ang II). Ang II is a vasoactive hormone produced primarily by the renin-angiotensin system in the kidneys. More recently, it has been shown that Ang II is also produced in local renin-angiotensin systems, including in the vasculature[27]. Ang II is a potent vasopressor that acts on smooth muscle cells via the AT_1R and AT_2R GPCRs[28]. These receptors have antagonistic effects, with AT_1R activation associated with the classical Gq11/PLC/IP-3/Ca^{2+}/calmodulin/MLCK contractile response, and AT_2R activation associated with antiproliferative, pro-apoptotic, and vasodilatory signalling pathways[28]. In addition to these core pathways, Ang II signalling has also been shown to induce downstream activation of several protein kinases including Wnk kinases, ALK1/2/4, and AMPK, as well as the transcription factors TGF, EGF, and VEGF. Importantly, chronic exposure to Ang II and subsequent activation of the AT_1R receptor has been associated

with VSMC proliferation and structural remodelling of the vasculature, as well as the activation of pro-inflammatory transcription factors[29].

1.3.2 VSMC Origin & Phenotype: Built to Contract, Born to Adapt

VSMCs are highly contractile cells that regulate vascular tone and provide structural support in the large arteries. In the mature vessel, VSMCs are quiescent and express a range of contractile proteins, including α-SMA (alpha-smooth muscle actin), SM22α, calponin, smoothelin, and SM-MHC (smooth muscle myosin heavy chain). Fate mapping studies have shown that VSMCs represent a highly heterologous cell population with diverse developmental origins[30]. It is now understood that different vessels, and even different segments of the same vessel, are composed of VSMC populations with distinct progenitors. Within the aorta, distinct populations of VSMCs with developmental origins in the cardiac neural crest, paraxial mesoderm-derived sclerotome, and the lateral plate mesoderm-derived second heart field have been observed. Interestingly, these cell populations have defined boundaries, with little intermixing of VSMCs of different lineages[31]. The heterologous nature of VSMC developmental origin provides some insight into the remarkable ability of VSMCs to modulate their phenotype.

Phenotypic switching refers to the ability of differentiated, contractile VSMCs to dedifferentiate into a proliferative, migratory, and secretory phenotype. This synthetic phenotype is associated with reduced expression of traditional contractile markers such as α-SMA, SM-MHC, and smoothelin and upregulated expression of markers associated with osteoblast, fibroblast, macrophage, and mesenchymal cells[32]. These dedifferentiated VSMCs have significantly increased proliferative capacity alongside upregulated expression of matrix metalloproteases (MMPs) and ECM components, which, in the healthy vessel, facilitate vascular remodelling and repair after injury. The synthetic phenotype is also associated with substantial morphogenic change from the defined, fibroblast-like spindle shape of differentiated SMCs to a more irregular epithelioid morphology[33]. Furthermore, the extensive intracellular network of contractile filaments found in differentiated SMCs is largely replaced by organelles associated with the synthesis and secretion of ECM and ECM-associated proteins in synthetic VSMCs[33].

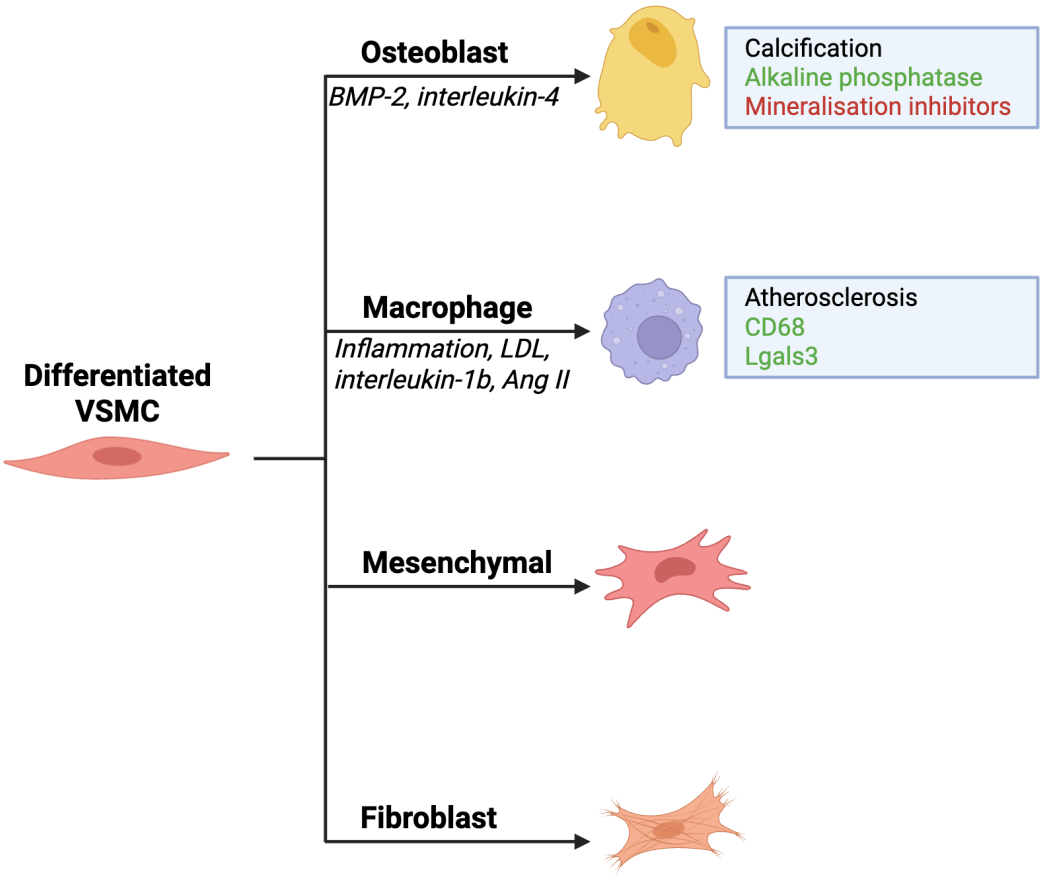

Figure 1.3. Diagrammatic representation of VSMC transdifferentiation into distinct cell types. *VSMCs retain the ability to transdifferentiate into several distinct cell types, including osteoblast-like cells, macrophage-like cells, mesenchymal-like cells and fibroblasts. (Figure generated using biorender: https://biorender.com)*

In addition to the contractile and synthetic phenotypes, recent studies have identified a number of other VSMC phenotypes with unique expression patterns[34]. This diverse group of phenotypes includes osteoblast, macrophage, mesenchymal, and fibroblast-like VSMCs (Figure 1.3). It is now understood that these phenotypes play diverse roles in vascular pathologies. For example, vascular calcification has been identified as a major contributor to vascular remodelling and is especially prevalent in diseases such as atherosclerosis. Work in mouse models has shown that transdifferentiation of VSMCs into osteochondrogenic precursor cells is a key driver of vascular calcification in disease[35]. These cells are associated with the presence of calcifying vesicles and the reduced expression of mineralisation inhibitory molecules, alongside upregulated expression of chondrocyte/osteoblast-like markers such as alkaline phosphatase[36]. Work by *Giachelli et al* has shown that knockout of the RUNX2 transcription factor prevents VSMCs transdifferentiation into osteoblast-like cells and prevents calcification

of atherosclerotic lesions in mouse[37]. Additionally, macrophage-like VSMCs have been observed under conditions of sustained vascular inflammation and atherosclerosis and have been linked to neointimal hyperplasia in mice[38]. These cells have reduced expression of contractile genes and upregulated expression of macrophage markers such as CD68 and Lgals3[34]. Work has shown that ~50% of foam cells found in atherosclerotic plaques are VSMC-derived macrophage-like cells[39]. It is understood that phagocytosis of low-density lipoprotein (LDL) and cholesterol are the primary metabolic drivers of VSMC transdifferentiation into macrophage-like cells. Additional pro-macrophage transdifferentiation factors include inflammatory chemokines, such as interleukin-1β, oxidative stress, and vasoactive molecules, such as Ang II[40]. Further work is required to fully elucidate the role of these VSMC-derived cells in disease. However, it is clear they contribute to arterial stiffening and chronic inflammation in atherosclerosis.

1.4 Determinants of VSMC Phenotypic Plasticity

The phenotypic plasticity of VSMCs is regulated through the integration of molecular and biomechanical signals from the extracellular environment. These signals include circulating factors in the blood, transcription factors, growth factors, inflammatory molecules, integrin signalling, non-coding RNAs, the Notch-pathway signalling pathway, and shear stress (Figure 1.4)[32]. Understanding these pathways in vital to understanding the behaviour of VSMC populations in cardiovascular disease.

1.4.1 Molecular Determinants of VSMC Phenotype

The transcription factor TGF-β appears to be essential for the induction and maintenance of the VSMC contractile phenotype[41]. TGF-β induces expression of serum response factor (SRF), which promotes contractile gene expression through its association with myocardin and its subsequent binding to CArG regulatory motifs[42]. SRF-Myocardin regulation of the contractile phenotype is complemented by TGF-β mediated activation of SMAD2/3/4 transcriptional complexes and their downstream regulation of contractile gene expression[43]. The activity of TGF-β is directly opposed by PDGF, which is released following vascular injury and promotes the rapid and sustained downregulation of contractile genes. PDGF activates KLF4, a transcription factor that blocks SRF-

Myocardin interaction[44], and can directly regulate the expression of contractile genes by binding to G/C repressor elements[45]. TGF-β has been shown to inhibit KLF4-mediated phenotypic switching through activation of microRNA143/145, which post-translationally inhibit KLF4 activity[46]. Additional growth factors involved in phenotypic regulation include FGF, which has been shown to induce the synthetic phenotype and promote the expression of inflammatory factors in atherosclerosis[47]. Other studies have found that the extent of VSMC dedifferentiation is proportional to the intensity of FGF signalling[32].

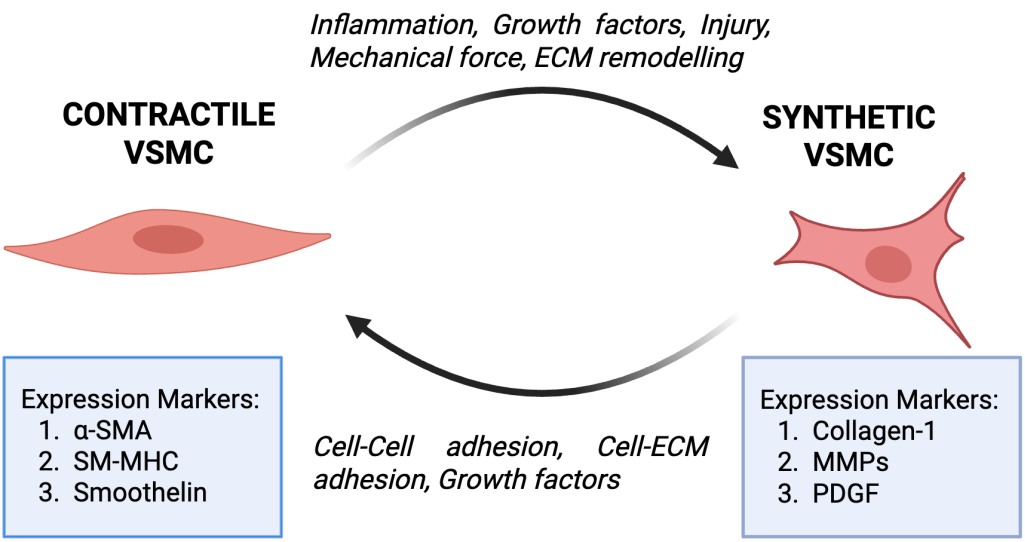

Figure 1.4. Schematic diagram showing VSMC dedifferentiation into the synthetic phenotype. *Dedifferentiation is driven by the integration of extracellular signalling pathways such as growth factors, inflammatory cytokines, mechanical forces and ECM remodelling. VSMC dedifferentiation results in the downregulation of contractile genes such as α-SMA, SM-MHC and smoothelin and the upregulation of synthetic genes such as collagen-I, MMPs and PDGF. (Figure generated using biorender: https://biorender.com)*

Other molecular regulators of the VSMC phenotypic switch include inflammatory cytokines. The binding of TNFs to the CD137 receptor is associated with phenotypic switching through downstream activation of the NFATc1 transcription factor and the subsequent inhibition of contractile gene expression[32]. Additionally, recent studies have identified products of endothelial exocytosis, such as NLRP3 inflammasome component IL-1β, as promoters of synthetic phenotype transition in VSMCs[48]. Work has shown that IL-1β induces the synthetic phenotype in a manner distinct from PDGF stimulation and that it promotes the expression of a discrete set of inflammatory genes. Additional

studies demonstrated that this IL-1β mediated phenotypic switch is mediated by NF-κB and leads to a primarily inflammatory phenotype[48].

1.4.2 Cell-Cell Interactions in Phenotype Regulation

Cell-cell interactions, particularly through Notch signalling, also play a role in VSMC phenotypic plasticity. The Notch-3 receptor is highly expressed in differentiated VSMCs and is associated with a range of cell processes. In canonical Notch signalling, activation of the Notch receptor by membrane-bound DLL or Jagged proteins results in downstream gene regulation through cleavage of the Notch intracellular domain (NICD). The NICD localises to the nucleus where it interacts with RBP-Jκ and MAML to promote transcription of the HES and HEY transcription factors[49]. These transcription factors act as suppressors of transcription, therefore influencing the expression of a range of downstream genes. *In vivo* studies have shown that Notch3$^{-/-}$ mice have a significantly thinner arterial medial layer and reduced expression of the VSMC marker protein smoothelin[50]. Additional studies have shown that Notch3$^{-/-}$ mice have pulmonary VSMCs with significantly reduced expression of contractile genes such as α-SMA, smoothelin, calponin, and SM-MHC compared to controls[51]. These studies suggest that Notch3 signalling is vital in the development and maintenance of the VSMC contractile phenotype. Conversely, overexpression of constitutively active NICD1 and NICD3 alongside activation of Notch3 has been shown to downregulate the expression of contractile markers in VSMCs, suggesting that dysregulated Notch signalling promotes the synthetic phenotype[52]. The mechanisms behind Notch-mediated phenotypic switching have yet to be fully elucidated. However, work has shown that several pathways underlie Notch3 activity, including KLF transcription factors, HES1 transcription factor, activation of p27Kip1, decreased activity of apoptotic promoters such as caspase-3, and upregulated MAPK signalling[53,54].

1.4.3 Epigenetic Determinants of VSMC Phenotype

VSMC phenotype is also modulated by epigenetic regulation of the transcriptome. DNA methylation is a vital component of the gene regulatory network and is mediated primarily through the activity of DNA methyltransferases. DNA methylation has been found to regulate several genes associated with VSMC phenotypic plasticity including

SRF, PDGF and TAGLN[55]. Recent work has shown that knockdown of the TET2 demethylating enzyme inhibits the expression of SRF and myocardin in VSMCs[56]. The authors additionally reported that TET2 knockdown induced upregulation of KLF4, promoting the synthetic phenotype[56]. Furthermore, hypermethylation has been associated with cardiovascular diseases such as atherosclerosis[55].

Additional epigenetic regulators of VSMC phenotype include histone modification through acetylation, methylation, and ubiquitinylation. These post-translational modifications often occur in combination. Acetylation typically promotes gene expression, whereas methylation and ubiquitylation have diverse transcriptional effects. In VSMCs, decreased methylation and increased acetylation of H3K9 and H3K27 has been observed in cells of advanced atherosclerotic plaques[57]. Additionally, work has shown that reduced methylation of H3K9 in VSMCs of arteries undergoing vascular remodelling and atherosclerotic plaque formation is associated with the upregulated expression of inflammatory cytokines such as IL-6 and matrix proteases MMP3/9/12[58]. Other groups have observed that methylation marker H3K4me2, found on genes specific to smooth muscle, is essential in maintaining VSMC contractile phenotype and that removal of methylation by the demethylase LSD1 leads to the loss of VSMC contractility[59]. Histone deacetylase 6 (HDAC6) is another important component in the epigenetic regulation of VSMC phenotype. As a histone deacetylase, HDAC6 is primarily involved in inhibiting gene expression by removing acetyl groups from histone proteins. However, HDAC6 is also found outside the nuclear envelope, where it deacetylates cytosolic proteins. Recent reports suggest that HDAC6 inhibition with Tubastatin A prevents PDGF-induced downregulation of the contractile genes α-SMA and SM-MHC[60]. Furthermore, the authors also found that HDAC6 inhibition result in increased transcriptional activity of SRF, alongside increased total protein level of the transcriptional regulator MRTF-A[60]. MRTF-A is a known regulator of contractile gene expression due to its role as a coactivator of SRF[61]. These results suggest that HDAC6 plays a crucial role in regulating the master contractile gene regulator, SRF, and therefore induces the VSMC synthetic phenotype.

1.4.4 ECM Determinants of VSMC Phenotype

ECM composition and organisation are also involved in the regulation of VSMC phenotype. The established dogma states that this interaction is mediated primarily through integrin receptors and their downstream signalling pathways. For example, previous work has shown that fibrillar collagen I binding to its αvβ3 integrin receptor promotes the contractile phenotype, whereas binding of monomeric collagen I is pro-synthetic and migratory[62]. Additionally, matricellular protein interactions with integrin receptors have also been shown to play a role in regulating VSMC phenotype. For example, Cartilage Oligomeric Matrix Protein (COMP), which binds directly to integrin α7β1, has been shown to be degraded by ADAMTS-7 in response to vascular injury. This decrease in COMP is associated with decreased expression of contractile markers such as α-SMA, SM22α, and calponin[63]. Interestingly, *in vitro* treatment of VSMCs with PDGF results in greatly inhibited COMP protein expression, whereas treatment with TGF-β was shown to significantly increase COMP expression[63]. This suggests an important link between growth factor signalling and ECM composition in the regulation of VSMC phenotype. Further evidence of this was reported by a group who found that the proteoglycan perlecan inhibits VSMC proliferation by sequestering FGF in its heparan sulphate side chains[64], and separate work found that different isoforms of collagen I regulate VSMC response to PDGF[65]. Another proteoglycan involved in the regulation of VSMC phenotype is heparin, which has been associated with the induction and maintenance of the contractile phenotype via activation of the heparin receptor protein and downstream activation of PKG[66].

More recently, the role of fibronectin in the VSMC phenotypic switch has been elucidated. *Chauhan* and colleagues report that Fibronectin extra domain A (Fn-EDA) drives phenotypic switching and promotes increased proliferation and migration of VSMCs in neointimal hyperplasia. They report that VSMC-specific Fn-EDA$^{-/-}$ mouse models show significantly reduced neointimal hyperplasia and reduced PDGF-induced phenotypic switching. The authors demonstrated that this Fn-EDA mediated VSMC migration and proliferation switch is regulated by both integrin and TLR4 signalling pathways[67]. Another recent finding is the role of the matricellular adhesion protein FBLN7 in VSMC phenotypic regulation. Work has shown that knockdown of FBLN7 ameliorates

AT_1R-induced vascular remodelling *in vivo* and that expression of VSMC contractile markers α-SMA and SM22α was elevated in FBLN7 knockout cells[68]. The authors identified FBLN7 binding to the syndecan-4 receptor and subsequent activation of the ROCK/MRTF-A signalling pathway as key to the VSMC phenotypic switch[68].

1.4.5 Mechanical Determinants of VSMC Phenotype

Finally, mechanical forces, such as stretch and shear stress, are key determinants of VSMC phenotype. These physical forces are transmitted through cell-cell and cell-ECM interactions. Shear stress is generated by blood flow and, therefore, exacts force on the longitudinal axis of the vessel wall. This force is primarily received by the endothelial cells of the tunica intima and transduced to VSMCs via cell-cell interactions. Studies *in vitro* have shown that endothelial cells co-cultured with VSMCs have increased expression of the E-selectin cell adhesion protein and that this increased expression is reversed by the application of shear stress[69]. This finding highlights the dynamic interaction between endothelial and smooth muscle cell populations in response to mechanical forces. Studies *in vitro* have shown that shear stress significantly reduces VSMC expression of contractile genes while increasing expression of matrix metalloproteases and inflammatory cytokines[70]. *Wu et al* linked this shear stress-induced phenotypic switch to an AMPK/mTOR/ULK1-mediated autophagy pathway[70]. Additional work in endothelial-VSMC co-culture has shown that when dysregulated low-flow is applied to endothelial cells, a concomitant increase in VSMC expression of PDGF and TGF-β occurs[71]. Furthermore, studies have shown that shear stress causes increased VSMC proliferation *in vitro*[72]. The authors demonstrated that the PI 3-kinase/Akt signalling pathway with downstream activation of p21 drives this response[72]. Interestingly, some groups have found contradictory evidence that rat aortic VSMCs exposed to varying amounts of shear stress show reduced proliferative and migratory activity compared to controls[73]. This result was repeated by *Dardik* and colleagues, who observed a similar reduction in proliferative activity in bovine aortic SMCs exposed to flow *in vitro*. However, the authors did observe an increase in SMC apoptosis, highlighting the role of shear stress in vascular remodelling[74].

Stretch is generated by hydrostatic pressure that opposes the intraluminal pressure produced by VSMCs in the vessel wall. Hydrostatic pressure within the lumen is increased under hypertensive conditions such as during atherosclerosis and stenosis. Studies in animal models of aortic coarctation have shown that arterial thickening occurs in a manner that is directly proportional to the extent of tensile wall stress[75]. In VSMCs, work has shown that MMP-2[76] and MMP-9[77] expression is upregulated in response to high intraluminal pressure, demonstrating the role of stretch in vascular remodelling. Stretch-induced MMP expression is understood to be regulated by PDGFR signalling and downstream activation of PI3K/Akt[78]. Interestingly, *in vitro* studies in animal-derived VSMCs have shown that low levels of cyclic stretch increase the expression of VSMC contractile markers. Counterintuitively, these studies also show that proliferative and migratory capacity is increased in both aberrantly low and aberrantly high stretch conditions[79]. In human VSMCs, high stretch simulation has been shown to induce reduced the expression of contractile markers and upregulation of the phenotypic master regulator KLF4[80]. This reduced contractile marker expression has been associated with the upregulation of inflammatory genes such as IL-8, IL-6 and, IL1β when exposed to high stretch[81]. Together, these findings highlight stretch as a critical biomechanical cue that modulates phenotypic plasticity and vascular remodelling.

1.5 VSMC Adhesion and Mechanotransduction

VSMCs are highly integrated into their extracellular environment. This integration facilitates VSMC phenotypic modulation in response to ECM composition and mechanical force transduction and enables the transfer of actomyosin derived contractile forces into the surrounding tissue. The multifaceted integration between VSMCs and their extracellular environment is mediated through a complex network of cell-ECM and cell-cell interactions.

1.5.1 Integrin-Mediated Mechanotransduction & Focal Adhesion Signalling in VSMCs

The primary mechanism through which VSMCs interact with the ECM is through integrin receptors. Integrins are heterodimeric, trans-membrane receptor proteins which link the extracellular ECM with the intracellular cytoskeleton. They consist of α and β subunits,

with ligand specificity primarily determined by specific subunit isoforms. There are 24 known integrins, consisting of 18 α subunits and 8 β subunits[82]. In VSMCs, β1 integrins are amongst the most abundantly expressed, and pair with several α subunits to provide binding specificity for ECM proteins such as collagen, fibronectin and laminin[83]. In particular, $\alpha 1\beta 1$ and $\alpha 2\beta 1$ integrins serve as the primary collagen receptors in VSMCs[83]. Also, expressed in VSMCs is the fibronectin binding α5β1 integrin, the laminin binding α7β1 integrin and the α8β1 integrin which has a wide range of ligands including fibronectin and vitronectin[84].

On binding of an integrin to its ECM substrate, the intracellular β domain recruits a range of adaptor and signalling proteins resulting in the formation of a focal adhesion[85]. These focal adhesions act as nucleation points for further protein-protein interactions and downstream signalling cascades. For example, the intracellular domain of the β subunit interacts with the actin cytoskeleton via the adaptor proteins talin, filamin, tensin and α-actinin; thus, enabling transmission of actomyosin generated forces into the extracellular environment[86]. The mechanistic phenomena of intracellular actomyosin derived forces imparting tension on the surrounding substrate is referred to as the molecular clutch, which can be dynamically engaged and disengaged depending on cellular requirements. Clutch proteins such as talin and vinculin are readily exchanged between their integrin-actomyosin associated state and their cytosolic pools, enabling the rapid formation and disassembly of actin associated integrin-ECM complexes[87]. The molecular clutch is highly sensitive to substrate stiffness. On stiff substrates talin has been shown to increase vinculin recruitment in a mechanism that reinforces the clutch and increases actomyosin force transduction. Studies utilising talin tension sensors have demonstrated the effects of different talin isoforms on ECM rigidity sensing and shown that differential expression of talin isoforms is essential in cell adaptation to extracellular stiffness[88].

Focal adhesion signalling is vital in mechanosensitive VSMC responses (Figure 1.5). There are two primary signalling axes in which focal adhesions play a role. The first is inside-out signalling or signalling involved in transduction of messages from the intracellular environment to the extracellular environment. The second is outside-in

signalling which involves the transduction of signals from the extracellular environment to the intracellular compartment[89]. Inside-out signalling is primarily involved in the formation of the focal adhesion complex. This process is commonly activated via the binding of ligand to GPCRs[90]. Outside-in signalling utilises the extensive signalling scaffold recruited during focal adhesion formation. One of the key components of focal adhesion signalling is focal adhesion kinase (FAK). FAK is a cytosolic tyrosine kinase that becomes phosphorylated upon integrin activation. It is involved in a range of cellular processes including proliferation, migration and differentiation. Its interactions with the actin cytoskeleton and membrane associated proteins such as PIP2 suggest it plays mechanosensitive roles with several studies linking it to force guided migration[91]. In VSMCs work has shown that increased fibronectin deposition in the ECM, a key ligand of integrin α5β1, induces enhanced FAK activation and induces VSMC proliferation and migration[92]. Additionally, VSMCs plated on stiff hydrogels have been shown to have elevated FAK activation and increased expression of cell cycle associated genes when compared to those plated on soft hydrogels[93].

1.5.2 The Dystrophin–Glycoprotein Complex in VSMCs: A Mechanical Stabiliser?

The dystrophin–glycoprotein complex (DGPC) is expressed in all types of muscle and is essential in the adhesion of myocytes to their basement membrane. In SMCs, the DGPC consists of α and β dystroglycans, β, δ, and ϵ-sarcoglycans, sarcospan, and dystrophin proteins (Figure 1.5)[94]. The DGPC is essential in preventing contraction-induced damage by providing mechanical stability to the plasma membrane and by distributing mechanical stress. This is achieved by linking the actin cytoskeleton with laminin and perlecan in the basal lamina. The exact role of the DGPC in VSMC adhesion and mechanotransduction is not fully understood. Currently, most studies utilise animal models of muscular dystrophy - an inherited neuromuscular disease characterised by mutations in DGPC components - to study the role of DGPC in the vasculature. For example, *Humphrey et al* found that arteries in mdx mice, which don't express the dystrophin gene, have structural abnormalities, distend less, and exhibit higher circumferential stresses when compared to controls[95]. This finding built on earlier work by *Henrion* and colleagues, who demonstrated that shear stress-induced dilation of arteries was reduced by 50-60% in mdx mice[96]. Further work is required to fully

understand the role of the DGPC in VSMCs; however, these studies suggest the DGPC plays a vital role in VSMC adhesion and mechanotransduction.

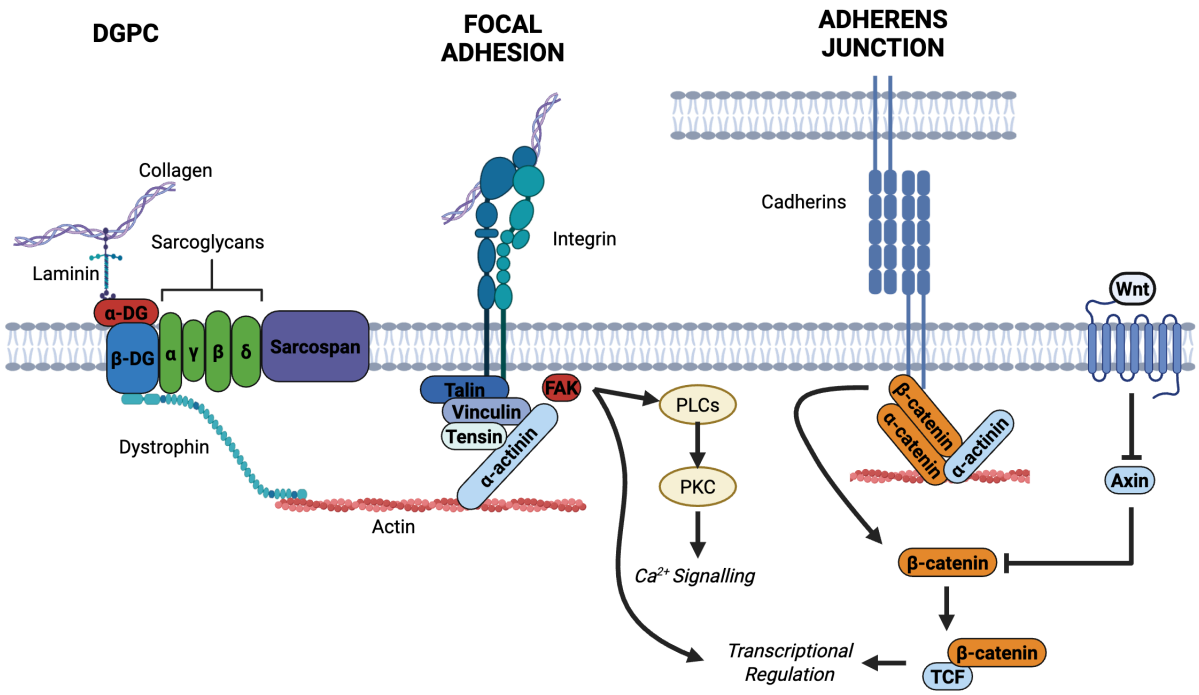

Figure 1.5. Schematic diagram showing the DGPC, focal adhesion and adherens junctions of VSMCs. *VSMCs possess a range of cell-cell and cell-ECM adhesion molecules. These adhesion molecules are vitally important in VSMC mechanotransduction and contractility. The DGPC is a vital cell-ECM adhesion complex that plays an important role in preventing contraction-induced cell damage by stabilising the plasma membrane. The DGPC consists of α and β dystroglycans, β, δ, and ϵ-sarcoglycans, sarcospan, and dystrophin proteins and adheres extracellular laminin proteins with the actin cytoskeleton. Focal adhesions are complex cell-ECM adhesion complexes mediated by integrin binding to diverse extracellular matrix ligands, and intracellular binding to the actin cytoskeleton via the talin-vinculin-αactinin scaffold. Focal adhesions also possess intrinsic signalling capability through recruitment and activation of focal adhesion kinase (FAK) and downstream promotion of Ca^{2+} signalling pathways. Adherens junctions are cell-cell adhesion complexes mediated by the formation of cadherin trans-dimers across the extracellular space. Adherens junctions also adhere the actin cytoskeleton via the support proteins α-actinin and vinculin. Adherens junctions also facilitate intracellular signalling through interaction with the Wnt signalling pathway and the translocation of β-catenin-TCF transcriptional complexes to the nucleus. (Figure generated using biorender: https://biorender.com)*

1.5.3 Cadherin-Mediated Adhesion & β-Catenin Signalling in VSMC Mechanotransduction

Cadherins are a diverse class of ubiquitous transmembrane, Ca^{2+} dependent cell-adhesion molecules vital in the formation of cell-cell adherens junctions. SMCs express several cadherin proteins, including the type I E-, N-, and R-cadherins, type II cadherin-6B and cadherin-11, and the atypical cadherins T-cadherin and cadherin-related FAT1[97]. The functionality of cadherins relies on their ability to form cadherin homodimers. These homodimers can then form cell-cell adhesions with cadherins present on neighbouring

cells through conformational change from cis- to trans-dimers[98]. The extracellular binding of neighbouring cadherins induces the recruitment of a range of cytosolic support and scaffold proteins, including α-, β-, and γ-catenins. This cadherin-catenin complex can then interact with actin via binding of support proteins α-actinin and vinculin (Figure 1.5)[99].

In addition to cell-cell adhesion, adherens junctions can also modulate a number of intracellular signalling pathways. The best characterised is the β-catenin/wnt pathway, which is involved in regulating a range of cell processes, including proliferation and migration. In canonical wnt signalling, the wnt ligand binds to the frizzled GPCR receptor. This prevents degradation of cytosolic β-catenin by initiating translocation of the negative wnt regulator, axin, to the plasma membrane. Free cytosolic β-catenin can then translocate into the nucleus, where it binds to and activates the transcription factor TCF, which regulates several downstream genes[99]. The role β-catenin/wnt signalling plays in cellular response to mechanical force is not well understood. However, work in endothelial cells has shown that the β-catenin/wnt signalling pathway is activated in cells exposed to aberrant hemodynamic flow states[100]. Additionally, *Tzima et al* previously identified an E-cadherin-VEGFR adhesion complex that appears to modulate endothelial cell response to shear stress[101]. The authors found that the interaction between E-cadherin and VEGFR is mediated by β-catenin. Furthermore, they found that knockout of β-catenin blocked integrin activation, preventing focal adhesion formation and inhibiting downstream signalling. Taken together, these results suggest that cadherins and β-catenin/wnt signalling play an important role in mechanotransduction in the vasculature. However, further work is required to fully elucidate their role in VSMC mechanotransduction.

1.5.4 Mechanosensitive Ion Channels in VSMC Signalling: Focus on Piezo1

Mechanosensitive ion channels are widely expressed membrane proteins. They are found in most cell types and can be grouped into three main categories: cation-selective channels, anion channels, and non-selective ion channels. Amongst the best characterized are the non-selective cation piezo family channels, consisting of piezo1 and 2. The piezo channels are large mechanosensitive ion channels that facilitate the

cross-membrane influx of Na^+, K^+, and Ca^{2+} ions. They have been implicated in a range of critical processes, including touch sensation, balance, and cardiovascular regulation[102]. Unlike most ion channels, piezo channels have been shown to possess intrinsic mechanosensitivity, where their primary gating modality is mechanical force. In the vasculature, early work in endothelial cells demonstrated that piezo1 is activated by shear stress (Figure 1.6)[103]. More recently, *Zhang et al* have shown that piezo1 is vital in endothelial cell response to shear stress through Ca^{2+} mediated PLC-β signalling and downstream activation of α5-integrin[104]. The role of piezo ion channels in VSMC mechanotransduction is not well understood. Work *in vivo* has focused on piezo-mediated VSMC response to intraluminal pressure with often contradictory results. *Honoré* and colleagues demonstrated that smooth muscle piezo1 knockout mice show no significant defects in vascular tone regulation or response to vasoactive compounds[105]. However, the authors also found that piezo1 deletion significantly reduced remodelling of caudal arteries in hypertensive mice[105]. Additionally, *Watt et al* report that the contractile properties of isolated rat arteries were not significantly altered by treatment with piezo1-modulating drugs[106].

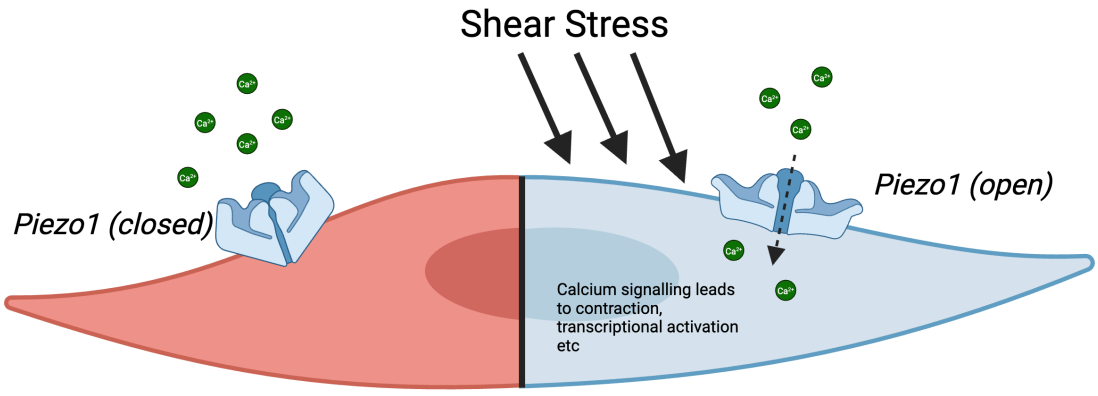

Figure 1.6. Diagrammatic representation of shear stress-induced activation of piezo1 channels. *Under low shear stress conditions, Piezo1 channels are closed preventing influx of Ca^{2+} ions. When mechanical stress is high, Piezo1 channels are opened, facilitating the influx of Ca^{2+} ions and initiating downstream calcium signalling. (Figure generated using biorender: https://biorender.com)*

Several other ion channels have been posited as having mechanosensitive roles in VSMCs, including TRPC6, TRPM4, TRPP1, TRPV4 and, P2X channels. These channels, while lacking intrinsic mechanosensitivity, play vital roles in integrating other mechanosensitive signalling pathways. For example, TRPC6 has been shown to play an important role in downstream signalling from mechanosensitive GPCRs such as the

angiotensin II receptor, AT_1R[107]. Additionally, due to the multimodal nature of ion channel gating, it is likely that many ion channels not currently associated with mechanosensing possess mechanical stimuli as a secondary or tertiary gating modality. Further work is needed to complete our understanding of ion-channel mediated mechanosensing in VSMCs.

1.6 Mechanisms of VSMC Contractility

The ability to contract is an essential element of the VSMC phenotype. As discussed, vascular smooth muscle contraction is regulated by both exogenous and endogenous factors. Exogenous factors include those found in the circulation, such as angiotensin, and factors released by the sympathetic nervous system, such as norepinephrine. These factors are usually associated with systemic vasoconstriction. Endogenous factors, including nitric oxide and endothelin, are released in response to localized stimuli and typically induce vasoconstriction within a specific organ or tissue[93].

Two primary mechanisms of VSMC contraction act synergistically to regulate vascular tone (Figure 1.7). The calcium-dependant pathway involves the binding of extracellular agonists to membrane-bound GPCRs. This interaction induces a conformational change in the receptor, enabling GDP-GTP exchange and the subsequent activation of the $G_{\alpha q}$ subunit. The activated $G_{\alpha q}$ subunit then disassociates from the G-protein complex and activates phospholipase C (PLCβ)[108]. Activated PLCβ can then bind to and hydrolyse the membrane component phosphatidylinositol 4,5-bisphosphate (PIP2) into two secondary messenger molecules: diacylglycerol (DAG) and inositol (1,4,5) trisphosphate (IP3). Cytosolic IP3 induces calcium release from the sarcoplasmic reticulum through the IP_3R receptor[109]. Levels of cytosolic Ca^{2+} can be further augmented through depolarisation of the plasma membrane and influx of extracellular Ca^{2+} through voltage-gated ion channels, transient receptor channels, and receptor-operated channels[110]. Free cytosolic Ca^{2+} binds to calmodulin, a calcium-binding protein involved in a range of signalling pathways. The calmodulin-Ca^{2+} complex subsequently activates myosin light chain kinase (MLCK), which phosphorylates serine-19 of the regulatory light chain MLC-20[109]. Phosphorylation of MLC-20 induces enhanced cross-bridge cycling, allowing the myosin-actin machinery to generate contractile force.

The calcium-dependent pathway is augmented by a separate, calcium-independent Rho/ROCK signalling cascade. RhoA, a member of the small GTPase family, is activated by guanine nucleotide exchange factor (GEF)-mediated exchange of GDP and GTP. The activity of GEFs is mediated by the activity of $G_{12/13}$ coupled GPCRs. In its GTP-bound state, RhoA binds to Rho-associated protein kinase (ROCK), which results in its autophosphorylation and activation. ROCK phosphorylates and inhibits myosin light chain phosphatase (MLCP). Inhibition of MLCP prevents it from dephosphorylating MLC-20 and, therefore, promotes the cross-bridge cycle[108].

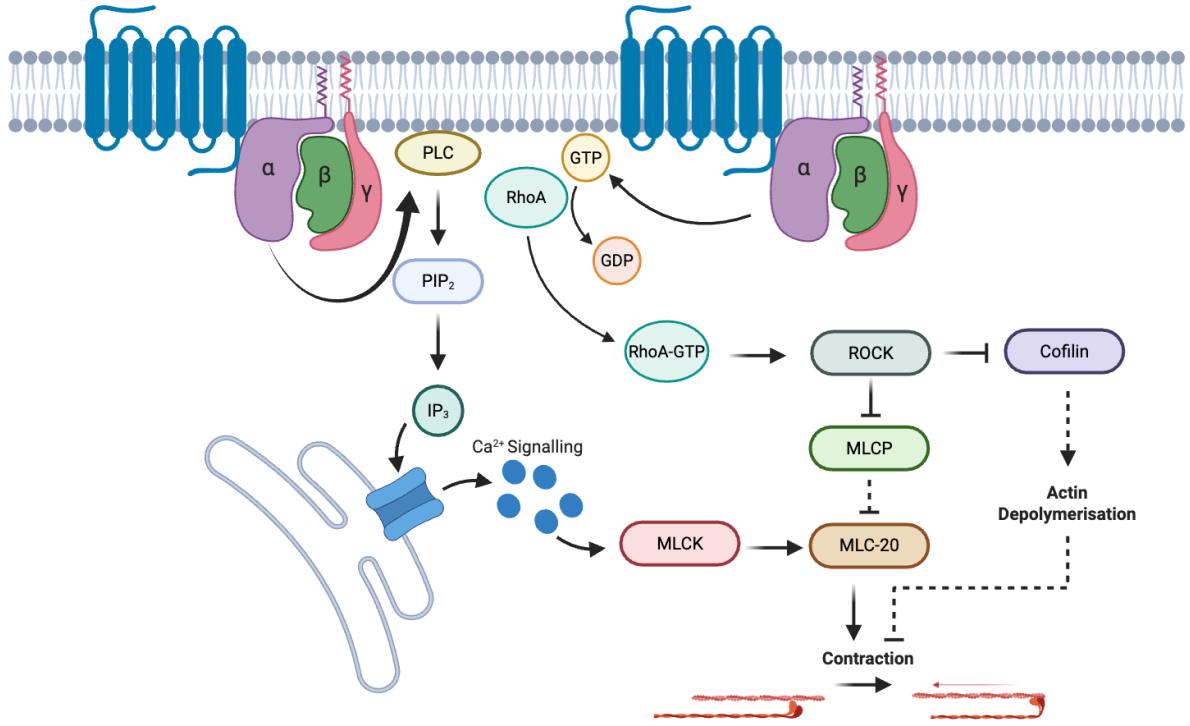

Figure 1.7. Schematic illustration of the calcium-dependent and the calcium-independent mechanisms of VSMC contraction. *The calcium dependent mechanism is activated by GPCR mediated activation of phospholipase C (PLC). Activated PLC hydrolyses phosphatidylinositol 4,5-bisphosphate (PIP_2) to inositol 1,4,5-trisphosphate (IP_3) which induces Ca^{2+} release from the sarcoplasmic reticulum through inositol trisphosphate receptor (IP_3R). Cytosolic Ca^{2+}binds to calmodulin which activates myosin light chain kinase (MLCK). MLCK phosphorylates MLC-20 inducing the cross-bridge cycle. The calcium-independent pathway is also activated by GPCR activation which leads to downstream activation of RhoA through GTP binding. Activated RhoA induces the autophosphorylation of Rho-associated protein kinase (ROCK) and the subsequent inhibition of myosin light chain phosphatase (MLCP), preventing the dephosphorylation of MLC-20, and promoting the cross-bridge cycle. (Figure generated using biorender: https://biorender.com)*

Both pathways promote greater cross-bridge cycling. At the beginning of the cross-bridge cycle, myosin hydrolyses ATP to ADP; this allows myosin to loosely associate with actin

filaments. The subsequent phosphorylation of myosin allows it to enter a pre-power stroke state where myosin and actin are strongly associated. Isomerisation of myosin into its force-generating state results in the sliding of actin microfilaments towards each other. This causes load to be exerted on the dense bodies, plastic structures analogous to the Z-disc in striated muscle, which act as anchoring points for the actin cytoskeleton[111], leading to contraction of the VSMC and transmission of tension into the surrounding substrate. Myosin then returns to its unbound state following exchange of ADP for ATP[110].

1.7 Extracellular Matrix in the Vasculature

As discussed, the composition and organisation of the ECM is a key element of the mature, mechanically appropriate blood vessel. In the aorta, this requires the coordinated expression of structural proteins, such as collagen (types I, III and, IV) and elastin, glycoproteins such as fibronectin and laminin, and proteoglycans such as versican and decorin. Combined, these macromolecules provide structural integrity, regulate cell behaviour, and enable adaption to mechanical stress.

Within the tunica intima, the ECM is predominantly comprised of the basement membrane, a specialised network of laminin, collagen IV, fibronectin, perlecan, and heparan-sulphate proteoglycans, which anchor the vascular endothelial cells[112]. The basement membrane plays a vital role in the cell signalling events that mediate endothelial cell migration, proliferation and, invasion[113]. The intimal basement membrane is separated from the tunica media by the internal elastic lamina (IEL). The IEL is a highly fenestrated sheet of elastic fibres that facilitates the diffusion of signalling molecules from the intima into the medial layer. Work has shown that endothelial cells are primarily responsible for the synthesis and secretion of elastin in the IEL and that knockdown of elastin in SMCs does not significantly affect IEL morphology[114].

The tunica media is rich in ECM proteins, including collagen I/III, elastin, proteoglycans, glycoproteins, and glycosaminoglycans, oriented in concentric elastic lamellae to support the circumferentially oriented VSMCs[115]. The structural proteins collagen and

elastin are the most abundantly expressed in the medial ECM, making up ~50% of the dry weight of large arteries. The elastin protein is initially synthesised by VSMCs and fibroblasts as tropoelastin monomers. During the formation of elastic fibres, tropoelastin monomers associate with fibrillin microfibers in the ECM. Fibrillin is a glycoprotein that is synthesised by fibroblasts, and which polymerises to form a scaffold for tropoelastin[116]. The tropoelastin monomers are then cross-linked by lysyl oxidase enzymes to form cross-linked elastin polymers. These highly cross-linked polymers form elastic fibres, which confer arteries with their compliance and recoil properties. Mature elastin contains approximately 15-20 cross-links per unit, which is essential to both the elastic properties of the protein and its substantial longevity. Work has shown that <1% of total body elastin is turned over within a year, with most elastin synthesis taking place mid-gestation and through the post-natal period, and only limited production occurring in adulthood[117].

Collagen is the main structural component of the vascular ECM and is responsible for imparting strength to the vessel wall. Collagen fibrils consist of a triple helix of three polypeptide chains. Each chain consists of a series of Gly-X-Y repeats where X is usually a proline residue, and Y is a 4-hydroxyproline residue[118]. This amino acid structure allows for tight packing of the chains into the triple helix structure, with the X and Y sidechains on the exterior of the procollagen molecule. Once secreted, the sidechains are enzymatically cleaved, allowing for the formation of large collagen fibrils[118]. In the tunica media, collagens associate with a range of glycoproteins such as fibrilin-1 and proteoglycans such as collagen-associated dermatan-sulfate proteoglycans and cell-associated heparin-sulfate proteoglycans which contribute to vessel elasticity[7]. Together, these structural interactions enable collagen to provide both mechanical strength and elastic support to be aortic wall. This finely tuned ECM architecture is vital to maintaining blood vessel homeostasis, and its remodelling underlies many forms of vascular pathology.

1.8 Extracellular Matrix Remodelling: The Primary Driver of Arterial Stiffening

Arterial stiffening is a multifactorial process that results in the loss of arterial compliance. A hallmark of vascular ageing and cardiovascular disease, arterial stiffening is associated with hypertension and increased shear stress and is a major risk factor for a range of cardiovascular events including aortic aneurism and stroke. The loss of arterial compliance also has systemic implications, with increased strain on the heart leading to heart failure and organ damage.

The best-characterised aspect of arterial stiffening is the remodelling of the medial ECM via enzymatic degradation of elastin and increased deposition and posttranslational modification of collagen. As discussed, elastin has a very low turnover rate in the mature artery; this allows for the accumulation of age-related changes such as MMP-mediated degradation, fragmentation, and calcification[119]. Work has shown that pulsatile wall stress causes fragmentation of elastin fibres over the life course[120], alongside the accumulation of Ca^{2+} on uncharged glycine residues[121]. As elastin fibres decay, they lose their elasticity, and mechanical load bearing is shifted to the stiffer collagen fibres. Enzyme-mediated degradation of elastin is driven primarily by the elastases MT1-MMP and MMP-2/7/9/12, as well as serine and cysteine proteases. Protease activity in the vasculature is regulated by the presence of inhibitors such as TIMPs; however, during ageing the balance between protease activity and their inhibitors becomes dysregulated, leading to increased elastolysis[122]. Combined, these factors result in increasingly disorganised, fragmented, and stiffer elastic fibres in the aged vasculature and result in reduced arterial compliance. The concurrent increase in collagen deposition further contributes to vascular stiffening. Increased collagen concentrations are observed in all three layers of the vessel wall during vascular ageing. This results in reduced compliance as the vessel wall gains tensile strength and loses the ability to deform under pressure. In addition to increased collagen concentrations, increased collaged glycation has been shown to increase arterial stiffening with age[119]. This non-enzymatic process involves the covalent binding of reducing sugars, such as glucose, to lysine residues on collagen[123]. As advanced glycation end products accumulate, they form crosslinks, further

contributing to vessel stiffening[124]. These structural changes in elastin and collagen not only stiffen the arterial wall but also create a microenvironment where the behaviour of vascular cells, such as VSMCs, is modulated, leading to the progression of disease and further stiffening.

Enhanced blood vessel rigidity and ECM remodelling directly alters the behaviour of medial VSMCs through the mechanosensitive machinery described above. As previously discussed, VSMC primarily sense changes in ECM stiffness via integrin-based adhesions, which attach the actin cytoskeleton to ECM components such as collagen and fibronectin. Work has shown that differential organisation of focal adhesions is a key mechanism by which mechanical signals are transmitted into VSMCs[125]. As focal adhesion organisation is partially determined by ECM composition[126], this signalling axis is vital in the VSMC response to matrix remodelling. These mechanically transduced signals regulate many processes within VSMC, including calcium signalling, cytoskeletal organisation, contraction, phenotypic state, and migration, thus linking ECM remodelling and stiffening in the vessel wall to functional changes in VSMCs[127].

1.9 Smooth Muscle Cell Stiffness Syndrome: A New Perspective in Vascular Stiffening

The role of ECM remodelling during arterial stiffening is well-established. However, a growing body of evidence now suggests that alterations in VSMC biomechanics are crucial contributors to the pathophysiological mechanisms underlying age- and disease-related arterial stiffening. This phenomenon has been tentatively described as *Smooth Muscle Cell Stiffness Syndrome (SMCSS)*[128]. The established dogma states that there are two primary mechanisms by which intrinsic VSMC stiffening contributes to arterial stiffening. The first, as outlined previously, is the transdifferentiation of contractile VSMCs to stiffer osteoblast-like and macrophage-like cells. The second is the extent of active tone generated by actomyosin-derived contractile forces within VSMCs.

1.9.1 The Actin Cytoskeleton in Arterial Stiffening

The actin cytoskeleton is a highly dynamic network that plays vital roles in actomyosin force generation via its interaction with myosin, cell adhesion, and cell signalling complexes[129]. Comprised of globular G-actin monomers which assemble to form F-actin microfilaments, the actin cytoskeleton exists in a state of flux and can rapidly assemble and disassemble in response to cell requirements. The extent to which actomyosin-generated forces contribute to vessel stiffening remains unknown. However, work in animal models has demonstrated that aortic VSMCs extracted from old monkeys have significantly higher elastic moduli - the unit of measurement applied to a material's resistance to being permanently deformed under stress - compared to younger monkeys when assessed using atomic force microscopy. The authors demonstrated that this increased stiffness is correlated with increased expression of genes associated with contractility, such as α-smooth muscle actin, and adhesion genes, such as integrin β1[130]. Similar findings have been observed in mouse models where ageing and hypertension were shown to have an additive effect on VSMC stiffness. In this study, VSMCs extracted from young hypertensive mice demonstrate a 2-fold increase in relative stiffness when compared to non-hypertensive controls. However, this effect was even greater in aged hypertensive mice, where VSMC stiffness underwent a 4-fold increase compared to young normotensive controls[131]. Work *in vitro* has shown that the actin cytoskeleton is remodelled in VSMCs exposed to cyclic stretch and that these cells are stiffer when assessed using AFM[132]. Similar findings have shown that cyclic stretching results in increased protein-protein interactions between focal adhesion-associated proteins vinculin and paxillin[133]. Taken together, these results suggest that the intrinsic contraction of VSMCs, driven by actomyosin activity and remodelling of the actin cytoskeleton, plays an important role in arterial stiffening.

1.9.2 The Microtubule Cytoskeleton in Arterial Stiffening

The microtubules are a key component of the cytoskeleton and play roles in a range of cellular processes, including intracellular transport, cell cycle, migration, maintenance of cell morphology, and cell contractility[134]. They are assembled from α/β-tubulin heterodimers, which polymerize, in a GTP dependent reaction, to form proto-filaments.

Approximately 13 proto-filaments combine to form the hollow microtubule structure. When β-tubulin is in its GTP-bound state, it possesses very high binding affinity for adjacent tubulin molecules. Shortly after polymerization, GTP is hydrolysed to GDP, which significantly reduces tubulin binding affinity and promotes depolymerization of the proto-filament[135]. This phenomenon is referred to as dynamic instability, whereby microtubules are always in a state of growth or shrinkage[134]. The ability to near-instantly polymerize and depolymerize allows the microtubule network to constantly remodel in response to intracellular and extracellular cues.

Microtubules are vital in resisting the contractile forces generated by actomyosin activity. This phenomenon is described by the tensegrity model of cell dynamics where microtubules act as compression-bearing struts to exert a protective force[136]. This protective force helps to oppose contraction, maintain cell shape, and protect organelle integrity[137]. Early research demonstrated that pharmacological inhibition of microtubule polymerization with vinblastine significantly increased Ca^{2+} dependant contraction of vascular smooth muscle *in vivo*[138]. Additionally, work conducted using isolated rat aortas demonstrated that treatment with microtubule destabilisers colcemid and vinblastine induced greater smooth muscle contractility in a Rho-kinase dependant fashion[139]. Previous work by the Warren lab has shown that pre-treatment with colchicine, a microtubule destabiliser, induces VSMCs to generate greater traction stress when treated with Angiotensin II *in vitro*. Importantly, total traction stress could be reduced by treating with paclitaxel, a microtubule stabiliser[140]. These studies suggest that microtubule stability is a key regulator of VSMC contractility.

Microtubule stability is regulated primarily through post-translation modifications. One such modification is α-tubulin acetylation, which is associated with enhanced proto-filament stabilisation[141]. Microtubule acetylation involves the transfer of an acetyl-moiety from the acetyl-coenzyme A to lysine 40 of the α-tubulin side chain. This process is mediated by the activity of acetyltransferase and deacetylase enzymes. One of the first mammalian acetyltransferases to be identified was ATAT1[142]. Studies in mouse have shown that knockout of the ATAT1 gene leads to an almost complete loss of embryonic tubulin acetylation[143]. The histone deacetylases (HDACs) are a large family of enzymes

involved in deacetylation of a range of nuclear and cytosolic proteins. HDAC6, in particular, has been identified as a cytosolic HDAC that deacetylases α-tubulin and causes microtubule destabilisation[144]. Previous work by the Warren lab has highlighted the role of HDAC6 activity in the regulation of VSMC contractility. Work in human fibroblasts has demonstrated that cells expressing acetyl-mimetic α-tubulin mutants have reduced cellular contractility compared to acetyl-null tubulin mutant cells. The authors confirmed this finding by treating cells with inhibitors of the actomyosin machinery, such as blebbistatin. They found that treated cells had increased microtubule acetylation. Importantly, they also observed that treatment with contractile promoters resulted in reduced microtubule acetylation[145]. The role of microtubule acetylation in CVDs is yet to be fully elucidated. However, it is clear that enzymes involved in regulating the acetylation of microtubules play vital roles in the control of dynamic instability. These enzymes, therefore, represent exciting novel targets for the treatment of CVD and CVD-related pathophysiologies such as arterial stiffening.

The microtubule cytoskeleton is also involved in regulating, and is regulated by, a range of intracellular signalling mechanisms. For example, early work found that increased intracellular Ca^{2+} induces microtubule depolymerisation[146]. Subsequent work demonstrated that this activity is driven by calmodulin and its downstream signalling pathways[147]. Conversely, porcine coronary VSMCs have been shown to have increased intracellular Ca^{2+} levels in response to treatment with the microtubule destabilising agent nocodazole[148]. These findings suggest that microtubule integration with signalling networks, such as the Ca^{2+} signalling pathway, is bidirectional and interdependent. Furthering our understanding of how microtubules contribute to vascular stiffening through their opposing interactions with actomyosin and interaction with intracellular signalling pathways will be key in understanding and treating SMCSS.

1.9.3 Aquaporins & VSMC Hypertrophy in Arterial Stiffening

VSMCs regulate their cell volume to maintain their physiological function and cardiovascular homeostasis. This process occurs in the context of fluctuating mechanical and osmotic stresses within the blood vessel wall. The two primary

mechanisms by which VSMC volume is modulated are regulatory volume decrease (RVD) and regulatory volume increase (RVI). RVD involves the release of osmolytes such as K^+ and Cl^- ions from the cell into the extracellular environment. This is mediated by the activation of voltage-gated and Ca^{2+}-activated channels as well as volume-regulated anion channels (VRACs)[149]. Water then follows the osmolyte gradient out of the cell, reducing cell volume. On the other hand, RVI is mediated by the activity of co-transporters such as the Na+/K+/2Cl- cotransporter (NKCC) and the Na+/Cl- symporter which increase the level of intracellular osmolytes, driving water down the osmotic gradient into the cell[150]. Both processes rely on aquaporins to facilitate transport of water across the cell membrane.

Aquaporins are ubiquitous transmembrane channels that facilitate osmotic water transport across membranes[151]. The ubiquitous nature of aquaporin expression highlights the diverse requirements for osmoregulation across all tissues and organ systems[152]. Aquaporins have been shown to play roles in the regulation of cell volume in a range of tissues in both health and disease. For example, aquaporin dysregulation in diseases such as cancer has been shown to contribute to aberrant regulation of cell volume[153]. Work has also shown that osmotic pressure plays a role in controlling cancer cell migration via an actomyosin independent mechanism[154]. In the vasculature, endothelial stiffening during inflammation has been associated with swelling of cells in a mechanism driven by aldosterone signalling and Na^+ influx[155]. The Warren lab has shown that VSMCs grown on stiff hydrogels have greater volume compared to cells grown on pliable hydrogels. One possible explanation for this phenomenon is the increased activity or expression of aquaporin channels in response to enhanced matrix stiffness. This would facilitate osmotic flow of water into the cells resulting in greater internal hydrostatic pressure and increased volume.

Aquaporins 1 and 4 are both widely expressed in cells of the cardiovascular system including VSMCs. Interestingly aquaporin 4 is also highly expressed in skeletal muscle, suggesting a possible role in contraction[156]. Investigating the role of aquaporins in this system, as well as the activity of ion channels such as NKCC, will help elucidate the wider role of VSMC volume regulation in vascular stiffening.

1.9.4 DNA Damage in Arterial Stiffening

DNA damage occurs in many forms including single strand breaks, base oxidation and telomere shortening. In the vasculature, DNA damage and has been identified as a key causative factor in vessel ageing. As DNA damage accumulates cells become increasingly senescent, undergo metabolic and signalling changes, and experience aberrant transcription[157]. Interestingly, VSMC senescence is associated with increased expression and secretion of pro-inflammatory factors[158]. Indeed, failure to repair VSMC DNA damage is associated with atherosclerotic lesion formation[159]. VSMCs from atherosclerotic plaques have considerably increased activation of DNA repair pathways alongside increased DNA damage[160]. Furthermore, work *in vivo* has shown that VSMC specific knockout of the DNA repair endonuclease ERCC1 results in progressive ageing of the vasculature[157]. These findings suggest that DNA damage plays an important role in vascular ageing and the occurrence of CVDs.

As VSMC contractility has been shown to increases on stiffer matrices[161], it is possible that enhanced ECM stiffness induces DNA damage through increased actomyosin activity. However, further work is needed to fully understand the causes and implications of age- and disease-induced DNA damage accumulation in VSMCs.

1.9.5 SMCSS: A New Target for Pharmacological Treatment of CVD?

The concept of cell stiffness syndrome was initially posited to describe stiffening of endothelial cells in response to vascular inflammation and aberrant mineralocorticoid signalling[162]. More recently this disease axis has been expanded to the VSMC to define the contributions of intrinsic VSMC stiffening to wholesale stiffening of the vasculature[128]. This new paradigm provides a range of novel investigative possibilities. Deepening our understanding of cytoskeletal and cell-adhesion dynamics will drastically enhance our overall understanding of how cell contraction contributes to VSMC stiffening. Of particular interest is the complex interplay between microtubule dynamics and intracellular signalling pathways such as Ca^{2+} flux. Additionally, elucidating the link between these axes and the regulation of VSMC volume and DNA damage in cell stiffness

will facilitate a more comprehensive understanding of SMCSS and contribute to our understanding of vascular stiffening.

SMCSS is an important concept as it raises the possibility of uncovering novel targets for pharmacological treatment of CVDs. Microtubules, with their central role in VSMC stiffening, represent a particularly exciting target for pharmacological intervention. As essential components of the cell division machinery, microtubules have already been extensively studied as targets for anti-cancer therapies. Several chemotherapy drugs which target microtubule dynamics have been approved for use in the clinic. One such drug is paclitaxel, a microtubule stabiliser which binds tubulin and prevents microtubule depolymerisation[163]. More recently, paclitaxel has been investigated for use in CVDs. Studies have demonstrated that paclitaxel is protective against ischemia-, stretch- and cholinergic-induced atrial fibrillation[164]. Other microtubule targeting drugs include Colchicine, a microtubule destabiliser used in the treatment of gout and to reduce the risk of myocardial infarction[164]. Additional strategies for targeting microtubules in VSMC stiffening involve targeting post-translational modifications such as acetylation and tyrosination[164]. For example, HDAC inhibitors have been examined *in vitro* and *in vivo* as anti-neoplastic drugs[165]. These studies have concentrated on the canonical HDAC regulation of histone deacetylation. Further work is required to understand the interaction between HDAC activity and microtubule dynamics in the context of VSMC stiffening.

In summation, deepening our understanding of SMCSS will enable us to identify the key molecular mechanisms that drive cell stiffening. By elucidating how cytoskeletal and adhesome remodelling intersects with signalling pathways, DNA damage and volume regulation to promote VSMC stiffening, we will be better equipped to develop pharmacological treatments that address the cell component of vascular stiffening.

1.10 VSMCs in the Lab

1.10.1 Current Limitations

There are several limitations to current assays used for growing and studying VSMCs *in vitro*. Firstly, as discussed, VSMCs are highly mechanosensitive cells, therefore, plating them on plastic, which is roughly 1000 times stiffer than the healthy aorta, is likely to substantially alter VSMC behaviour. Previous work has demonstrated that VSMCs maintained on plastic or glass substrates undergo transition to the synthetic phenotype[166]. This supports *in vivo* findings in terms of VSMC response to ECM remodelling. Additionally, growing VSMCs on rigid substrates precludes any representative investigation into the role of substrate stiffness on VSMC stiffness and contractility. Therefore, any study aiming to investigate mechanosensitive pathways in VSMCs must utilise a system where extracellular substrate stiffness can by modulated to physiological, or even pathophysiological stiffnesses.

1.10.2 The Polyacrylamide Hydrogel System

This project utilises polyacrylamide hydrogels to study VSMCs (Figure 1.8). This system is useful as it allows substrate stiffness to be tuned to represent physiological conditions and therefore more accurately represent the extracellular environment of the VSMC *in vitro*. Additionally, hydrogels can be fabricated which replicate the stiffer extracellular environment observed in aged and diseased blood vessels. This system is therefore unique in enabling easy comparison between cells grown on healthy and aged/diseased substrates. Use of the polyacrylamide system confers two distinct advantages. Firstly, it is relatively cheap and requires little in terms of specialist equipment or training. Secondly, it allows for the use of common laboratory techniques such as drug screening, cell staining and confocal microscopy.

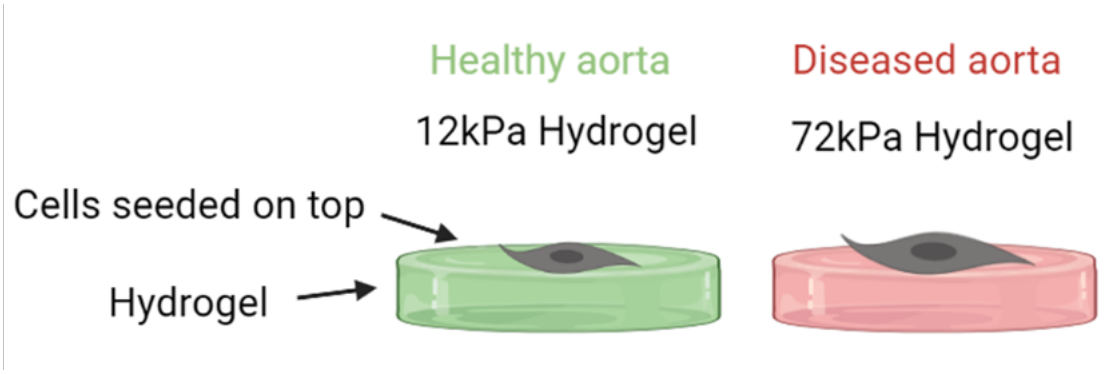

Figure 1.8. The polyacrylamide hydrogel system. *This study uses a polyacrylamide hydrogel system. Cells are seeded onto hydrogels that represent extracellular matrix of either healthy (12 kPa - represented here as a green hydrogel) or aged/diseased (72 kPa - represented here as a red hydrogel) stiffness. (Figure generated using biorender: https://biorender.com)*

The use of this system also allows for the use of other common molecular biology techniques. For example, in this study I utilise pharmacological inhibitors of known mechanosensory pathways, to unpick the signalling pathways involved in VSMC response to matrix rigidity. This is easy to do using this system as cells are cultured on hydrogels as normal without any additional steps that would otherwise complicate this process. The use of hydrogels also allows for relatively easy assessment of cell parameters through confocal and live cell timelapse microscopy, both of which I utilise extensively in my investigation.

1.10.3 Overview of Pharmacological Agents Used

The primary methodology used in this project is the targeted inhibition and activation of intracellular signalling pathways using pharmacological agents. These agents were chosen due to their ability to perturb key signalling pathways involved in the VSMC response to matrix rigidity.

Table 1.1. List of pharmacological compounds used in this study. *Shows their molecular target, and the assay they're used in.*

Compound	**Target**	**Assay**
TCAQP1	Aquaporin 1	Cell area/TFM
TGN020	Aquaporin 4	Cell area
Furosemide	NKCC	Cell area
STOCK2S 26	Wnk	Cell area
Go6983	PKC	Cell area
Xestospongin C	IP_3R	Cell area
Dantrolene	RyR	Cell area
Epothilone B	Microtubules (Stabilises)	Cell area
Nocodazole	Microtubules (Destabilises)	Cell area
A1070722	GSK3	Cell area/TFM
AZD7762	Chk2	Cell area
Ku5933	ATM	Cell area
EB47	PARP-1	Cell area
Colchicine	Microtubules (Destabilises)	Ca^{2+} flux
Paclitaxel	Microtubules (Stabilises)	Ca^{2+} flux
MS275	HDAC1	Ca^{2+} flux/TFM
Santacruzamate A	HDAC2	Ca^{2+} flux
RGFP966	HDAC3	Ca^{2+} flux
Tubastatin	HDAC6	Ca^{2+} flux
GsMTx-4	SACs (piezo, TRP families)	Ca^{2+} flux
Yoda1	Piezo1 (Activates)	Ca^{2+} flux /TFM
Jedi1	Piezo1 (Activates)	TFM
Vas 2870	NAPDH-oxidase	TFM

These pharmacological agents can be broadly categorised into groups, such as water transport regulators, cytoskeletal organisers, calcium signalling, and ion transport, depending on their target.

1.10.3.1 Ion and Water Transport Regulators

Water and ion transport regulators were used to unpick the effects of matrix rigidity on VSMC volume response. Volume response is a key element of cell homeostasis and has been shown to be dysregulated by enhanced matrix rigidity in unpublished work by the Warren lab.

The water transport regulating compounds used in this study include TCAQP1 and TGN020 which blockade the AQP1 and AQP4 channels respectively. The inhibitory

mechanism of these compounds not fully understood. However, it is believed that direct blockade of the water channel is a key mechanism. Furthermore, it has been suggested that TGN020 may induce ubiquitin-proteasome mediated alterations to AQP4 trafficking and degradation, thus reducing the prevalence of AQP4 at the cell membrane[167].

The NKCC inhibitor, Furosemide was used due to NKCCs role in driving increased osmolarity through chloride ion flux. Furosemide is known to inhibit the activity of NKCC by binding to and occluding the Cl^- binding site[168].

1.10.3.2 Cytoskeletal Modulators

Cytoskeletal modulators were used due to the role the cytoskeleton plays in both sensing matrix rigidity and in the mechanical response to changes in matrix stiffness. In this study, cytoskeletal modulators were used to assess how changes in microtubule stability altered the cell area and intracellular signalling response to altered matrix rigidity.

The key cytoskeletal stabilisers used in this study include epothilone B and paclitaxel which promote microtubule polymerisation through binding to the taxane site on β-tubulin. Binding of these compounds causes a conformational change in the M-loop of β-tubulin which promotes proto-filament formation and inhibits depolymerisation[169].

The microtubule destabilising compounds nocodazole and colchicine were also used. Colchicine promotes destabilisation of microtubules by binding to the colchicine binding site of β-tubulin, inducing a conformational change that prevents inclusion of the tubulin heterodimer into microtubule filaments[170]. Similarly, nocodazole promotes destabilisation of microtubules by binding to β-tubulin and preventing formation of microtubule protofilaments. Nocodazole has additionally been shown to increase activity of tubulin GTPase, increasing the rate of microtubule depolymerisation[171].

1.10.3.3 Calcium Signalling Modulators

Several pharmacological modulators of calcium signalling were used. Ca^{2+} signalling was investigated due its involvement in regulating diverse processes associated with volume control, matrix rigidity response and microtubule dynamics.

The intracellular Ca^{2+} store release channels, IP_3R and the ryanodine receptor, were inhibited by treatment with xestospongin C and dantrolene respectively. Xestospongin C is believed to bind to IP_3R, however, the exact mechanisms by which it inhibits IP3 induced Ca^{2+} release is not known. The ryanodine receptor inhibitor dantrolene selectively binds to the RyR1/3 isoforms and inhibits Ca^{2+} release. Dantrolene's inhibitory action is believed to involve the activity of the calcium binding protein calmodulin and favourable Mg^{2+} and ATP conditions, however the exact mechanism in which Ca^{2+} release is prevented has yet to be fully elucidated[172].

Targeted modulation of mechanosensitive cell-surface channels was also conducted using pharmacological compounds. The piezo1 ion channel was activated using the small molecule activators jedi1 and yoda1. Yoda1 acts as a molecular wedge, causing a decoupling of the piezo arm domain from the rest of the channel and promoting activation in response to sub-threshold stimuli[173]. Jedi1 is an allosteric activator of piezo1. It binds to extracellular blade-like domains, causing them to become sensitised to mechanical stimuli and lowering the threshold for channel activation[174]. Finally, the non-specific cation channel inhibitor GSMTx4 was used to inhibit piezo1 activity. GSMTx4 is a compound extracted from the Chilean rose tarantula, it inhibits piezo1 by inducing a decoupling of the lipid bilayer and the piezo1 channel. This decoupling is believed to be driven by GSMTx4 binding to the bilayer and the subsequent alteration of the membrane's mechanical properties[175].

1.10.3.4 Kinase Signalling Modulators

Key intracellular kinases were also targeted for pharmacological inhibition. These kinases were targeted due to their broad roles in downstream signalling from Ca^{2+} machinery and their integration into cytoskeletal processes and mechanotransduction.

PKC was inhibited using Go6983, a small-molecule broad-spectrum PKC inhibitor that competes with ATP for PKC binding, blocking its activation and inhibiting its kinase activity[176]. The cell-cycle and DNA damage repair kinases Chk2 and ATM were inhibited using AZD7762 and Ku55933 which have similar ATP-competitive mechanisms[177]. Wnk was inhibited using STOCK2S 26 which works by inhibiting the binding of Wnk to downstream signalling kinases SPAK and OSR1 and preventing the activation of downstream effectors NKCC1 and NCC[178]. GSK3 was inhibited with the small molecule inhibitor A1070722. The exact mechanism of A1070722 inhibition has not been conclusively established, however, it is known to bind to the catalytic domain of GSK3 and is believed to prevent ATP binding[179].

1.10.3.5 HDAC Modulators

HDACs were targeted due to their diverse cellular roles, including, proliferation, cell-motility, and differentiation. Additionally, recent work has highlighted their involvement in cytoskeletal regulation and signalling.

HDAC1 was inhibited with MS275, a benzamide derivative which binds to the catalytic site of HDAC1 and prevents it binding to and removing histone proteins[180]. HDAC2 was inhibited with Santacruzamate A. Santacruzamate A has been shown to be structurally similar to other benzamide-type inhibitors and as such is assumed to have a similar mechanism of action, namely, physical blockade through catalytic pocket binding, although this is yet to be conclusively shown[181]. Other benzamide-type inhibitors include RGFP966 which was used to inhibit HDAC3 by chelating zinc ions in the active site[182]. Additional zinc-sequestering compounds include Tubastatin, used here to inhibit HDAC 6[183].

1.10.3.6 Metabolic Signalling Modulators

The metabolic and redox signalling modulators used in this study include EB47 and VAS2870. EB47 was used to selectively inhibit PARP-1, an important enzyme involved in NAD^+ signalling in the cell stress-response and has been lined to Ca^{2+} signalling and transcriptional regulation. EB47 works by mimicking the NAD^+ substrate and blocking the

PARP catalytic domain[184]. Similarly, VAS2870 was used to inhibit NAPDH-oxidase, a major source of ROS in VSMCs. ROS are involved in several processes including contractility, Ca^{2+} signalling, and cytoskeletal organisation. The molecular mechanism of VAS2870 involves covalent alkylation of a cysteine residues in the NOX active site and the subsequent inhibition of ROS generation from NAPDH[185].

1.11 Aims of the Project & Hypotheses

The primary aim of this project is to better understand VSMCSS by examining the VSMC response to enhanced matrix rigidity. This will be achieved through use of the previously described polyacrylamide hydrogel system, in conjunction with targeted inhibition of key VSMC mechanotransduction and signalling pathways. The impacts of this pharmacological intervention will be assessed using confocal microscopy to investigate changes in cell morphology, and live-cell timelapse fluorescence microscopy to investigate Ca^{2+} flux and traction force generation. This will enable me to identify the key signalling and mechanistic pathways involved in the VSMC response to enhanced matrix rigidity. This study will provide targets for future work developing pharmacological interventions for VSMC stiffening in vascular ageing and disease.

I propose that matrix rigidity regulates VSMC signalling pathways involved in:

1. VSMC morphology – specifically VSMC area and volume.

2. Regulation of calcium handling and calcium signalling.

3. Downstream effects of these matrix rigidity responses – specifically traction stress generation.

I therefore hypothesise that:

1. Inhibition of mechanosensitive signalling pathways with pharmacological inhibitors will facilitate rescue of normal VSMC morphology on rigid hydrogels.

2. Matrix rigidity alone will modulate Ca^{2+} ion flux, and that targeted pharmacological intervention of calcium handling pathways will facilitate rescue of normal Ca^{2+} flux on rigid hydrogels.

3. Matrix rigidity will increase VSMC traction stress generation, and that targeted inhibition of signalling pathways identified in the previous two steps will rescue normal traction force generation on rigid hydrogels.

Chapter 2: Materials and Methods

2.1 Lab Consumables

Consumable	Source	Product No./Identifier
(3-Aminopropyl)triethoxysilane (APES)	Sigma	A3678
30mm Coverslip	VWR	631-0174
6-well plate	Thermo Scientific	130184
100% Acrylamide	Sigma	A7802
Bis-acrylamide	BioRad	1610142
Bovine Serum Albumin (BSA)	Sigma	A2153
Collagen-1	Thermo Scientific	A1048301
CSOW 620 – static confiner	4D Cell	N/A
Dimethyl sulfoxide (DMSO)	Sigma	D8418
Earle's Balanced Salt Solution	Sigma	E6267
FluoSpheres™ Carboxylate-Modified Microspheres (Red)	Thermo Scientific	F8812
Glutaraldehyde	Sigma	G6257
Mounting Media	Vector Labs	H-1400-10
Mounting Media (with DAPI)	Vector Labs	H-1500-10
NP40	Thermo Scientific	85124
Parafilm	Sigma	P7793
Paraformaldehyde (PFA)	Sigma	P6148
Phosphate Buffered Saline (PBS)	Sigma	R014G
Sulfo-SANPAH	Abcam	Ab145610
Tetramethyl-ethylenediamine (TEMED)	Thermo Scientific	17919
T75 Flasks	Fisher Scientific	11884235
Triton X-100	Sigma	X100
Trypsin-EDTA	Sigma	T3924

2.2 Antibodies & Dyes

Antibody/Dye	Source	Product No./Identifier
Alexa Fluor® 488 (anti-mouse)	Thermo Scientific	A32723
Fluo-4	Thermo Scientific	F14201
Lamin A/C	Sigma	MABT1341
Rhodamine Phalloidin	Thermo Scientific	R415

2.3 Compounds & Drugs

Compound	Source	Product No./Identifier
Angiotensin II	Thermo Scientific	A9525
A1070722	Tocris	4431
AZD7762	MedChem	HY-10992
Colchicine	Sigma	C9754
Dantrolene	Tocris	0507
EB47	Tocris	4140
Epothilone B	Sigma	E2656
Furosemide	Tocris	3109
Go6983	Tocris	2285
GSMTX4	Abcam	ab141871
Ku 55933	Tocris	3544
MS275	Tocris	6208
Nocodazole	Tocris	1228
Paclitaxel	Sigma	T7402
Remodelin	Sigma	5.31066
RGFP 966	Tocris	6728
Santacruzamate A	Tocris	7191
STOCK2S 26	Tocris	5570
TC AQP1	Tocris	5412
TGN 020	Tocris	5425
Tubastatin A	Sigma	382187
Vas 2870	Tocris	6654
Xestospongin C	Tocris	1280
Yoda1	Tocris	5586

2.4 Coverslip Activation

Coverslips (30 mm) were treated with approximately 200 µL (3-Aminopropyl)-triethoxysilane (APES) (Sigma A3648) on a sheet of parafilm for 3 min at RT before washing with dH2O. They were then immersed in 2 mL of 0.5% glutaraldehyde (Sigma G6257) in dH_2O solution and incubated at RT for 40 min. Coverslips were subsequently washed with dH2O x3 and left to dry overnight.

2.5 Polyacrylamide Hydrogel Fabrication

Polyacrylamide solutions were prepared to the required stiffness and aliquoted. 12 kPa buffer was prepared in dH20 to give the following final percentages: 7.5% Acrylamide, 0.15% bis-acrylamide. 72 kPa buffer was prepared to give the following final percentages: 10% Acrylamide, 0.5% bis-acrylamide.

Polymerisation of the acrylamide/bis-acrylamide solution was initiated via the addition of 10% Ammonium persulphate (APS) (Sigma A3678) and N,N,N,N' tetramethyl-ethylenediamine (TEMED) (Thermo Scientific #17919) in ratios of 1:100 and 1:1000 respectively. Next, once thoroughly mixed, 50 µL of solution was placed onto glass slides with coverslips lowered on top, activated side down, and incubated for 2-4 min at RT. Once suitably polymerised, coverslips were removed and placed into 6 well plates, washed with dH2O x3 and stored at 4 °C in dH2O for a maximum of 2 weeks.

For traction force assays, red fluorescent beads (Thermo Scientific F8812) 1:1000 were added to the hydrogel solution prior to polymerisation.

2.6 Cell Culture

Adult aortic VSMCs (Sigma 354-05A) were used for all experiments. As described in the supplier's documentation, these cells were pooled from 3 patients aged between 25 and 60 years old, with no underlying health conditions. Cells were cultured in growth media (Sigma 311-500) with VSMC supplement (Sigma 311-GS) at 37 °C and 5% CO_2. Cells were passaged upon reaching a confluency of approximately 80%. Cells were used in experiments between passage 4-11 to minimise phenotypic drift. Cells were not used

after P11 and were disposed of. Prior to seeding, cells were visually assessed for morphological indications that they had undergone a phenotypic transition (eg. epithiloid morphology as opposed to spindle shaped). Cells that were obviously atypical were also not used in experiments. Where possible, experimental comparisons were made with cells with matched or similar passage numbers to reduce variability. During cell splitting media was removed and cells were washed with Earl's Balanced Salt Solution (Sigma E6267), trypsinised (Sigma T3924) and resuspended in growth media. Cells were split at roughly 1:2 to maintain growth. For storage, cells were initially stored at -80 °C in freezing media before being transferred to liquid nitrogen.

2.6.1 Cell Seeding

Prior to seeding, hydrogels were crosslinked using 2 mL Sulfo-SANPH (Merck) in dH2O at 1:3000 and 5 min exposure to 365 nm UV light in a benchtop UV transilluminator. Hydrogels were then sterilized for 40 min using 365 nm UV light. All subsequent steps were carried out in an aseptic tissue culture hood. The crosslinked and sterilised hydrogels were next washed in PBS and incubated in 2 mL collagen I (0.3 mg/mL) at RT for 10 min. Excess collagen solution was removed with a further PBS wash.

Cells were seeded onto hydrogels approximately 24 hours before use in experiments. During seeding, growth media was removed, and cells were washed with Earle's Balanced Salt Solution. Cells were trypsinised and seeded onto hydrogels in growth media. For immunofluorescence assays cells were seeded from a confluent T75 at a ratio of 1:4 into a 6-well plate. For traction force assay, cells were seeded at a ratio of 1:6 to ensure adequate space between cells.

Cells intended for area and Ca^{2+} imaging experiments had their media removed and replaced with basal media approximately 18h prior to treatment to induce quiescence.

For confinement studies the CSOW 620 static confiner from 4D cell was prepared as per the manufacturer's instructions. PDMS pistons and confinement slides were sterilised

with 70% EtOH before washing with sterile PBS. Cells were seeded into 6-well plates and confined for 24 hours prior to imaging.

2.6.2 Drug Treatments

2.6.2.1 VSMC Area Experiments

Drugs were diluted to desired concentration in basal media. Drug treatments in basal media were applied, and cells were incubated for 30 min at 37 ^{o}C and 5% CO_2. Following this, cells were co-treated with 10 μM angiotensin II and incubated for a further 30 min at 37 ^{o}C and 5% CO_2.

2.6.2.2 Calcium Imaging Experiments

Cells were treated with compounds of interest and angiotensin II at point of imaging. See below.

2.6.2.3 Traction Force Experiments

Drugs were diluted to desired concentrations in growth media. Drug treatments in growth media were applied, and cells were incubated for 24 hours at 37 ^{o}C and 5% CO_2.

2.6.2.4 Confinement Experiments

When performing confinement experiments the PDMS pistons and confinement slides were incubated in drugs diluted in basal media for 1 hour prior to cell drug treatment at RT. Following this, cells were treated with drugs for 30 min while confined before co-treatment with 10 μM Ang II and confined for a further 30 min.

2.7 Immunocytochemistry & Cell Staining Techniques

2.7.1 VSMC Area & Volume Experiments

Prior to imaging, cell media was removed from the wells before washing with PBS. Cells were then fixed for 10 min with 4% PFA (Sigma P6148) at RT. PFA was removed and cells were further washed with PBS. Subsequently, cells were permeabilised with 10% NP40 for 5 min. Following fixing and permeabilisation, cells were incubated overnight with

primary antibody solution anti-lamin A/C (Sigma) 1:400 in 3% BSA. Cells were incubated in an incubation chamber at 4°C to maintain humidity and prevent light ingress. After 24 hours, antibody solution was removed, and coverslips were washed with PBS. Cells were incubated with secondary antibody solution Alexa Fluor® 488 1:200 and rhodamine phalloidin 1:200 in 3% BSA/PBS for 2 hours at RT in a humidity chamber in the dark. Secondary antibody solution was removed, and coverslips were washed x3 with PBS and stored at 4 °C. Prior to imaging, coverslips were mounted on slides with 30µL of mounting media without DAPI.

2.7.2 Calcium Imaging

Cells were transported to the microscopy room prior to drug treatment. Cell media was refreshed, and cells were loaded with 3 µM of Fluo-4 diluted in DMSO for 30 min at 37 ºC and 5% CO_2. For some conditions, cells were pre-treated with compounds of interest at this point (where this is the case, it will be stated in the text). After 30 min, cells were washed with PBS and incubated in basal media prior to imaging.

2.8 Immunofluorescence microscopy

Confocal microscopy was used to assess cell area and volume. Images were captured at 20x magnification. 5 separate images were taken per condition with a total of approx. 25 cells imaged per condition. When volume was being assessed a Z-stack of approx. 20 slices was taken at an interval of 1.4 µm.

Images were analysed using FIJI[186]. Scale was automatically imported from image meta data. Image brightness and contrast was adjusted so that cells could be easily distinguished. The “freehand selection” tool was used to manually draw around cells. Cells were excluded where the boundary between cells was unclear.

To assess cell volume raw stacks were first converted to hyperstacks. Contrast and brightness were not changed. Hyperstacks were thresholded using the brightest image as the template. When thresholding, the Otsu algorithm was applied so that cells were fully coloured in with as little background noise as possible. Following this, cells were

selected using FIJI's freehand selection tool and the inbuilt ROI manager. The following macro was used to assess the volume of each ROI individually:

```
// ImageJ Macro Code
// Measure Volume of Thresholded Pixels in an Image Stack
//
//

macro "Measure Stack" {
   run("Clear Results");   // First, clear the results table

   // loop through each slice in the stack. Start at n=1 (the first slice),
   // keep going while n <= nSlices (nSlices is the total number of slices in the stack)
   // and increment n by one after each loop (n++)
   for (n=1; n<=nSlices; n++) {
     setSlice(n);  // set the stack's current slice to n
     run("Measure");   // Run the "Measure" function in ImageJ
   }

                // Create a variable that we will use to store the area measured in each slice
   totalArea = 0;
   // Loop through each result from 0 (the first result on the table) to nResult (the total number of
results on the table)
   for (n=0; n < nResults; n++)
   {
     totalArea += getResult("Area",n);   // Add the area of the current result to the total
   }
   // Get the calibration information from ImageJ and store into width, height, depth, and unit variables.
   // We will only be using depth and unit
   getVoxelSize(width, height, depth, unit);
   // Calculate the volume by multiplying the sum of area of each slice by the depth
   volume = totalArea*depth;
   // Print the result of the volume calculation to the log
   print(volume);
}
```

2.9 Fluo-4 calcium imaging

Ca^{2+} imaging was performed using a Zeiss Axiovert 200 M. Cells were incubated at 37 ^{o}C/5% CO_2 throughout imaging. Images were captured at 10x magnification every 500 ms for a total of 30 min. After 5 min, cells were stimulated with Ang II (10 μM). For conditions where cells were not pre-treated, compounds of interest were added at this stage. Cells were imaged for a further 20 min. Finally, cells were stimulated with the ionophore A23187 to confirm the assay had worked.

Images were analysed using FIJI. Z-stacks were trimmed to exclude the ionophore control. Following this, the image was split into 2 ROIs roughly corresponding to the left

and right sides of the frame. Background ROIs with no cells within each analysis ROI were also selected. Areas with obvious anomalies, such as cell debris, were excluded. To extract fluorescence intensities for each time-point the "Plot Z-axis profile" tool was used. The background ROI was subtracted from the analysis ROI and ΔF and $\Delta F/F_0$ values were calculated. GraphPad Prism was used to plot graphs and perform statistical analysis.

2.10 Traction Force Microscopy (TFM)

Traction force imaging was performed using a Zeiss Axiovert 200 M. Cells were incubated at 37 ^{o}C/5% CO_2 throughout imaging. Images were captured at 20x magnification every second for a total of 20 min or until image focus had been lost. After 3 min, 25% Triton X-100 in PBS was added to lyse cells.

Images were analysed using FIJI. Pixel width and height were set to 0.325 microns, the appropriate scale for a x20 objective with eyepiece lens of x10. First, Z-stacks were aligned using the 'Linear Stack Alignment with SIFT" tool. Following this, "before lysis" and "post lysis" images were generated. This was achieved using the "Slice Keeper" tool to select slices across the time-period from immediately before lysis up until bead movement had ceased. The 'Slice Remover" tool was then used so that only the first and last slices of this new "Kept Stack" remained. Next, bead displacement between these two time points was measured using the 'Partical Image Velocimetry" (PIV) plugin[187]. Following this, the PIV output file was analysed with the "Fourier Transform Traction Cytometry" (FTTC) plugin[188] to generate a traction stress heatmap. Pixel size was set to 0.325 microns and regularisation factor was set at 0. The appropriate young's modulus was set for each condition. This traction stress heatmap was then used to measure integrated traction force by overlaying the corresponding phase image. ROIs were then drawn around individual cells using the "freehand selection" tool and XY coordinates were saved.

2.11 Statistical Analysis

Data were collected from multiple replicates (N) of experiments. Where necessary, the number of cells analysed (n) is also reported in figure legends. All statistical analysis was carried out using GraphPad Prism 10.5.0. Normality was assessed using the Shapiro-Wilk normality test. Bar charts represent the mean with error bars displaying standard error of the mean (SEM). Concentration response curves are presented as mean ± SEM plotted on a logarithmic scale and generated using non-linear regression. To determine significance between two groups an un-paired students T-test was performed. Where homogeneity of variance needed to be tested a Brown-Forsythe test was used. Where variances were unequal, Welch's correction was applied to T-tests. For assessing significance between multiple groups a one-way ANOVA was used, followed by Tukey's multiple comparisons test. Where necessary, outliers in data sets were identified and removed using the ROUT (Q = 1%) non-linear regression test. Statistical significance is represented by: * = $p<0.05$, ** < 0.01, *** <0.001 and **** < 0.0001. Results that fall below the threshold for statistical significance are represented by "ns".

Chapter 3: Unpicking the signalling pathways that drive matrix stiffness-induced VSMC morphological dysfunction

3.1 Introduction

Stiffening of blood vessels is a major risk factor in the development of cardiovascular disease such as atherosclerosis and is strongly associated with hypertension and the loss of circulatory efficiency[119]. Traditionally, arterial stiffening has been associated with remodelling of the vascular ECM, however, it is now understood to additionally involve VSMCs and their interactions with the stiffened or otherwise structurally aberrant vascular matrix.

Previous work by the Warren lab has demonstrated that matrix rigidity modulates VSMC response to contractile agonist stimulation. Specifically, work using our polyacrylamide hydrogel system has shown that cells seeded on pliable (12 kPa – healthy mimicking) substrates undergo a normal contractile response to angiotensin II stimulation. This was assessed by measuring cell area and volume. However, when cells were cultured on stiff (72 kPa – disease/aged mimicking) substrates and treated with angiotensin II they underwent a dysfunctional hypertrophy-like response, where both cell area and volume were found to be increased in a concentration dependent fashion (Figure 3.1).

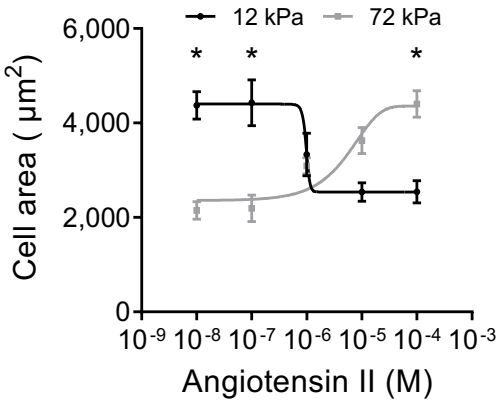

Figure 3.1. Cell area of VSMCs cultured on 12 kPa and 72 kPa hydrogels treated with angiotensin II. *Previous work conducted by the Warren lab demonstrated that when VSMCs are seeded on pliable (12 kPa) hydrogels and treated with the contractile agonist Ang II they undergo a concentration dependent reduction in cell area. However, when VSMCs are seeded on rigid (72 kPa) hydrogels and treated with Ang II they undergo an aberrant, hypertrophy-like response and increase in area. (Work conducted by previous members of the Warren lab and published in the British Journal of Pharmacology[189].)*

The mechanisms underlying this aberrant hypertrophy-like response have yet to be fully elucidated. Here, I utilise the polyacrylamide hydrogel system developed by the Warren lab in conjunction with pharmacological inhibitors and confocal microscopy to

interrogate the signalling pathways involved in this dysfunctional response. To do this, I fabricated hydrogels of both 12 and 72 kPa stiffnesses (which mimic the healthy and diseased/aged aorta), seeded them with VSMCs and co-treated them with concentration ranges of known inhibitors and 10 μM of the contractile agonist Ang II. I then assessed morphological response by measuring changes in cell area. Previous work by the Warren lab has shown that cell area is representative of cell volume[190]. Thus, quantifying changes in cell area provided a reliable readout of the hypertrophy-like response and facilitated interrogation of the signalling pathways driving this matrix-dependent response.

3.2 Aims

This chapter aims to unpick the signalling pathways that drive the dysfunctional hypertrophy-like response observed in VSMCs cultured on rigid matrices and stimulated with contractile agonist Ang II. This will be achieved by:

1. Utilising the polyacrylamide hydrogel assay developed by the Warren lab to conduct biased concentration response screens. These screens will focus on known pharmacological inhibitors of cell components involved in volume regulation, contraction, mechanosensing, and intracellular signalling.

2. Use this data to extract IC_{50} data for the compounds of interest.

3.3 Hypotheses

I predict that targeted, pharmacological inhibition of specific cellular signalling pathways will enable me to modulate the aberrant hypertrophy-like response observed in VSMCs treated with Ang II on rigid matrix.

Specifically, I hypothesise that:

1. Targeted inhibition of cell components involved in volume regulation (e.g. aquaporins), mechanosensing (e.g. the microtubule cytoskeleton) and signalling molecules (e.g. Ca^{2+} ion channels, nuclear kinases), will result in reduced cell area of VSMCs cultured on rigid hydrogels.

2. Changes in VSMC area will be concentration dependent.

3.4 Materials and Methods

Table 3.1. List of compounds used in Chapter 3. *Shows their molecular target and the concentration range used.*

Compound	**Target**	**Concentration Range**
TCAQP1	Aquaporin 1	*0.00001 – 10 μM*
TGN020	Aquaporin 4	*0.001 – 1000 nM*
Furosemide	NKCC	*0.01 – 100 μM*
STOCK2S 26	Wnk	*0.01 – 100 μM*
Go6983	PKC	*0.01 – 100 nM*
Xestospongin C	IP_3R	*0.001 – 10 μM*
Dantrolene	RyR	*0.001 – 10 nM*
Epothilone B	Microtubules (Stabilises)	*0.001 – 10 nM*
Nocodazole	Microtubules (Destabilises)	*0.001 – 10 nM*
A1070722	GSK3	*0.001 – 10 nM*
AZD7762	Chk2	*0.001 – 10 nM*
Ku5933	ATM	*0.001 – 10 nM*
EB47	PARP-1	*0.001 – 10 nM*

3.5 Results

3.5.1 AQP1 blockade reduces VSMC area on both pliable and rigid matrix

Aquaporin mediated water flux across the plasma membrane is a known regulator of volume across cell types. I therefore sought to examine the effect of AQP1 inhibition on VSMCs cultured on both 12 and 72 kPa hydrogels. AQP1 is a ubiquitously expressed aquaporin and has been implicated in a range of processes, including volume regulation, calcium handling[191] and, cell migration[192]. Furthermore, AQP1 blockade has been shown

to inhibit proliferation and motility in cancer cells[193] and inhibits oxidative stress accumulation and senescence in endothelial cells[194].

Cells were seeded in basal media on 12 and 72 kPa hydrogels and treated with the AQP1 channel blocker TCAQP1 (0.00001-10 µM) for 1 hour. Cells were additionally co-treated with 10 µM Ang II for 30 min prior to fixing. Representative images were captured using confocal microscopy and cell area was assessed using Fiji.

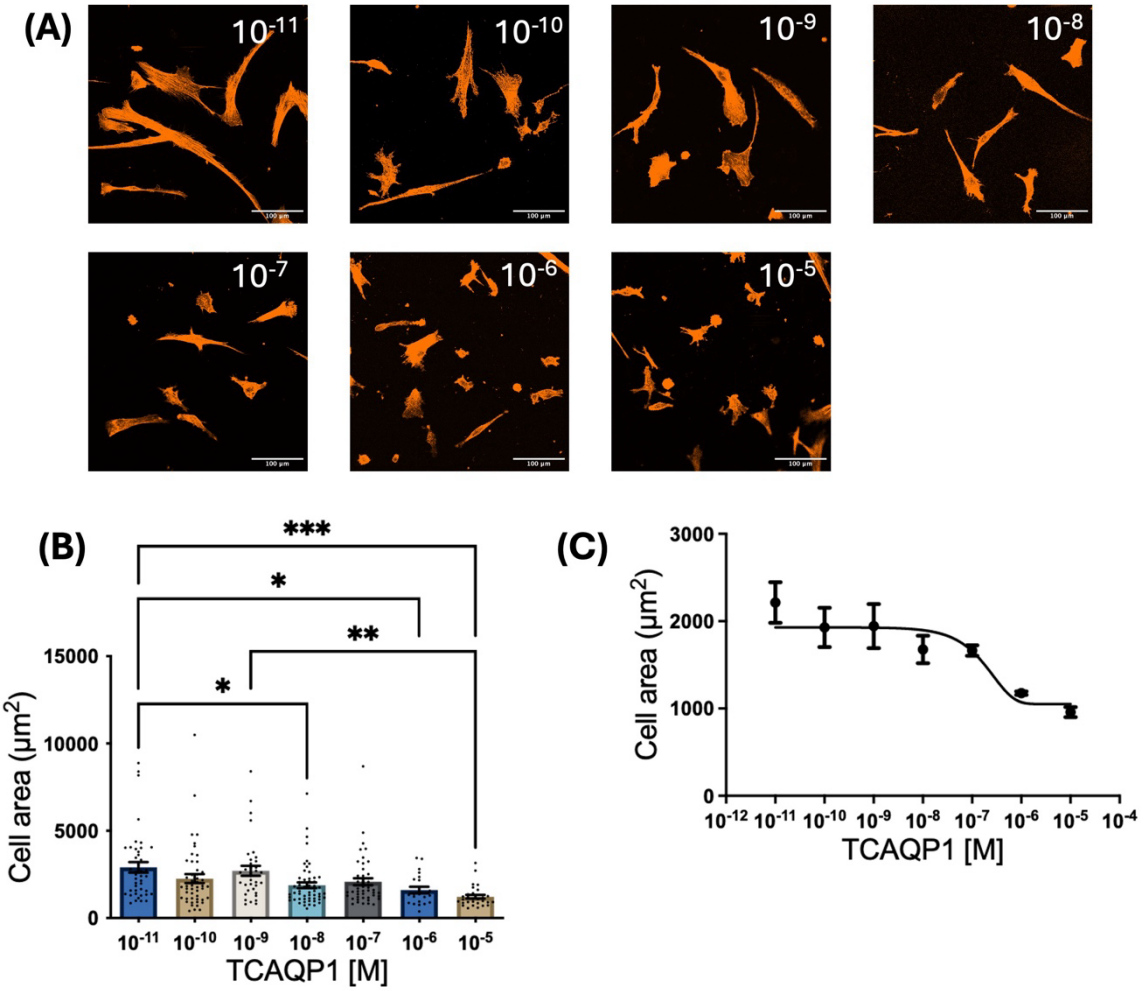

Figure 3.2. TCAQP1 concentration response assay on 12 kPa hydrogels. ***(A)*** *Representative images. Scale bars represent 100 µm.* ***(B)*** *VSMC area on 12 kPa hydrogels treated with TCAQP1 (0.00001-10 µM). Shows means and SEM. Statistical significance assessed by One-way ANOVA and Tukey's multiple comparisons test (* = p<0.05, ** < 0.01, *** < 0.001).* ***(C)*** *Dose response curve showing VSMC area in response to TCAQP1 treatment. Shows means and SEM. Data are based on measurements of 307 VSMCs from 3 independent experiments.*

Analysis revealed that TCAQP1 treatment induced a significant, concentration-dependent reduction in area of VSMCs seeded on pliable hydrogels (Figure 3.2B). Mean cell area decreased from 2964 µm^2 at the lowest tested concentration (0.00001 µM) to

1220 μm² at the highest (10 μM) concentration. Additionally, regression analysis determined the half-maximal inhibitory concentration (IC_{50}) to be approximately 10^{-7} M (Figure 3.2C).

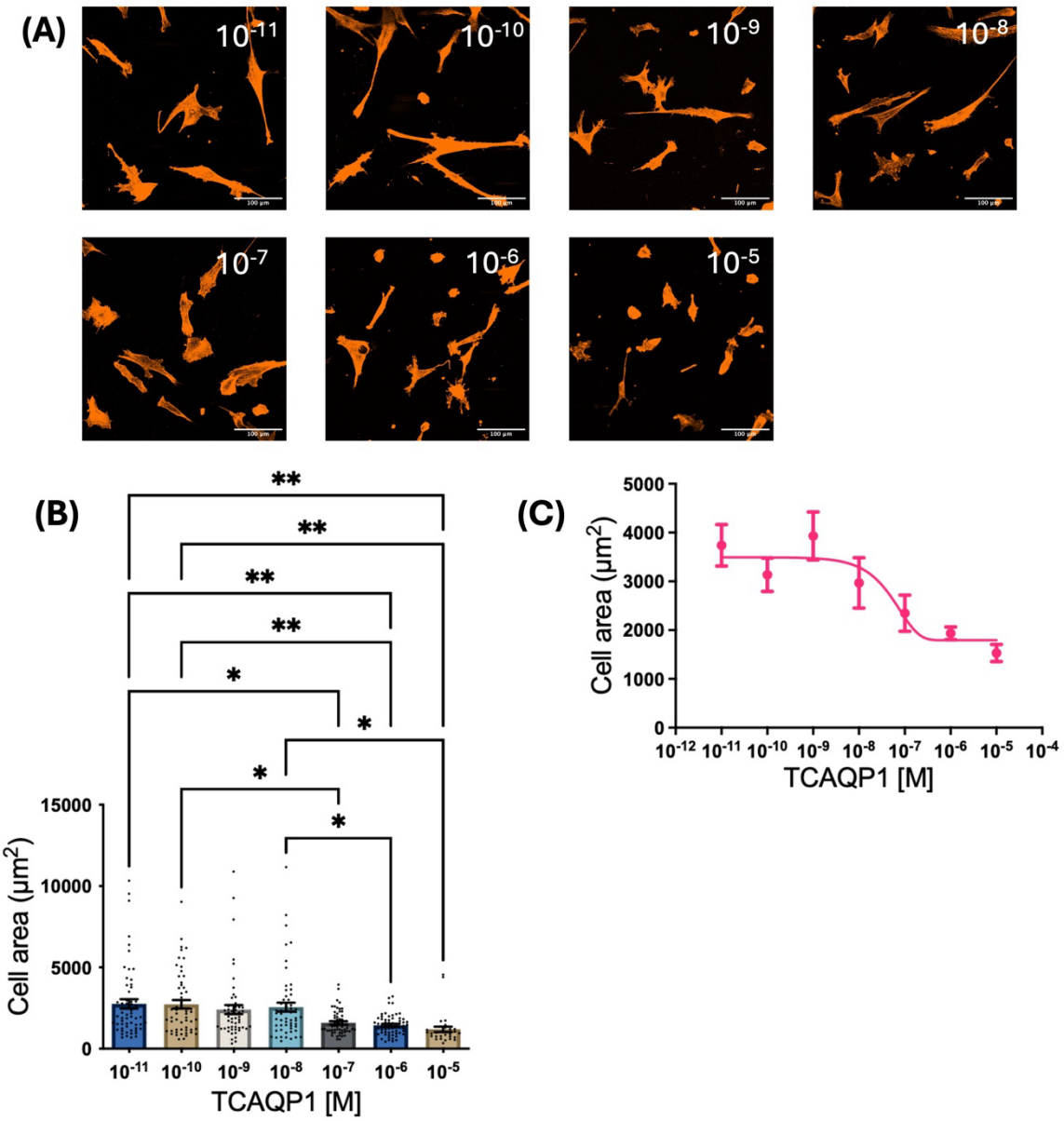

Figure 3.3. TCAQP1 concentration response assay on 72 kPa hydrogels. ***(A)*** *Representative images. Scale bars represent 100 μm.* ***(B)*** *VSMC area on 72 kPa hydrogels treated with TCAQP1 (0.00001-10 μM). Shows means and SEM. Statistical significance assessed by One-way ANOVA and Tukey's multiple comparisons test (* = p<0.05, ** < 0.01).* ***(C)*** *Dose response curve showing VSMC area in response to TCAQP1 treatment. Shows means and SEM. Data are based on measurements of 372 VSMCs from 3 independent experiments.*

A similar reduction in cell area was observed in VSMCs cultured on rigid matrix and treated with TCAQP1 (Figure 3.3B). Cell area was reduced from 2761 μm² at the lowest tested concentration (0.00001 μM) to 1188 μm² at the highest (10 μM) concentration.

Additionally, regression analysis determined the half-maximal inhibitory concentration (IC_{50}) to be approximately 10^{-7} M (Figure 3.3C).

3.5.2 AQP4 blockade reduces VSMC area on rigid matrix

Following this, I investigated VSMC response to blockade of another ubiquitously expressed aquaporin. AQP4 has been previously identified in both smooth and striated muscle and is known to play roles in congenital heart disease, hypertension and angiogenesis[195]. Interestingly, AQP4 possess the strongest water permeability among aquaporins and is therefore central to regulating intracellular pressure and cell volume[151]. In mouse models, knockdown of AQP4 was found to be protective against myocardial ischemia[196]. Additionally, inhibition of AQP4 has been shown to alter expression of chemokine receptors[197] and the kinases AMP and Akt[151].

Here, cells were seeded in basal media on 12 and 72 kPa polyacrylamide hydrogels, treated with AQP4 channel blocker TGN020 (0.001-1000 nM) for 1 hour and co-treated with 10 μM Ang II for 30 min.

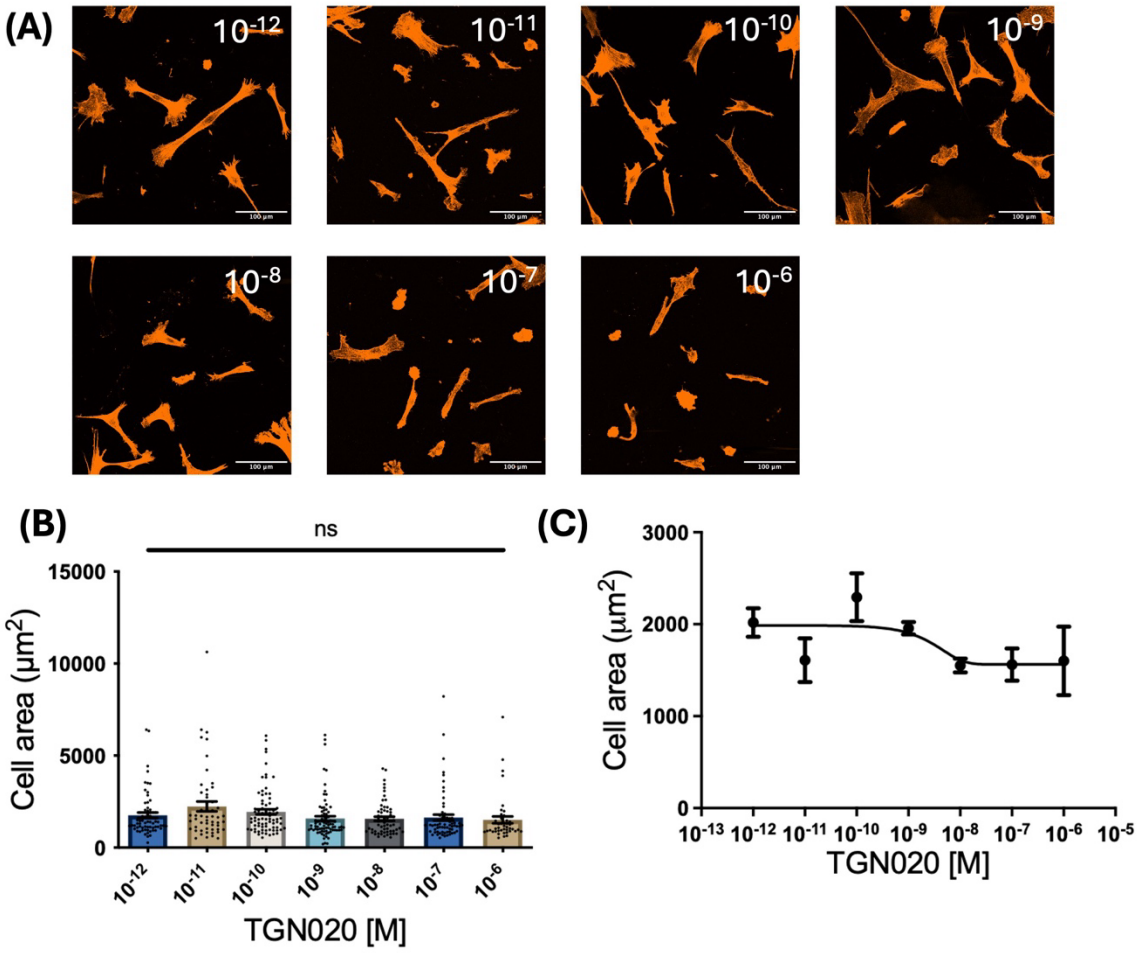

Figure 3.4. TGN020 concentration response assay on 12 kPa hydrogels. ***(A)*** *Representative images. Scale bars represent 100 µm.* ***(B)*** *VSMC area on 12 kPa hydrogels treated with TGN020 (0.001-1000 nM). Shows means and SEM. Statistical significance assessed by One-way ANOVA and Tukey's multiple comparisons test.* ***(C)*** *Dose response curve showing VSMC area in response to TGN020 treatment. Shows means and SEM. Data are based on measurements of 449 VSMCs from 3 independent experiments.*

Analysis of these data revealed that TGN020 had no significant effect on the area of VSMC cultured on pliable hydrogels (Figure 3.4B).

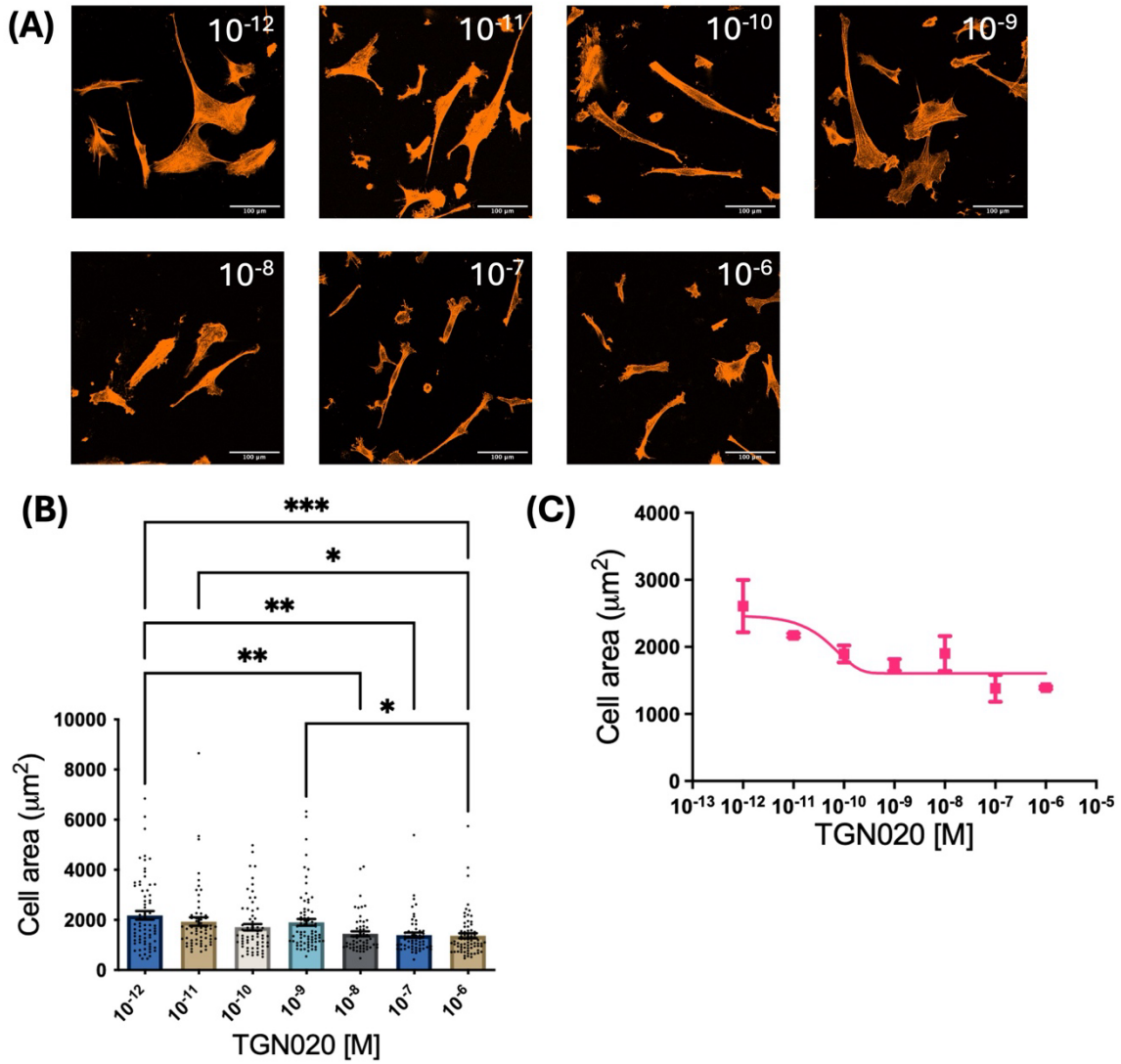

Figure 3.5. TGN020 concentration response assay on 72 kPa hydrogels. (A) *Representative images. Scale bars represent 100 µm.* ***(B)*** *VSMC area on 72 kPa hydrogels treated with TGN020 (0.001-1000 nM). Shows means and SEM. Statistical significance assessed by One-way ANOVA and Tukey's multiple comparisons test (* = p<0.05, ** < 0.01, *** < 0.001).* ***(C)*** *Dose response curve showing VSMC area in response to TGN020 treatment. Shows means and SEM. Data are based on measurements of 454 VSMCs from 3 independent experiments.*

TGN020 treatment induced a concentration-dependent reduction in VSMC area on rigid hydrogels (Figure 3.5B). Cell area was reduced from 2182 µm^2 at the lowest tested concentration (0.001 nM) to 1369 µm^2 at the highest concentration (1000 nM). Regression analysis determined the half-maximal inhibitory concentration (IC_{50}) to be approximately 10^{-10} M (Figure 3.5C).

3.5.3 NKCC inhibition has no effect on VSMC area on rigid matrix

Following these findings, I investigated the effect of NKCC inhibition on VSMC area response to enhanced matrix rigidity. NKCC is an important membrane-bound

symporter which mediates the inward flux of Na^+, K and Cl ions into the cytosol[198]. NKCC is a known regulator of volume in other cell types through its interaction with pro-proliferative proteins such as mTORC1[199] and through modulation of intracellular water potential. Additionally, work in astrocytes has revealed that inhibition of NKCC prevents the upregulation of AQP4 in cell damage conditions[200].

Cells were seeded in basal media on 72 kPa polyacrylamide hydrogels, treated with the NKCC inhibitor Furosemide (0.01-100 μM) for 1 hour and co-treated with 10 μM Ang II for 30 min.

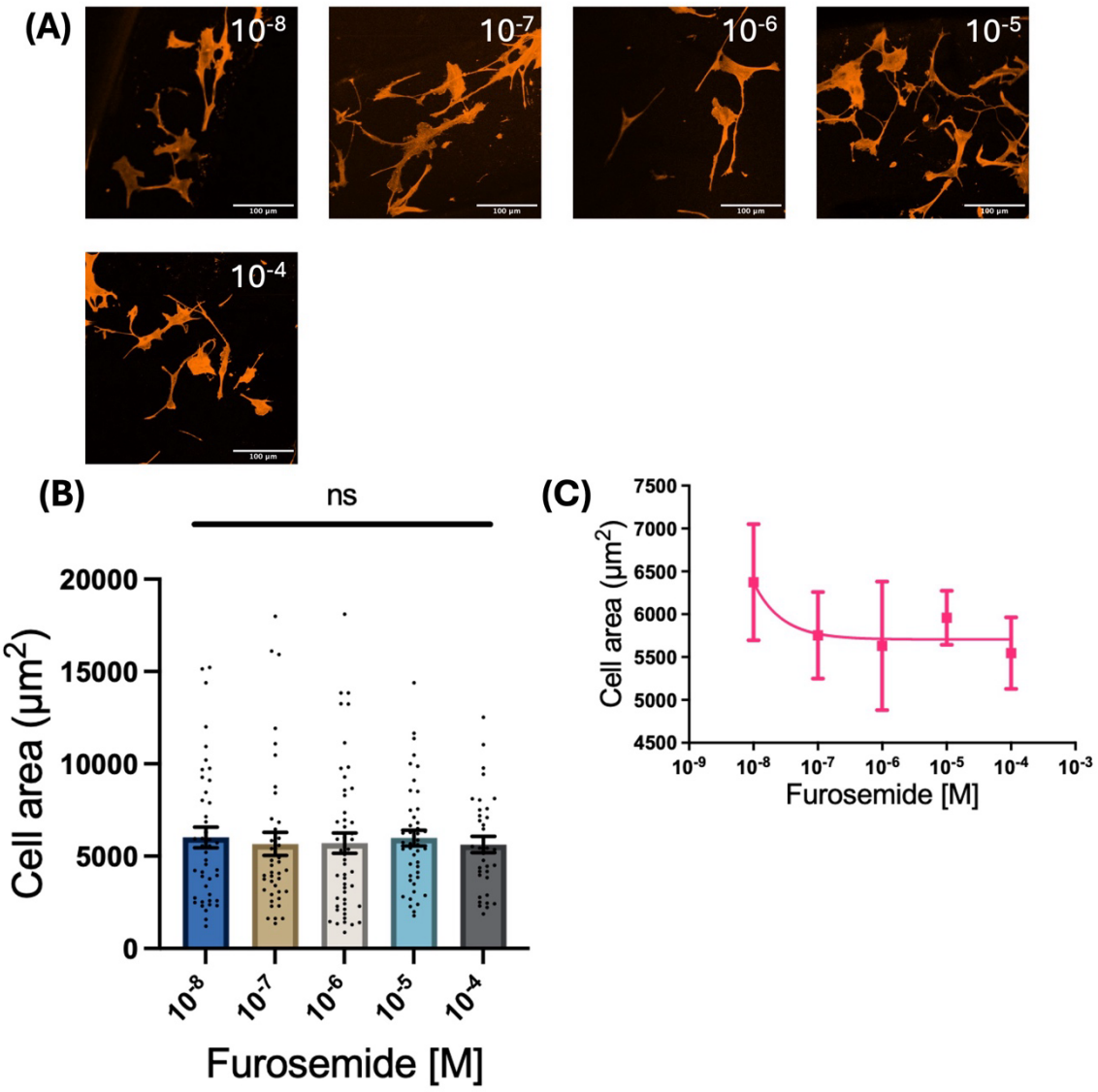

Figure 3.6. Furosemide concentration response assay on 72 kPa hydrogels. ***(A)*** *Representative images. Scale bars represent 100 µm.* ***(B)*** *VSMC area on 72 kPa hydrogels treated with furosemide (0.01-100 µM). Shows means and SEM. Statistical significance assessed by One-way ANOVA and Tukey's multiple comparisons test.* ***(C)*** *Dose response curve showing VSMC area in response to furosemide treatment. Shows means and SEM. Data are based on measurements of 215 VSMCs from 3 independent experiments. N = 1 conducted by another member of the Warren lab.*

Analysis of these data revealed that Furosemide treatment had no significant effect on the area of VSMCs cultured on rigid hydrogels (Figure 3.6B).

3.5.4 Wnk inhibition has no effect on VSMC area on rigid matrix

I additionally investigated the effect of Wnk inhibition on VSMC morphology response to enhanced matrix rigidity. Wnk1 and Wnk2 have been linked to cell volume regulation through their interactions with SPAK. A kinase involved in the phosphorylation and

activation of ion cotransporters such as NKCC[201]. I used STOCK2S 26 to inhibit Wnk which works by blocking the interaction between the Wnk and SPAK proteins.

Here, cells were seeded in basal media on 72 kPa polyacrylamide hydrogels, treated with Wnk inhibitor STOCK2S 26 (0.01-100 µM) for 1 hour and co-treated with 10 µM Ang II for 30 min.

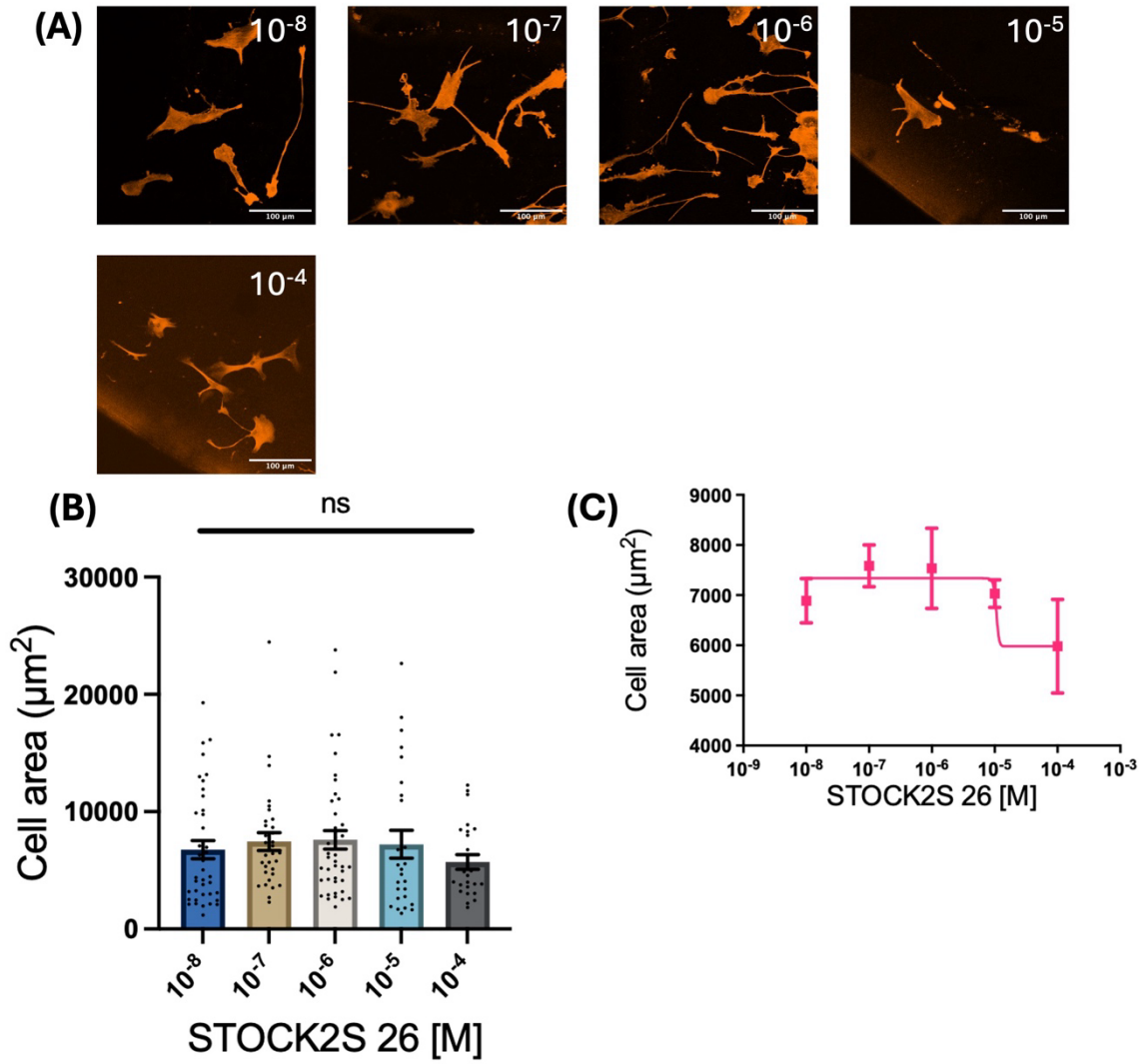

Figure 3.7. STOCK2S 26 concentration response assay on 72 kPa hydrogels. ***(A)*** *Representative images. Scale bars represent 100 µm.* ***(B)*** *VSMC area on 72 kPa hydrogels treated with STOCK2S 26 (0.01-100 µM). Shows means and SEM. Statistical significance assessed by One-way ANOVA and Tukey's multiple comparisons test.* ***(C)*** *Dose response curve showing VSMC area in response to STOCK2S 26 treatment. Shows means and SEM. Data are based on measurements of 164 VSMCs from 3 independent experiments. N = 1 conducted by another member of the Warren lab.*

Analysis of these data revealed that STOCK2S 26 treatment had no significant effect on the area of VSMCs cultured on rigid hydrogels (Figure 3.7B).

3.5.5 PKC inhibition reduces VSMC area on rigid matrix

Following these findings, I investigated the PKC inhibitor Go6983. PKC is a ubiquitous protein kinase involved in the downstream regulation of a range of proteins. One of the key activators of PKC is Ca^{2+}. This association means that PKC is vital to several intracellular signalling cascades. As a result, PKC is involved in range of processes including contraction, migration and proliferation. PKC has also been shown to regulate the localisation of aquaporins, highlighting its key role as a regulator of cell volume[202].

The Go6983 inhibitor is a broad-spectrum inhibitor with proven efficacy against a number of PKC isoforms, including PKCα, PKCβ, PKCγ, PKCδ, PKCζ and PKCμ. It has been shown to exert a cardioprotective effects in myocardial ischemia and prevents superoxide-mediated cardiac contractile dysfunction[203].

Here, cells were seeded in basal media on 72 kPa polyacrylamide hydrogels, treated with PKC inhibitor Go6983 (0.01-100 nM) for 1 hour and co-treated with 10 μM Ang II for 30 min.

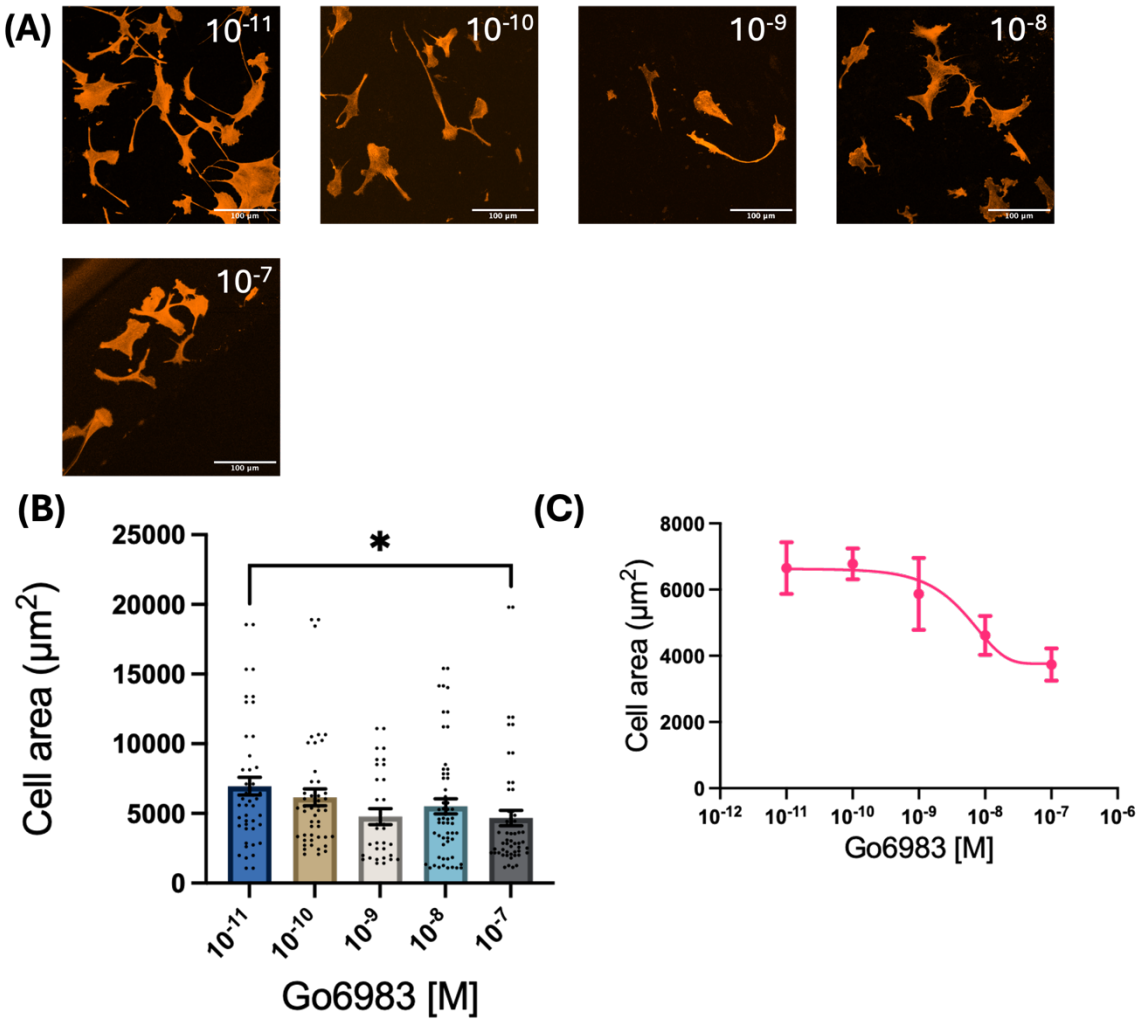

Figure 3.8. Go6983 concentration response assay on 72 kPa hydrogels. ***(A)*** *Representative images. Scale bars represent 100 µm.* ***(B)*** *VSMC area on 72 kPa hydrogels treated with Go6983 (0.01-100 nM). Shows means and SEM. Statistical significance assessed by One-way ANOVA and Tukey's multiple comparisons test (* = p<0.05).* ***(C)*** *Dose response curve showing VSMC area in response to Go6983 treatment. Shows means and SEM. Data are based on measurements of 238 VSMCs from 3 independent experiments.*

These data show that Go6883 treatment induced a concentration dependant reduction in cell area of VSMCs seeded on rigid matrix (Figure 3.8B). Mean area was reduced from 6957 µm^2 at the lowest tested concentration (0.01 nM) to 4668 µm^2 at the highest concentration (100 nM). Regression analysis determined the half-maximal inhibitory concentration (IC_{50}) to be approximately 10^{-9} M (Figure 3.8C).

3.5.6 IP_3R inhibition increases VSMC area on pliable matrix and decreases area on rigid matrix

I next examined the effect of inhibiting inositol 1,4,5-trisphosphate (IP_3) mediated Ca^{2+} release with the IP_3R antagonist, xestospongin C. IP_3R is a vital sarcoplasmic calcium

channel, activated downstream of GPCR agonist binding and the subsequent cleavage of PIP_2 into IP_3 and DAG. IP_3 mediated Ca^{2+} release from the sarcoplasmic reticulum is involved in a range of cell processes such as contraction, migration and proliferation.

Cells were seeded in basal media on 12 kPa polyacrylamide hydrogels, treated with xestospongin C (0.001-10 µM) for 1 hour and co-treated with 10 µM Ang II for 30 min.

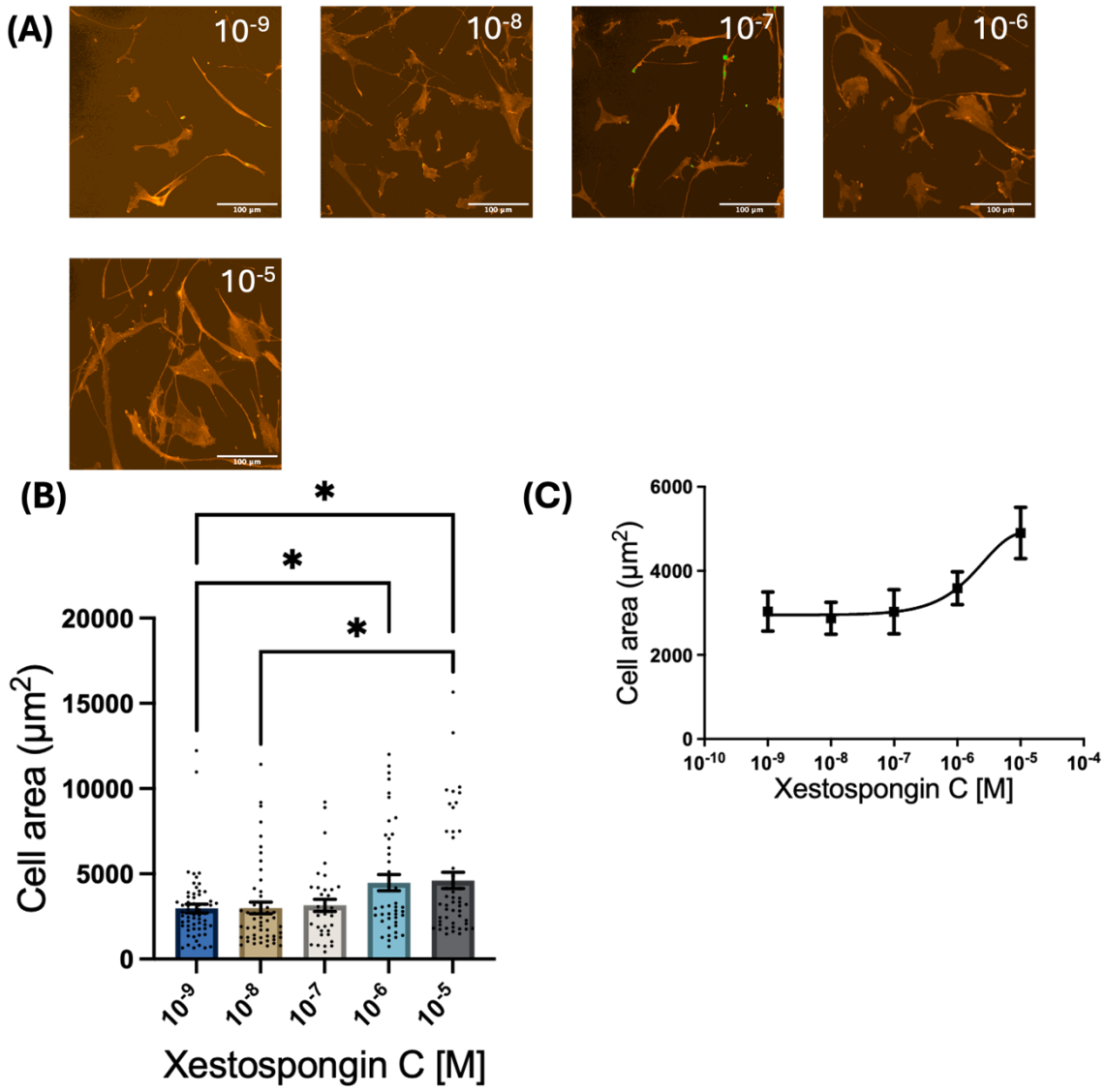

Figure 3.9. Xestospongin C concentration response assay on 12 kPa hydrogels. ***(A)*** *Representative images. Scale bars represent 100 µm.* ***(B)*** *VSMC area on 12 kPa hydrogels treated xestospongin C (0.001-10 µM). Shows means and SEM. Statistical significance assessed by One-way ANOVA and Tukey's multiple comparisons test (* = p<0.05).* ***(C)*** *Dose response curve showing VSMC area in response to xestospongin C treatment. Shows means and SEM. Data are based on measurements of 241 VSMCs from 3 independent experiments.*

Interestingly, analysis revealed that xestospongin C induced a concentration dependant increase in area of VSMCs cultured on pliable matrix (Figure 3.9B). Mean area was

increased from 2970 µm^2 at the lowest tested concentration (0.001 µM) to 4612 µm^2 at the highest concentration (10 µM). Regression analysis determined the half-maximal inhibitory concentration (IC_{50}) to be approximately 10^{-6} M (Figure 3.9C).

Following this, VSMCs were seeded on 72 kPa hydrogels, treated with xestospongin C and co-treated with 10 µM Ang II as previously stated.

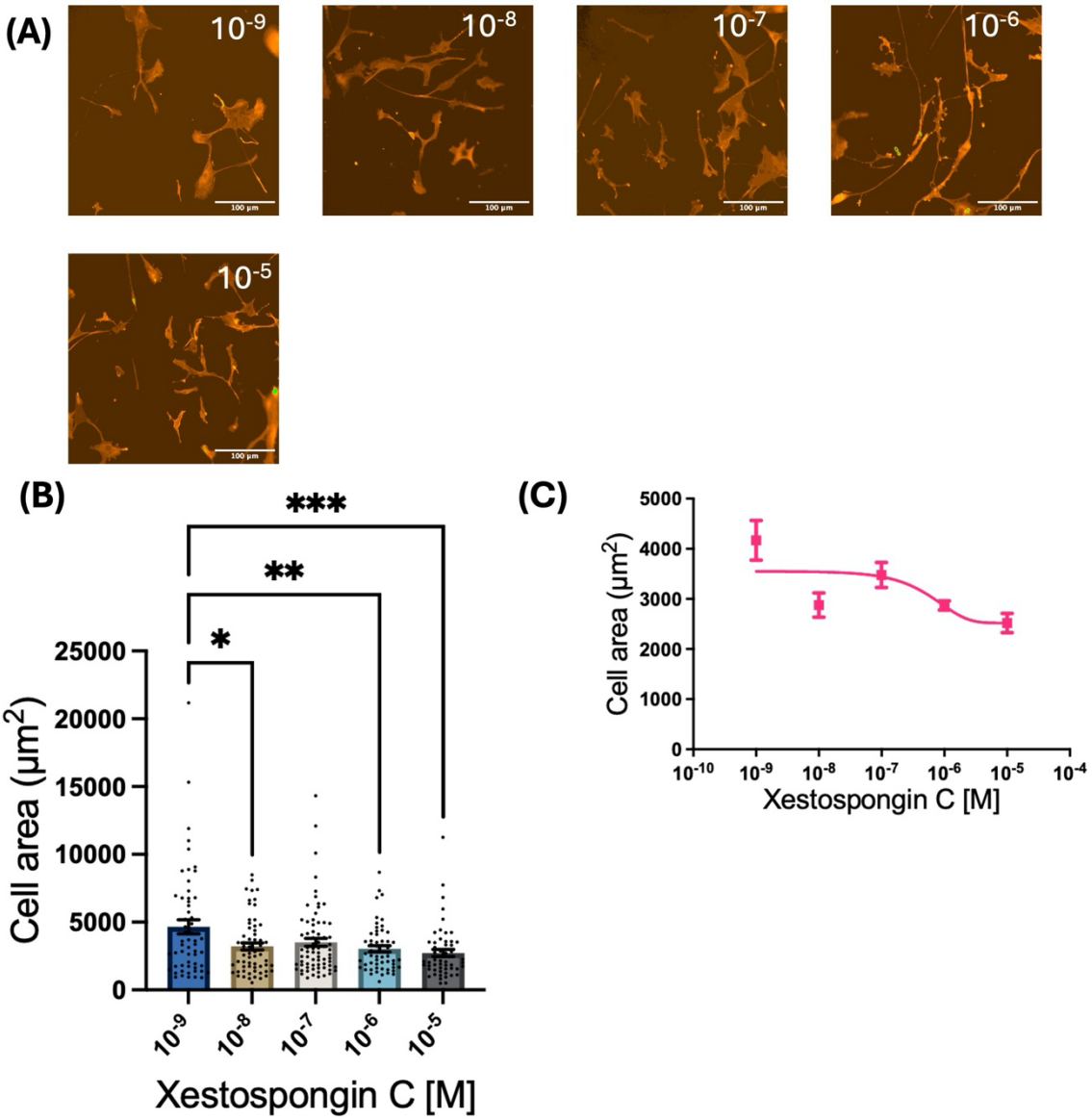

Figure 3.10. Xestospongin C concentration response assay on 72 kPa hydrogels. ***(A)*** *Representative images. Scale bars represent 100 um.* ***(B)*** *VSMC area on 72 kPa hydrogels treated Xestospongin C (0.001-10 uM). Shows means and SEM. Statistical significance assessed by One-way ANOVA and Tukey's multiple comparisons test (* = p<0.05, ** < 0.01, *** < 0.001).* ***(C)*** *Dose response curve showing VSMC area in response to xestospongin C treatment. Shows means and SEM. Data are based on measurements of 301 VSMCs from 3 independent experiments.*

These data show that on rigid matrix, VSMCs treated with xestospongin C underwent a concentration dependent reduction in cell area (Figure 3.10B). Area was reduced from 4658 μm^2 at the lowest tested concentration (0.001 μM) to 2727 μm^2 at the highest concentration (10 μM). Regression analysis determined the half-maximal inhibitory concentration (IC_{50}) to be approximately 10^{-6} M (Figure 3.10C).

3.5.7 RyR inhibition increases VSMC area on pliable matrix and decreases area on rigid matrix

Following these results, I next examined the effects of ryanodine receptor inhibition on VSMC area response to enhanced matrix rigidity. Ryanodine receptors (RyR) are multidomain, intracellular calcium channels that facilitate Ca^{2+} ion flux from the sarcoplasmic reticulum into the cytosol. Compared to the agonist mediated release of Ca^{2+} though IP_3R channels, RyR mediated Ca^{2+} release is complex and less well understood. Traditionally, RyR mediated Ca^{2+} release has been associated with amplification of Ca^{2+} transients through calcium induced calcium release (CICR), where small amounts of Ca^{2+} in the cytosol cause RyR to release even more Ca^{2+} ions[204]. Additionally, RyR can be activated by Ca^{2+} flux through membrane bound L-type voltage-gated calcium channels. Release of Ca^{2+} from RyR is associated with core VSMCs processes such as maintenance of vascular tone, regulation of contractility and cell signalling[205].

Here, VSMCs were seeded in basal media on 12 kPa polyacrylamide hydrogels, treated with the RyR inhibitor dantrolene (0.001-10 nM) for 1 hour and co-treated with 10 μM Ang II for 30 min.

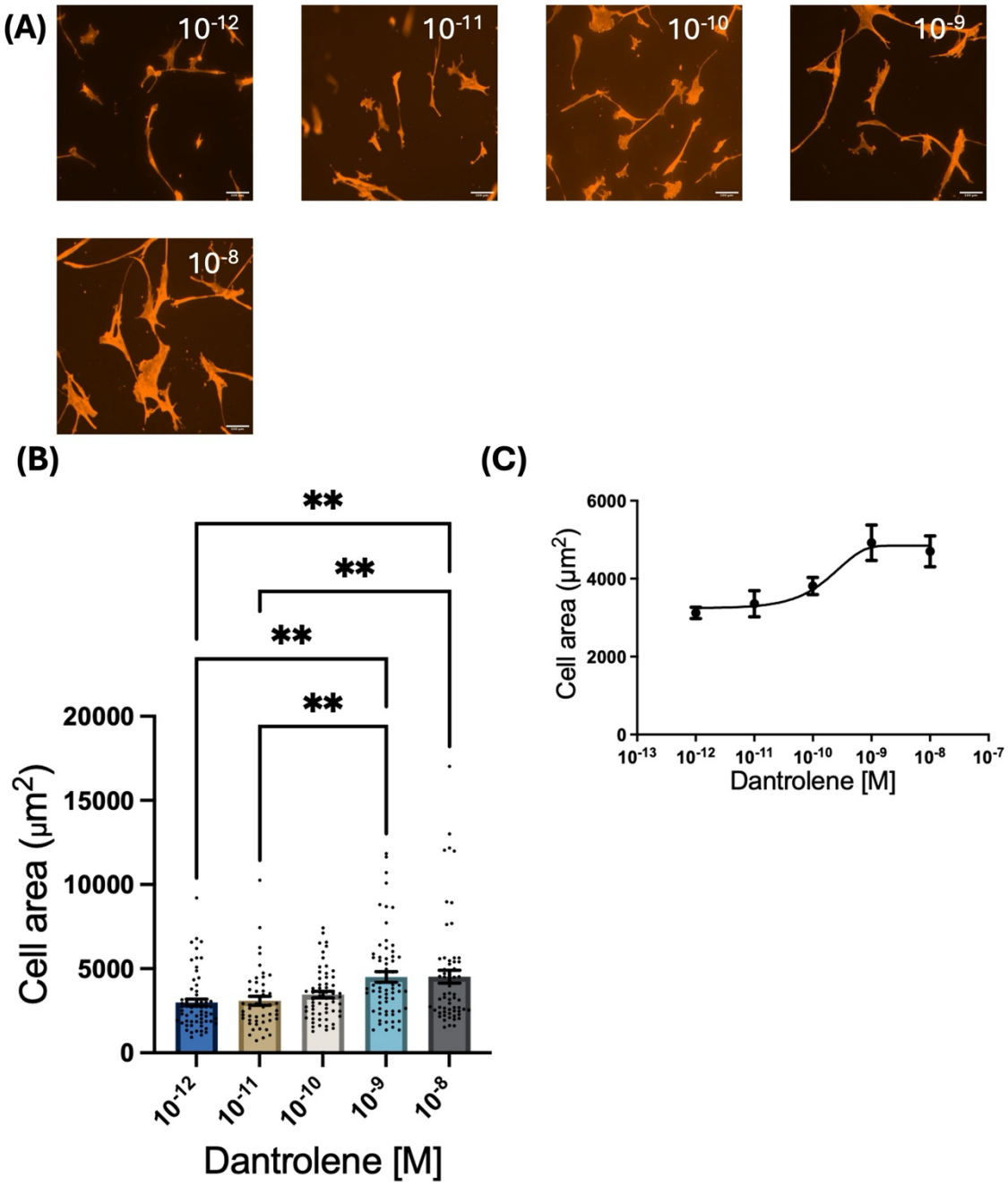

Figure 3.11. Dantrolene concentration response assay on 12 kPa hydrogels. ***(A)*** *Representative images. Scale bars represent 100 µm.* ***(B)*** *VSMC area on 12 kPa hydrogels treated dantrolene (0.001-10 nM). Shows means and SEM. Statistical significance assessed by One-way ANOVA and Tukey's multiple comparisons test (* = p<0.05, ** < 0.01).* ***(C)*** *Dose response curve showing VSMC area in response to dantrolene treatment. Shows means and SEM. Data are based on measurements of 298 VSMCs from 4 independent experiments. N = 1 conducted by another member of the Warren lab.*

This data shows that inhibition of RyR with dantrolene induces a concentration dependent increase in VSMC area when cultured on pliable hydrogels and co-treated with Ang II (Figure 3.11B). Mean area was increased from 2984 µm^2 at the lowest tested concentration (0.001 nM) to 4527 µm^2 at the highest concentration (10 nM). Regression

analysis determined the half-maximal inhibitory concentration (IC_{50}) to be approximately 10^{-10} M (Figure 3.11C).

Following this, VSMCs were seeded on 72 kPa hydrogels, treated with dantrolene and co-treated with 10 μM Ang II as previously described.

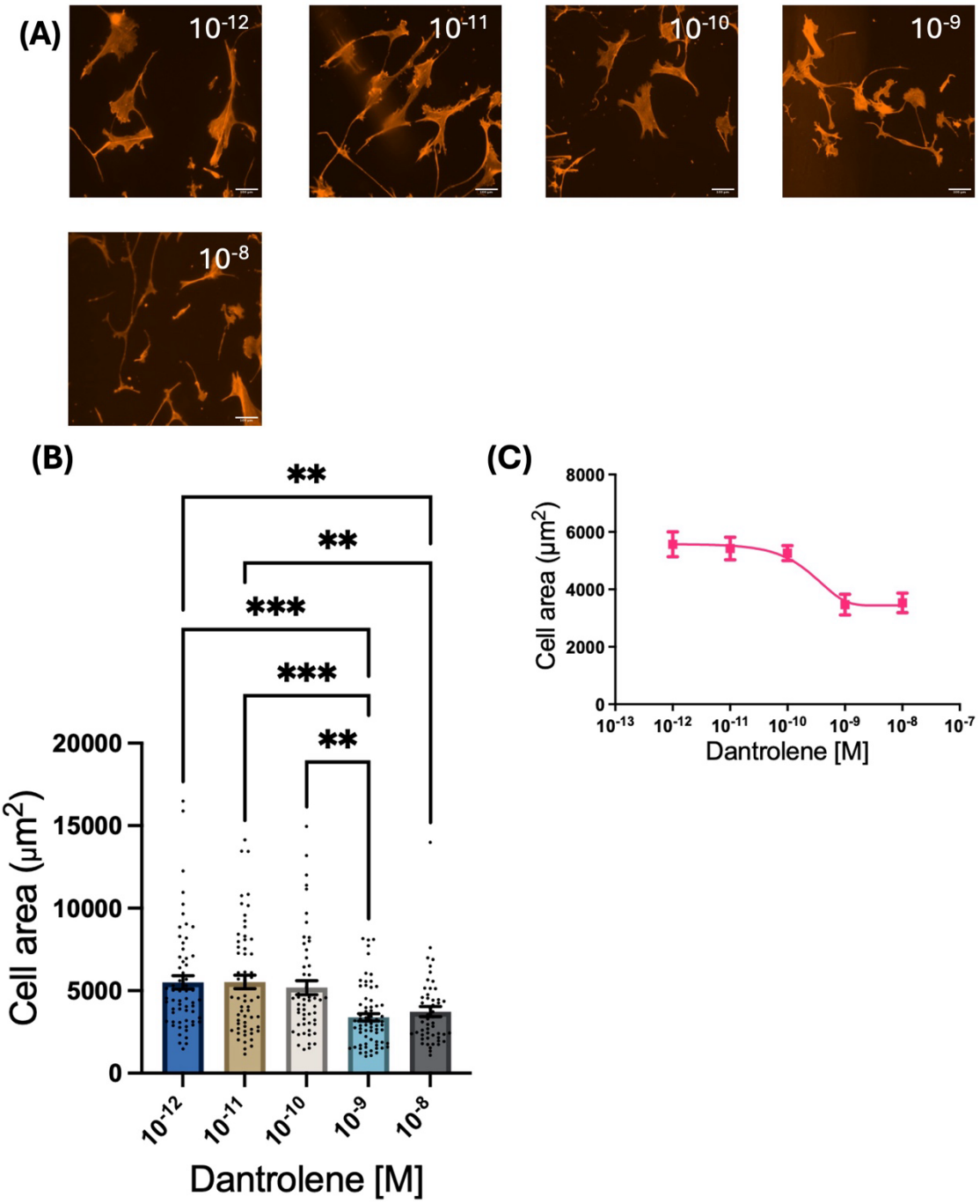

Figure 3.12. Dantrolene concentration response assay on 72 kPa hydrogels. ***(A)*** *Representative images. Scale bars represent 100 µm.* ***(B)*** *VSMC area on 72 kPa hydrogels treated dantrolene (0.001-10 nM). Shows means and SEM. Statistical significance assessed by One-way ANOVA and Tukey's multiple comparisons test (* = p<0.05, ** < 0.01, *** < 0.001).* ***(C)*** *Dose response curve showing VSMC area in response to dantrolene treatment. Shows means and SEM. Data are based on measurements of 295 VSMCs from 4 independent experiments. N = 1 conducted by another member of the Warren lab.*

This analysis revealed that treatment with dantrolene induced a concentration dependent reduction in cell area in VSMCs seeded on rigid hydrogels and co-treated with Ang II (Figure 3.12B). Mean area was reduced from 5509 μm^2 at the lowest tested concentration (0.001 nM) to 3728 μm^2 at the highest concentration (10 nM). Regression

analysis determined the half-maximal inhibitory concentration (IC_{50}) to be approximately 10^{-10} M (Figure 3.12C).

3.5.8 Microtubule stabilisation reduces VSMC area on rigid matrix

Additional experiments were conducted to examine the role of microtubule stability in regulating VSMC area response to pliable and rigid matrix. As discussed, microtubules act to resist the compressive forces of actomyosin activity. Therefore, the tensegrity model predicts that microtubule stabilisation will reduce contractile force generation.

To test this, VSMCs were first treated with the microtubule stabilising agent epothilone B. Epothilone binds to αβ-tubulin heterodimer subunits. This reduces the rate of tubulin dissociation resulting in stabilised microtubules[206]. Here, cells were seeded on pliable matrices in basal media, treated with epothilone B (0.001-10 nM) for 1 hour, and co-treated with 10 μM Ang II for 30 min.

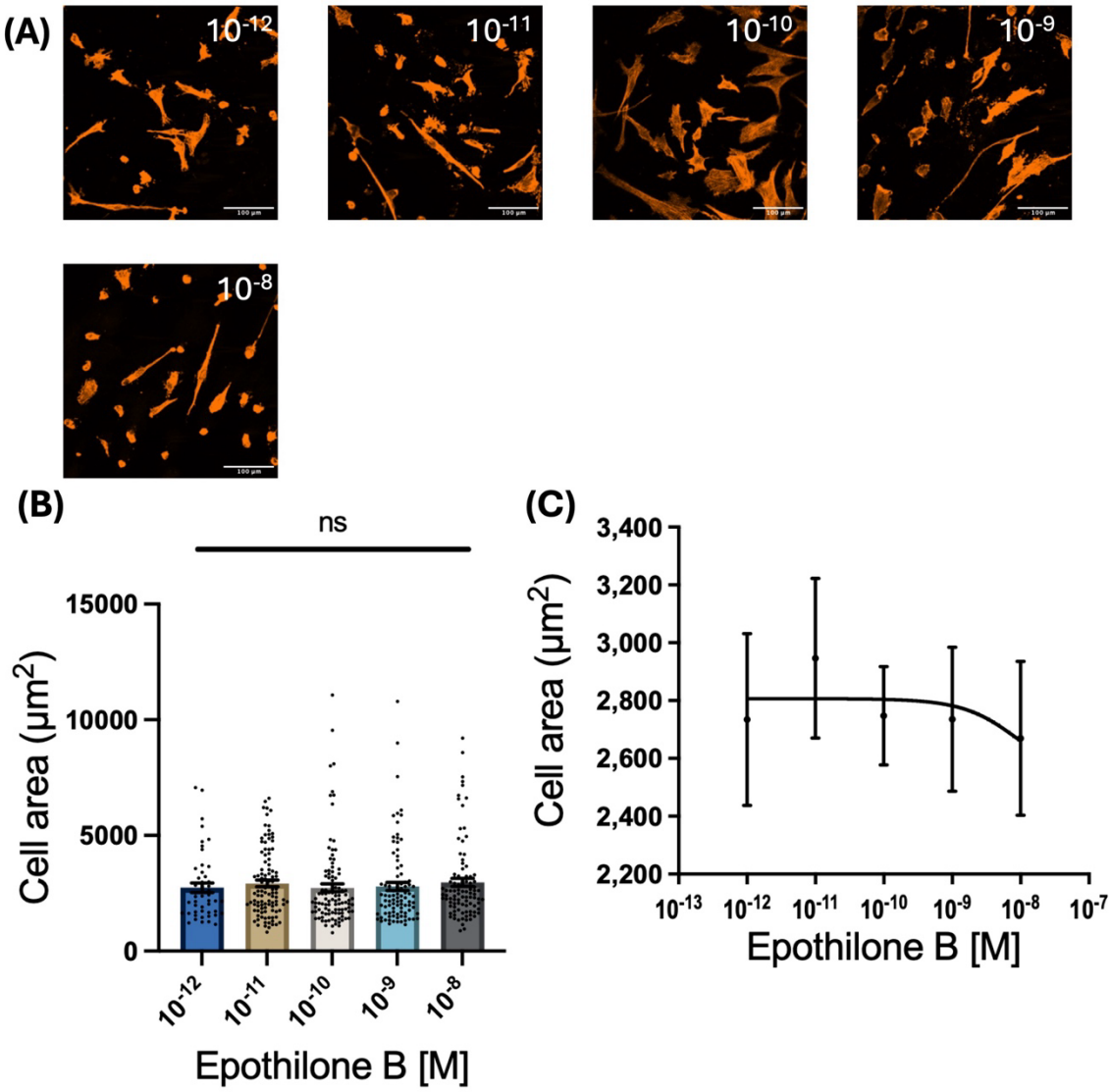

Figure 3.13. Epothilone B concentration response assay on 12 kPa hydrogels. ***(A)*** *Representative images. Scale bars represent 100 µm.* ***(B)*** *VSMC area on 12 kPa hydrogels treated epothilone B (0.001-10 nM). Shows means and SEM. Statistical significance assessed by One-way ANOVA and Tukey's multiple comparisons test.* ***(C)*** *Dose response curve showing VSMC area in response to epothilone B treatment. Shows means and SEM. Data are based on measurements of 445 VSMCs from 5 independent experiments.*

Analysis of this data revealed that Epothilone B treatment had no significant effect on VSMC area when seeded on pliable matrix (Figure 3.13B).

Following this, VSMCs on rigid matrix were also co- treated with epothilone B and 10 µM Ang II as previously described.

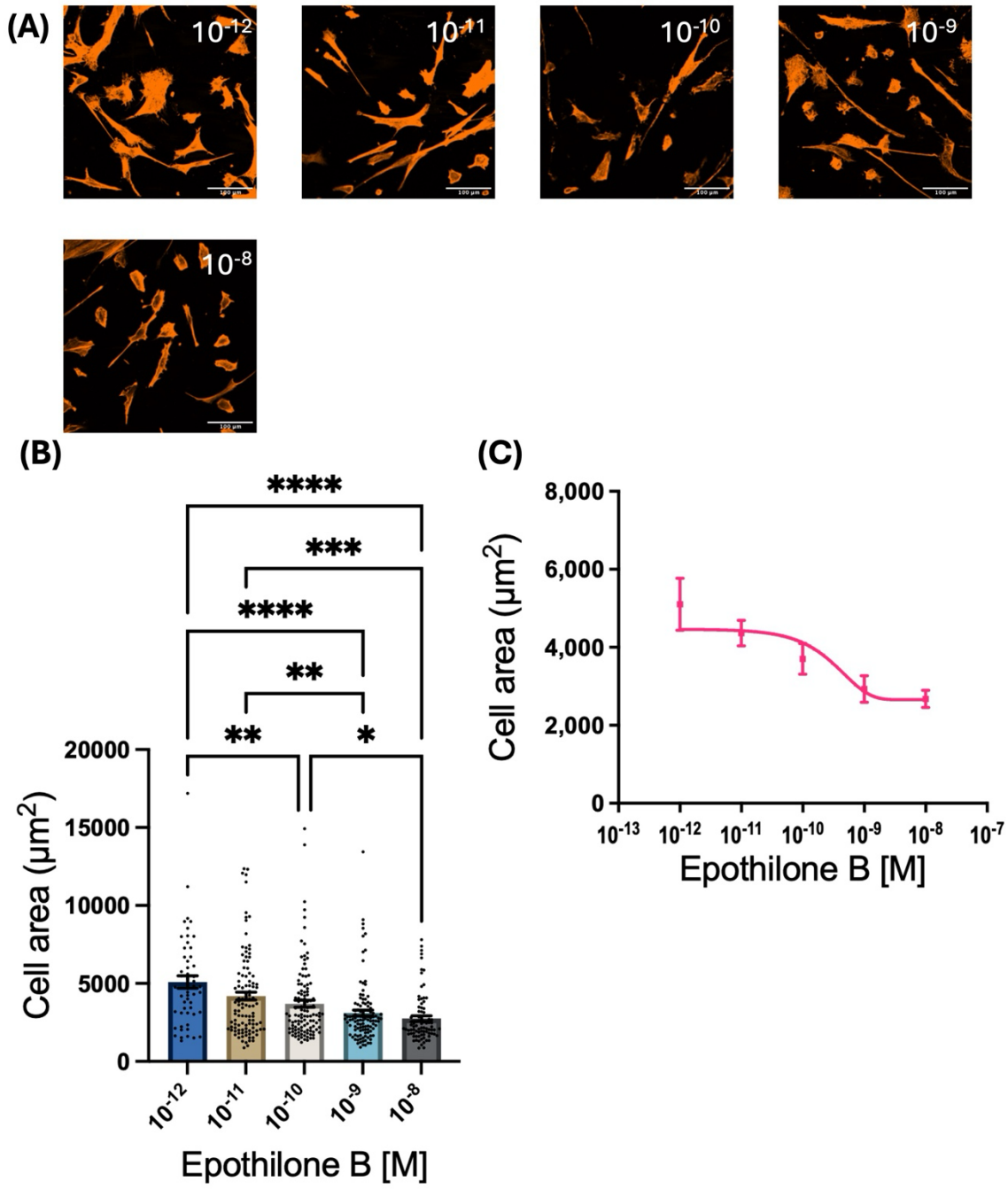

Figure 3.14. Epothilone B concentration response assay on 72 kPa hydrogels. ***(A)*** *Representative images. Scale bars represent 100 µm.* ***(B)*** *VSMC area on 72 kPa hydrogels treated epothilone B (0.001-10 nM). Shows means and SEM. Statistical significance assessed by One-way ANOVA and Tukey's multiple comparisons test (* = p<0.05, ** < 0.01, *** < 0.001, **** < 0.0001).* ***(C)*** *Dose response curve showing VSMC area in response to epothilone B treatment. Shows means and SEM. Data are based on measurements of 473 VSMCs from 5 independent experiments.*

These results show that on rigid matrices, VSMCs treated with epothilone B undergo a concentration dependent reduction in cell area (Figure 3.14B). Area was reduced from 5089 µm^2 at the lowest tested concentration (0.01 nM) to 2753 µm^2 at the highest

concentration (100 nM). Regression analysis determined the half-maximal inhibitory concentration (IC_{50}) to be approximately 10^{-10} M (Figure 3.14C).

3.5.9 Microtubule destabilisation increases VSMC area on pliable matrix

Next, to further investigate the role of microtubule stability in VSMC area response to enhanced matrix rigidity, the microtubule destabilising agent Nocodazole was used. The tensegrity model predicts that microtubule destabilisation should induce an increase in contractile force generation.

Here, cells were seeded on pliable hydrogels in basal media, treated with Nocodazole (0.001-10 nM) for 1 hour and co-treated with 10 μM Ang II for 30 min.

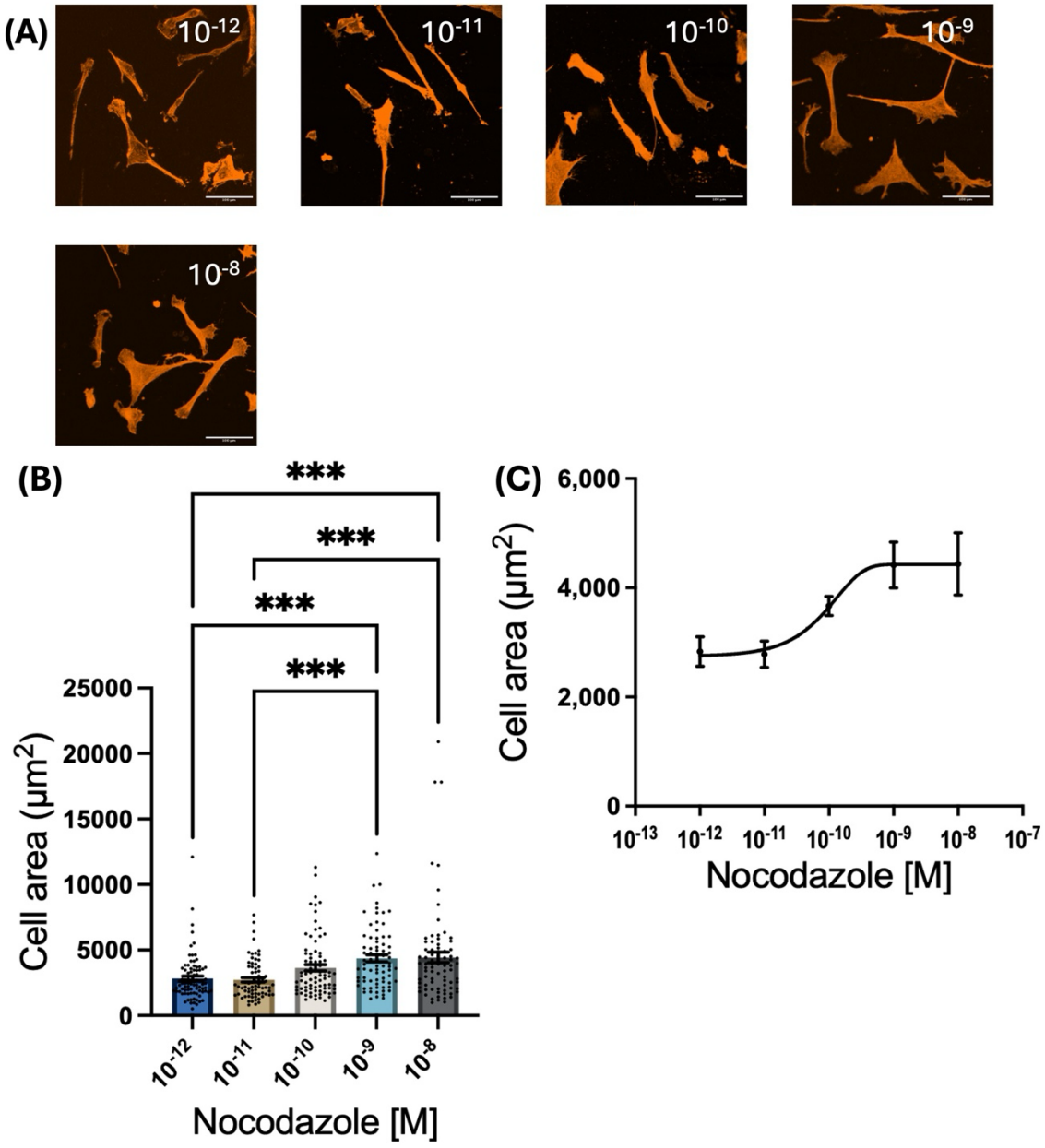

Figure 3.15. Nocodazole concentration response assay on 12 kPa hydrogels. ***(A)*** *Representative images. Scale bars represent 100 µm.* ***(B)*** *VSMC area on 12 kPa hydrogels treated with nocodazole (0.001-10 nM). Shows means and SEM. Statistical significance assessed by One-way ANOVA and Tukey's multiple comparisons test (*** p< 0.001).* ***(C)*** *Dose response curve showing VSMC area in response to nocodazole treatment. Shows means and SEM. Data are based on measurements of 396 VSMCs from 5 independent experiments.*

Analysis revealed that Nocodazole treatment induced a concentration dependent increase in the area of VSMCs cultured on pliable matrix (Figure 3.15B). Area was increased from 2820 µm^2 at the lowest tested concentration (0.01 nM) to 4430 µm^2 at the highest concentration (100 nM). Regression analysis determined the half-maximal inhibitory concentration (IC_{50}) to be approximately 10^{-10} M (Figure 3.15C).

Next, this experiment was repeated on VSMCs seeded on rigid hydrogels.

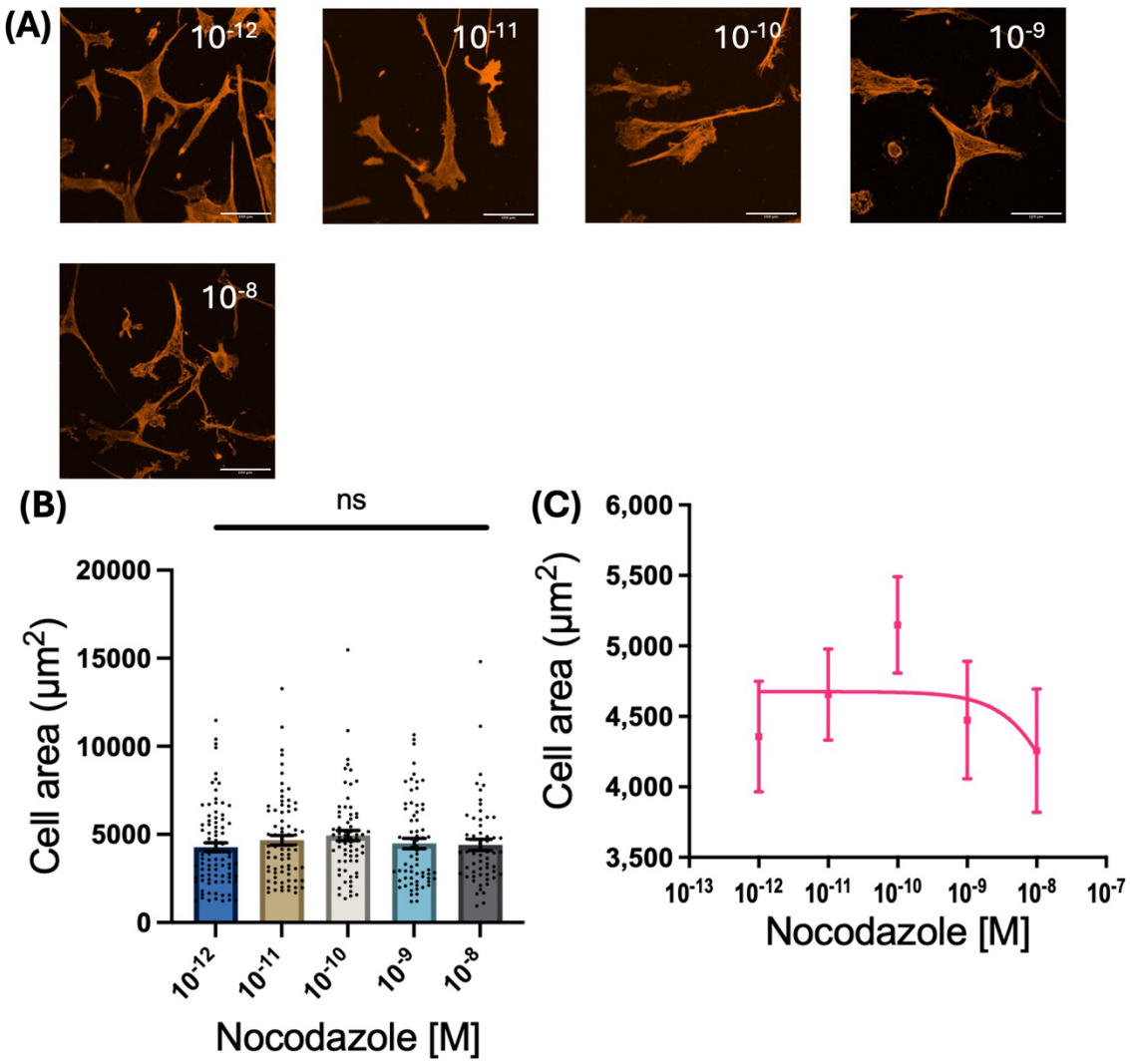

Figure 3.16. Nocodazole concentration response assay on 72 kPa hydrogels. ***(A)*** *Representative images. Scale bars represent 100 um.* ***(B)*** *VSMC area on 72 kPa hydrogels treated with nocodazole (0.001-10 nM). Shows means and SEM. Statistical significance assessed by One-way ANOVA and Tukey's multiple comparisons test.* ***(C)*** *Dose response curve showing VSMC area in response to nocodazole treatment. Shows means and SEM. Data are based on measurements of 357 VSMCs from 5 independent experiments.*

Analysis of this data revealed that Nocodazole treatment had no significant effect on VSMC area when seeded on rigid matrix (Figure 3.16B).

3.5.10 GSK3 inhibition reduces VSMC area on rigid matrix

Following this, I examined the effect of inhibiting GSK3b with inhibitor A1070722. GSK3b is a serine-threonine kinase involved in several intracellular signalling pathways. Notably it is involved in modulating the Wnt and Notch pathways, suggesting a key role in the regulation of cell proliferation, repair and tissue development. Its activity has also been linked to processes including metabolic regulation, DNA repair and regulation of

microtubule dynamics through its interaction with the microtubule-associated protein Tau[207].

Cells were seeded on pliable hydrogels in basal media and treated with A1070722 (0.001-10 nM) for 1 hour. Cells were also co-treated with Ang II (10 µM) for 30 min prior to imaging.

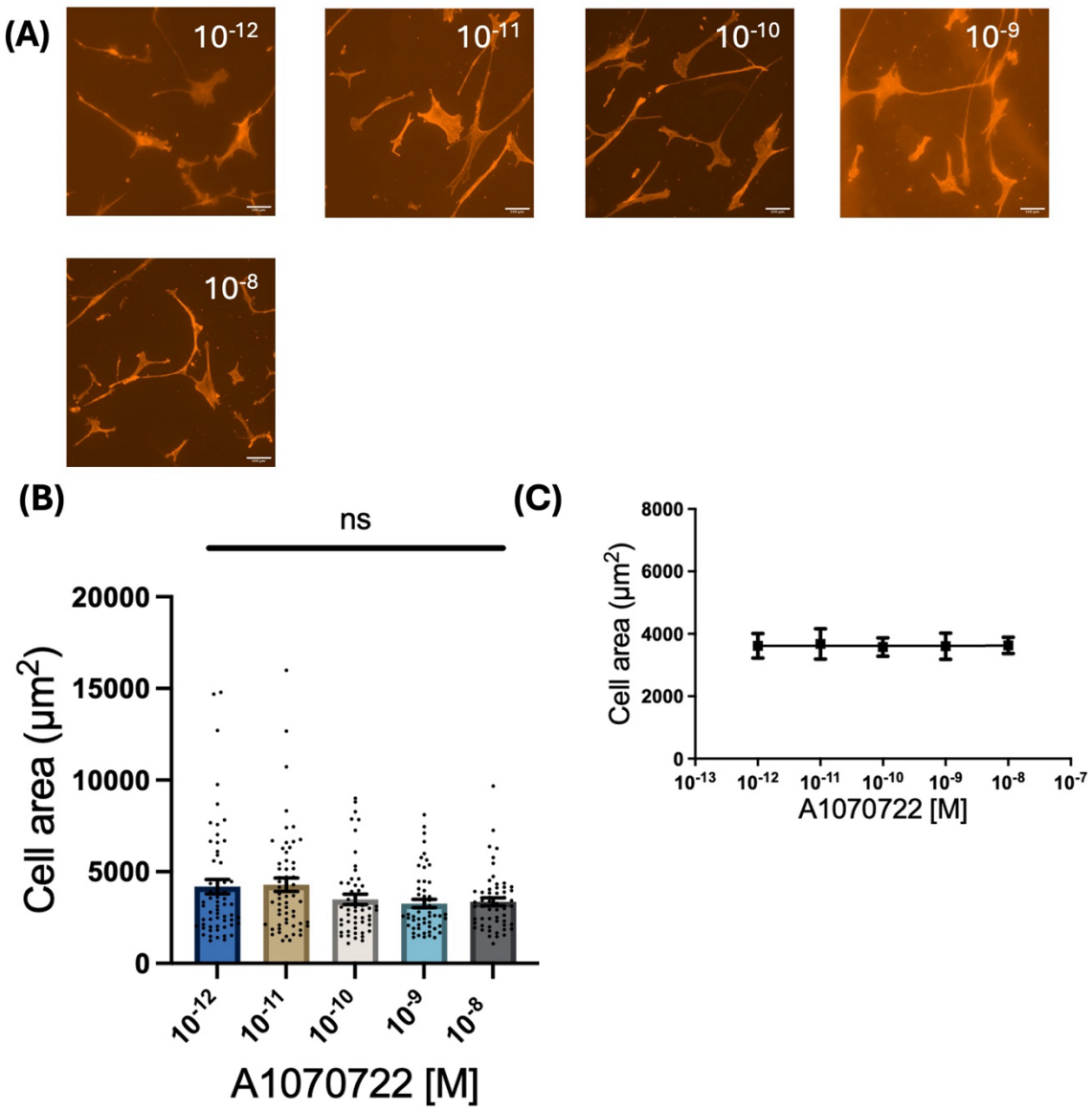

Figure 3.17. A1070722 concentration response assay on 12 kPa hydrogels. ***(A)*** *Representative images. Scale bars represent 100 µm.* ***(B)*** *VSMC area on 12kPa hydrogels treated with A1070722 (0.001-10 nM). Shows means and SEM. Statistical significance assessed by One-way ANOVA and Tukey's multiple comparisons test.* ***(C)*** *Dose response curve showing VSMC area in response to A1070722 treatment. Shows means and SEM. Data are based on measurements of 281 VSMCs from 4 independent experiments.*

Analysis of this data revealed that A1070722 treatment had no significant effect on VSMC area when seeded on pliable matrix (Figure 3.17B).

Next, cells were seeded on rigid matrices and treated with A1070722.

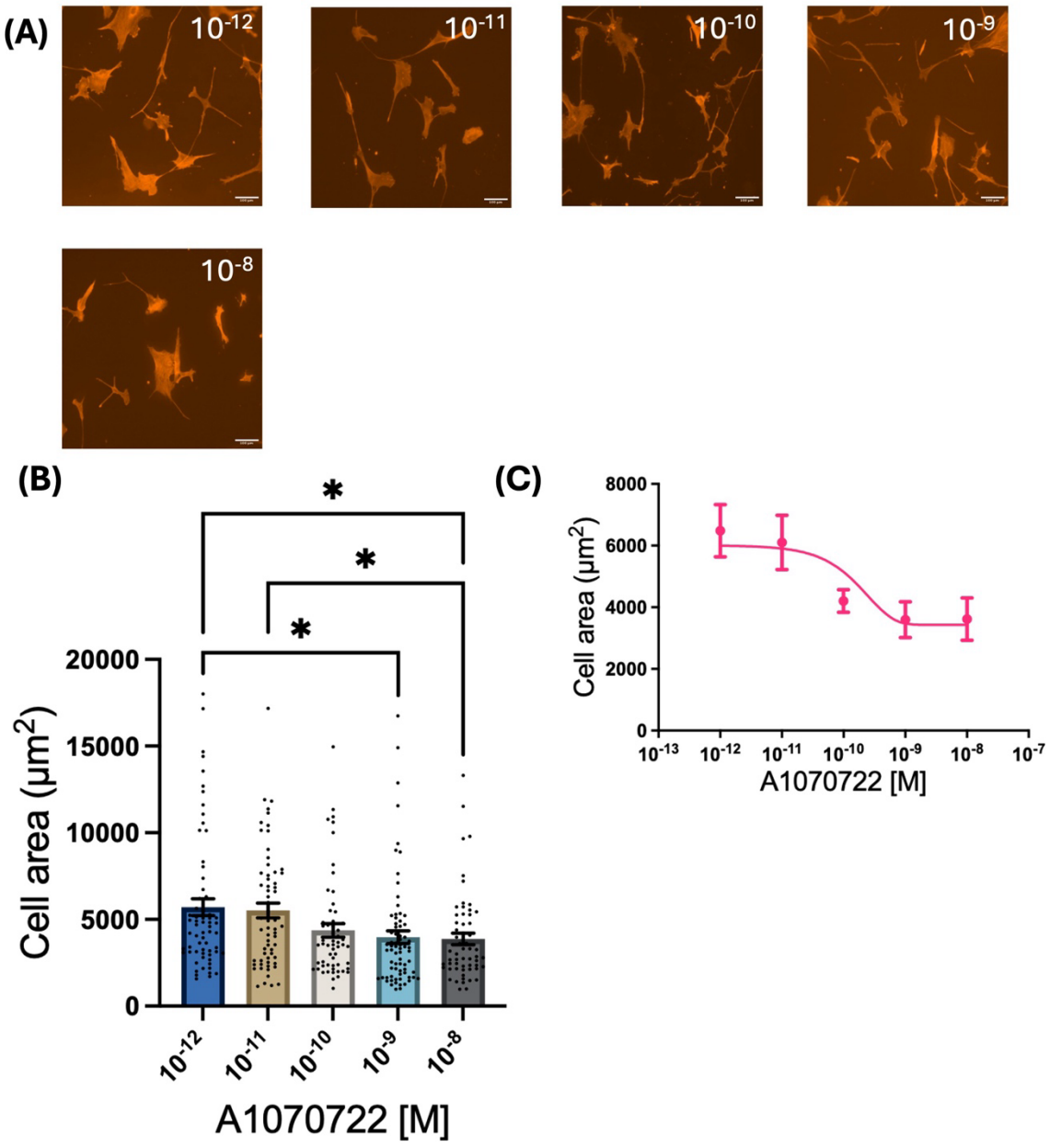

Figure 3.18. A1070722 concentration response assay on 72 kPa hydrogels. ***(A)*** *Representative images. Scale bars represent 100 µm.* ***(B)*** *VSMC area on 72 kPa hydrogels treated with A1070722 (0.001-10 nM). Shows means and SEM. Statistical significance assessed by One-way ANOVA and Tukey's multiple comparisons test (* = p<0.05).* ***(C)*** *Dose response curve showing VSMC area in response to A1070722 treatment. Shows means and SEM. Data are based on measurements of 314 VSMCs from 4 independent experiments.*

This data shows that A1070722 treatment induced a concentration dependent reduction in the area of VSMCs seeded on rigid matrix (Figure 3.18B). Cell area was reduced from

5708 μm^2 at the lowest tested concentration (0.001 nM) to 3873 μm^2 at the highest concentration (10 nM). Regression analysis determined the half-maximal inhibitory concentration (IC_{50}) to be approximately 10^{-10} M (Figure 3.18C).

3.5.11 Chk2 inhibition reduces VSMC area on rigid matrix

Next, I examined the effect of inhibiting Chk2 on VSMC area response to matrix stiffness. Chk2 is a serine-threonine kinase involved in the response to DNA damage which it mediates through its pro-apoptotic and pro-DNA repair activity. An important tumour suppressor gene, Chk2 is integrated into anti-proliferative pathways such as ATM-Chk2 and interacts with several known regulators of cell cycle, including P53 and E2F1[208]. To examine the role of Chk2 in this system, the inhibitor AZD7762 was used. AZD7762 is a selective ATP-competitive inhibitor under investigation as a potential adjuvant therapy in the treatment of some cancers.

Cells were first seeded on pliable hydrogels in basal media, treated with AZD7762 (0.001-10 nM) for 1 hour and co-treated with 10 μM Ang II for 30 min.

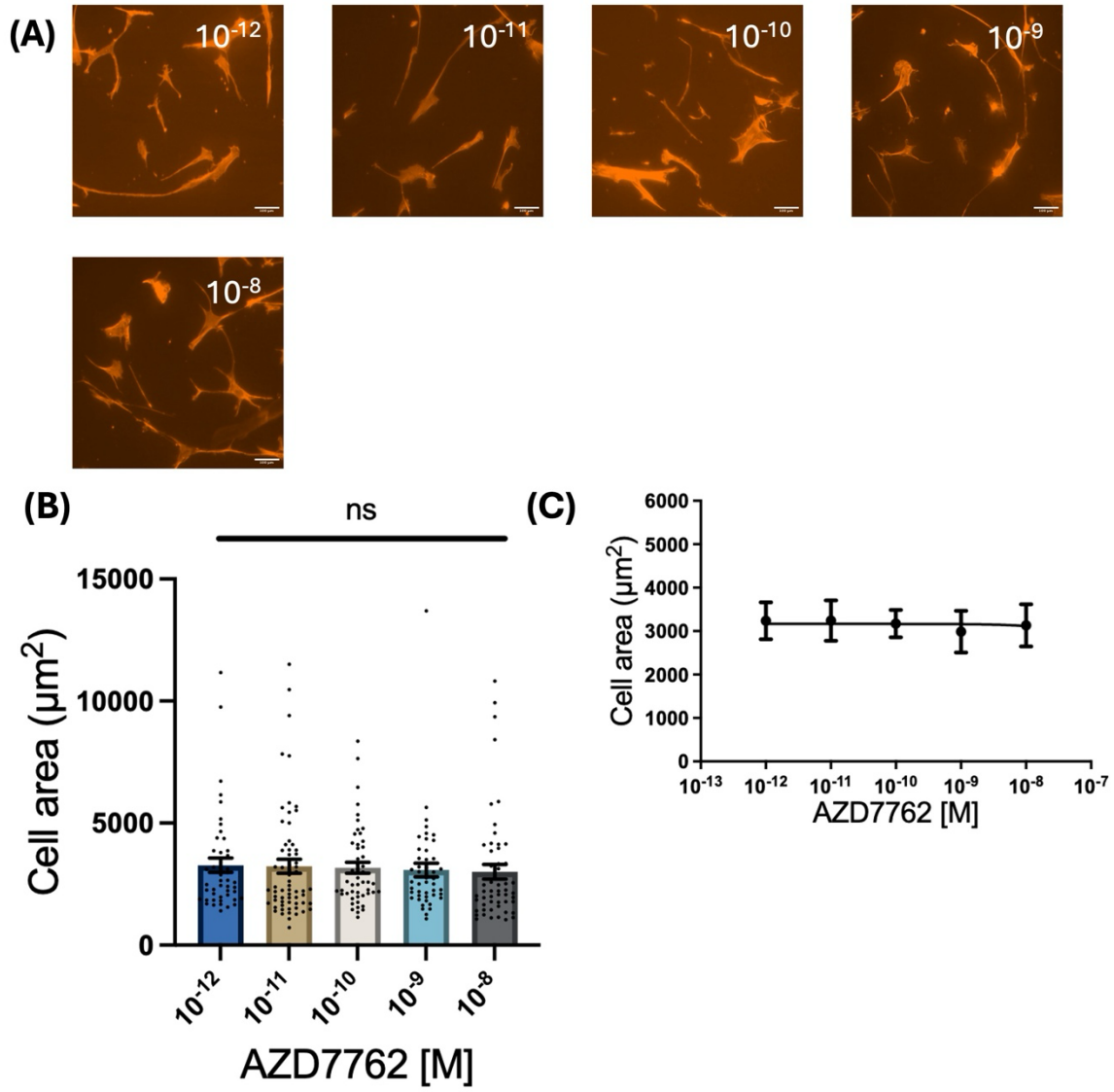

Figure 3.19. AZD7762 concentration response assay on 12 kPa hydrogels. ***(A)*** *Representative images. Scale bars represent 100 µm.* ***(B)*** *VSMC area on 12 kPa hydrogels treated with AZD7762 (0.001-10 nM). Shows means and SEM. Statistical significance assessed by One-way ANOVA and Tukey's multiple comparisons test.* ***(C)*** *Dose response curve showing VSMC area in response to AZD7762 treatment. Shows means and SEM. Data are based on measurements of 263 VSMCs from 3 independent experiments.*

Analysis revealed that AZD7762 treatment had no significant effect on VSMC area when seeded on pliable hydrogels (Figure 3.19B).

Next, cells were seeded on rigid matrices and treated with AZD7762.

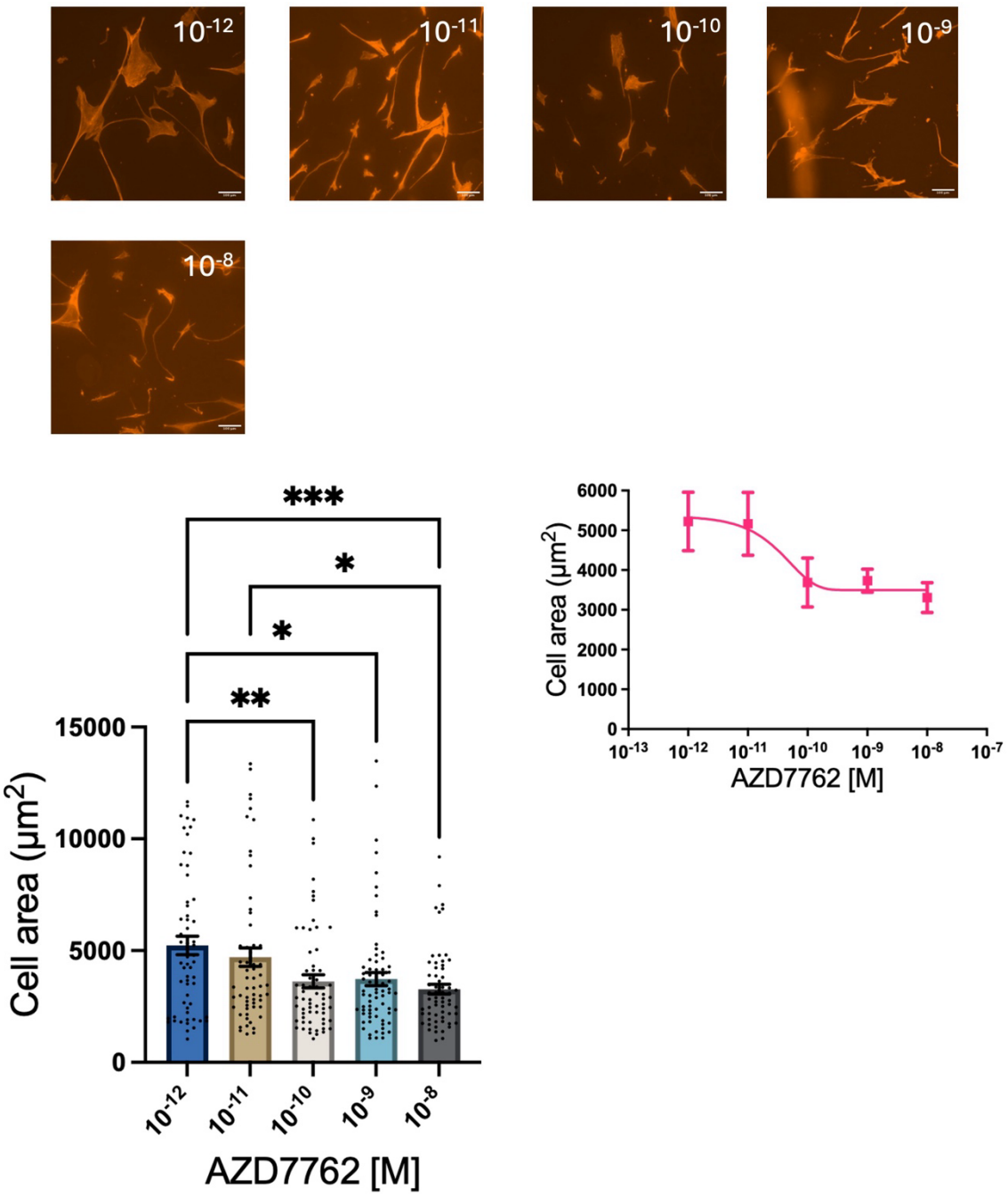

Figure 3.20. AZD7762 concentration response assay on 72 kPa hydrogels. ***(A)*** *Representative images. Scale bars represent 100 µm.* ***(B)*** *VSMC area on 72 kPa hydrogels treated with AZD7762 (0.001-10 nM). Shows means and SEM. Statistical significance assessed by One-way ANOVA and Tukey's multiple comparisons test.* ***(C)*** *Dose response curve showing VSMC area in response to AZD7762 treatment. Shows means and SEM. Data are based on measurements of 315 VSMCs from 3 independent experiments.*

This data shows that AZD7762 induced a concentration dependent reduction in area of VSMCs seeded on rigid hydrogels and co-treated with Ang II (Figure 3.20B). Mean cell area was reduced from 5232 μm^2 at the lowest tested concentration (0.001 nM) to 3275 μm^2 at the highest tested concentration (10 nM). Regression analysis determined the half-maximal inhibitory concentration (IC_{50}) to be approximately 10^{-10} M (Figure 3.20C).

3.5.12 ATM inhibition reduces VSMC area on rigid matrix

Following these findings, I investigated the effects of ATM inhibition on VSMC response to matrix stiffness. ATM is another important serine-threonine kinase involved in DNA damage response. In the vasculature ATM is known to be protective against oxidative stress and DNA damage accumulation in atherosclerosis[209]. Here, cells were seeded on pliable hydrogels in basal media, treated with the ATM inhibitor Ku55933 (0.001-10 nM) for 1 hour and co-treated with 10 µM Ang II for 30 min.

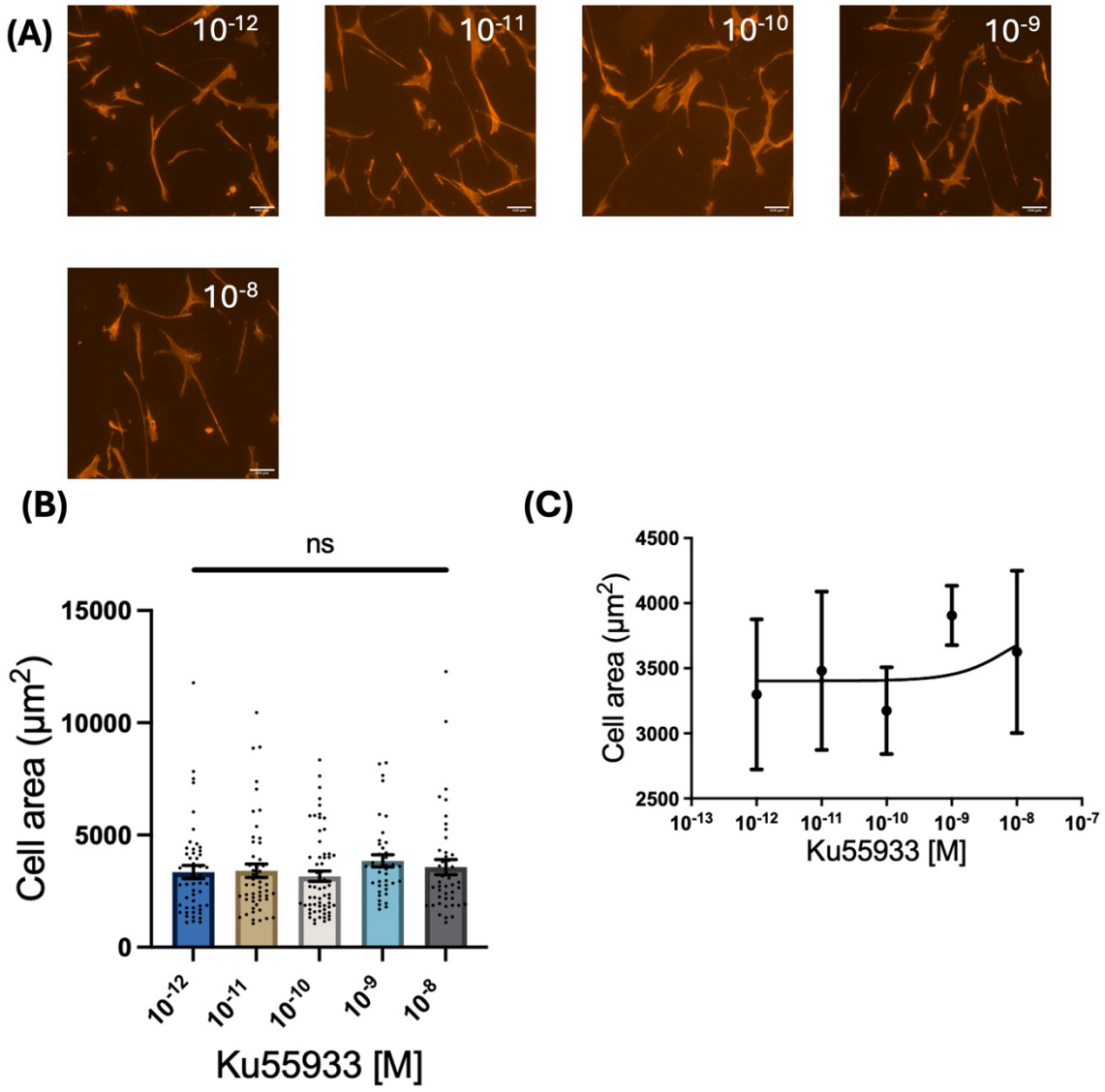

Figure 3.21. Ku55933 concentration response assay on 12 kPa hydrogels. ***(A)*** *Representative images. Scale bars represent 100 µm.* ***(B)*** *VSMC area on 12 kPa hydrogels treated with Ku55933 (0.001-10 nM). Shows means and SEM. Statistical significance assessed by One-way ANOVA and Tukey's multiple comparisons test.* ***(C)*** *Dose response curve showing VSMC area in response to Ku55933 treatment. Shows means and SEM. Data are based on measurements of 248 VSMCs from 3 independent experiments.*

Analysis revealed that Ku55933 treatment had no significant effect on VSMC area when seeded on pliable hydrogels (Figure 3.21B).

Next, cells were seeded on rigid matrices and treated with Ku55933.

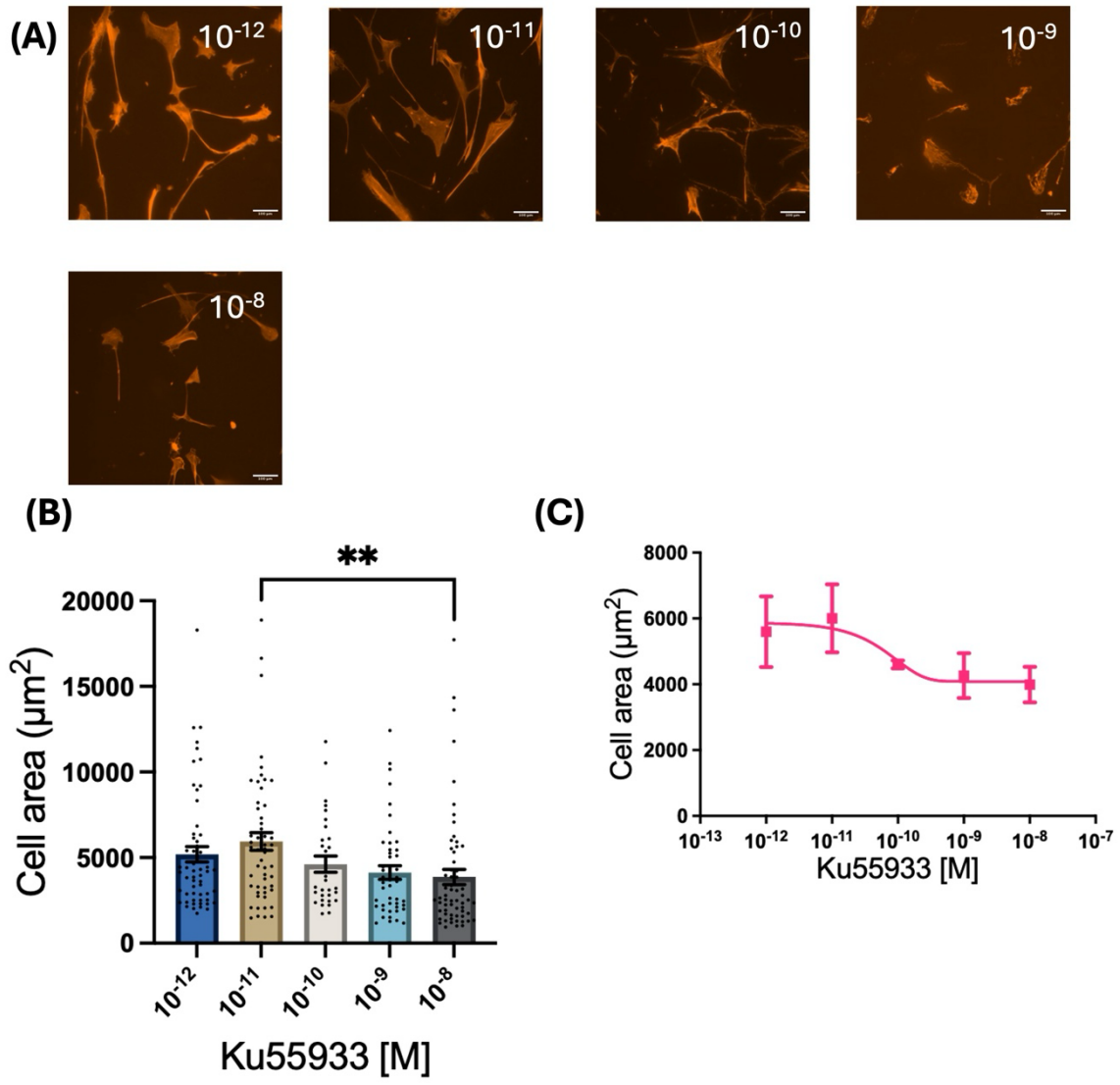

Figure 3.22. Ku55933 concentration response assay on 72 kPa hydrogels. ***(A)*** *Representative images. Scale bars represent 100 µm.* ***(B)*** *VSMC area on 72 kPa hydrogels treated with Ku55933 (0.001-10 nM). Shows means and SEM. Statistical significance assessed by One-way ANOVA and Tukey's multiple comparisons test.* ***(C)*** *Dose response curve showing VSMC area in response to Ku55933 treatment. Shows means and SEM. Data are based on measurements of 248 VSMCs from 3 independent experiments.*

These data show that Ku55933 treatment induced a significant reduction in cell area of VSMCs seeded on rigid hydrogels (Figure 3.22B). Mean cell area was reduced from 5189 μm^2 at the lowest tested concentration (0.001 nM) to 3868 μm^2 at the highest

concentration (10 nM). Regression analysis determined the half-maximal inhibitory concentration (IC_{50}) to be approximately 10^{-10} M (Figure 3.22C).

3.5.13 PARP-1 inhibition reduces VSMC area on rigid matrix

Finally, I examined the effect of PARP-1 inhibition on VSMC are response to matrix stiffness. PARP-1 is an ADP-ribosyltransferase involved in DNA damage repair, proliferation, and inflammation[210]. Like ATM, PARP-1 is known to be especially important in regulating the response to oxidative stress induced DNA damage. In VSMCs this pathway has been shown to be vital in post-DNA damage apoptosis in atherosclerosis[211].

Cells were seeded on pliable hydrogels in basal media, treated with EB47 (0.001-10 nM) for 1 hour, and co-treated with 10 μM Ang II for 30 min.

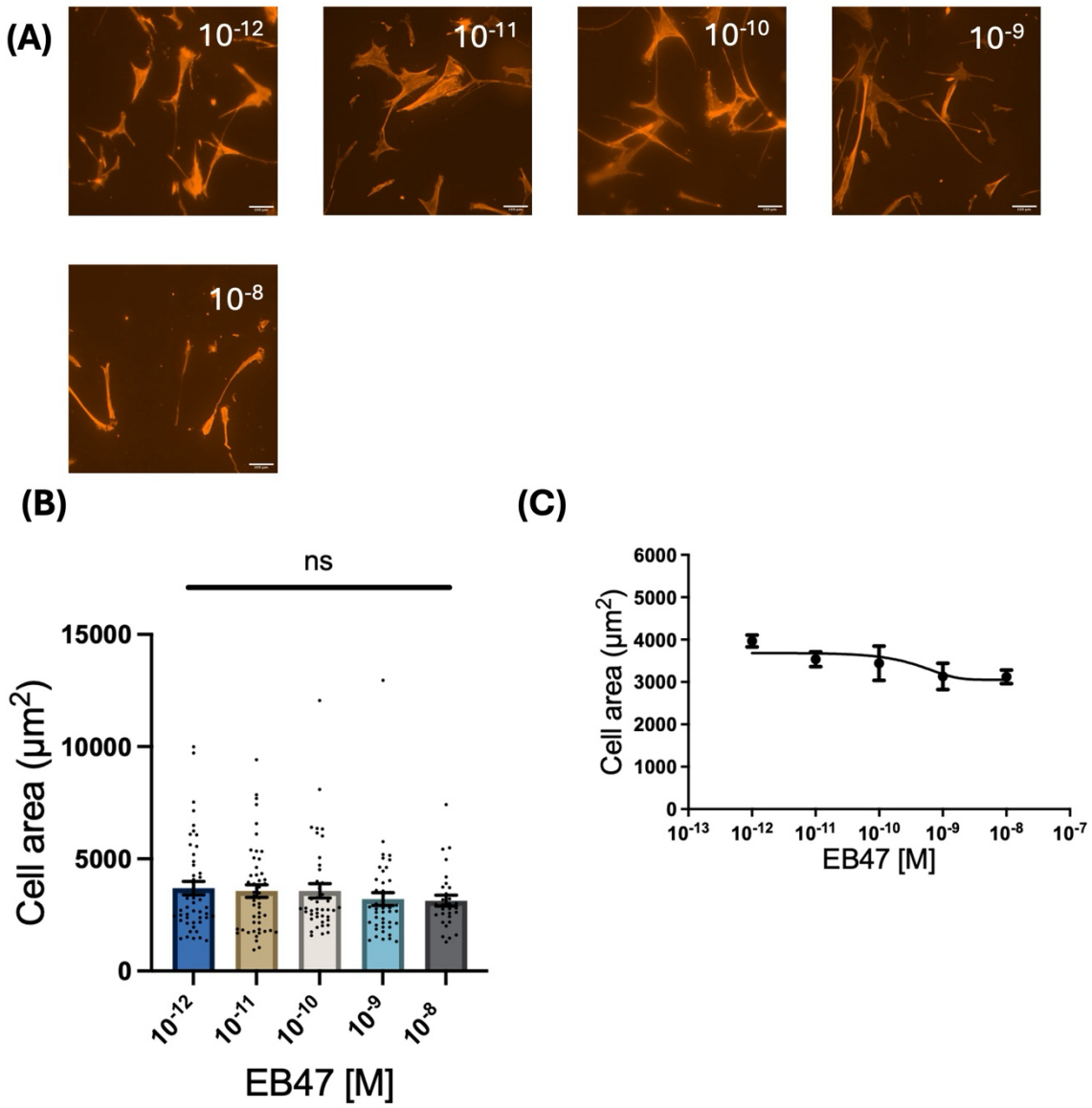

Figure 3.23. EB47 concentration response assay on 12 kPa hydrogels. ***(A)*** *Representative images. Scale bars represent 100 µm.* ***(B)*** *VSMC area on 12 kPa hydrogels treated with EB47 (0.001-10 nM). Shows means and SEM. Statistical significance assessed by One-way ANOVA and Tukey's multiple comparisons test.* ***(C)*** *Dose response curve showing VSMC area in response to EB47 treatment. Shows means and SEM. Data are based on measurements of 214 VSMCs from 3 independent experiments.*

Analysis revealed that EB47 treatment had no significant effect on VSMC area when seeded on pliable hydrogels (Figure 3.23B).

Next, cells were seeded on rigid matrices and treated with EB47.

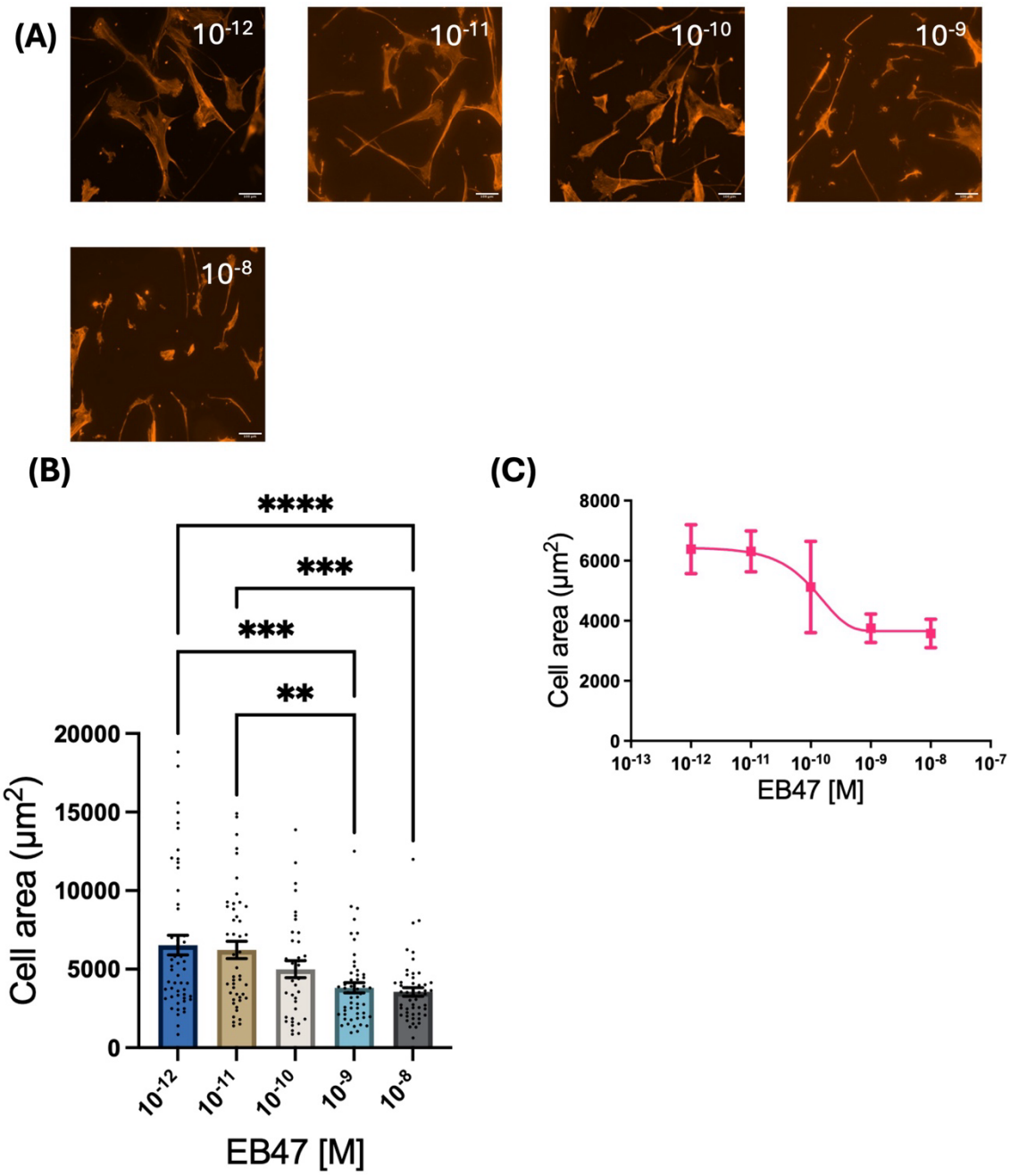

Figure 3.24. EB47 concentration response assay on 72 kPa hydrogels. ***(A)*** *Representative images. Scale bars represent 100 µm.* ***(B)*** *VSMC area on 72 kPa hydrogels treated with EB47 (0.001-10 nM). Shows means and SEM. Statistical significance assessed by One-way ANOVA and Tukey's multiple comparisons test.* ***(C)*** *Dose response curve showing VSMC area in response to EB47 treatment. Shows means and SEM. Data are based on measurements of 238 VSMCs from 3 independent experiments.*

These data show that EB47 treatment induced a concentration dependent reduction in cell area of VSMCs cultured on rigid hydrogels (Figure 3.24B). Mean cell area was reduced from 6528 µm^2 at the lowest tested concentration (0.001 nM) to 3557 µm^2 at the highest concentration (10 nM). Regression analysis determined the half-maximal inhibitory concentration (IC_{50}) to be approximately 10^{-10} M (Figure 3.24C).

3.6 Discussion

Previous work in the Warren lab has shown that VSMCs cultured on stiff (72kPa) hydrogels undergo a dysfunctional, hypertrophy-like response when treated with the contractile agonist AngII. Our working hypothesis for this phenomenon is that VSMCs cultured on 72kPa hydrogels undergo the same increase in actomyosin force generation when treated with Ang II that VSMCs on pliable hydrogels do. However, unlike cells on pliable hydrogels, VSMCs on stiff hydrogels are unable to contract, due to a failure to adequately deform their extracellular matrix. This subsequently results in dysregulation of other volume regulating processes, such as aquaporin localisation and Ca^{2+} flux, possibly driven by microtubule dynamics. This has been explored in two recent papers by the Warren group[189,212]. This response likely contributes to increased vessel wall stiffness in ageing and cardiovascular disease and is a key part of the 'smooth muscle cell stiffness syndrome' outlined in the introduction to this thesis. Therefore, identifying the signalling and mechanistic components involved in this process will provide us with a better understanding of the VSMC contribution to vessel stiffening and thus provide us with potential targets for pharmacological treatment of cardiovascular disease in clinical settings.

To achieve this, the work in this chapter focussed on utilising the Warren lab's tuneable polyacrylamide hydrogel system in conjunction with confocal microscopy. This approach enabled me to conduct biased concentration response screens, with the aim of investigating changes in VSMC area in response to targeted inhibition of key intracellular signalling components, on both pliable and rigid matrices.

***Table 3.2. List of compounds used in Chapter 3**. Shows their molecular target and their effect on VSMC area on both 12 and 72 kPa hydrogels.*

		Area Response	
Drug	**Target**	**12 kPa**	**72 kPa**
TCAQP1	Aquaporin 1	Reduced	Reduced
TGN020	Aquaporin 4	No change	Reduced
Furosemide	NKCC	N/A	No change
STOCK2S 26	Wnk	N/A	No Change
Go6983	PKC	N/A	Reduced
Xestospongin C	IP_3R	Increased	Reduced
Dantrolene	RyR	Increased	Reduced
Epothilone B	MTs (Stabilises)	No change	Reduced
Nocodazole	MTs (Destabilises)	Increased	No change
A1070722	GSK3	No change	Reduced
AZD7762	Chk2	No change	Reduced
Ku55933	ATM	No change	Reduced
EB47	PARP-1	No change	Reduced

The first component I chose to investigate were aquaporins. Aquaporins are membrane bound water channels found in all cell types, which facilitate the flow of water into cells from the extracellular environment. It is unsurprising therefore that aquaporins play a vital role in volume regulation across diverse cell types. In VSMCs, the most prevalent aquaporin is AQP1, which is known to be highly expressed, with expression of AQP4, AQP7 and AQP9 also reported[195]. In my experiments, I decided to focus on AQP1 and 4 due to their prevalence in VSMCs and the availability of proven pharmacological inhibitors.

I first examined AQP1 with the inhibitor TCAQP1. The results of this experiment were interesting as they showed that VSMC area is reduced on both pliable and stiff hydrogels when co-treated with TCAQP1 and Ang II. The reduction in cell area was similar in both conditions. This is likely because AQP1 is highly expressed in VSMCs in normal physiological conditions, and therefore inhibiting its activity has a significant effect on cell area on both healthy (pliable) and diseased/aged (rigid) hydrogels. The potential therapeutic benefit of targeting AQP1 with the aim of ameliorating vessel stiffening is therefore limited. This is because any pharmacological agent targeting AQP1 would have a significant effect on healthy VSMCs as well as diseased/aged VSMCs. In contrast, inhibition of AQP4 with TGN020 had no effect on the area of VSMCs cultured on pliable

hydrogels. This may be due to the lower expression of AQP4 in VSMCs, but could also point to increased expression, differential localisation or increased activity of AQP4 in VSMCs under pathophysiological conditions. Previous work has highlighted the differential expression of AQP4 in disease conditions of other cell types, especially in the central nervous system[213]. Less is known regarding the expression or activity of AQP4 in disease of the cardiovascular system. However, this data provides strong evidence that aquaporins play an important role in VSMC stiffening and that targeting them may be represent a novel therapeutic strategy for treating vessel wall stiffening. AQP4 in particular, due to its null effect on VSMCs on pliable healthy hydrogels, represents an interesting potential target.

Following this, I examined the role of NKCC. NKCC is an interesting target due to its important role in volume regulation in other cell types. NKCC regulates cell volume through chloride ion influx[214] which increases osmolarity and therefore water flow through aquaporins, down the osmotic gradient. Surprisingly, the data presented here shows that inhibiting NKCC with Furosemide had no statistically significant effect on VSMC area on rigid hydrogels. However, previous work by several groups has shown that NKCC is primarily activated in response to cell shrinkage[215,216]. Therefore, as VSMCs seeded on rigid hydrogels undergo volume increase it is possible that NKCC is already downregulated in these cells. It is also possible that the lack of response observed here is due to altered ion handling within these cells. This could be caused by changes in the activity of mechanosensitive ion channels such as Piezo, or changes to mechanisms involved in release of Ca^{2+} ions from intracellular stores. Additionally, previous in vitro work has shown that inhibition of NKCC leads to hyperpolarisation of rat VSMCs[217]. This means that the minimum stimulus required for depolarisation of the membrane and contraction is reduced. We might therefore expect that the contractile response to Ang II treatment, and subsequent swelling of VSMCs on rigid matrix, would increase with Furosemide concentration in this system. Therefore, the results here suggest that NKCC is not involved in the aberrant hypertrophy-like response we observe in our VSMCs.

These findings were complemented by the finding that Wnk inhibition with STOCK2S 26 also had no significant effect on VSMC area on rigid hydrogels. Wnk was investigated as

it plays an important role in regulating the activity of ion cotransporters such as NKCC through its interaction with the kinase SPAK. Furthermore, the role of Wnk in cardiovascular health and disease is well established. For example, inhibition of Wnk has been extensively studied as a potential anti-hypertensive strategy as mutations in the Wnk gene are associated with a type of inherited hypertension known as Gordon's syndrome[218]. Currently, there is little published data regarding the role of Wnk in VSMCs in either health or disease. However, it is known that inhibition of Wnk affects cell volume in other cell types. For example, it has been shown that inhibition of Wnk in natural killer cells results in reduced volume and cell motility[219]. Wnk activity is known to be regulated by Ca^{2+} flux, further suggesting that changes to intracellular ion handling play a role in VSMC response to matrix stiffness.

PKC inhibition with Go6983 caused a significant reduction in VSMC area on rigid hydrogels. PKC is an important intracellular signalling molecule involved in a range of processes, including localisation of aquaporins to the cell membrane[202]. One of the key activators of PKC is Ca^{2+} signalling. This suggests a direct link between contractile activity, which itself results from increased cytosolic Ca^{2+} levels, and the movement of aquaporins to the membrane, resulting in increased water flow into the cell and increased volume. To further investigate the role of Ca^{2+} flux, I examined the effects of the IP_3R inhibitor xestospongin C, and the RyR inhibitor dantrolene, on VSMC area response to matrix rigidity. IP_3R is the sarcoplasmic receptor for the signalling molecular IP_3 which is released downstream of activated GPCRs, such as by the agonist AngII. Interestingly, my results show a significant increase in cell area when treated with Xestospongin C on pliable hydrogels, and a concomitant reduction of cell area on rigid hydrogels. This finding was repeated when cells were treated with the ryanodine receptor inhibitor, dantrolene. The involvement of Ca^{2+} in the contractile process is well established. However, these results appear to directly link Ca^{2+} flux, induced by AngII stimulation, to the dysfunctional, hypertrophy-like swelling of VSMCs on rigid hydrogels. Currently, most work examining the role of Ca^{2+} in cardiovascular disease has focussed on the cardiomyocyte and endothelial cell populations, with little focus on the VSMC. However, the results here highlight a significant issue regarding the pharmacological treatment of disease, which is, in this context, the matrix-dependent divergence in drug

response. As Ca^{2+} signalling is a ubiquitous signalling pathway it is unsurprising that inhibiting IP_3R and RyR resulted in equally significant effects in VSMCs cultured on the pliable (healthy mimicking) hydrogel as on the rigid (disease mimicking) hydrogel. It is therefore necessary to examine other pathways and mechanisms that regulate Ca^{2+} that may allow for more targeted treatment of diseased VSMCs.

One possible target is the microtubule cytoskeleton. It is known that Ca^{2+}-Microtubule crosstalk is an important part of Ca^{2+} signal modulation[220]. For example, activation of calmodulin by Ca^{2+} results in the recruitment of MAPK, and the subsequent phosphorylation of microtubule-associated proteins (MAPs) which modulate microtubule dynamics[221]. Conversely, work has also shown that microtubules possess the ability to sequester Ca^{2+}, thus modulating downstream Ca^{2+} signalling[222]. I first examined the effect of microtubule stabilisation with the compound epothilone B. This resulted in a significant reduction in area of VSMCs cultured on stiff substrate and no significant change in cell area on pliable substrate. This finding supports the tensegrity model of microtubule dynamics. The tensegrity model states that microtubules act as compression bearing struts, where contractile forces generated by actomyosin, and the resistance generated by microtubules, are held in a state of constant tension[223]. This compression resisting force helps to oppose contractile forces and enables cells to maintain their shape. The findings here suggest that increased microtubule stabilisation leads to decreased contractile force generation. This finding is supported by other work, for example it has been shown that stabilisation of microtubules in fibroblasts leads to reduced contractile activity *in vitro*[224]. The same group found that microtubule destabilisation caused an increase in contractile activity in fibroblasts[224]. My results appear to corroborate this finding. Treatment with the microtubule destabilising compound Nocodazole caused the area of VSMCs on pliable hydrogels to increase with no significant effect on cells cultured on rigid hydrogels. Together, these findings suggest that microtubules are already maximally stabilised on pliable hydrogels and maximally destabilised on stiff hydrogels. Further work is required to further investigate the role of microtubules in VSMC stiffening. However, at this stage targeting microtubule dynamics looks like a promising avenue for developing drugs to treat smooth muscle cell stiffness syndrome.

Following these experiments, I examined the effects of inhibiting several important serine-threonine kinases. Inhibition of all three of these kinases, GSK3b, Chk2 and ATM, resulted in a significant reduction of VSMC area when seeded on rigid matrix, while having no effect on VSMCs seeded on pliable hydrogels. GSK3b is a known regulator of microtubule dynamics through its interaction with Tau. Tau is most understood in the context of neurological disease such as Alzheimer's and Parkinson's, where its aberrant accumulation causes neurons to become damaged. Interestingly, recent work in this field has shown that the Tau protein exhibits crosstalk with extracellular matrix proteins[225], and that pathological accumulation of Tau in these diseases leads to reorganisation of the ECM[226]. Tau may therefore represent an interesting target in the treatment of arterial stiffening and may be particularly interesting to examine in the context of vascular dementias.

The ATM-Chk2 pathway is a vitally important DNA damage signalling pathway and has been implicated in a range of diseases. The role of ATM-Chk2 in VSMC health and disease is not well understood. However, it is likely that both ATM and Chk2 are activated when mechanical stress is applied to the nucleus. This is relevant in the context of VSMC stiffening as we know these cells undergo dysfunctional mechanosensitive and morphological responses to matrix stiffening. It is highly likely therefore that the nucleus in these cells is placed under significant strain, possibly leading to chromatin stretching and DNA breaks[227]. Furthermore, we know these kinases are involved in microtubule reorganisation through their role as cell cycle regulators during cytokinesis[228]. It is therefore possible that Chk2 and ATM are involved in the regulation of microtubule dynamics in the context of VSMC stiffening. Further work is required to fully elucidate the role these kinases play in cardiovascular disease and arterial stiffening. However, this early work suggests they represent a promising target. Finally, the inhibition of PARP-1 with EB47 resulted in a significant reduction in VSMC area when cultured on rigid hydrogels but had no effect on those cultured on pliable hydrogels. The fact that inhibition of several kinases involved in DNA damage and chromosomal stability resulted in the same effect suggests a potentially important role for DNA damage and repair pathways in VSMC stiffening. This is unsurprising as DNA damage has been associated with VSMC ageing[229], senescence[230] and ECM remodelling[229,231].

3.6.1 Summary and Limitations

In conclusion, this chapter has interrogated some key signalling pathways involved in VSMC response to matrix stiffening. This was achieved using a tuneable polyacrylamide hydrogel system and confocal microscopy to assess changes in cell area in response to different pharmacological inhibitors. My results have identified several components that contribute to VSMC stiffening in the wider context of arterial stiffening in cardiovascular disease and ageing. I identify aquaporins as a key regulator of VSMC area increase in response to matrix stiffness. Follow-up experiments revealed that this pathway appears to be associated with regulation of Ca^{2+} flux and microtubule dynamics and possibly involves the activity of Ca^{2+} associated kinases such as PKC.

This data does have some limitations. The polyacrylamide system itself, while highly tuneable, easy to use, and cheap to perform, is a 2D system with monocultured cells. This means that our system is not able to accurately mimic the true 3D environment in which VSMCs reside *in vivo*. This is an important consideration when dealing with cells such as VSMCs which are highly mechanosensitive and are deeply integrated into their extracellular environment. Future work will be able to build on the findings here to examine the effects of these inhibitors in 3D systems such as organoids, and other co-culture systems, where VSMCs are seeded in the presence of endothelial cells and fibroblasts.

Chapter 4: Calcium Handling in VSMC Response to Matrix Stiffness

4.1 Introduction

The previous chapter identified several signalling pathways involved in the VSMC response to matrix stiffness. One of the key pathways identified was calcium signalling and its interactions with Ca^{2+}-dependent kinases and microtubules. In this chapter, I aim to further investigate the role of Ca^{2+} handling in the VSMC response to enhanced matrix rigidity.

Ca^{2+} ions are one of the most widespread and versatile intracellular signalling messengers, with involvement in nearly all cell processes, including, proliferation, migration, metabolism, cell death, transcription/translation, immune response and intracellular trafficking[232–235]. As a result of modern imaging techniques, we now know that information is encoded within the complex spatial dynamics, frequency, kinetics and amplitude of calcium signals[236]. This complexity is reflected in VSMCs, where Ca^{2+} signalling is tightly regulated to control cell contractility and homeostasis. Under resting conditions, Ca^{2+} levels in the cytosol are low. Upon stimulation, Ca^{2+} is released from intracellular stores into the cytosol where it activates several downstream signalling effectors. In VSMCs, calcium signalling is induced primarily through the binding of agonists, such as angiotensin II, to membrane bound GPCRs. This causes activation of downstream signalling molecules that induce the release of calcium from the sarcoplasmic reticulum through IP_3R and RyR[237]. As discussed, this signalling axis is central to driving the VSMC contractile machinery which is vital to VSMC function.

Of particular interest here is the cross-talk between Ca^{2+} signalling and microtubule dynamics. As previously discussed, microtubule dynamics and Ca^{2+} signalling are closely linked. Ca^{2+} mediated phosphorylation of MAPs has been shown to regulate microtubule reorganisation, and microtubules have been shown to sequester Ca^{2+} ions, thus modulating Ca^{2+} signalling. For this reason, microtubule stability and its effect on Ca^{2+} signalling in VSMC response to matrix stiffening was investigated in this chapter using the microtubule modulators colchicine and paclitaxel. Additionally, HDACs have been shown to regulate microtubule dynamics through direct deacetylation of β-tubulin[238]. This mechanism has been most clearly linked to the activity of cytosolic

HDAC6, a protein which is also associated with a range of cardiovascular diseases, including atherosclerosis and hypertension[239]. For these reasons, the role of HDACs in this signalling axis was also investigated using targeted inhibitors of HDAC1/2/3 & 6.

Remodelling of Ca^{2+} handling is a known component of disease, including cardiovascular disease such as hypertension, cardiac hypertrophy and atrial arrhythmias[240]. Matrix stiffness induced remodelling of calcium flux has been reported in epithelial-to-mesenchymal transition in prostate cancer cells[241], and in breast cancer cells, where matrix stiffness was found to attenuate Ca^{2+} influx[242]. However, our current understanding of the role Ca^{2+} signalling plays in disease and ageing of VSMCs is limited.

To investigate the role of Ca^{2+} flux in VSMC response to enhanced matrix rigidity I again utilised our polyacrylamide hydrogel system in conjunction with pharmacological agonists and antagonists of known calcium handling components. Specifically, Ca^{2+} flux was observed using fluorescence video time-lapse microscopy to detect changes in Fluo-4 fluorescence. Fluo-4 is a cell-permeable calcium indicator that exhibits Ca^{2+}-induced changes in fluorescent intensity, which can be observed when excited with a 488 nm laser[243]. VSMCs were seeded on 12 kPa and 72 kPa hydrogels and incubated in basal media for 48 hours. Approximately 30 min prior to imaging, the cells were loaded with 3 μM Fluo-4. For some conditions, cells were also treated with the compound of interest at this stage. VSMCs were incubated for 30 min prior to imaging. After 5 min of imaging, VSMCs were treated with 10 μM Ang II. For conditions where VSMCs were not pre-treated, compounds of interest were also added at this point. Cells were then imaged for a further 20 min, before treatment with the ionophore A23187.

4.2 Aims

This chapter aims to investigate Ang II induced calcium handling in VSMCs cultured on pliable and stiff hydrogels and treated with pharmacological compounds of interest. This will be achieved by:

1. Conducting video time-lapse microscopy to compare changes in Ang II induced Ca^{2+} flux over time on pliable vs rigid hydrogels.

2. Conducting video time-lapse microscopy to observe changes in Ang II induced Ca^{2+} flux over time in VSMCs co-treated with compounds of interest.

4.3 Hypotheses

I predict that Ang II induced calcium flux in VSMCs will be modulated by matrix stiffness. Additionally, I predict that this modulation will be further altered by co-treatment with various pharmacological compounds that target Ca^{2+} handling pathways.

Specifically, I hypothesise that:

1. Enhanced matrix rigidity will cause Ca^{2+} flux to be increased in VSMCs treated with Ang II.

2. Co-treatment with Ang II and compounds of interest will differentially effect VSMCs cultured on pliable and rigid substrates, revealing stiffness dependent regulation of Ca^{2+} handling in VSMCs.

4.4 Materials and Methods

Table 4.1. List of compounds used in Chapter 4. *Shows their molecular target and working concentration.*

Compound	**Target**	**Working Concentration**
Colchicine	Microtubules (destabilises)	100 nM
Paclitaxel	Microtubules (stabilises)	1 nM
MS275	HDAC1	1 nM
Santacruzamate A	HDAC2	10 nM
RGFP966	HDAC3	10 µM
Tubastatin	HDAC6	1 µM
GsMTx-4	SACs (piezo, TRP families)	500 nM
Yoda1	Piezo1 (activates)	1 µM

4.5 Results

4.5.1 VSMC Ca2+ flux is modulated by matrix rigidity

Previous work by the Warren lab has shown that matrix rigidity affects VSMC area/volume. In the previous chapter I identified components of the Ca^{2+} signalling pathway as vital elements of this matrix rigidity response. Therefore, I wanted to examine the effect of matrix rigidity on Ca^{2+} flux in VSMCs. To achieve this, cells were seeded on both 12 kPa and 72 kPa hydrogels in basal media, treated with 3 μM of the calcium dye Fluo-4 for 30 min, imaged for 5 min prior to treatment with 10 μM Ang II, and then imaged for a further 20 min. Live cell imaging videos were then analysed using FIJI and GraphPad Prism.

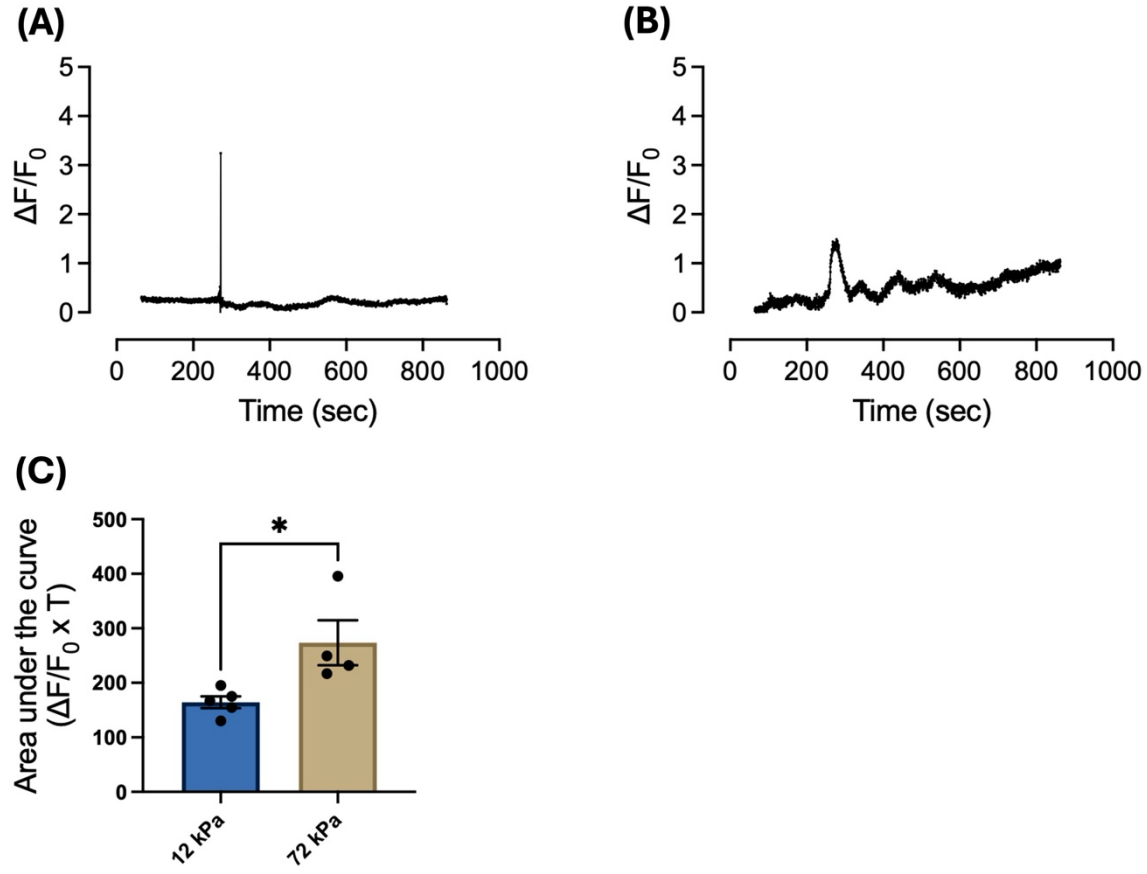

Figure 4.1. Matrix rigidity modulates Ang II induced Ca^{2+} flux in VSMCs. *Graphs show representative $\Delta F/F_0$ values over time for VSMCS cultured on **(A)** 12 kPa hydrogels and **(B)** 72 kPa hydrogels and treated with Ang II. **(C)** Graph shows area under the curve (ΔF/F0×T) for 12 kPa vs 72 kPa curves. Shows means and SEM. Statistical significance assessed by unpaired (independent) 2-sample T-test (* = p< 0.05). Mean data for individual repeats of 3 independent experiments are shown as black dots.*

Analysis of this data revealed that matrix rigidity had a significant effect on calcium flux in VSMCs. On 12 kPa hydrogels, Ang II stimulation induced a rapid spike in Ca^{2+} levels

which then rapidly returned to baseline (Figure 4.1A). This contrasts with 72 kPa hydrogels where Ang II stimulation induced a much smaller initial peak with a prolonged increase in intracellular Ca^{2+} level (Figure 4.1B). Analysis of area under the curve (AUC) showed that VSMCs cultured on stiff matrix have significantly higher AUC (Figure 4.1C). This suggests that VSMCs cultured on rigid hydrogels have elevated levels of Ca^{2+} signalling compared to those cultured on pliable hydrogels.

4.5.2 Microtubule destabilisation increases Ca^{2+} flux on pliable hydrogels

Following these findings, I wanted to examine the role of microtubules in regulating Ca^{2+} flux in VSMC response to matrix stiffness. As discussed in the previous chapter, Ca^{2+}-microtubule crosstalk is a known modulator of Ca^{2+} signalling, and my previous results suggest that microtubule dynamics play a role in regulating the VSMC response to matrix stiffness. To examine the link between microtubule dynamics and Ca^{2+} flux in VSMCs I first investigated the effect of colchicine, a microtubule destabilising agent, on Ca^{2+} flux in VSMCs.

To do this, cells were seeded on 12 kPa and 72 kPa hydrogels in basal media for 48 hours prior to imaging. Cells were treated with colchicine (100 nM), or vehicle control (DMSO) during Fluo-4 loading. Cells were further incubated for 30 min, washed, returned to basal media and imaged for 30 min, during which Ang II (10 μM) was applied after 5 min, and the ionophore A23187 (20 μM) after 25 min.

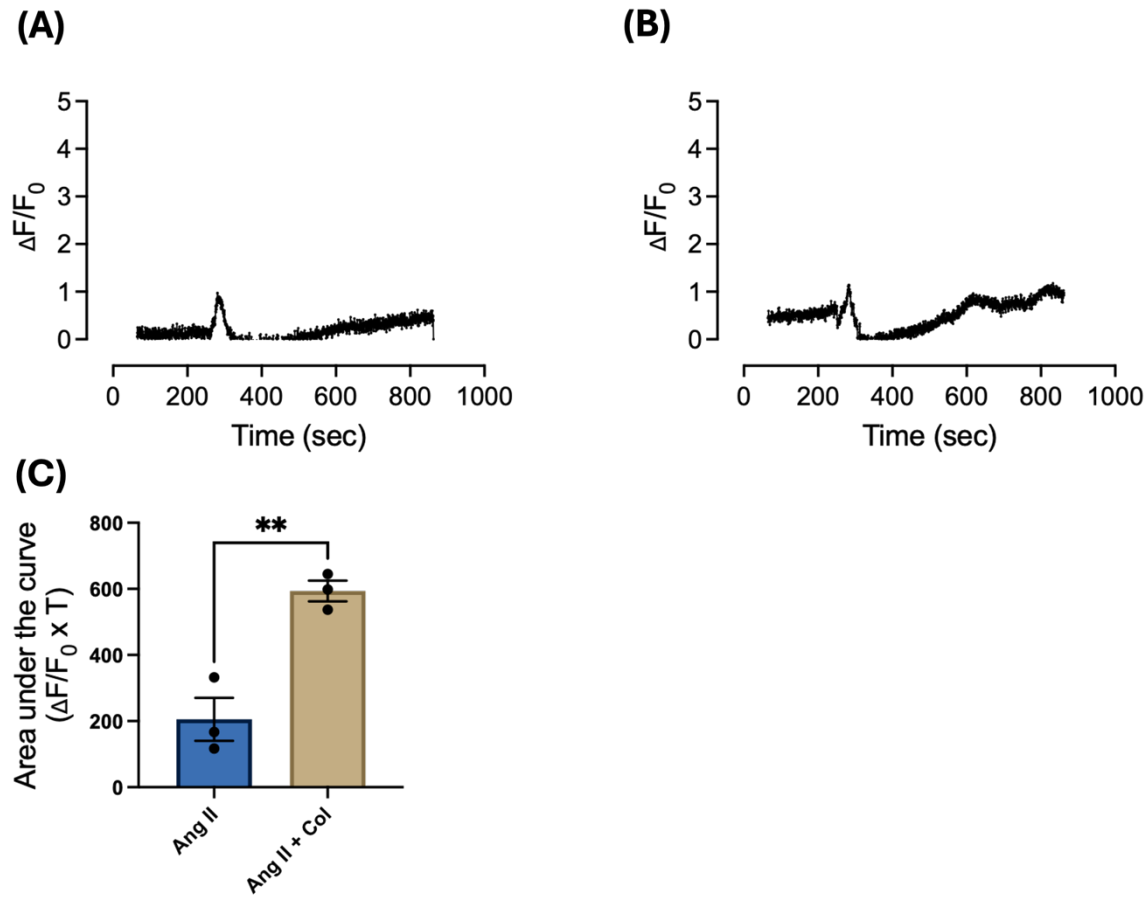

Figure 4.2. Colchicine treatment increases Ang II induced Ca^{2+} flux in VSMCs cultured on pliable hydrogels. *Graphs show representative $\Delta F/F_0$ values over time for VSMCS treated with **(A)** vehicle control and **(B)** colchicine (100 nM) and co-treated with Ang II on 12 kPa hydrogels. **(C)** Graph shows area under the curve (ΔF/F0×T) for vehicle control vs colchicine treated curves. Shows means and SEM. Statistical significance assessed by unpaired (independent) 2-sample T-test (** = p< 0.01). Mean data for individual repeats of 3 independent experiments are shown as black dots.*

Analysis of this data revealed that microtubule destabilisation with colchicine significantly increased Ca^{2+} flux compared to the vehicle control. Treatment with colchicine induced a small initial peak, similar to the vehicle control, that was followed by a gradual increase in intracellular Ca^{2+} which persisted throughout the timelapse and didn't return to baseline (Figure 4.2B). Further analysis revealed that VSMCs treated with Colchicine had significantly higher AUC (Figure 4.2C).

Following this, Ca^{2+} flux was investigated in VSMCs treated with colchicine on rigid hydrogels.

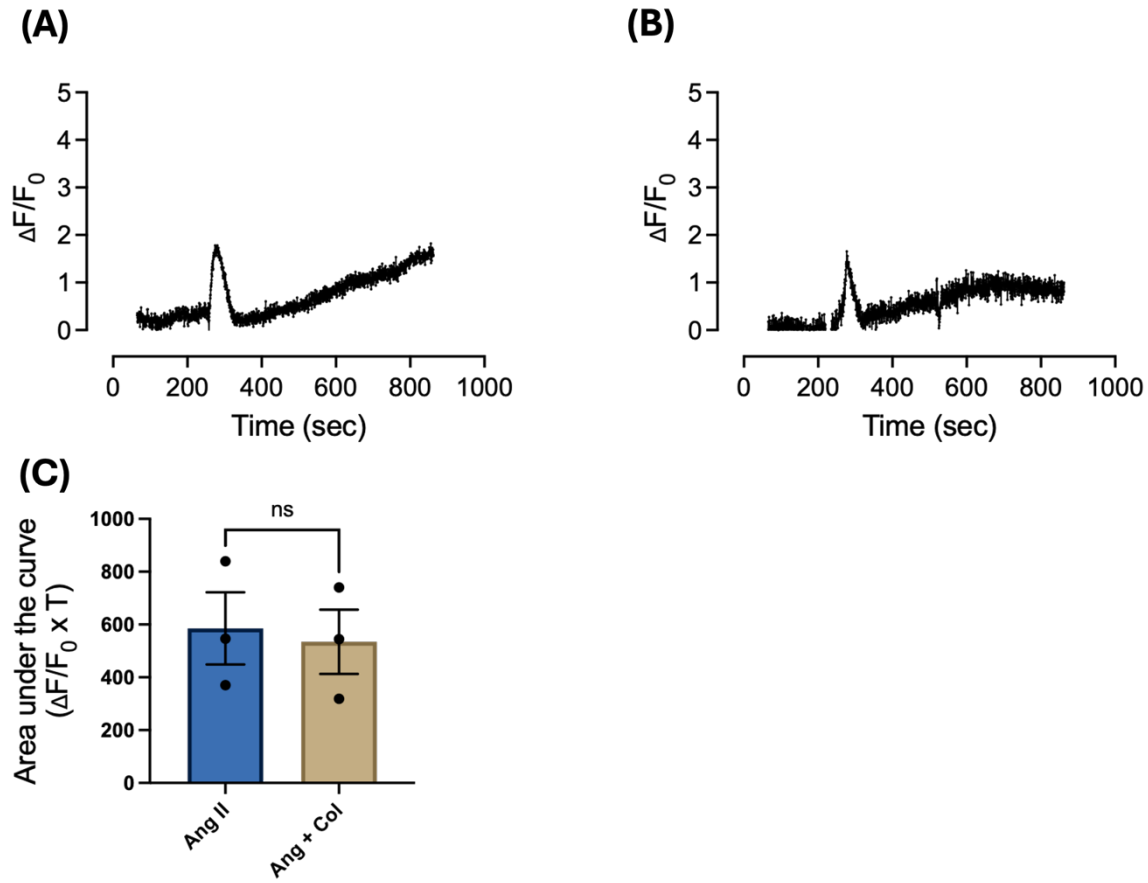

Figure 4.3. Colchicine treatment has no effect on Ang II induced Ca^{2+} flux in VSMCs cultured on rigid hydrogels. *Graphs show representative $\Delta F/F_0$ values over time for VSMCS treated with **(A)** vehicle control and **(B)** colchicine (100 nM) and co-treated with Ang II on 72 kPa hydrogels. **(C)** Graph shows area under the curve (ΔF/F0×T) for vehicle control vs colchicine treated curves. Shows means and SEM. Statistical significance assessed by unpaired (independent) 2-sample T-test. Mean data for individual repeats of 3 independent experiments are shown as black dots.*

Analysis of these results found that colchicine treatment had little effect on Ca^{2+} flux in VSMCs on rigid hydrogels compared to vehicle control (Figure 4.3A/B). No significant difference in was observed in AUC (Figure 4.3C).

4.5.3 Microtubule stabilisation increases Ca^{2+} flux on pliable hydrogels and reduces Ca2+ flux on rigid hydrogels

Next, I investigated the effect of microtubule stabilisation on Ca^{2+} flux in VSMCs. To do this I utilised the microtubule stabilising agent paclitaxel.

Here, cells were seeded on 12 kPa and 72kPa hydrogels in basal media and incubated for 48 hours. Cells were treated with paclitaxel (1 nM) or vehicle control (DMSO) during

the Fluo-4 loading step. Cells were imaged and treated with Ang II and A23187 as previously described.

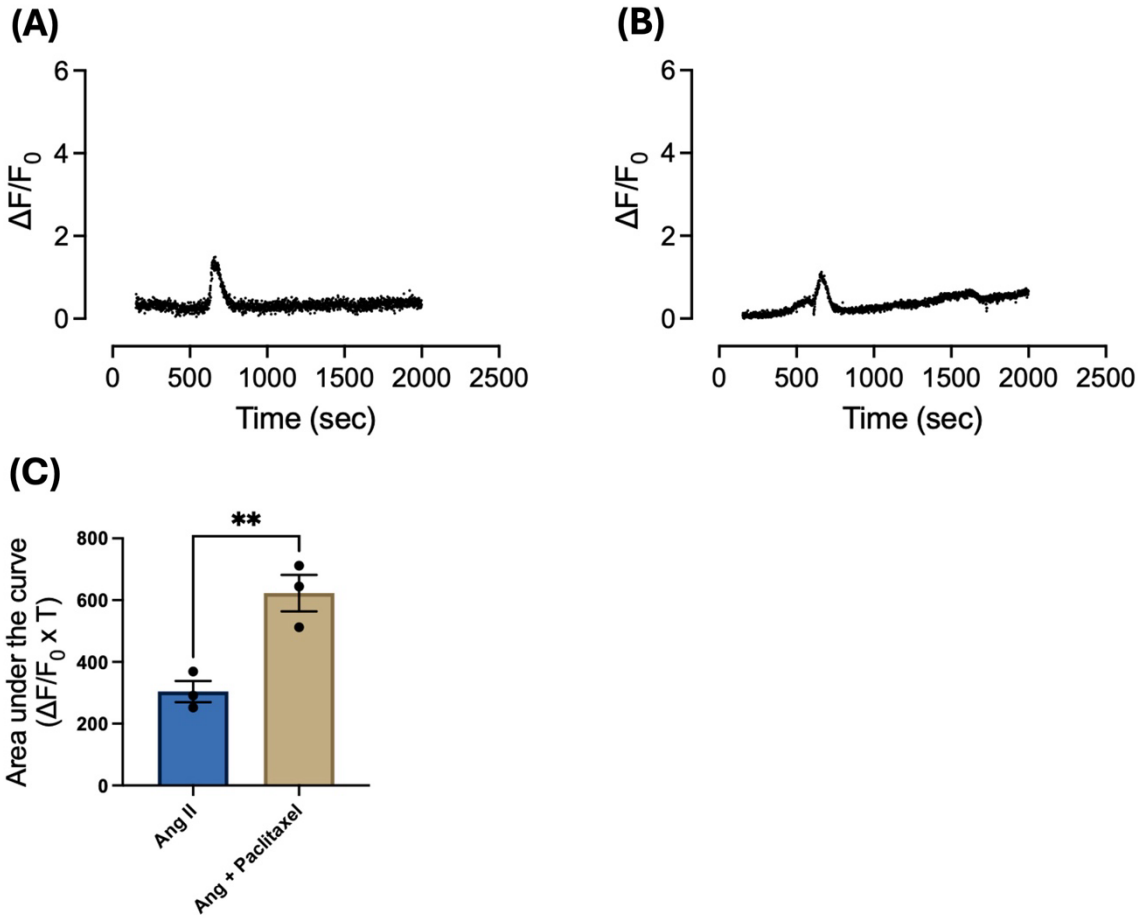

Figure 4.4. Paclitaxel treatment increases Ang II induced Ca^{2+} flux in VSMCs cultured on pliable hydrogels. *Graphs show representative $\Delta F/F_0$ values over time for VSMCS treated with **(A)** vehicle control and **(B)** paclitaxel (1 nM) and co-treated with Ang II on 12 kPa hydrogels. **(C)** Graph shows area under the curve (ΔF/F0×T) for vehicle control vs paclitaxel treated curves. Shows means and SEM. Statistical significance assessed by unpaired (independent) 2-sample T-test (** = p< 0.01). Mean data for individual repeats of 3 independent experiments are shown as black dots.*

These data show that paclitaxel treatment had a significant effect on Ca^{2+} flux in VSMCs cultured on pliable hydrogels. The initial Ca^{2+} spike did not appear to be significantly altered compared to vehicle control. However, paclitaxel appeared to induce a slightly prolonged increase in Ca^{2+} flux which was not present in vehicle control (Figure 4.4A/B). AUC analysis showed that paclitaxel treated cells have a significantly higher AUC compared to controls on pliable hydrogels (Figure 4.4C).

Next, this experiment was repeated on VSMCs seeded on rigid hydrogels.

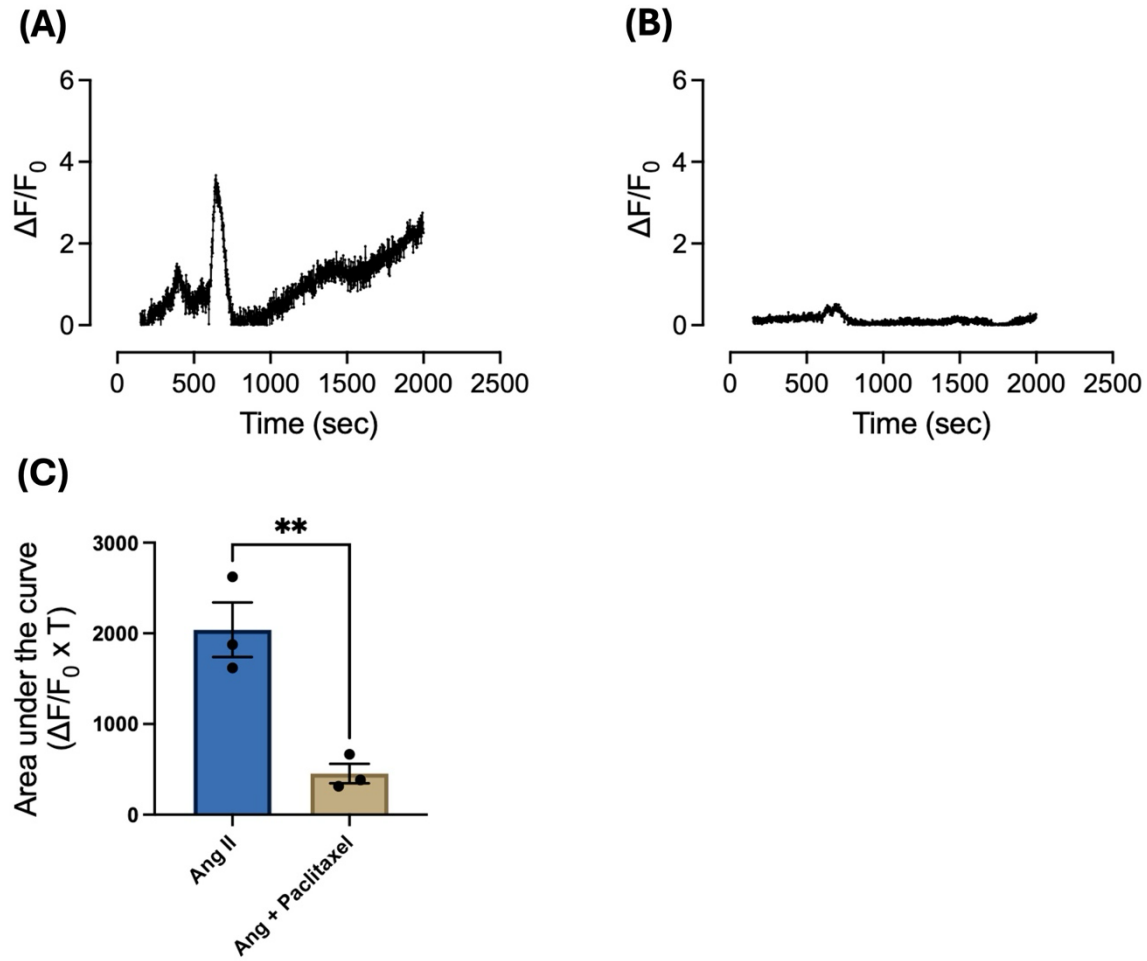

Figure 4.5. Paclitaxel treatment reduces Ang II induced Ca^{2+} flux in VSMCs cultured on rigid hydrogels. *Graphs show representative $\Delta F/F_0$ values over time for VSMCS treated with **(A)** vehicle control and **(B)** paclitaxel (1 nM) and co-treated with Ang II on 72 kPa hydrogels. **(C)** Graph shows area under the curve (ΔF/F0×T) for vehicle control vs paclitaxel treated curves. Shows means and SEM. Statistical significance assessed by unpaired (independent) 2-sample T-test (** = p< 0.01). Mean data for individual repeats of 3 independent experiments are shown as black dots.*

This analysis revealed that paclitaxel significantly reduced Ca^{2+} flux on rigid hydrogels. The initial spike was substantially reduced compared to vehicle control and Ca^{2+} flux rapidly returned to baseline. This is in sharp contrast to the vehicle control where a prolonged increase in Ca^{2+} flux was observed (Figure 4.5A/B). AUC analysis revealed that paclitaxel treated cells had a significantly reduced AUC compared to vehicle control on rigid hydrogels (Figure 4.5C).

4.5.4 Inhibition of Class I HDAC had no significant effect on Ca^{2+} flux on either pliable or rigid hydrogels

Following this I wanted to examine the role of the HDAC1 in regulation of Ca^{2+} flux in VSMC response to matrix stiffness. Previous work by the Warren group has identified

HDACs as key players in the regulation of the VSMC response to matrix stiffness[190]. HDAC1 is a class I HDAC, ubiquitously expressed across tissues and involved primarily in regulation of cell cycle, differentiation, DNA repair and transcriptional repression[244]. Loss of HDAC1 function has been associated with vascular calcification and the progression of cardiovascular disease[245]. To investigate the activity of HDAC1 I used one of its known pharmacological inhibitors, MS275.

Here, cells were seeded on 12 kPa and 72kPa hydrogels in basal media and incubated for 48 hours. Cells were treated with MS275 (1 nM) or vehicle control (DMSO) during Fluo-4 loading. Cells were imaged and treated with Ang II and A23187 as previously described.

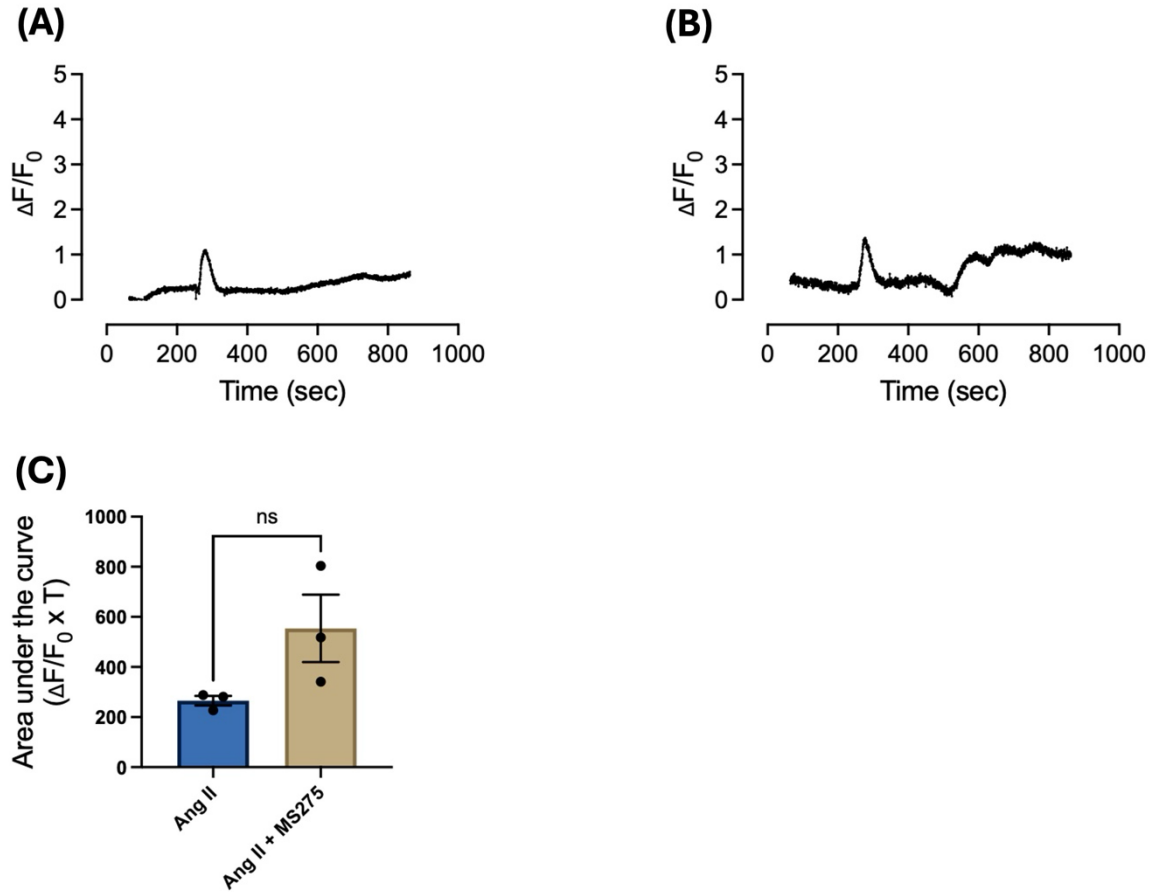

Figure 4.6. MS275 treatment increases Ang II induced Ca^{2+} flux in VSMCs cultured on pliable hydrogels. *Graphs show representative $\Delta F/F_0$ values over time for VSMCS treated with **(A)** vehicle control and **(B)** MS275 (1 nM) and co-treated with Ang II on 12 kPa hydrogels. **(C)** Graph shows area under the curve (ΔF/F0×T) for vehicle control vs MS275 treated curves. Shows means and SEM. Statistical significance assessed by unpaired (independent) 2-sample T-test. Mean data for individual repeats of 3 independent experiments are shown as black dots.*

These data show that MS275 treatment had no statistically significant increase in Ca^{2+} flux compared to vehicle control on pliable hydrogels. Interestingly, MS275 appeared to

induce a series of follow-up peaks after the initial peak as part of a prolonged increase in intracellular Ca^{2+} (Figure 4.6B). However, AUC analysis showed that VSMCs treated with MS275 had no statistically significant change in Ca^{2+} flux compared to vehicle control (Figure 4.6C).

Following this, VSMCs seeded on rigid hydrogels were also treated with MS275 as described above.

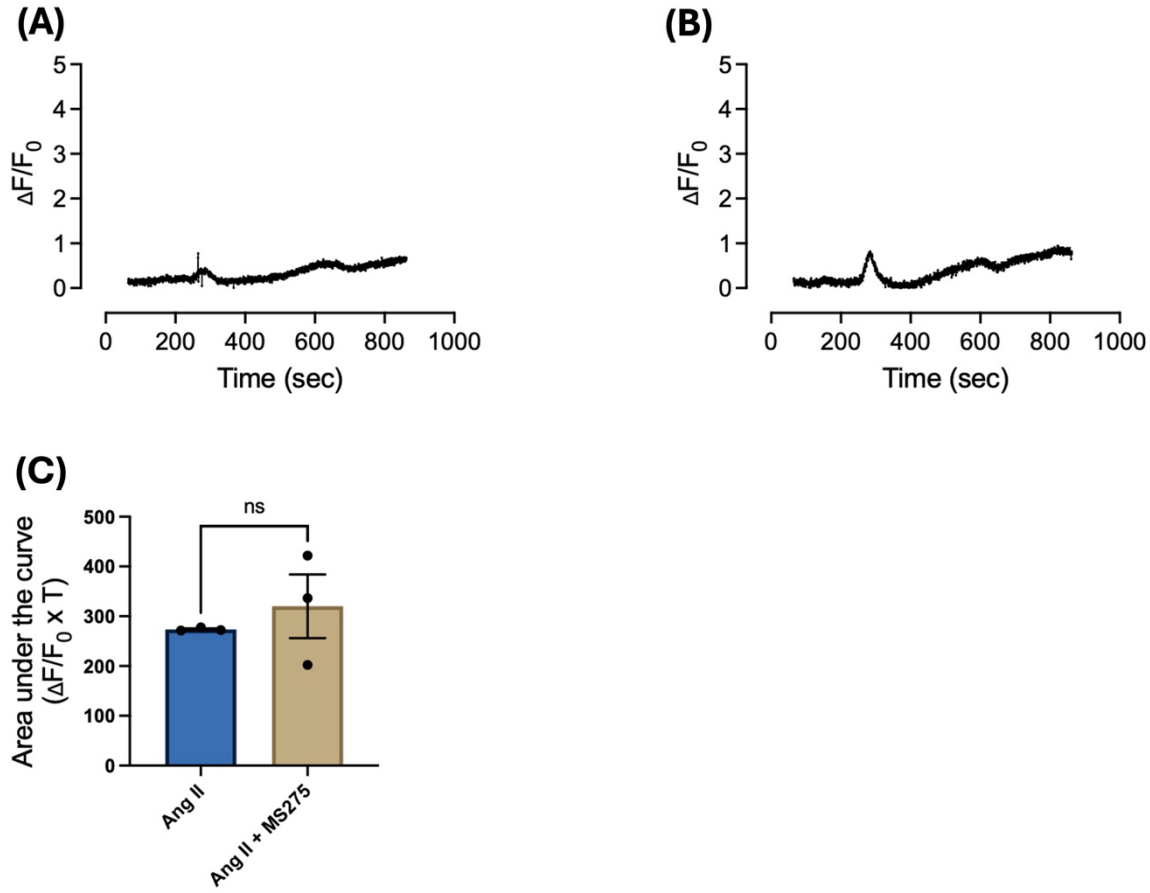

Figure 4.7. MS275 treatment has no effect on Ang II induced Ca^{2+} flux in VSMCs cultured on rigid hydrogels. *Graphs show representative $\Delta F/F_0$ values over time for VSMCS treated with **(A)** vehicle control and, **(B)** MS275 (1 nM) and co-treated with Ang II on 72 kPa hydrogels. **(C)** Graph shows area under the curve (ΔF/F0×T) for vehicle control vs MS275 treated curves. Shows means and SEM. Statistical significance assessed by unpaired (independent) 2-sample T-test. Mean data for individual repeats of 3 independent experiments are shown as black dots.*

This analysis revealed that there was no statistically significant change in Ca^{2+} flux in VSMCs seeded on rigid hydrogels and treated with MS275 compared to vehicle controls. AUC analysis confirmed that there was no significant difference in AUC between vehicle and MS275 treated cells (Figure 4.7C).

4.5.5 Effects of HDAC2/3 inhibition on Ca2+ flux in VSMCs on pliable and rigid hydrogels

Following these findings, I wanted to investigate the role of two additional class I HDACs in Ca^{2+} handling in VSMC response to matrix stiffness. Firstly, I wanted to investigate HDAC2. HDAC2 is an important transcriptional repressor with vital roles in cardiac development[246], cytokine signalling and cell-cycle progression[247]. Aberrant expression of HDAC2 is frequently observed in solid tumour neoplasm and has been linked with cardiac hypertrophy[248], cardiac ageing/failure[249] and Alzheimer's disease. I used santacruzamate A, a pharmacological inhibitor of HDAC2, to investigate its role in Ca^{2+} handling.

I also investigated the role of HDAC3 in VSMC Ca^{2+} handling. HDAC3 plays similar physiological roles to the other class I HDACs and is especially important in regulation of the inflammatory response[250]. In the cardiovascular system upregulation of HDAC3 has been associated with atherosclerosis and myocardial infarction[250]. Dysregulation of HDAC3 is also associated with neurodegenerative disease, kidney disease and autoimmune disease, usually driven by the aberrant activation of pro-inflammatory pathways[251]. To investigate the role of HDAC3 in Ca^{2+} handling I employed the widely used HDAC3 inhibitor RGFP966.

Here, cells were seeded on 12 kPa and 72kPa hydrogels in basal media and incubated for 48 hours. The cells were then loaded with fluo-4 (3 μM). VSMCs were treated with either santacruzamate A (10 nM), RGFP966 (10 μM) or DMSO vehicle control during the Ang II co-treatment step.

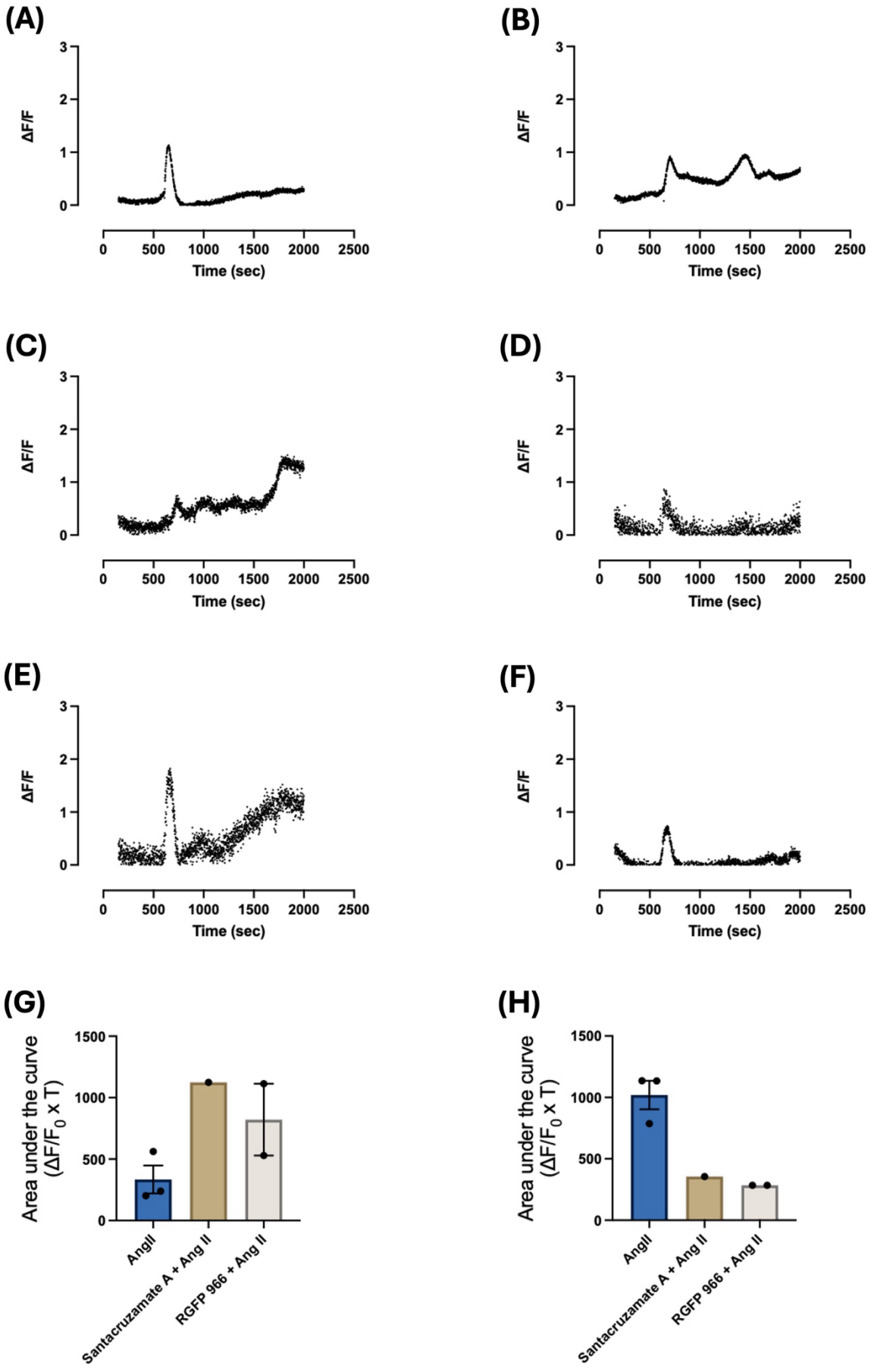
(A)
(B)
(C)
(D)
(E)
(F)
(G)
(H)
ΔF/F
Time (sec)
0
500
1000
1500
2000
2500
1
2
3
Area under the curve
(ΔF/F0 x T)
AngII
Santacruzamate A + Ang II
RGFP 966 + Ang II

Figure 4.8. Effect of class I HDAC inhibition on Ang II induced Ca^{2+} flux in VSMCs cultured on pliable and rigid hydrogels. Graphs *show representative $\Delta F/F_0$ values over time for VSMCS treated with **(A)** loading control on 12 kPa hydrogel or, **(B)** loading control on 72 kPa hydrogel or, **(C)** santacruzamate A (10 nM) on 12 kPa hydrogel or, **(D)** santacruzamate A (10 nM) on 72 kPa hydrogel or, **(E)** RGFP966 (10 μM) on 12 kPa hydrogel or, **(F)** RGFP966 (10 μM) on 72 kPa hydrogel. **(G)** Graph shows area under the curve (ΔF/F0×T) for vehicle control vs santacruzamate A vs RGFP966 treated curves on 12 kPa hydrogels. **(H)** Graph shows area under the curve (ΔF/F0×T) for vehicle control vs santacruzamate A vs RGFP966 treated curves on 72 kPa hydrogels. Shows means and SEM. Statistical analysis not performed due to N = 1 (Santacruzamate A) and N = 2 (RGFP966). Mean data for individual repeats of 1/2 independent experiments are shown as black dots.*

Analysis of these data suggest that santacruzamate A treatment results in a reduced initial Ca^{2+} spike, followed by a gradual increase in intracellular Ca^{2+} levels on pliable hydrogels (Figure 4.8C). However, on rigid hydrogels a small initial peak was observed that rapidly returned to baseline (Figure 4.8D). A similar trend was observed in RGFP966 treated cells, however on pliable hydrogels, RGFP966 appeared to induce a greater initial spike, followed by a gradual increase in intracellular Ca^{2+} (Figure 4.8E). On rigid hydrogels, RGFP966 appeared to induce a smaller initial Ca^{2+} spike that rapidly returned to baseline (Figure 4.8F). AUC analysis showed that both santacruzamate A and RGFP966 treated cells appeared to have greater AUC compared to vehicle controls on pliable hydrogels (Figure 8G). This contrasts with AUC analysis of cells on rigid hydrogels where both santacruzamate A and RGFP966 treated cells appear to have reduced AUC compared to vehicle controls (Figure 4.8H). These experiments will need to be repeated in order to statistically validate these preliminary findings.

4.5.6 Inhibition of HDAC6 has no effect on Ca^{2+} flux on pliable hydrogels

Next, I wanted to examine the role of HDAC6 in regulation of Ca^{2+} flux in VSMC response to matrix stiffness. HDAC6 is a class II histone deacetylase and has been implicated in a range of diseases including cancers, neurological disease and pathological autoimmune conditions[252]. In the cardiovascular system, HDAC6 has been associated with atherosclerosis, hypertension and myocardial hypertrophy[239]. Of note in the context of this work is the role HDAC6 plays in deacetylating α-tubulin, thus contributing to microtubule destabilisation[253]. Here, I utilised tubastatin, a potent pharmacological inhibitor of HDAC6 to investigate its role in Ca^{2+} flux in VSMCs response to matrix stiffness.

VSMCs were seeded on 12 kPa and 72kPa hydrogels in basal media and incubated for 48 hours. The cells were treated with tubastatin (1 μM) or vehicle control (DMSO) during Fluo-4 loading and then imaged and treated with Ang II and A23187 as previously described.

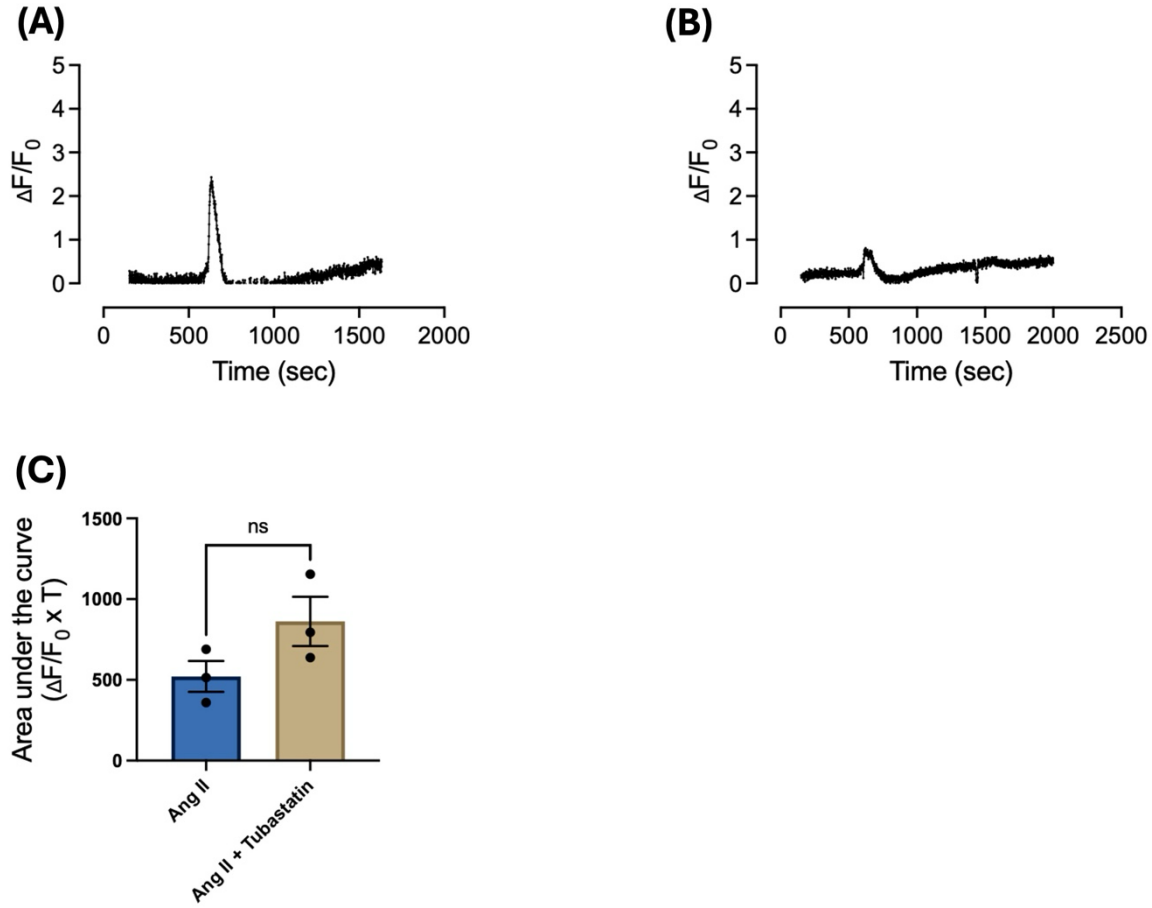

Figure 4.9. Tubastatin treatment has no effect on Ang II induced Ca^{2+} flux in VSMCs cultured on pliable hydrogels. *Graphs show representative $\Delta F/F_0$ values over time for VSMCS treated with **(A)** vehicle control and **(B)** tubastatin (1 μM) and co-treated with Ang II on 12 kPa hydrogels. **(C)** Graph shows area under the curve (ΔF/F0×T) for vehicle control vs tubastatin treated curves. Shows means and SEM. Statistical significance assessed by unpaired (independent) 2-sample T-test. Mean data for individual repeats of 3 independent experiments are shown as black dots.*

This analysis found that there was no statistically significant change in Ca^{2+} flux in VSMCs seeded on pliable hydrogels and treated with tubastatin compared to vehicle controls. AUC analysis showed no significant difference between tubastatin treated and control cells (Figure 4.9C).

Following this, VSMCs seeded on rigid hydrogels were also treated with tubastatin as described above.

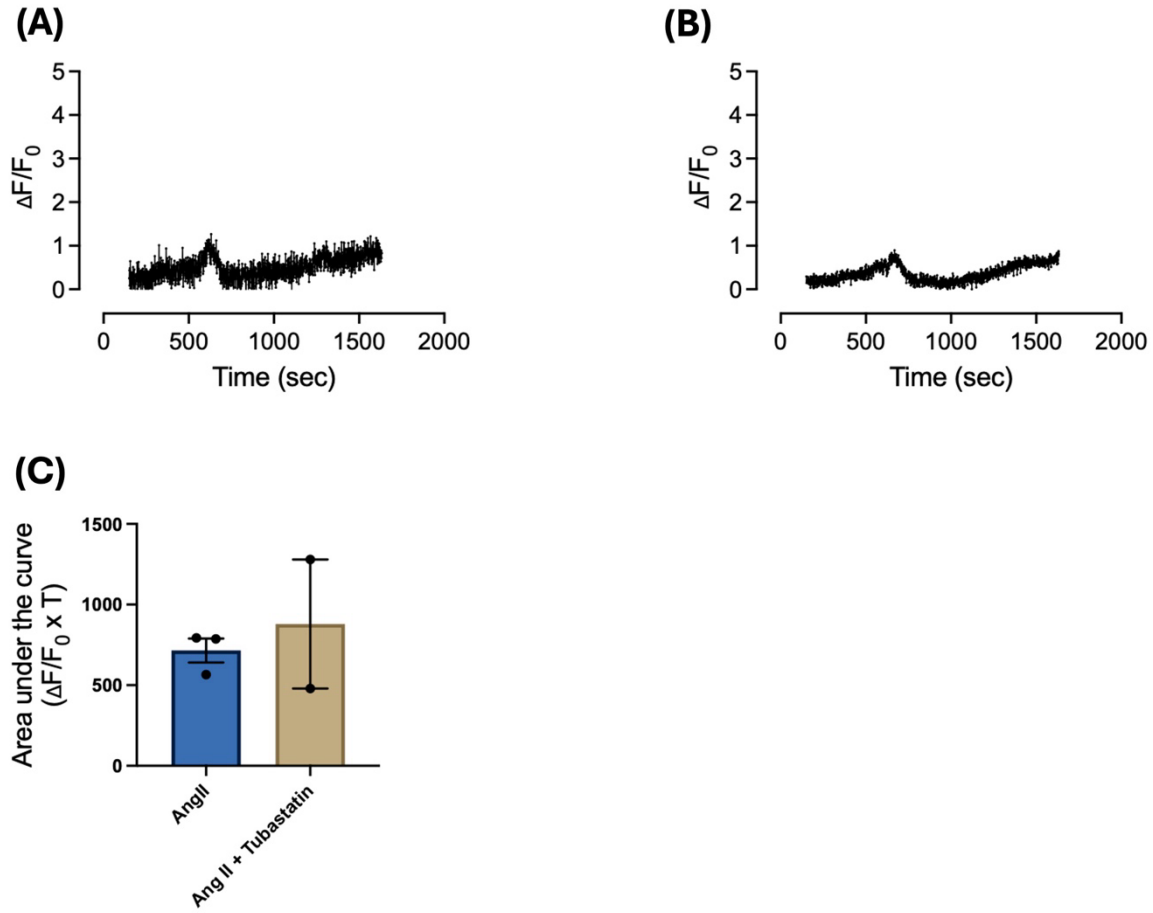

Figure 4.10. Tubastatin treatment has no effect on Ang II induced Ca^{2+} flux in VSMCs cultured on rigid hydrogels. *Graphs show representative $\Delta F/F_0$ values over time for VSMCS treated with **(A)** vehicle control and **(B)** tubastatin (1 μM) and co-treated with Ang II on 72 kPa hydrogels. **(C)** Graph shows area under the curve (ΔF/F0×T) for vehicle control vs tubastatin treated curves. Shows means and SEM. Statistical analysis not performed due to N = 2. Mean data for individual repeats of 2 independent experiments are shown as black dots.*

Analysis of these data suggest that there is no significant difference in Ca^{2+} flux in VSMCs seeded on rigid hydrogels and treated with tubastatin (Figure 4.10). Further repeats are needed to confirm this finding.

4.5.7 Blockade of stretch activated channels reduces Ca^{2+} flux on rigid hydrogels

Next, I investigated the role of stretch activated ion channels in Ca^{2+} flux in VSMC response to matrix stiffness. As discussed, VSMCs are highly mechanosensitive cells which are tightly integrated into their extracellular environment through mechanosensitive ion channels. Here, I utilised the neurotoxin GsMTx-4, a non-specific ion channel blocker, that primarily inhibits mechanosensitive channels of the Piezo and TRP families[254,255].

VSMCs were seeded on 72 kPa hydrogels in basal media and incubated for 48 hours. The cells were treated with GsMTx-4 (500 nM) or vehicle control (DMSO) during Fluo-4 loading and then imaged and treated with Ang II and A23187 as previously described.

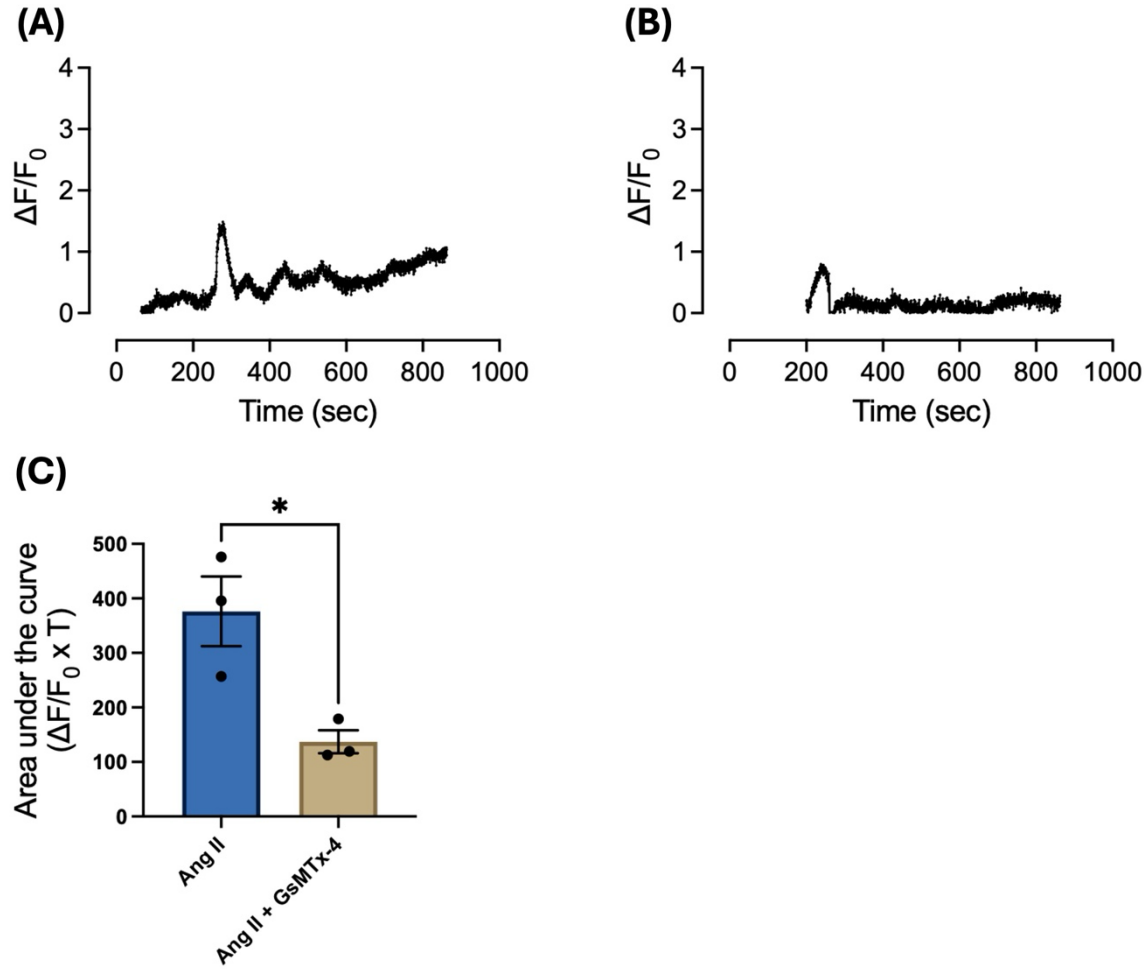

Figure 4.11. GSMTx4 treatment reduces Ang II induced Ca^{2+} flux in VSMCs cultured on rigid hydrogels. *Graphs show representative $\Delta F/F_0$ values over time for VSMCS treated with **(A)** vehicle control and **(B)** GsMTx-4 (500 nM) and co-treated with Ang II on 72 kPa hydrogels. **(C)** Graph shows area under the curve (ΔF/F0×T) for vehicle control vs GsMTx-4 treated curves. Shows means and SEM. Statistical significance assessed by unpaired (independent) 2-sample T-test (* = p< 0.05). Mean data for individual repeats of 3 independent experiments are shown as black dots.*

Analysis of these data show that GsMTx-4 treatment induced a reduction in Ca^{2+} flux in VSMCs on rigid hydrogels. GsMTx-4 caused Ca^{2+} flux to rapidly return to baseline after the initial peak (Figure 4.11A/B). AUC analysis shows that GsMTx-4 treated cells had a significantly lower AUC compared to vehicle control (Figure 4.11C).

4.5.8 Activation of Piezo1 increases Ca^{2+} flux on both pliable and rigid hydrogels

Next, I examined the role of the mechanosensitive, non-selective, cation channel, Piezo1 on Ca^{2+} handling in VSMC response to matrix stiffness. Piezo1's mechanosensitive

capabilities suggest it plays a role in a range of processes such as volume regulation, where it responds to increased osmotic stress through Ca^{2+}-mediated activation of volume-regulated ion channels, and Ca^{2+}-mediated regulation of cell cycle and cell death pathways[256]. To investigate Piezo1 I used the allosteric activator yoda1.

Here, cells were seeded on 12 kPa and 72kPa hydrogels in basal media and incubated for 48 hours. Cells were treated with yoda1 (1 μM) or vehicle control (DMSO) during Fluo-4 loading. Cells were imaged and treated with Ang II and A23187 as previously described.

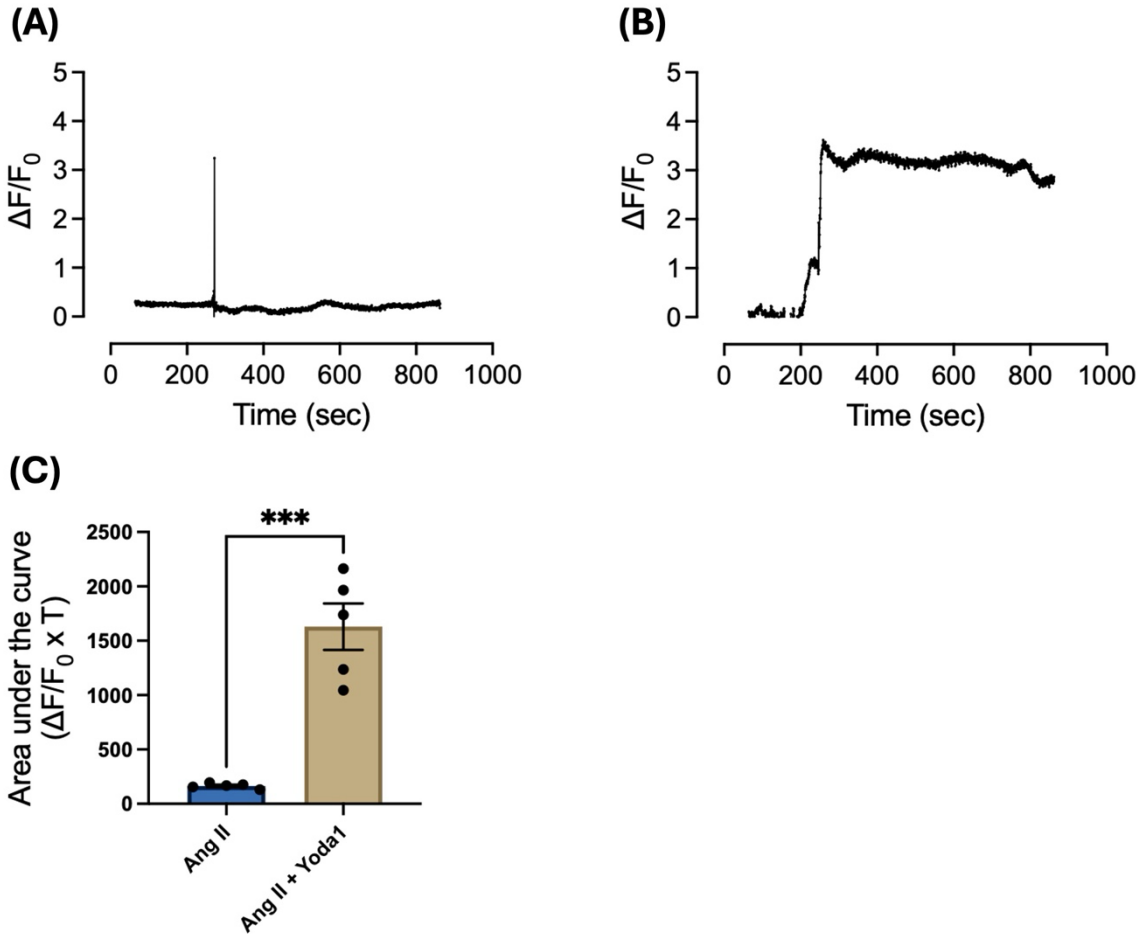

Figure 4.12. Yoda1 treatment increases Ang II induced Ca^{2+} flux in VSMCs cultured on pliable hydrogels. *Graphs show representative $\Delta F/F_0$ values over time for VSMCS treated with **(A)** vehicle control and **(B)** yoda1 (1 μM) and co-treated with Ang II on 12 kPa hydrogels. **(C)** Graph shows area under the curve (ΔF/F0×T) for vehicle control vs yoda1 treated curves. Shows means and SEM. Statistical significance assessed by unpaired (independent) 2-sample T-test (*** = p< 0.001). Mean data for individual repeats of 5 independent experiments are shown as black dots.*

This analysis found that activation of Piezo1 with yoda1 induced a significant increase in Ca^{2+} flux in VSMCs seeded on pliable hydrogels compared to vehicle control (Figure 4.12A/B). Yoda1 treatment induced a significantly higher peak Ca^{2+} level and caused

intracellular Ca^{2+} levels to remain continuously elevated post-treatment with Ang II. AUC analysis revealed that yoda1 treated cells had a significantly higher AUC compared to the control (Figure 4.12C).

Following this, VSMCs were seeded on rigid hydrogels and treated with yoda1.

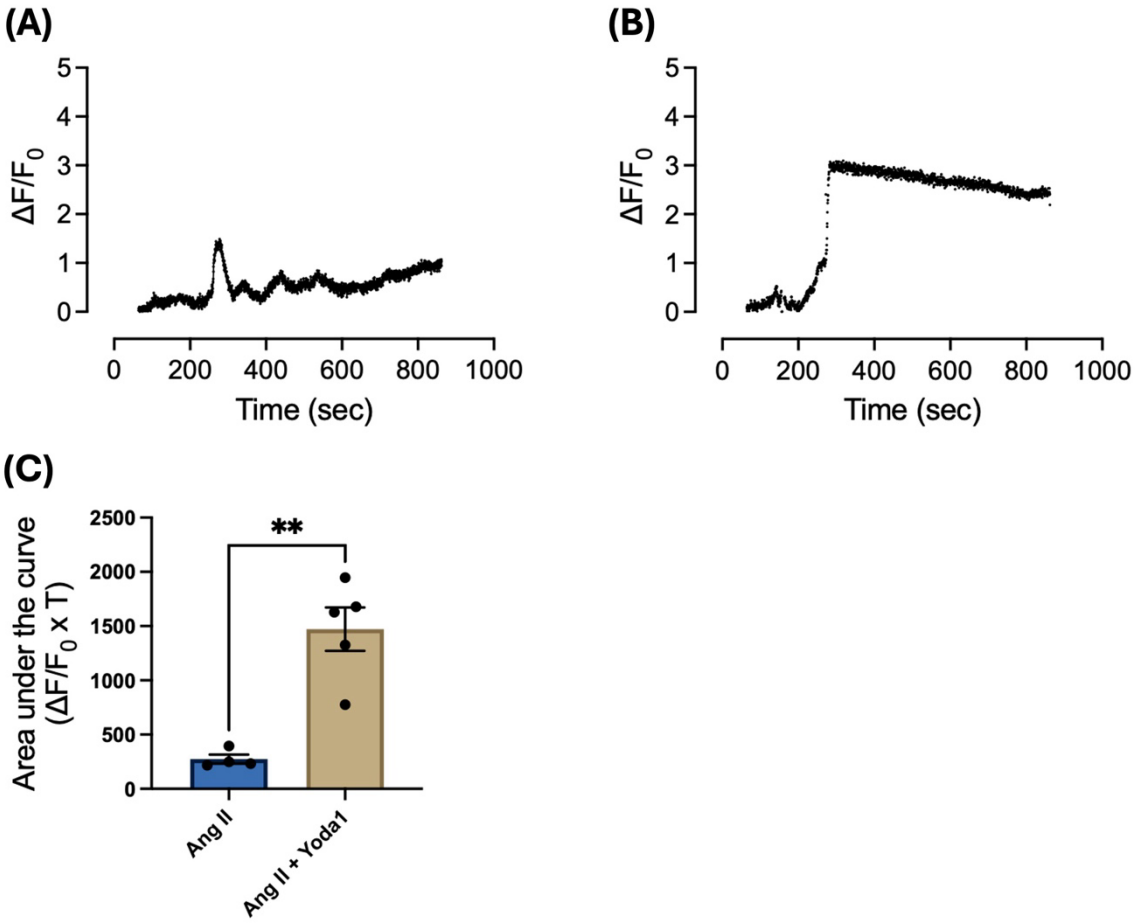

Figure 4.13. Yoda1 treatment increases Ang II induced Ca^{2+} flux in VSMCs cultured on rigid hydrogels. *Graphs show representative $\Delta F/F_0$ values over time for VSMCS treated with **(A)** vehicle control and **(B)** yoda1 (1 μM) and co-treated with Ang II on 72 kPa hydrogels. **(C)** Graph shows area under the curve (ΔF/F0×T) for vehicle control vs yoda1 treated curves. Shows means and SEM. Statistical significance assessed by unpaired (independent) 2-sample T-test (** = p< 0.01). Mean data for individual repeats of 5 independent experiments are shown as black dots.*

Analysis of these data revealed that activation of Piezo1 with yoda1 induced a significant increase in Ca^{2+} flux in VSMCs seeded on rigid hydrogels compared to vehicle control (Figure 4.13A/B). AUC analysis showed that yoda1 treated cells had a significantly higher AUC compared to vehicle control (Figure 4.13C).

4.6 Discussion

In this chapter I have utilised the Warren Lab's polyacrylamide hydrogel system in conjunction with Fluo-4 video time-lapse microscopy to assess fluctuations in intracellular Ca^{2+} content of VSMCs. This builds on the work of the previous chapter where I identified several mechanistic pathways involved in regulation of, or downstream signalling from, Ca^{2+} signals in the context of VSMC response to matrix stiffness. Specifically, I found that Ca^{2+} signalling appeared to be a key driver of the dysfunctional hypertrophy-like response that VSMCs undergo when seeded on rigid hydrogels and treated with the contractile agonist Ang II. Central to these findings was the role of microtubule dynamics in the regulation of Ca^{2+} flux, the downstream activity of Ca^{2+} regulated kinases such as PKC and Wnk, and the wider ion handling machinery within VSMCs, such as NKCC. In this chapter, I developed these findings further by directly investigating changes in Ca^{2+} flux between pliable and rigid hydrogels. I then examined how Ca^{2+} flux is modulated by targeted inhibition or activation of key signalling and mechanistic components, on both pliable and rigid hydrogels. This allowed me to identify key components of the Ca^{2+} handling toolkit that become dysregulated in VSMC stiffness syndrome and identify potential pharmacological targets for the treatment of cardiovascular disease.

4.6.1 Matrix Rigidity Modulates Ca^{2+} Flux

I first investigated how Ca^{2+} flux was modulated by matrix rigidity. The results of this experiment were very interesting as it showed a distinct difference in not only the quantity of Ca^{2+} signalling, but also in the spatial and kinetic elements of the Ca^{2+} signal. On the pliable hydrogel, Ca^{2+} rapidly spiked in response to Ang II stimulation but then quickly returned to baseline. Conversely, on the rigid hydrogel, the initial Ca^{2+} spike in response to Ang II stimulation was lower but was then followed by a gradual increase in intracellular Ca^{2+} level over time. When area under the curve was assessed, it was found that VSMCs on the rigid hydrogel had significantly greater AUC. This corroborates the finding that Ca^{2+} signalling is heightened and prolonged in VSMCs on rigid hydrogels compared to those on pliable hydrogels. This finding supports the established dogma that ECM stiffness plays a key role in the regulation of VSMC phenotype, proliferation and

contractility. As discussed, Ca^{2+} signalling is a ubiquitous messenger and is vitally important in contraction and maintenance of the contractile phenotype. Therefore, the current finding that matrix rigidity alone can modulate Ca^{2+} signalling is not without precedent as VSMCs are highly mechanosensitive cells and the link between ECM stiffness and SMC contractility has been extensively reported[257–259].

This finding provides us with an enhanced view of some of the established mechanistic frameworks through which we view arterial and VSMC stiffening. Firstly, this finding supports the idea that arterial stiffening is partly driven by increased actomyosin force generation. As outlined in the introduction, VSMCs contraction requires Ca^{2+} mediated cross-bridge cycling. Therefore, it is probable that elevated Ca^{2+} signalling in response to enhanced matrix rigidity results in greater actomyosin derived forces and enhanced traction stress. Activation of the AT1 GPCR through stimulation with its agonist, angiotensin II, as replicated in this study, is one of the key mechanisms by which Ca^{2+} is released from intracellular stores in VSMCs. AT1 activation is a known driver of cardiovascular disease such as hypertension and atherosclerosis[260]. Additionally, previous work has linked the activation of AT1 to mechanosensitive pathways through the close interplay between the AT1 receptor and α8, β1, β3 integrins[261]. Furthermore, work in rat cardiac myocytes has shown that stretch of integrin β1 results in activation of Cl^- SACs, release of angiotensin II and subsequent activation of AT1[262]. AT1 activation has been shown to stimulate FAK, highlighting crosstalk between AT1 and mechanosensitive integrins. In VSMCs, α1β1 integrin has been shown to modulate the effects of Ang II in a pathway mediated by ILK/AKT/NOX2 signalling[263]. The interaction between AT1 and mechanosensitive cell-surface proteins, such as integrins and SACs, suggests that the differential Ca^{2+} flux observed between pliable and rigid matrices when stimulated with Ang II is modulated at the receptor level. Work has shown that the AT1 receptor is regulated by several factors including growth factors, cytokines, NO, insulin, sex hormones, and numerous other molecular regulators[260]. The heterologous regulation of the AT1 receptor suggests it is likely to be differentially regulated under diseased and aged conditions, and therefore, possibly explains the differences in Ang II induced Ca^{2+} flux reported here. AT1 may therefore represent a disease specific target for the treatment of cardiovascular disease.

4.6.2 Microtubule Dynamics in VSMC Ca^{2+} Handling: A stability switch?

It is clear from this finding that Ca^{2+} handling is differentially regulated in VSMCs seeded on pliable and rigid matrix. To further investigate this finding, I next examined the role of microtubule dynamics in the regulation of Ca^{2+} flux in VSMCs. In the literature microtubules are reported as compression bearing struts that act to resist the compressive forces generated by actomyosin activity. This tensegrity equilibrium can be used to define VSMC behaviour in response to changes in matrix rigidity, whereby healthy VSMCs exist in a balance between microtubule stability and actomyosin derived tension[212]. However, under diseased conditions, microtubules become destabilised leading to increased actomyosin force generation, enhanced traction stress and subsequent VSMC stiffening.

Here, I first utilised the microtubule destabilising agent colchicine. Colchicine is an FDA approved medication used in the treatment of gout and familial mediterranean fever. It's cardio-protective activity is well known, and it is frequently used to reduce the risk of heart attacks, stroke, and cardiovascular death. It is also used to prevent cardiovascular events in patients with atherosclerosis[264]. Colchicine works by binding to $\alpha\beta$-tubulin heterodimers and preventing their polymerisation into the microtubule protofilament[265]. My work here shows that colchicine treated VSMCs on pliable hydrogels had significantly increased Ca^{2+} flux compared to vehicle controls when treated with Ang II. Furthermore, analysis of the Ca^{2+} fluorescence over time appears to show that Ang II/colchicine co-treatment of VSMCs on pliable hydrogels mimics the spatial and kinetic elements of Ang II induced Ca^{2+} flux on rigid hydrogels. Interestingly, colchicine treatment had no significant effect on Ca^{2+} flux in VSMCs seeded on rigid hydrogels compared to vehicle controls. This finding suggests that on rigid hydrogels, microtubules are already maximally destabilised, and that colchicine treatment has no additional effect.

This finding, while novel, is largely supported by the literature. For example, work in rat myocardial slices has shown that colchicine treatment results in accelerated contractile kinetics[266]. Furthermore, this result appears to support the tensegrity model described above, where destabilisation of microtubules results in the loss of balance between the

compression resisting microtubules and the contractile forces generated by actomyosin. This loss of balance may result in “runaway” actomyosin tension and increased traction force generation. Increased actomyosin activity is likely to exert significant deformational force on the plasma membrane, especially in the context of contraction-induced VSMC swelling observed on rigid matrices. This deformational force would increase membrane tension resulting in the activation of stretch activated ions channels such as Piezo and TRPC family channels, resulting in Ca^{2+} influx and further microtubule destabilisation. The data presented here show that this altered tensegrity balance can be induced through destabilisation of microtubules on pliable hydrogels.

The ability of Ca^{2+} to regulate microtubule dynamics is well documented. For example, in vitro work has shown that free Ca^{2+} binding to microtubule ends increases the probability of catastrophe by accelerating the rate of GTP hydrolysis[267]. Furthermore, studies in hereditary neuropathies have shown that calcium dysfunction leads to microtubule destabilisation through Ca^{2+}-mediated activation of calpain. Interestingly, the authors also found that microtubule associated proteins (MAPs) such as MAP2 and Tau were significantly reduced under dysregulated Ca^{2+} conditions[268]. Additionally, research in rat neurons has shown that stabilisation of microtubules through post-translational addition of polyamines is driven by a Ca^{2+}-dependent transglutaminase enzyme[269]. Furthermore, recent work has shown that microtubule detyrosination, a hallmark of stable microtubules, is regulated by Ca^{2+}-dependent calpains[270]. Finally, as mentioned in the previous chapter, Ca^{2+}-dependent activation of calmodulin results in recruitment and activation of MAPK and the subsequent phosphorylation of MAPs which regulate microtubule dynamics[221]. These findings strongly implicate calcium signalling as a regulator of microtubule dynamics and highlight the need for further research to elucidate this mechanism in VSMCs.

Following this, I also examined the effect of the stabilising agent paclitaxel on Ca^{2+} handling in VSMCs. This experiment provided further evidence for the involvement of a microtubule stability switch regulating Ca^{2+} flux in response to matrix stiffness. Here, on pliable hydrogels, paclitaxel treatment induced a statistically significant increase in intracellular Ca^{2+} in response to Ang II treatment compared to vehicle control. However,

there appeared to be little change in the spatial and kinetic elements of the Ca2+ signal between paclitaxel and vehicle treated cells. These data are in sharp contrast to the results of paclitaxel treatment of VSMCs seeded on rigid hydrogels. Here, the Ang II induced Ca^{2+} signal was significantly reduced with extensive remodelling of the spatial and kinetic flux. Paclitaxel treatment appeared to drastically reduce the initial Ca^{2+} peak and prevent the prolonged Ca^{2+} increase observed in vehicle treated cells. This data suggests that the tensegrity equilibrium described above can be restored, in relation to its effects on Ca^{2+} flux, through treatment with microtubule-stabilising agents. This is a significant finding and raises the possibility of using microtubule-stabilising agents as pharmacological interventions for stiffening related disease of the vasculature. However, current microtubule targeting agents are highly toxic, even at relatively low doses, due to their ability to arrest cell cycle, leading to checkpoint-induced cell death[271]. In cancer treatment, microtubule targeting agents are frequently conjugated to carriers, such as antibodies, to increase target specificity and reduce systemic toxicity. A similar approach may be beneficial in treatment of CVDs.

The finding that paclitaxel induced an increase in intracellular Ca^{2+} on pliable hydrogels is surprising and suggests that there are additional, unidentified mechanisms involved. One possible explanation is enhanced VSMC mechanosensitivity in high microtubule stability conditions. For example, preprint work has shown that paclitaxel sensitises the Ca^{2+} permeable Piezo1 SAC to mechanical activation[272]. Additionally, un peer reviewed research has shown that stabilisation of microtubules through acetylation leads to focal adhesion maturation. This suggests that enhanced levels of mechano-integration with the extracellular environment may exist under conditions where microtubules are stable[273]. Further research is required to elucidate the role of enhanced microtubule stability on mechanotransduction and calcium signalling on pliable matrices.

In summary, microtubule dynamics appear to play an important role in the regulation of Ca^{2+} handling in VSMC response to matrix rigidity. Viewing microtubules through the lens of the tensegrity model allows us to define VSMC behaviour in relation to their role as mechanical struts that balance the compressive forces of actomyosin activity. I have shown that interventions to promote microtubule stability on rigid hydrogels serve to

reduce Ca^{2+} flux in response to Ang II stimulation. Furthermore, I find that microtubule destabilisation on pliable matrices increases Ang II induced Ca^{2+} flux. These findings suggest that microtubule dynamics are maintained in a balance that directly contributes to regulation of Ca^{2+} flux. This system is likely to be reciprocal, as Ca^{2+} itself is a known regulator of microtubule stability, and fluctuations in intracellular Ca^{2+} can influence microtubule-associated proteins and post-translational modification of tubulin. Such feedback loops may enable VSMCs to fine-tune their mechanosensitive and contractile responses through remodelling of the microtubule cytoskeleton, in a process that becomes dysregulated during vascular stiffening.

4.6.3 HDACs: Regulators of the Microtubule Stability Switch?

Following these findings, I examined the role of HDACs in the regulation of Ca^{2+} flux in VSMCs. HDACs are a class of enzymes involved in the removal of acetyl groups from histone and non-histone proteins[274]. This process is vital in the epigenetic regulation of gene transcription, where the removal of acetyl groups from the histone protein promotes gene transcription. The non-histone protein activity of HDACs has been revealed as a somewhat analogous mechanism to that of protein phosphatases. However, instead of removing phosphate groups, HDACs removed acetyl groups from lysine residues to regulate protein function and interactions[274]. There is an established link between Ca^{2+} signalling and the activity of HDACs. Activation of the class II HDACs is known to be regulated by Ca^{2+}-calmodulin dependent protein kinases (CaMKs) which transmit biochemical signals from cell-surface GPCRs to HDACs[275]. Furthermore, the role of HDACs in cardiovascular diseases such as cardiac hypertrophy, coronary heart disease, atherosclerosis and hypertension is well known[275–277].

Here, I first examined the role of HDAC1 and found that inhibition of HDAC1 using MS275 resulted in no significant change in Ca^{2+} flux on either pliable or rigid hydrogels when co-treated with Ang II compared to vehicle controls. This result appears to suggest that HDAC1 isn't a modulator of Ca^{2+} signalling under these conditions. A possible explanation for this, following up from my previous findings, is that HDAC1 is not directly involved in the regulation of microtubule dynamics. Additionally, the IC50 for MS275 inhibition of HDAC1 is usually reported in the micromolar or high nanomolar range for *in*

vitro experiments[278]. We previously determined an effective MS275 concentration range of *0.01-100* nM in our system, with an IC50 of approximately 1 nM[190]. However, it is possible that our working concentration of MS275 was too low to see an effect in this assay.

These data contrasted with the finding that inhibition of HDAC2 and 3 appeared to alter Ca^{2+} flux. It is important to note that these findings are preliminary and require further repeats before any statistically backed conclusions can be drawn. However, at this stage it appears that inhibition of both HDAC2 (with santacruzamate A) and HDAC3 (with RGFP 966) induces an increase in Ca^{2+} flux on pliable hydrogels compared to vehicle controls. Additionally, both compounds appeared to induce a prolonged increase in intracellular Ca^{2+} levels over time. This contrasts with the effect on rigid hydrogels where both compounds appeared to reduce levels of intracellular Ca^{2+} and prevented any longer-term increase in Ca^{2+}. Here, Ca^{2+} levels rapidly returned to baseline, mimicking the result seen on untreated pliable hydrogels. The finding that different class I HDACs appear to have different effects on Ca^{2+} flux in VSMCs is surprising and further suggests that the MS275 concentration used here isn't sufficient to illicit a response in this system.

Approached through the lens of microtubule stability as a key regulator of Ca^{2+} flux, there is some evidence to support the activity of class I HDACs as regulators of microtubule dynamics. Firstly, it is widely reported that acetylation of tubulin in microtubules contributes to microtubule stability (Figure 4.14)[279,280]. Furthermore, inhibition of HDAC3 with MI192 has been shown to modulate tubulin acetylation in a non-linear, time-variable manner. The authors of this study found that when HDAC3 was inhibited at low concentrations of inhibitor for a long period, tubulin acetylation was slightly increased. However, when HDAC3 was inhibited over the short term (<1 hour), as done in this thesis, significantly increased levels of tubulin acetylation were observed[281]. Another study found that HDAC3 promotes formation of the meiotic apparatus in mouse oocytes by modulating tubulin acetylation. The authors found that knockdown of HDAC3 expression inhibits kinetochore-microtubule attachment. They linked this finding the ability of HDAC3 to maintain tubulin hypoacetylation and therefore its destabilised, highly dynamic state[282]. It is clear that the class I HDACs may play a role in regulating

microtubule dynamics, and that this axis may be involved in the microtubule stability-linked modulation of Ca^{2+} flux in VSMCs. Further repeats are required to validate the findings of these preliminary experiments.

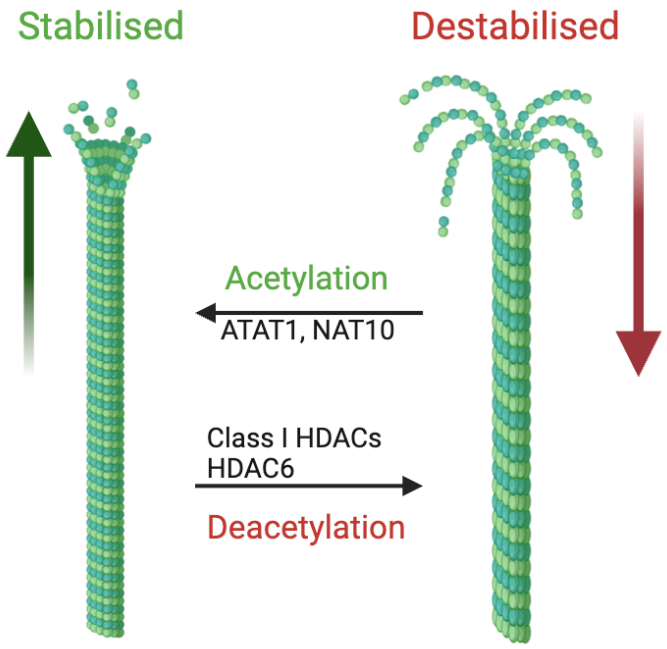

Figure 4.14. Schematic diagram of the interplay between tubulin acetylation and microtubule dynamics. *When tubulin is acetylated by acetyltransferases such as ATAT1 and NAT10 it becomes stabilised. When acetyl groups are removed by deacetylases such as HDAC2/3/6 microtubules become destabilised.*

I additionally investigated the effect of HDAC6 inhibition with tubastatin. Here, I found that tubastatin treatment had no significant effect on Ca^{2+} flux in VSMCs seeded on either pliable or rigid matrices. Previous work conducted by the Warren lab has shown that tubastatin treatment causes VSMCs on rigid matrix to undergo a reduction in area in a concentration dependent fashion[190]. It therefore appears that this HDAC6 inhibitor mediated reduction in cell area is not linked to fluctuations in intracellular Ca^{2+} levels. It is worth noting the HDACs, including HDAC6, have many protein targets. Therefore, inhibiting HDAC activity is likely to have several off-target effects that are difficult to predict. We should therefore be cautious drawing firm conclusions from these results. There is some evidence in the literature to suggest that HDAC6 targets and deacetylates microtubules. For example, an *in vitro* study in mouse cells found that knockout of HDAC6 resulted in significantly higher levels of α-tubulin acetylation[238]. Another study found that HDAC6 inhibition prevented the microtubule-mediated translocation of STIM1 to the plasma membrane. STIM 1 is an important endoplasmic reticulum calcium

sensor that drives Ca^{2+} flow across the plasma membrane in response to reduced Ca^{2+} levels in the endoplasmic reticulum due to IP_3R activation[283]. Taken together these data suggest that HDAC6 plays an important role in the regulation of microtubule stability and Ca^{2+} handling. It is interesting therefore that the experiments conducted here do not show a significant change in Ca^{2+} flux in tubastatin treated cells. Further work is required to fully understand the role of HDAC6 plays in regulating VSMC calcium flux. In conclusion, it is possible that during VSMC stiffening, the normal mechanisms that regulate microtubule dynamics become uncoupled such that altering HDAC6 activity, or indeed HDAC1 activity, no longer translates into a measurable change in intracellular Ca^{2+} handling. Furthermore, it is possible that under these stiff conditions, Ca^{2+} handling becomes dominated by the activity of stretch activated channels such as Piezo1 and TRPC.

4.6.4 Stretch Activated Channels: The Drivers of Ca^{2+} Flux in VSMC Stiffness Response

Finally, I investigated the effect of pharmacological intervention of stretch activated channels on Ca^{2+} flux in VSMC response to matrix stiffness. I first used the inhibitor GsMTx-4, a neurotoxin isolated from the Chilean rose tarantula, which selectively inhibits cationic mechanosensitive channels[284]. Here, I found that inhibition of MSCs resulted in significantly reduced Ca^{2+} flux on rigid hydrogels. This result suggests that the increased Ca^{2+} flux observed in VSMCs seeded on rigid hydrogels is primarily the result of increased flow of Ca^{2+} ions across the plasma membrane from the extracellular environment. Furthermore, this result aligns with my, and the Warren lab's, previous findings that Ca^{2+} flux is driven by destabilised microtubules, leading to uncontrolled actomyosin force generation and increased deformational stress exerted on the plasma membrane.

Next, I used Yoda1, an allosteric activator of the Piezo1 channel. I found that Yoda1 treatment induced significantly increased Ca^{2+} flux on both pliable and rigid hydrogels. This result suggests that the stiffness induced Ca^{2+}-pathway is already fully saturated on rigid hydrogels. Previous work by the Warren lab has linked Piezo1 activity to the aberrant VSMCs volume response on rigid hydrogels. This result suggests that Piezo1 activity in

this response is complex and is driven by more than just persistent channel activation on rigid hydrogels. We have previously hypothesised that actomyosin activity contributes to transient activation of Piezo1 channels and that this may be linked to the localisation of a subset of Piezo1 channels to integrin cell-adhesion sites.

The complex force-dependent localisation of Piezo1 was explored in a recent study in human fibroblasts. The authors found that recruitment of Piezo1 to focal adhesions required myosin-derived contractile forces. Furthermore, they found that this localisation resulted in transient and highly localised Ca^{2+} signals[285]. This suggests that Piezo1's involvement in force response is subtle and context dependent. The experiment conducted here, utilising a potent activator of Piezo1 and then doing low resolution imaging to identify general Ca^{2+} trends, is likely to miss these subtle changes in Ca^{2+} signalling in response to matrix stiffness. The Warren lab has also hypothesised that Piezo1 off-kinetics are modulated by stiffness, with Piezo1 channels on pliable hydrogels rapidly returning to their off configuration after Ang II stimulation but not on rigid matrices[189].

4.6.5 Summary and Limitations

In conclusion, this chapter demonstrates that Ca^{2+} handling is regulated by matrix stiffness. I have utilised targeted inhibition and activation Ca^{2+} handling components to highlight the mechanistic role of microtubules, HDACs and mechanosensitive ion channels in this model (Table 4.2). On pliable substrate, microtubule destabilisation and HDAC2/3 inhibition appeared to enhance Ang II induced Ca^{2+} flux, whereas on rigid matrices the lower Ca^{2+} baseline can be recapitulated through microtubule stabilisation, inhibition of HDAC2/3 and blockade of mechanosensitive ion channels. Additionally, these results support the key role of the Piezo1 ion channel in the downstream response to membrane deformation on rigid hydrogels. Importantly, these results show the potential stiffness-sensitive efficacy of pharmacological interventions targeting microtubules, HDACs or mechanosensitive ion channels in the treatment of cardiovascular disease.

Table 4.2. List of the compounds used in Chapter 4. *Shows their molecular target and their effect on calcium flux compared to vehicle control when co-treated with Ang II. NA, significance not assessed.*

		Calcium Flux	
Drug	**Target**	**12 kPa**	**72 kPa**
No treatment (rigidity only)	N/A	*Low*	*High*
Colchicine	Microtubules (destabilises)	Increase	No effect
Paclitaxel	Microtubules (stabilises)	Increase	Decrease
MS275	HDAC1	No effect	No effect
Santacruzamate A	HDAC2	NA	NA
RGFP966	HDAC3	NA	NA
Tubastatin	HDAC6	No effect	NA
GsMTx-4	SACs (piezo, TRP families)	NA	Decrease
Yoda1	Piezo1 (activates)	Increase	Increase

This data has some limitations. For example, all compounds were administered as short-term treatments over minutes and hours. This means that many chronic adaptive effects, such as those seen in response to matrix stiffness, may not be captured. Furthermore, many of the compounds used such as HDAC inhibitors have multiple targets and varying isoform selectivity leading to hard to predict off-target effects. Finally, the live-cell imaging with Fluo-4 technique used here has limited resolution beyond observing global changes in Ca^{2+} flux. Future work could aim to utilise a higher resolution approach to image localised fluctuations in Ca^{2+} level.

Chapter 5: Downstream Effects of VSMC Matrix Rigidity Response

5.1 Introduction

Aortic stiffening is a major risk factor for the development of cardiovascular disease and is associated with several vascular events such as stroke and heart failure. In the previous two chapters I have identified key signalling pathways involved in the VSMC contribution to this stiffening. In particular, I have identified that aquaporins, microtubule dynamics and Ca^{2+} flux are vitally important components of vascular smooth muscle cell stiffness syndrome (VSMCSS). In this chapter I aim to investigate the downstream effects of pathological modification of these pathways on vital VSMC processes.

Regulation of vascular tone through cell contraction is the key function of VSMCs. Previous work in this thesis and by the Warren lab has shown that the contractile machinery of VSMCs becomes dysregulated on rigid matrices leading to an aberrant hypertrophy-like response. I have also shown that Ca^{2+} flux and microtubule dynamics become dysregulated during arterial stiffening. As key regulators of cell contractility, this dysregulation is likely to contribute to the dysfunctional contraction-induced hypertrophy-like response observed in VSMCSS. Investigating VSMCs contractility is therefore likely to develop our understanding of VSMCSS and elucidate downstream effects of the signalling axis I have identified in the previous chapters.

To investigate VSMC contractility I utilised traction force microscopy (TFM). TFM is a widely used microscopy technique used to measure traction forces. Traction forces are mechanical forces generated by cells which are transmitted into the extracellular matrix and neighbouring cells through cell-ECM and cell-cell junctions such as focal adhesions and adherens junctions. When cells contract, they exert deformational forces on their underlying matrix. In TFM, fluorescently labelled beads are inserted into the matrix to measure this deformational force. When cells contract and deform their underlying substrate, the fluorescent beads move, facilitating tracking of deformation. Typically, the position of beads is recorded when cells are attached their substrate and then again after they have detached. This detachment is usually precipitated through a lysis step, such as through treatment with triton X-100. A displacement field can then be generated by

comparing the before and after images [286]. This methodology can be used in conjunction with the targeted inhibition and activation approach I have used throughout this work. This will enable me to assess matrix-dependent and pathway-dependent contractile responses.

Finally, I also investigate the effect of cell confinement on VSMC area response. During vascular stiffening, the ECM undergoes wholesale remodelling resulting in stiffening and altered cell-ECM interaction. Under these conditions, VSMCs are likely to undergo increased confinement as the ECM solidifies around them. Previous work has shown that confinement of SMCs results in increased phenotypic plasticity[287]. To assess VSMC response to confinement I utilised the 4D cell CSOW 620 static confiner[288] . This device is used with a standard glass-bottom 6-well plate and enables confinement of cells through micro PDMS pillars which can be controlled to nanometre precision (Figure 5.1).

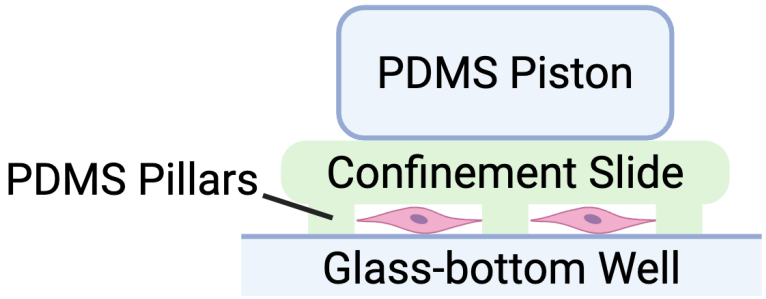

Figure 5.1. Schematic diagram of the 'CSOW 620 static confiner' in use with VSMCs. *Cells are seeded as normal onto a glass-bottom six-well plates. The cell confiner is then placed on top, with PDMS pistons of pre-selected height used to limit vertical space.*

Again, this methodology can be used alongside pharmacological co-treatment with Ang II and compounds of interest. I can then examine changes in cell characteristics such as area and volume. This experiment will allow me to examine changes in the VSMC contractile activity in response to varying levels of confinement.

5.2 Aims

This chapter aims to investigate downstream effects of the pro-stiffening signalling pathways identified in the previous chapters. This will be achieved by:

1. Performing TFM to assess changes in traction stress of VSMCs seeded on pliable and rigid hydrogels and co-treated with Ang II and compounds of interest.

2. Performing cell confinement assays to assess VSMC area response to confinement and treatment with Ang II.

5.3 Hypotheses

I predict that matrix rigidity will modulate VSMC contractility as measured by traction force microscopy. Furthermore, I propose that targeted inhibition of previously identified signalling components will facilitate stiffness-differentiated modulation of VSMC contractility. Additionally, I predict that mechanical confinement of VSMCs will modulate cell area. Specifically, I hypothesise that:

1. Enhanced matrix rigidity will increase VSMC traction force generation.

2. Pharmacological inhibition of previously identified signalling pathways will rescue normal levels of traction force generation on rigid hydrogels.

3. Mechanical confinement of VSMCs will decrease cell area and volume.

5.4 Materials and Methods

Table 5.1. List of compounds used in Chapter 5. *Shows their molecular target and working concentration.*

Compound	Target	Working Concentration
A1070722	GSK3	1 nM
MS275	HDAC1	1 nM
TCAQP1	Aquaporin 1	100 nM
Jedi1	Piezo1 (activates)	1 µM
Yoda1	Piezo1 (activates)	1 µM
Vas 2870	NAPDH-oxidase	100 µM

5.5 Results

5.5.1 Matrix rigidity has no impact on VSMC traction force generation

First, to investigate the direct effect of matrix rigidity on VSMC traction stress generation I utilised TFM. As described above, cells were seeded on both 12 kPa and 72 kPa hydrogels that contained fluorescent microbeads. Live-timelapse microscopy was conducted to image cells both pre- and post-lysis with triton X-100. Bead movement between the pre- and post-lysis images was used to generate displacement fields.

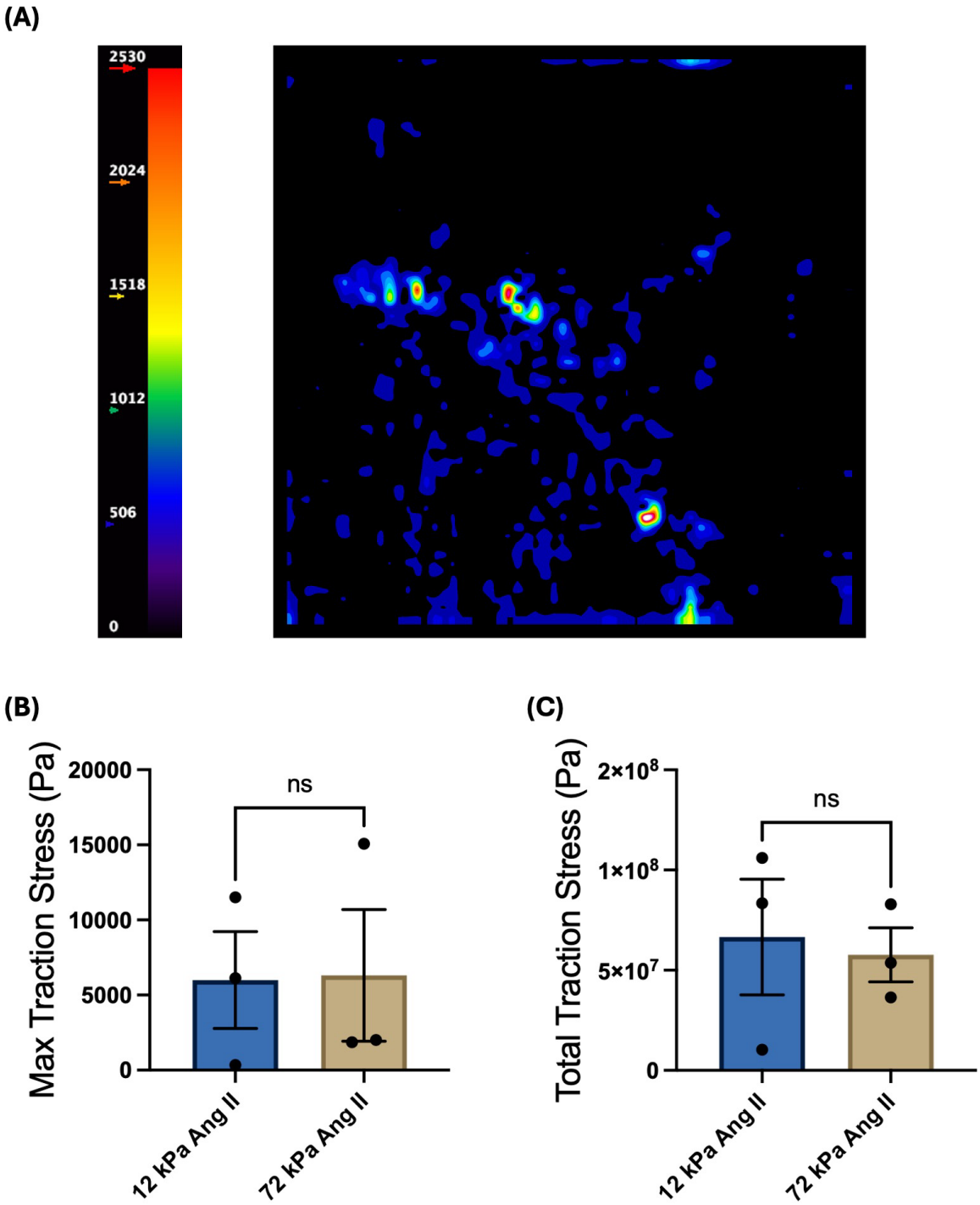

Figure 5.2. Matrix rigidity has no effect on VSMC traction stress generation. ***(A)*** *Representative traction stress heatmap generated by Fourier Transform Traction Cytometry (FTTC) from 12 kPa Ang II condition. Scale bar shows Pa. Graphs show* ***(B)*** *maximum traction stress generation and,* ***(C)*** *total traction stress generation for 12 vs 72 kPa hydrogels. Mean and SEM displayed. Black dots show means of N = 3 individual experiments. Statistical significance determined with unpaired T-test.*

This analysis found that there was no significant change in traction stress generated by VSMCs when seeded on either 12 or 72 kPa hydrogels (Figure 5.2B/C). The mean total traction stress generated by cells on 12 kPa and 72 kPa hydrogels was 5997 Pa and 6312

Pa respectively. For total traction stress generation, means of 66603742 Pa and 57678126 Pa were recorded for 12 and 72 kPa hydrogels respectively.

5.5.2 GSK3 inhibition has no impact on VSMC traction force generation

I have previously shown that inhibition of GSK3 with A1070722 induces a reduction in cell area of VSMCs on 72 kPa hydrogels in a concentration dependent fashion. To see if this effect is driven by increased traction stress generation, I conducted TFM with A1070722 treated VSMCs.

First, I seeded cells on 12 kPa hydrogels and treated them with A1070722 (1 nM). TFM was performed as previously described.

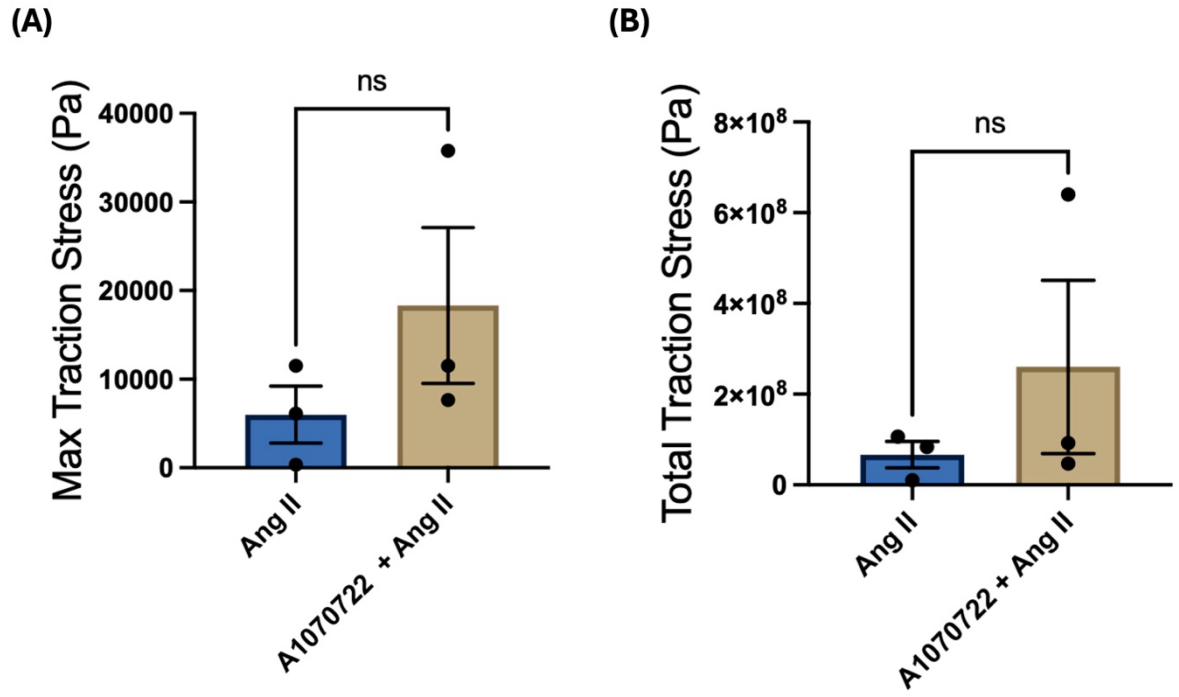

Figure 5.3. A1070722 treatment has no effect on VSMC traction force generation on pliable hydrogels. *Graphs show **(A)** maximum traction stress generation and, **(B)** total traction stress generation for Ang II controls vs A1070722 treated cells on 12 kPa hydrogels. Mean and SEM displayed. Black dots show means of N = 3 individual experiments. Statistical significance determined with unpaired T-test.*

Analysis of these data showed that A1070722 treatment had no significant effect on VSMC traction force generation on pliable hydrogels (Figure 5.3).

Next this experiment was repeated on rigid hydrogels.

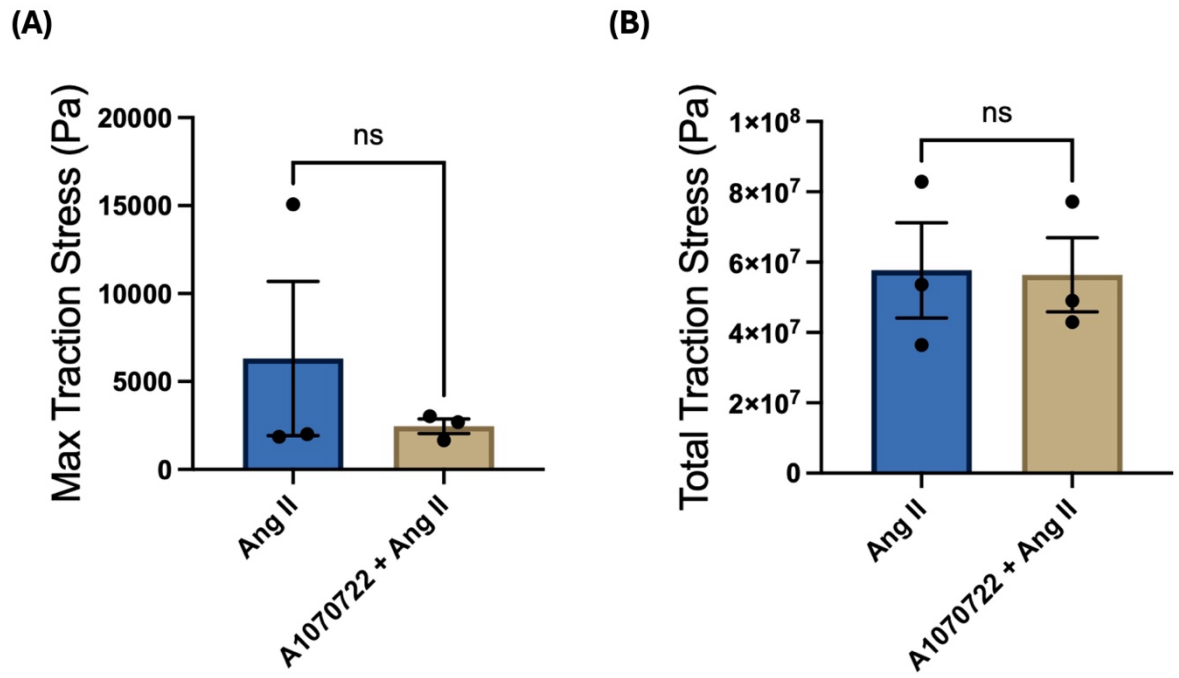

Figure 5.4. A1070722 treatment has no effect on VSMC traction force generation on rigid hydrogels. *Graphs show* ***(A)*** *maximum traction stress generation and,* ***(B)*** *total traction stress generation for Ang II controls vs A1070722 treated cells on 72 kPa hydrogels. Mean and SEM displayed. Black dots show means of N = 3 individual experiments. Statistical significance determined with unpaired T-test.*

These results suggest that A1070722 treatment had no significant effect on VSMC traction stress generation on rigid hydrogels (Figure 5.4).

5.5.3 HDAC1 inhibition has no impact on VSMC traction force generation

Following this I examined the effect of HDAC1 inhibition on VSMC traction stress generation. In the previous chapter I showed that inhibition of HDAC1 with MS275 has no significant effect on Ca^{2+} flux in VSMCs cultured on both 12 and 72 kPa hydrogels. To determine whether HDAC1 inhibition had any impact on VSMC traction stress generation I conducted TFM with MS275 treated cells.

Cells were seeded on 12 kPa hydrogels and treated with MS275 (1 nM). TFM was performed as previously described.

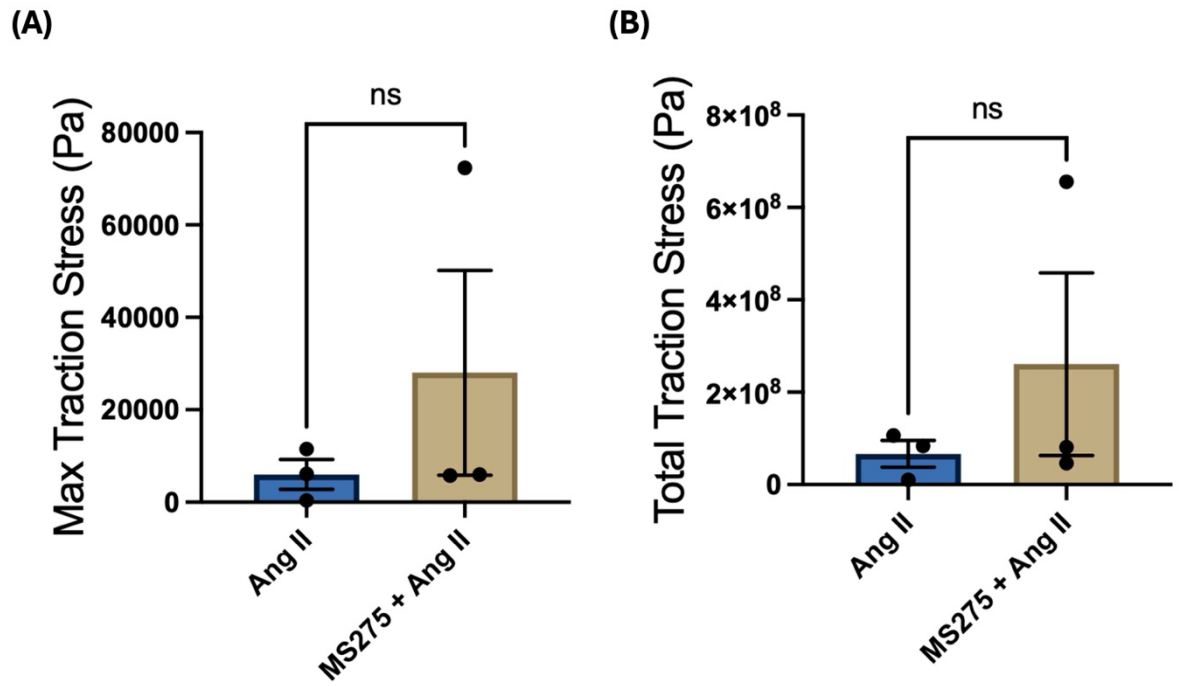

Figure 5.5. MS275 treatment has no effect on VSMC traction force generation on pliable hydrogels. *Graphs show* ***(A)*** *maximum traction stress generation and,* ***(B)*** *total traction stress generation for Ang II controls vs MS275 treated cells on 12 kPa hydrogels. Mean and SEM displayed. Black dots show means of N = 3 individual experiments. Statistical significance determined with unpaired T-test.*

These results show that MS275 treatment has no significant effect on VSMC traction force generation on pliable hydrogels (Figure 5.5).

Next, this experiment was repeated on rigid hydrogels.

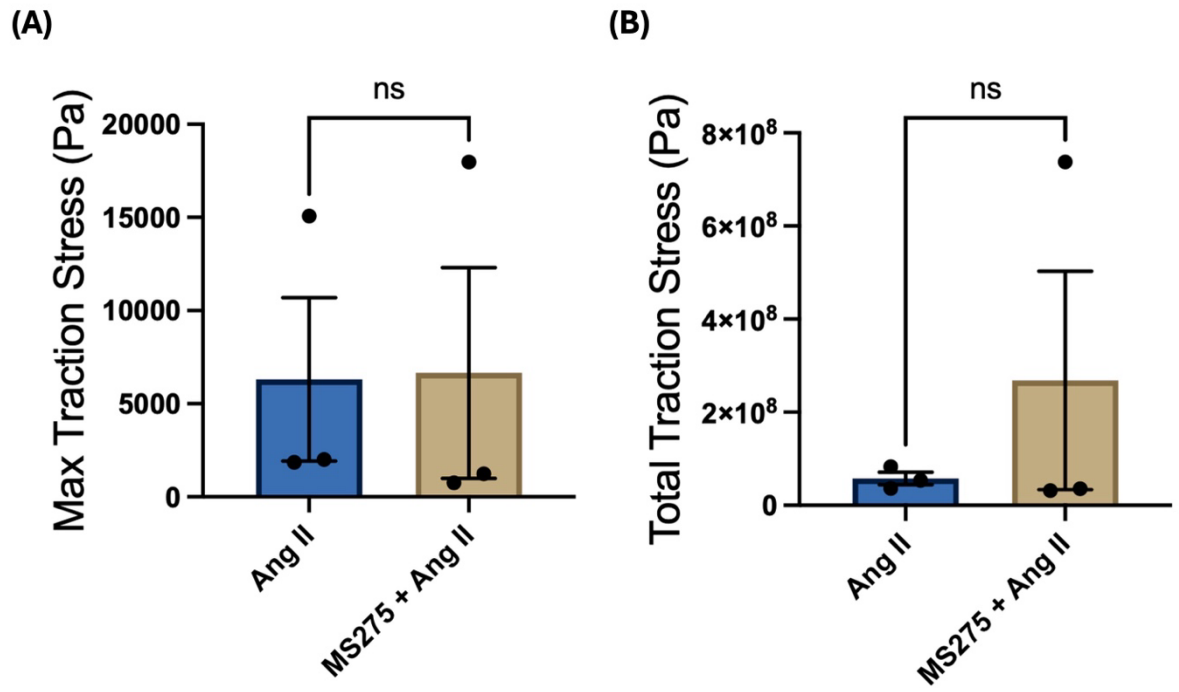

Figure 5.6. MS275 treatment has no effect on VSMC traction force generation on rigid hydrogels. *Graphs show* ***(A)*** *maximum traction stress generation and,* ***(B)*** *total traction stress generation for Ang II controls vs MS275 treated cells on 72 kPa hydrogels. Mean and SEM displayed. Black dots show means of N = 3 individual experiments. Statistical significance determined with unpaired T-test.*

These results suggest that there is no statistically significant difference in traction force generation in VSMCs cultured on rigid hydrogels and treated with MS275 (Figure 5.6).

5.5.4 Assessing data set distribution

During analysis of the previous experiments, it was observed that several data points appeared as potential outliers. To ensure robust interpretation of my results I conducted an evaluation of data distribution across experiments. This included graphical inspection and formal testing for distribution.

I first plotted Q-Q plots for each experiment to visualise data distribution. Q-Q plots were generated for each experiment to assess whether maximum and total displacement values were normally distributed. Plots were separated by experiment and by matrix stiffness. As an example, Q-Q plots for the Ang II vs A1070722 vs MS275 experiments are shown here. (Figure 5.7/8).

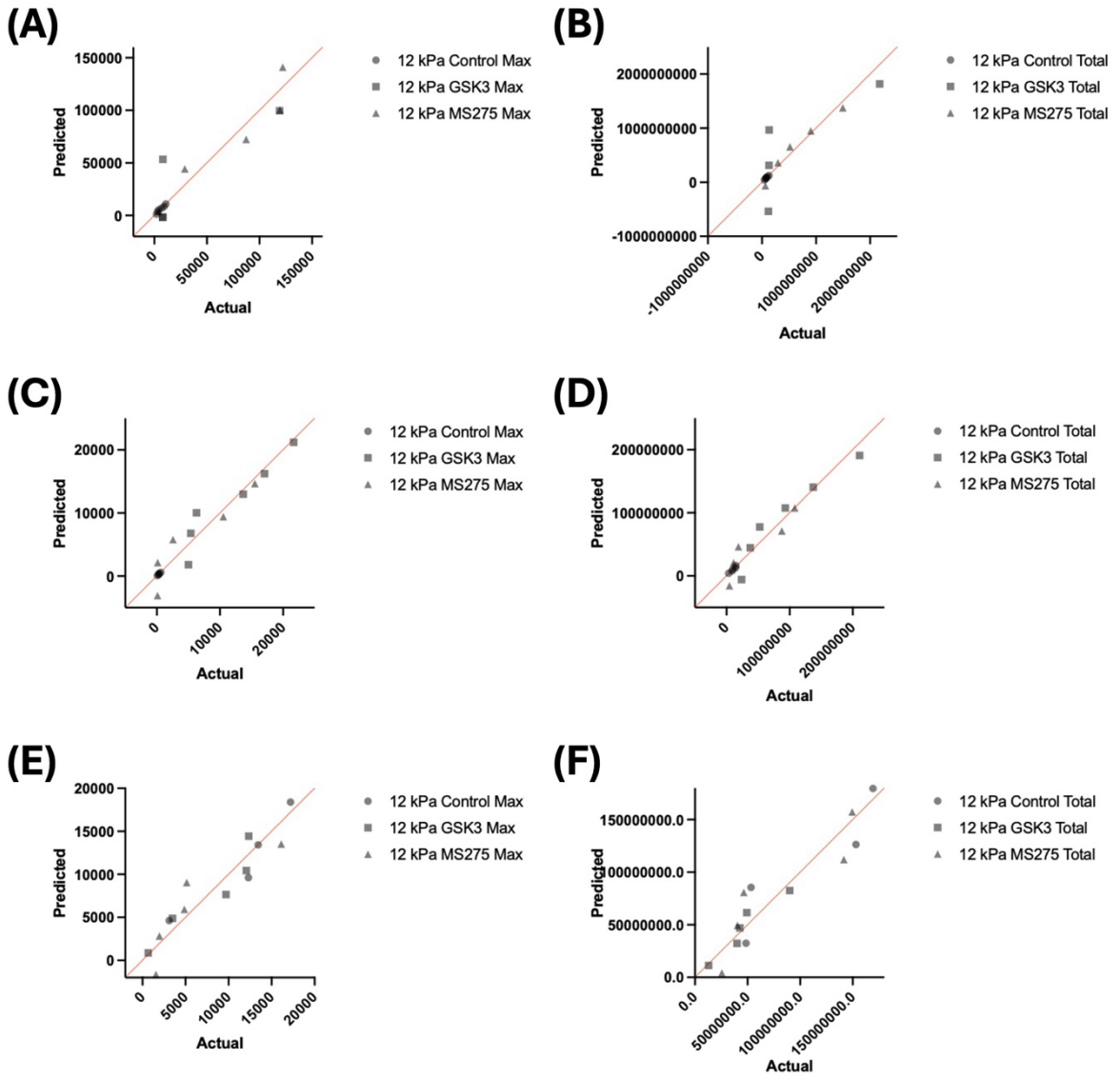

Figure 5.7. Q-Q plot showing distribution of maximum and total traction stress generation from TFM datasets on pliable hydrogels. *Plot shows observed vs predicted distribution with red line representing 1:1 perfect normality. Each point represents an observed value plotted against the expected value in a normal distribution. Data lying close to the red line is approximately normal whereas deviation from the line indicates non-normal distribution.*

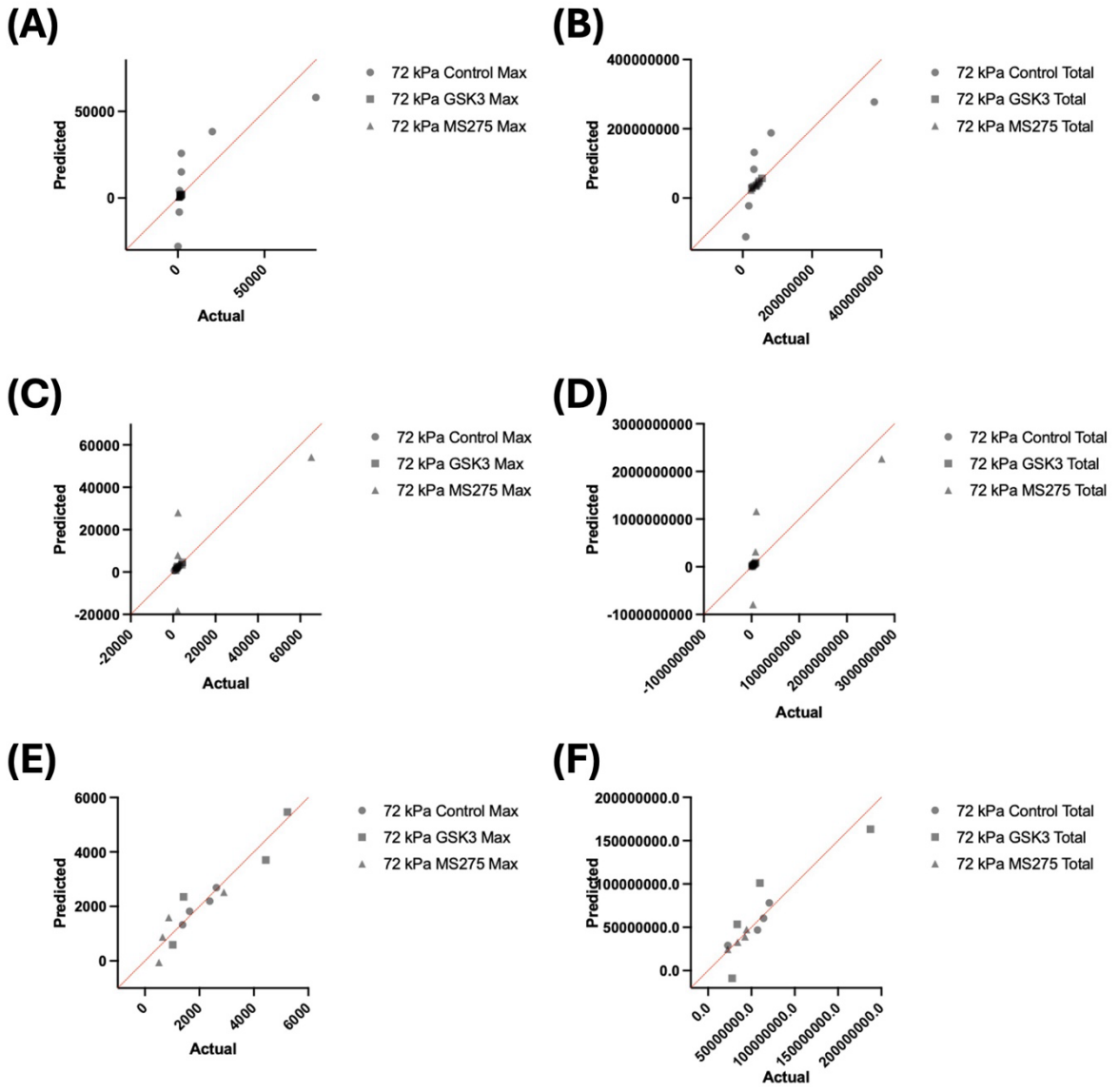

Figure 5.8. Q-Q plot showing distribution of maximum and total traction stress generation from TFM datasets on rigid hydrogels. *Plot shows observed vs predicted distribution with red line representing 1:1 perfect normality. Each point represents an observed value plotted against the expected value in a normal distribution. Data lying close to the red line is approximately normal whereas deviation from the line indicates non-normal distribution.*

Visual inspection of these plots suggests that most data sets in these experiments are normally distributed, but that a small number appear to follow a non-normal distribution. To statistically confirm this, I conducted a formal assessment of normality for each experiment, using the Shapiro-Wilk test for normality (Table 5.1).

Table 5.2. Normality testing of TFM datasets across A1070722 and MS275 experimental conditions. *Table shows results of normality assessment for maximum and total traction stress in VSMC seeded on 12 and 72 kPa hydrogels, with or without inhibition of GSK3 (A1070722) or HDAC1 (MS275). Normality was assessed using the Shapiro-Wilk test. "Yes" indicates that the experiment did not significantly deviate from normality. "No" indicates deviation from normal distribution.*

	Experiment 1	Experiment 2	Experiment 2
Condition	**Normally Distributed?**	**Normally Distributed?**	**Normally Distributed?**
12 kPa Control Max	Yes	Yes	Yes
12 kPa A1070722 Max	No	Yes	Yes
12 kPa MS275 Max	Yes	Yes	Yes
12 kPa Control Total	Yes	Yes	Yes
12 kPa A1070722 Total	No	Yes	Yes
12 kPa MS275 Total	Yes	Yes	Yes
72 kPa Control Max	No	Yes	Yes
72 kPa A1070722 Max	Yes	Yes	Yes
72 kPa MS275 Max	Yes	No	No
72 kPa Control Total	No	Yes	Yes
72 kPa A1070722 Total	Yes	Yes	Yes
72 kPa MS275 Total	Yes	No	Yes

5.5.5 Outlier Removal with ROUT

The normality assessments conducted above found that most data sets were normally distributed but that a small number had non-normal distribution, suggesting the presence of outliers (Figure 5.7/8, Table 5.1). As outliers can significantly skew mean values and statistical assessment, I conducted a systematic outlier removal step using the "robust regression and outlier removal" (ROUT) method available in GraphPad Prism. The ROUT method works by first calculating a curve which is less influenced by extreme values. This curve acts as a best fit and the distance of each data point from this robust curve is calculated. Data points that deviate more than expected are flagged as outliers. During this step a false discovery rate control (Q) is used to reduce the number of false positives. Here, I utilised the ROUT method (Q = 1%) to reduce the influence of extreme values while limiting the probability of incorrectly labelling a data point as an outlier.

As an example, data points identified as outliers from one A1070722 vs MS275 experiment are plotted below (Figure 5.9).

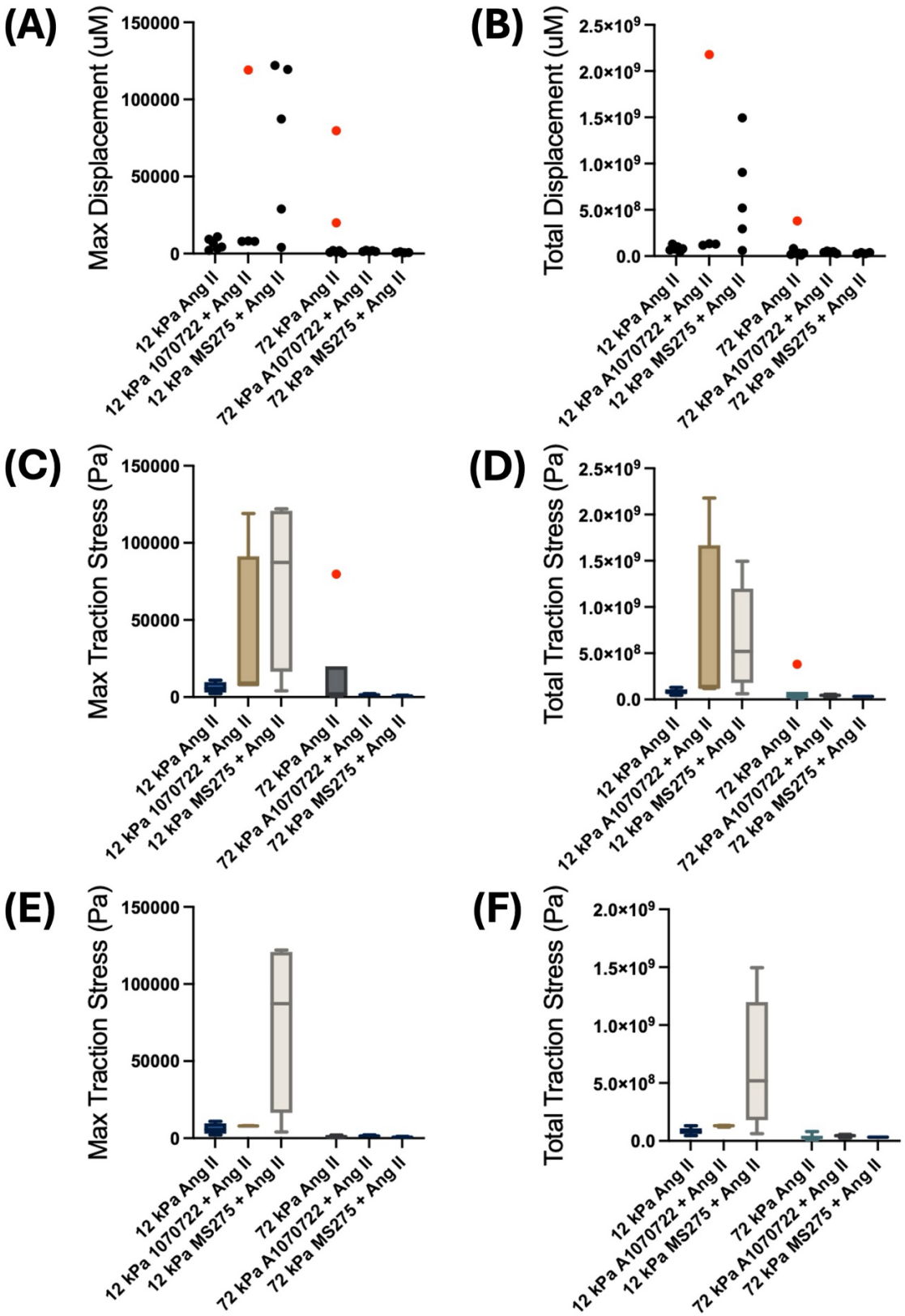

Figure 5.9. Data points removed from Ang II vs A1070722 vs MS275 in TFM experiment 1 by ROUT. *Data points from* ***(A)*** *Maximum traction stress and,* ***(B)*** *Total traction stress. Graphs show all data points from N = 1. Data points in red were identified as outliers by ROUT method (Q = 1%).* ***(C).*** *Tukey box and whisker plot showing max traction stress and,* ***(D)*** *total traction stress before outlier removal.* ***(E)*** *Tukey box and whisker plot showing max traction stress and,* ***(F)*** *total traction stress after outlier removal. Box and whisker graphs show distribution of values, boxes represent interquartile range, whiskers show 1.5 × IQR.*

Table 5.3. Statistical summary of Ang II vs A1070722 vs MS275 TFM experiment 1 before and after outlier removal. *Lists n (no. cells), mean and SEM for each condition and repeat (N = 3). Values highlighted in red are conditions with at least one outlier.*

Condition	Experiment 1			Experiment 2			Experiment 3		
	n	**Mean**	**SEM**	**n**	**Mean**	**SEM**	**n**	**Mean**	**SEM**
12 kPa Ang II Max	6	6132	1436	5	341.6	86.25	4	11516	2992
12 kPa Max Ang II Cleaned	6	6132	1436	5	341.6	86.25	4	11516	2992
12 kPa Ang II Total	6	83444419	12022408	5	10322736	2125463	4	106044070	32008030
12 kPa Ang II Total Cleaned	6	83444419	12022408	5	10322736	2125463	4	106044070	32008030
72 kPa Ang II Max	7	15079	11090	5	1851	427.0	4	2007	295.5
72 kPa Ang II Max Cleaned	5	1184	361.1	5	1851	427.0	4	2007	295.5
72 kPa Ang II Total	7	82893554	50219360	5	36491088	9056426	4	53649736	10663656
72 kPa Ang II Total Cleaned	6	33444244	10365805	5	36491088	9056426	4	53649736	10663656
12 kPa A1070722 Max	4	35768	27773	6	11515	2865	5	7657	2367
12 kPa A1070722 Max Cleaned	3	7995	66.81	6	11515	2865	5	7657	2367
12 kPa A1070722 Total	4	640582140	512737110	6	92557621	29049493	5	46963288	12436878
12 kPa A1070722 Total Cleaned	3	127856083	4761099	6	92557621	29049493	5	46963288	12436878
72 kPa A1070722 Max	5	1656	179.1	5	2696	645.0	4	3028	1060
72 kPa A1070722 Max Cleaned	5	1656	179.1	5	2696	645.0	4	3028	1060
72 kPa A1070722 Total	5	42967154	4885269	5	49076705	14152877	4	77178466	37412301
72 kPa A1070722 Total Cleaned	5	42967154	4885269	5	49076705	14152877	4	77178466	37412301

12 kPa MS275 Max	5	72359	23950	5	5780	3098	5	5936	2648
12 kPa MS275 Max Cleaned	5	72359	23950	5	5780	3098	5	5936	2648
12 kPa MS275 Total	5	655451759	251750909	5	46038446	21493730	5	80716965	26714137
12 kPa MS275 Total Cleaned	5	655451759	251750909	5	46038446	21493730	5	80716965	26714137
72 kPa MS275 Max	4	754.9	136.6	4	17967	15762	4	1234	560.4
72 kPa MS275 Max Cleaned	4	754.9	136.6	3	2205	44.38	4	1234	560.4
72 kPa MS275 Total	4	31884979	3805318	4	737374576	664434466	4	35964777	4981026
72 kPa MS275 Total Cleaned	4	31884979	3805318	3	73098621	20523832	4	35964777	4981026

I then plotted the results of the previous experiment again using the cleaned data sets.

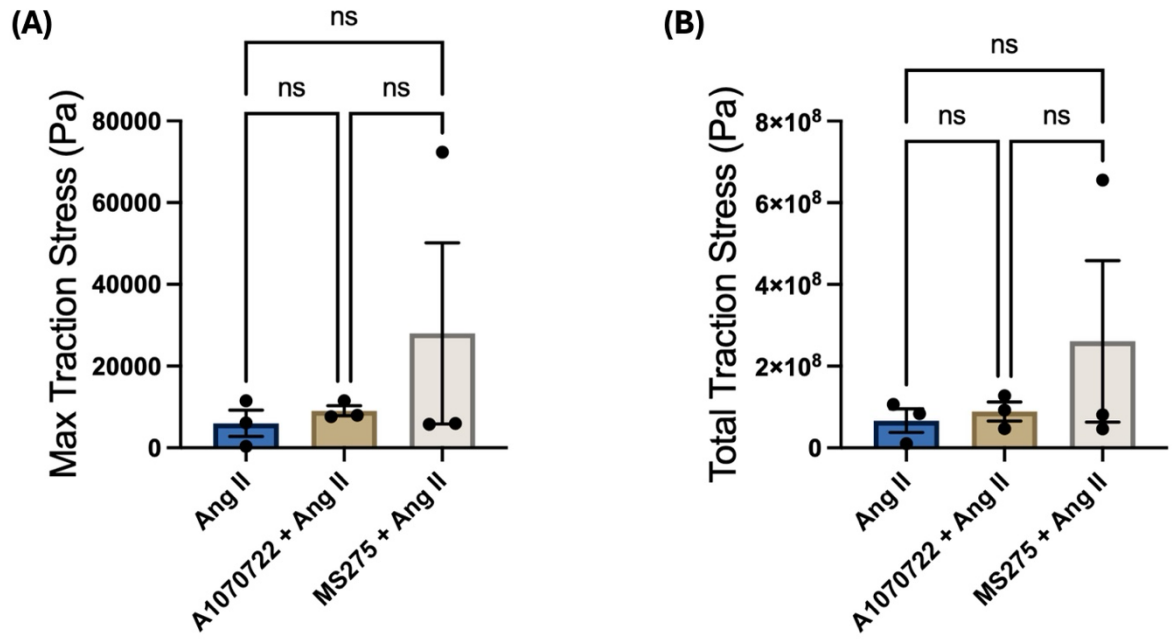

Figure 5.10. A1070722 and MS275 treatment has no effect on VSMC traction force generation on pliable hydrogels. *Graphs show* ***(A)*** *maximum traction stress generation and,* ***(B)*** *total traction stress generation for Ang II controls vs MS275 vs A1070722 treated cells on 12 kPa hydrogels. Mean and SEM displayed. Black dots show means of N = 3 individual experiments. Statistical significance determined with unpaired T-test.*

On 12 kPa hydrogels, I again found that there was no statistically significant difference in traction stress generation between VSMCs treated with A1070722 or MS275 and co-treated with Ang II compared to the Ang II control when outliers were removed (Figure

5.10). It appears that MS275 treatment increased the mean maximum and total traction force generation, however, this finding was driven primarily by a single experiment where very high values were observed, and the difference was not significant.

I also plotted the experiment on 72 kPa hydrogels with outliers removed.

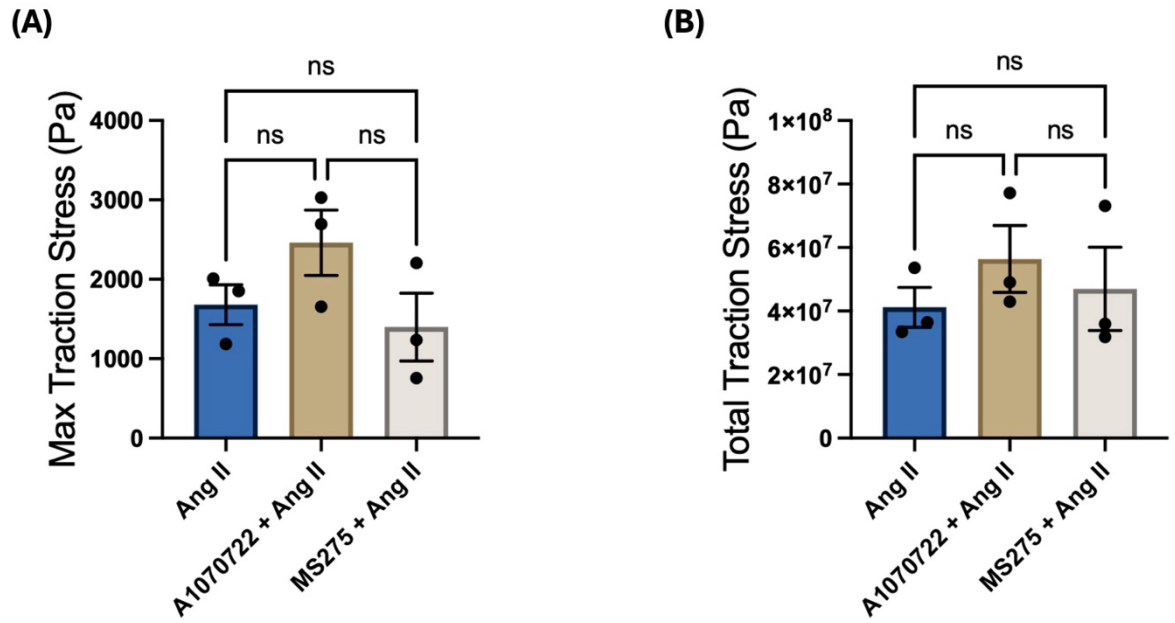

Figure 5.11. A1070722 and MS275 treatment have no effect on VSMC traction force generation on rigid hydrogels. *Graphs show* ***(A)*** *maximum traction stress generation and,* ***(B)*** *total traction stress generation for Ang II controls vs MS275 vs A1070722 treated cells on 72 kPa hydrogels. Mean and SEM displayed. Black dots show means of N = 3 individual experiments. Statistical significance determined with unpaired T-test.*

On rigid hydrogels, there was a slight increase in traction force generation by cells treated with A1070722, however, this result was not significant. Likewise, MS275 treatment had no significant effect on either maximum or total traction force generation compared to Ang II control on rigid hydrogels (Figure 5.11).

Following these findings I also reanalysed the results of the original pliable vs rigid hydrogel experiment, applying the same process of normality checking and outlier removal as described above.

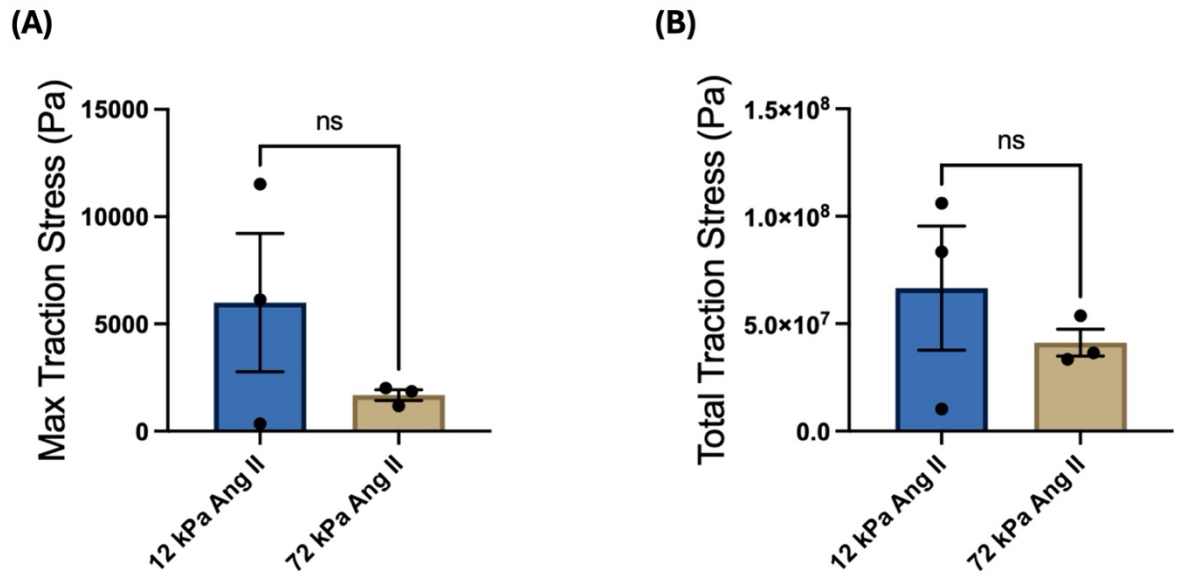

Figure 5.12. Reanalysis of the pliable vs rigid TFM experiment with outliers removed. *Graphs show* ***(A)*** *maximum traction stress generation and,* ***(B)*** *total traction stress generation for cells on 12 vs 72 kPa hydrogels. Mean and SEM displayed. Black dots show means of N = 3 individual experiments. Statistical significance determined with unpaired T-test.*

This reanalysis suggested that maximum and total traction stress generation was reduced on rigid hydrogels compared to 12 kPa substrates (Figure 5.12). However, statistical analysis revealed that these results were not significant. Notably, even after outlier removal, the range of values for the 12 kPa condition remained very broad, indicating significant variability within the dataset and suggesting that there may be technical issues with this experiment.

Having established that outliers were present in some data sets, I applied the ROUT method (Q = 1%) to all subsequent analyses. Unless otherwise stated, the results presented in the remainder of this chapter reflect data sets with outliers removed. Additionally, due to the high variability of some data sets, homogeneity of variances was assessed for each data set using the Brown-Forsythe test. Where variance was found to be unequal, Welch's correction was applied to T-tests.

5.5.6 AQP1 blockade has no impact on VSMC traction stress generation

In the first chapter I demonstrated that AQP1 blockade with TCAQP1 induces a reduction in VSMC area in a concentration dependent fashion. To determine whether this result was driven by increased traction force generation I performed TFM on VSMCs treated with TCAQP1.

Cells were first seeded on 12 kPa hydrogels and treated with TCAQP1 (100 nM). TFM was conducted as previously described.

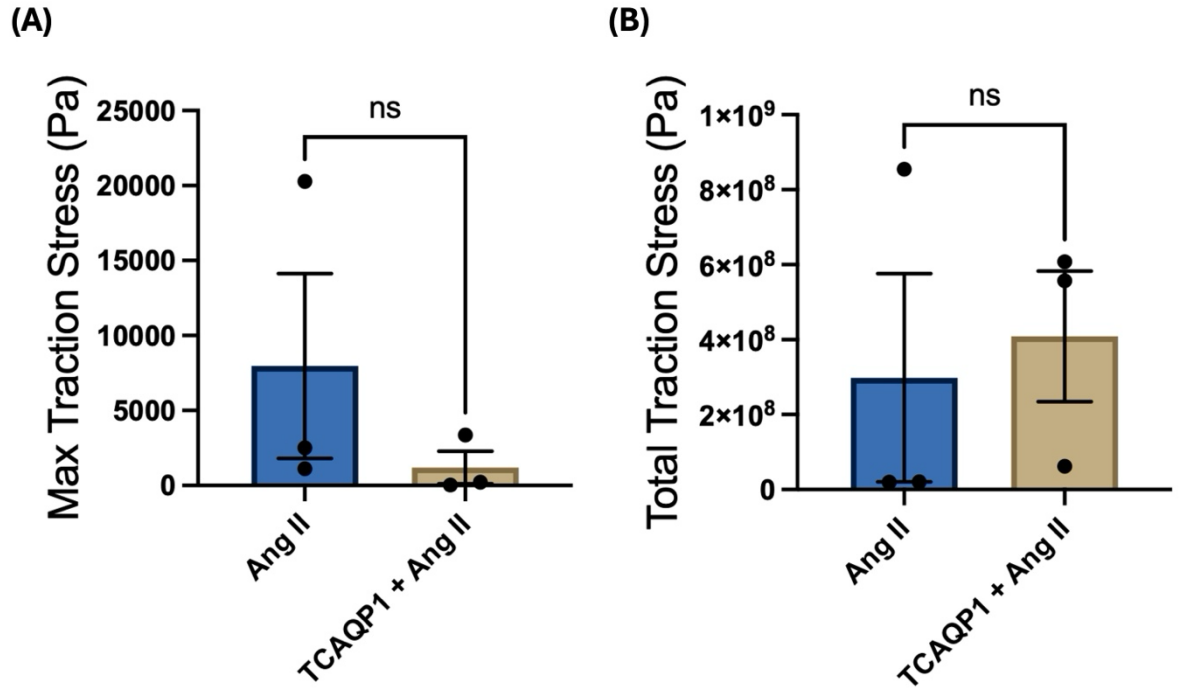

Figure 5.13. AQP1 blockade has no effect on VSMC traction force generation on pliable hydrogels. *Graphs show **(A)** maximum traction stress generation and, **(B)** total traction stress generation for Ang II controls vs TCAQP1 treated cells on 12 kPa hydrogels. Mean and SEM displayed. Black dots show means of N = 3 individual experiments. Statistical significance determined with unpaired T-test.*

Analysis of these data provided contradictory results. TCAQP1 appeared to decrease maximum VSMC traction stress generation, while total traction stress appeared to be slightly increased compared to the Ang II control (Figure 5.13). However, statistical analysis showed that neither of these results were significant. Again, substantial variation was observed in both conditions, highlighting the possibility of technical issues with this experiment.

Next, this experiment was repeated on rigid hydrogels.

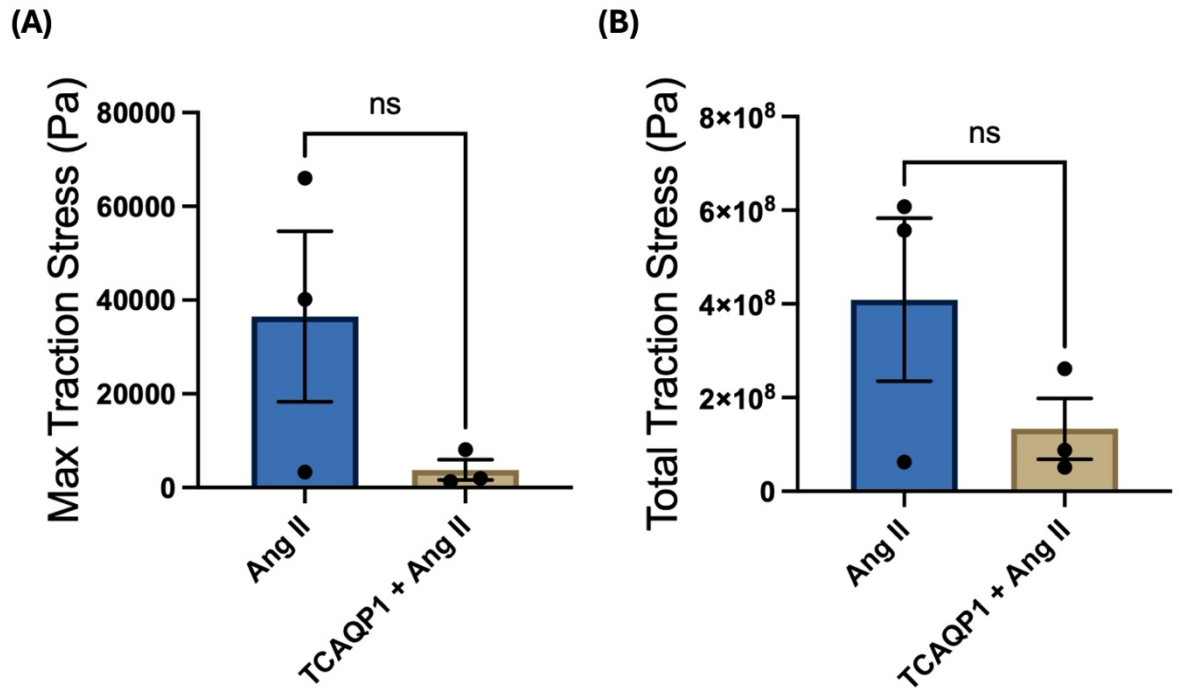

Figure 5.14. AQP1 blockade has no effect on VSMC traction force generation on rigid hydrogels. *Graphs show **(A)** maximum traction stress generation and, **(B)** total traction stress generation for Ang II controls vs TCAQP1 treated cells on 72 kPa hydrogels. Mean and SEM displayed. Black dots show means of N = 3 individual experiments. Statistical significance determined with unpaired T-test.*

On rigid hydrogels blockade of AQP1 appeared to substantially reduce both maximum and total traction stress generation compared to Ang II controls (Figure 5.14). However, analysis revealed that these results were not statistically significant. Notably, the Ang II control condition had a broad range of data, indicating underlying variability, and suggesting a more general issue with the dataset.

5.5.7 Activation of piezo 1 appears to have diverse effects of VSMC traction stress generation

In the previous chapters I demonstrated that activation of piezo1 increases Ca^{2+} flux in VSMCs on both pliable and rigid substrates. To assess whether this increased Ca^{2+} flux has downstream effects on traction force generation I conducted TFM with the Piezo1 activators yoda1 and jedi1.

VSMCs were first seeded on 12 kPa hydrogels and treated with yoda1 (1 μM) and jedi1 (1 μM). TFM was carried out as previously described.

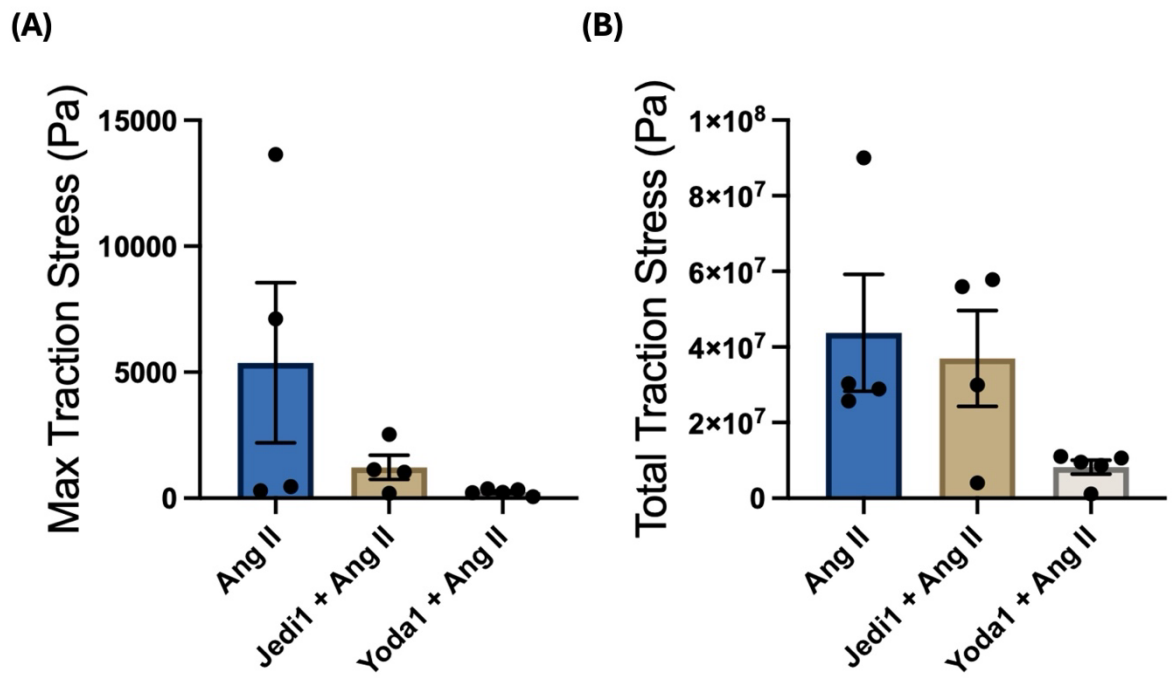

Figure 5.15. Piezo1 activation with Yoda1 or Piezo1 appears to reduce traction stress generation on pliable hydrogels. *Graphs show* ***(A)*** *maximum traction stress generation and,* ***(B)*** *total traction stress generation for Ang II controls vs jedi1 vs yoda1 treated cells on 12 kPa hydrogels. Mean and SEM displayed. Black dots show individual cells (n) from N = 1 experiments. No statistical analysis performed.*

Analysis of this data suggested that activation of piezo1 channels with either yoda1 or jedi1 resulted in reduced traction stress generation by VSMCs seeded on pliable hydrogels. Yoda1 induced the greatest reduction in both maximum and total traction stress generation (Figure 5.15).

Next, this experiment was repeated on rigid hydrogels.

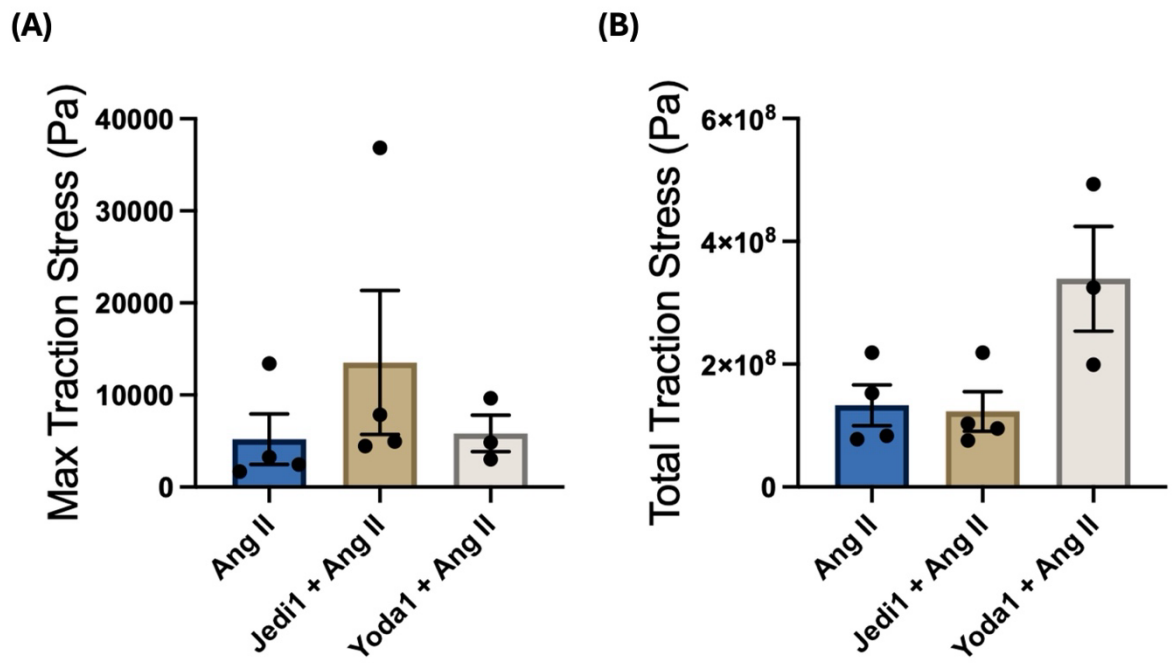

Figure 5.16. Piezo1 activation with Yoda1 or Piezo1 appears to have diverse effects on traction stress generation on rigid hydrogels. *Graphs show **(A)** maximum traction stress generation and, **(B)** total traction stress generation for Ang II controls vs jedi1 vs yoda1 treated cells on 72 kPa hydrogels. Mean and SEM displayed. Black dots show individual cells (n) from N = 1 experiments. No statistical analysis performed.*

On rigid hydrogels, jedi1 treatment appeared to induce a slight increase in maximum traction stress generation compared to the Ang II control, whereas yoda1 treatment induced no noticeable change. However, total traction stress generation was notably increased by yoda1 treatment compared to Ang II controls but remained unchanged by jedi1 treatment (Figure 5.16). No statistical analysis was carried out on this *N = 1* experiment. Further repeats will be required to confirm these preliminary findings.

5.5.8 NAPDH-oxidase (NOX) inhibition has no effect on VSMC traction stress generation

I next investigated the effect of inhibiting NAPDH-oxidase (NOX) on VSMC traction stress generation. NOX is an important multi-subunit enzyme complex that generates ROS such as superoxide anion (O_2^-). In combination with NAPDH, NOX maintains the redox balance within cells, regulating processes such as inflammation and cell signalling. In the vasculature, NOX and ROS-mediated processes have been associated with Ca^{2+} signalling regulation, myogenic tone regulation and expression of genes such as α-SMA and E-cadherin[289]. To assess whether NOX plays a role in VSMC traction force generation I conducted TFM on cells treated with the NAPDH-oxidase inhibitor Vas 2870.

VSMCs were first seeded on 12 kPa hydrogels and treated with Vas 2870 (100 μM). TFM was conducted as previously described.

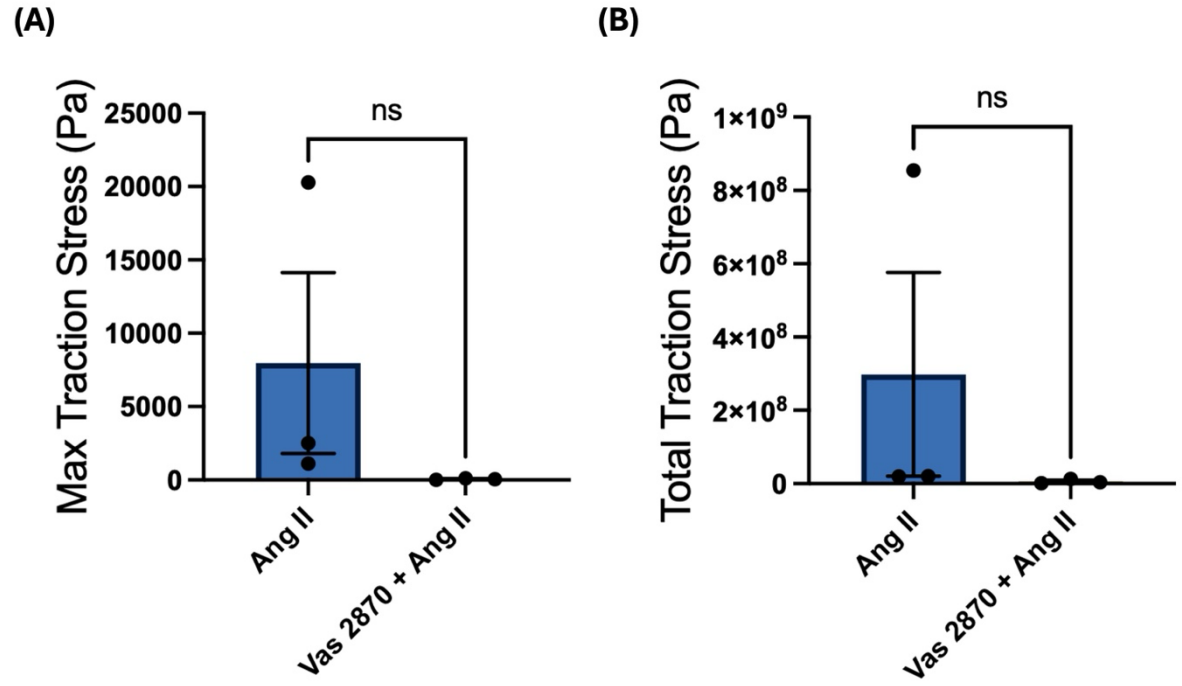

Figure 5.17. NOX inhibition with Vas 2970 has no effect on VSMC traction stress generation on pliable hydrogels. *Graphs show **(A)** maximum traction stress generation and, **(B)** total traction stress generation for Ang II controls vs Vas 2870 treated cells on 12 kPa hydrogels. Mean and SEM displayed. Black dots show means of N = 3 individual experiments. Statistical significance determined with unpaired T-test.*

Analysis of these data suggest that Vas 2870 treatment notably reduced maximum and total traction stress generation by VSMCs on pliable hydrogels. However, these results were found to be non-significant (Figure 5.17).

Next, this experiment was repeated on rigid hydrogels.

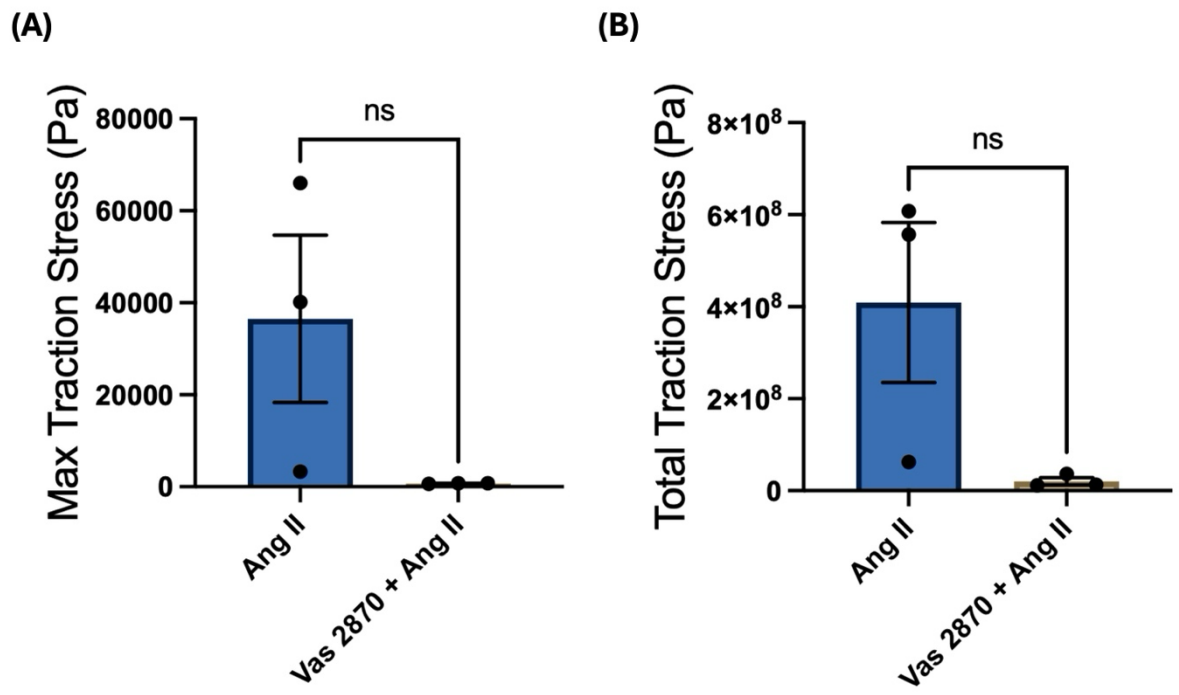

Figure 5.18. NOX inhibition with Vas 2970 has no effect on VSMC traction stress generation on rigid hydrogels. *Graphs show* ***(A)*** *maximum traction stress generation and,* ***(B)*** *total traction stress generation for Ang II controls vs Vas 2870 treated cells on 72 kPa hydrogels. Mean and SEM displayed. Black dots show means of N = 3 individual experiments. Statistical significance determined with unpaired T-test.*

Analysis of these results revealed a similar trend, where treatment with Vas 2870 appeared to reduce maximum and total traction stress generation by VSMCs, however, this result was again found to be non-significant (Figure 5.18).

5.5.9 Confinement *in vitro* appears to influence VSMC area and volume

I next examined the effect of confinement on VSMC area and volume when treated with Ang II. This experiment allows for examination of VSMC behaviour while mimicking the restricted microenvironment of VSMCs *in vivo*. This is particularly interesting in the context of vascular stiffening in disease, where the mechanical forces exerted on VSMCs, such as confinement, are dysregulated.

Here, VSMCs were treated with either TCAQP1, an AQP1 inhibitor, or A1070722, a GSK3 inhibitor, and co-treated with Ang II. These compounds were picked due to their previously demonstrated role in regulating cell area in chapter 3.

To conduct this assay, VSMCs were seeded onto glass-bottomed 6-well plates. Cells were confined with the CSOW 620 static confiner as previously described and treated with TCAQP1 (100 nM) or A1070722 (1 nM) before co-treatment with Ang II (10 μM).

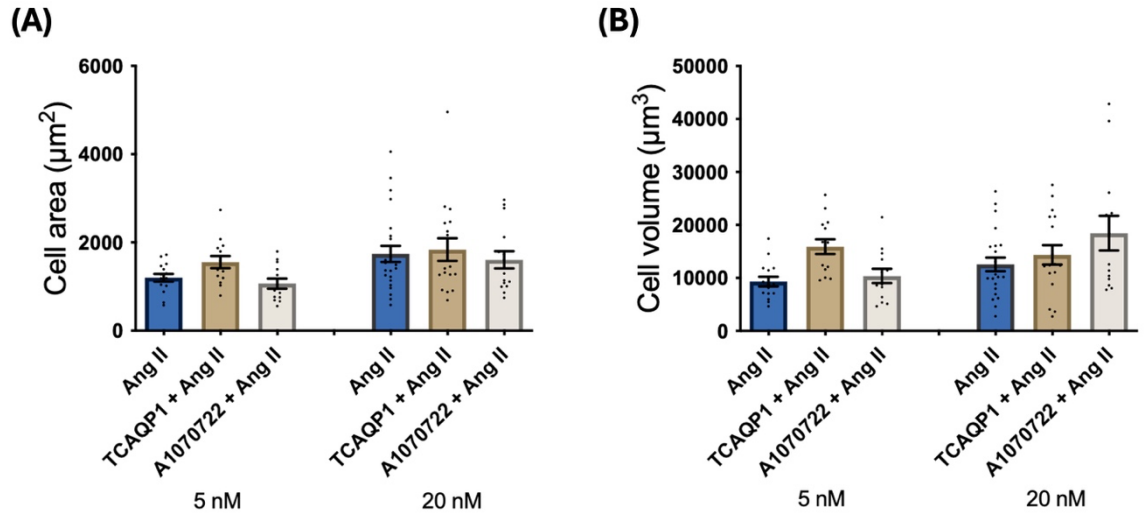

Figure 5.19. Confinement appears to have diverse effects on VSMC area/volume response. *Graphs show* ***(A)*** *cell area and,* ***(B)*** *cell volume of VSMCs treated with Ang II vs TCAQP1 vs A1070722 and confined with 5 nm and 20 nm confinement slides. Mean and SEM displayed. Black dots show individual cells (n) from N = 1 experiments. No statistical analysis performed.*

Analysis of these results appeared to suggest that cell area is slightly decreased under high confinement (5 nm) conditions compared to under less confined (20 nm) conditions. There appeared to be very little difference in cell area of VSMCs treated with TCAQP1 or A1070722 when compared to the Ang II control for either high or low confinement conditions (Figure 5.19A). A similar trend was observed in cell volume. VSMC volume appeared to be slightly decreased under high confinement conditions compared to low confinement conditions (Figure 5.19B). Under high confinement conditions, TCAQP1 treated cells appeared to have a larger volume compared to the Ang II control and A1070722 treated cells. However, no statistical analysis was carried out on this *N = 1* experiment. Further repeats are required to validate these preliminary findings.

5.6 Discussion

In this chapter I have examined the downstream effects of VSMC response to enhanced matrix rigidity. I first examined whether the pro-stiffening pathways observed in the previous chapters (eg. AQP1, GSK3, HDAC1, Piezo1 and NOX) effect traction stress generation in VSMCs seeded on both pliable and rigid matrices. I then briefly examined

the effects of mechanical confinement on VSMC area and volume. These data suggest that matrix rigidity alone had no significant effect on traction force generation. Additionally, inhibition of AQP1, GSK3, HDAC1 and NOX produced no significant change in traction stress generation. However, these results appeared highly variable, even after outlier removal, indicating potential technical issues with these experiments. Piezo1 activation appeared to produce variable responses depending on the drug treatment, with some indication of increased traction stress generation in some conditions. Confinement data indicted a trend towards reduced cell area and volume in high confinement conditions. However, these results were only pilot data (N = 1) and will require further repeats to validate the findings.

The finding that matrix rigidity alone did not affect VSMC traction stress generation is surprising. It is especially surprising that the data appeared to trend towards decreased traction stress generation on rigid hydrogels despite the lack of statistical significance. I have previously shown that matrix rigidity modulates VSMC area response and Ca^{2+} flux in a stiffness dependent fashion. Previous work in endothelial cells has shown that traction force, as assessed by TFM, and cell area are increased with enhanced substrate stiffness[290]. Furthermore, work in fibroblasts has shown that peak and total traction force is increased by increased matrix stiffness[291]. Both groups linked these observations to increased contractility of their cells *in vitro*. The Warren lab has previously linked increased VSMC contractility to the dysfunctional hypertrophy-like response observed in cells seeded on rigid hydrogels. This finding therefore appears to refute the established literature, and our own previous findings. Firstly, assuming the results of this experiment are accurate, it is possible that VSMCs are able to maintain their contractile homeostasis under conditions of enhanced matrix rigidity. Furthermore, it is possible that enhanced matrix rigidity, such as that simulated by our 72 kPa hydrogel, causes usually contractile VSMCs to dedifferentiate into a less contractile phenotype. As outlined in the introduction to this thesis, the phenotypic plasticity of VSMCs in response to extracellular cues is well-established[292]. Additionally, it is possible that TFM may not capture the subtler aspects of tone regulation in VSMCs. VSMC contraction drives subtle changes in isometric tone, in contrast to the wholescale isotonic contraction of skeletal muscle cells. It is possible that the experiments conducted here were not of high enough

resolution to measure subtle differences in VSMC contraction on rigid compared to pliable hydrogels.

It is also surprising that targeted inhibition of previously identified VSMC stiffening pathway components didn't translate into measurable changes in traction stress generation. Of these inhibitors, I have directly linked TCAQP1 (AQP1) and A1070722 (GSK3) to VSMC area control. The results presented here suggest that this area control is not directly linked to changes in traction force generation. We know that VSMCs have multiple overlapping signalling pathways that regulate smooth muscle contractility[293]. It is possible therefore that VSMCs possess compensatory signalling pathways that help to maintain contractile homeostasis when key signalling pathways are inhibited. This redundancy may enable VSMCs to maintain continuous levels of contractile activity when core signalling pathways are inhibited and between pliable and rigid substrates. This may explain why inhibiting these signalling pathways didn't induce statistically significant changes in traction stress generation.

Activation of piezo1 appeared to induce a notable, but not statistically significant, reduction in traction stress generation on pliable hydrogels. I have previously shown that activation of piezo1 induces a significant increase in intracellular Ca^{2+} levels in VSMCs seeded on both pliable and rigid hydrogels. The contractile machinery of VSMCs is intrinsically linked to Ca^{2+} flux, it is therefore surprising that influx of Ca^{2+} appeared to reduce traction stress generation in this experiment. Additionally, on rigid substrate, the finding that yoda1 increased total traction stress, and Jedi1 increased maximum traction stress, further highlights the role of piezo1 in stiffness-dependent contractile response. Further repeats of this experiment will need to be carried out before any firm conclusions can be drawn from these data. However, the literature, and my findings, support a highly dynamic role for piezo1 in VSMC contractility. Work has shown that traction forces drive piezo1 localisation to focal adhesions and induces localised Ca^{2+} flickers[294]. Furthermore, a group working with macrophages has shown that piezo1 activation is modulated by matrix stiffness[295]. Together, these results suggest that piezo1 acts as stiffness-dependent mechanosensor in VSMCs, however, additional experiments will be required to determine the significance of this response.

Having examined the effects of matrix rigidity on traction force generation, I next examined the impact of physical confinement on VSMC morphology. My key finding that confinement at 5 nm (high confinement) appeared to induce a slight reduction in both cell area and volume is as expected. Previous work has shown that VSMCs seeded in tightly confined microchannels exhibit a highly contractile phenotype with increased expression of SMC specific genes[287]. I have previously shown that AQP1 blockade reduces VSMC area on both pliable and rigid substrates. Therefore, the finding that AQP1 blockade appeared to slightly increase cell area in high confinement conditions compared to Ang II controls is interesting. Previous work by the Warren lab has shown that AQP1 regulation is closely linked to extracellular cues. For example, we have previously shown that enhanced matrix rigidity causes AQP localisation to the plasma membrane. It is possible that under high-confinement conditions normal osmotic regulation becomes uncoupled from AQP1 activity, leading to impaired osmotic balance. However, we cannot draw firm conclusions from the N = 1 data, and further work is required to fully understand the effects of spatial confinement on VSMC area/volume response.

It is clear from the data presented here that several of the TFM datasets have significant limitations. Firstly, the spread of data appears to be very broad in most data sets. This is especially prevalent in 12 kPa conditions. Attempts to limit the statistical impact of this variance through application of outlier removal with the ROUT method, while justifiable from a data hygiene perspective, do not remove underlying noise in the datasets. Furthermore, the nature of these experiments mean that the number of cells (n) for each condition is relatively low, limiting statistical power. Furthermore, as previously discussed, the application of TFM in this context may not allow for sufficiently high resolution to observe the micro-adjustments of VSMC contractility. This phenomenon has been previously reported on[296]. It may therefore be useful to design an experiment with higher resolution. For example, atomic force microscopy (AFM) could be used to examine local tension at the membrane in VSMCs on substrates of different stiffnesses. Finally, it is worth noting the heterogenous nature of primary cell cultures such as the VSMCs used here. As these experiments were carried out over a relatively short time

span, utilising the same cell lines, it is possible that these cells were in some way abnormal (differences in phenotype, passage history, proliferative state etc). These so called 'batch effects' may have contributed to the unexpected and highly noisy results presented here.

As discussed above, the data presented in this chapter are highly variable, limiting the strength of any conclusions. However, if taken at face value, these results suggest that VSMC contractility, as measured by traction stress, may not be a key contributor to VSMCSS and vascular stiffening. Taken together, the Warren lab's previous findings, and the results I have presented in this thesis, suggest that this non-hypercontraction driven model involves remodelling of signalling pathways such as Ca^{2+}, and structural reorganisation of cytoskeletal networks, and aquaporin expression and localisation dynamics. This model repositions VSMC stiffening as a disorder involving intrinsic stiffening driven by cytoskeletal remodelling, phenotypic plasticity and osmotic balance.

5.6.1 Summary and Limitations

In conclusion, this chapter has examined downstream effects of VSMC response to enhanced matrix rigidity. Overall, TFM experiments showed no significant difference between pliable and rigid matrix or between control and inhibitor-treated cells on traction stress generation, although preliminary trends were observed for piezo1 activation and confinement experiments. These data sets were highly variable, and despite the application of rigorous normality testing and outlier removal steps, remained highly limited. However, despite limited statistical power, these results suggest that VSMC contraction is not the main driver of VSMC stiffening and that changes in cell signalling, phenotypic plasticity and cell morphology drive this dysfunction. Going forward, refined experimental approaches and new models will be needed to validate these findings.

Chapter 6: Discussion and Conclusion

Overall, this thesis has examined the signalling pathways and mechanisms by which VSMCs respond to enhanced matrix rigidity. This is a significant field of research as stiffening of the major arteries, such as the aorta, is a major component of cardiovascular disease such as atherosclerosis, and is an important risk factor for cardiovascular events such as stroke and aneurism. My main aim therefore was to identify the key signalling pathways and mechanisms by which VSMCs contribute to arterial stiffening. To do this, I have investigated VSMC response to enhanced matrix rigidity through the lens of "smooth muscle cell stiffness syndrome". This syndrome posits that the SMC contribution to tissue stiffening results from altered mechanical and adhesive properties of SMCs. In VSMCs these properties include increased stiffening of the cortical cytoskeleton and increased adhesion to ECM proteins such as fibronectin[128]. To achieve this aim, I utilised a hydrogel-based assay previously developed by the Warren group[297]. This assay utilises hydrogels of tuneable stiffnesses, which can be adhered to 30 mm coverslips and used in conjunction with 6-well plates for cell culture. We use hydrogels of 12 kPa, which possess a stiffness equivalent to a healthy blood vessel, and 72 kPa, which are roughly equivalent to the stiffness of an aged or early-stage diseased blood vessel.

In chapter 3, I used this assay in conjunction with immunofluorescence microscopy to conduct concentration response screens on several inhibitors of key VSMC signalling pathways. Previous work by the Warren lab has found that VSMCs seeded on rigid hydrogels undergo a dysfunctional hypertrophy-like response. I therefore conducted targeted screens focused on inhibiting pathways involved in volume regulation, calcium handling, microtubule dynamics and key cell-signalling protein kinases. By assessing cell area, I identified key pathways involved in VSMC response to enhanced matrix stiffening. My key findings from this chapter are that aquaporins, Ca^{2+} handling and microtubules all play important roles in the VSMC response to enhanced matrix rigidity. Specifically, I found that inhibition of aquaporins induced a reduction in cell area on rigid matrix, as did inhibition of calcium store channels IP_3R and RyR. Interestingly, I found that microtubule stabilising agent epothilone B induced a reduction in cell area on rigid matrix, and that microtubule destabilising agent nocodazole caused a contrasting increase in VSMC area on pliable matrix.

In chapter 4, I developed the findings of the first chapter by examining changes in Ca^{2+} flux in response to co-treatment of VSMCs with Ang II and compounds that target Ca^{2+} handling pathways. This allowed me to identify pathways involved in stiffness-dependent regulation of Ca^{2+} handling in VSMCs. To achieve this, I used Fluo-4, a cell-permeable calcium indicator which can be used to measure Ca^{2+} concentrations inside living cells. My key findings from this chapter are that enhanced matrix rigidity induces a wholescale remodelling of calcium dynamics in VSMC treated with Ang II, with significantly increased cytosolic Ca^{2+} concentrations observed on 72 kPa hydrogels. Furthermore, I found that microtubule stabilisation with paclitaxel caused a significant increase in Ca^{2+} flux in VSMCs on pliable hydrogels, and a significant reduction in Ca^{2+} flux in cells on rigid hydrogels. Importantly, I found that inhibition of mechanosensitive ion channels such as piezo 1 prevented the increase of intracellular Ca^{2+} concentration in VSMCs on rigid hydrogels. Additionally, I found that activation of piezo1 induced significantly increased Ca^{2+} flux on both pliable and rigid hydrogels.

In the final results chapter, I examined the downstream effects of the VSMC response to matrix rigidity such as contractility. To achieve this, I used TFM in conjunction with our polyacrylamide hydrogel assay. TFM is a microscopy technique used to examine the traction forces exerted by cells on their extracellular matrix. TFM works by inserting fluorescently labelled beads into the extracellular substrate. When cells contract, they exert deformational forces on the matrix which causes the embedded beads to move. This bead movement can be tracked to generate a displacement field. The TFM results presented in this thesis are highly variable, which, despite the application of rigorous data quality control steps, precludes drawing any firm conclusions. However, taken at face value, the key finding of this chapter is that vascular stiffening is not primarily driven by VSMC hyper-contractility. I additionally conducted preliminary work utilising a cell-confinement device to examine the effect of restricted microenvironments on VSMC behaviour. My main finding here is that VSMCs under high confinement conditions appear to have reduced area and volume compared to cells under moderate confinement conditions.

Overall, the main findings from this work are that VSMC response to enhanced matrix rigidity involves several complementary pathways, that calcium flux drives this matrix dependent response, and that SMCSS is not a dysfunction of hyper-contractility.

6.1 VSMC response to enhanced matrix rigidity involves several complementary pathways

One of the key takeaways from my first chapter is the diversity of pathways involved in regulation of VSMC area response to enhanced matrix rigidity (Table 6.1).

***Table 6.1. Table showing compounds used in chapter 3**. Shows their molecular target, their effect on VSMC area on pliable and rigid hydrogels, and their cell area range at lowest and highest concentration.*

		Area Response		Cell Area Range (μm²)	
Drug	**Target**	**12 kPa**	**72 kPa**	**12kPa**	**72kPa**
TCAQP1	Aquaporin 1	Reduced	Reduced	2907-1220	2761-1188
TGN020	Aquaporin 4	No change	Reduced	1756-1506	2182-1369
Furosemide	NKCC	N/A	No change	N/A	6021-5633
STOCK2S 26	Wnk	N/A	No Change	N/A	6762-5719
Go6983	PKC	N/A	Reduced	N/A	6957-4668
Xestospongin C	IP_3R	Increased	Reduced	2970-4612	4658-2727
Dantrolene	RyR	Increased	Reduced	1966-5126	5010-1864
Epothilone B	MTs (Stabilises)	No change	Reduced	2742-2963	5089-2753
Nocodazole	MTs (Destabilises)	Increased	No change	2820-4430	4271-4409
A1070722	GSK3	No change	Reduced	4186-3362	5708-3873
AZD7762	Chk2	No change	Reduced	3274-3012	5232-3275
Ku55933	ATM	No change	Reduced	3347-3571	5189-3868
EB47	PARP-1	No change	Reduced	3693-3133	6528-3557

The table above shows that many of the pathways involved in VSMC response to enhanced matrix rigidity are membrane channels and cytoskeletal regulators. One of the key findings of this chapter is the role of aquaporin water channels in VSMC morphological response. As the primary facilitators of osmosis across the plasma membrane, aquaporins are key regulators of cell area/volume in many cell types. Here, I

show that inhibition of AQP1 induced a reduction in VSMC area on both pliable and rigid hydrogels. Interestingly, the finding that AQP4 inhibition had no effect on cell area in VSMCs seeded on pliable hydrogels suggests that AQP4 possesses substrate-depended dynamics. These results suggest that substrate-dependent water flux through aquaporins plays a key role in the VSMC response to enhanced matrix rigidity. Another pathway of particular interest is the Ca^{2+} signalling pathway. My results show that inhibition of intracellular Ca^{2+} release through IP_3R and RyR induces an increase in VSMC area on pliable hydrogels, but a reduction on rigid hydrogels. Additionally, the finding that inhibition of PKC, an important Ca^{2+} signalling protein, reduced VSMC area on rigid hydrogels further highlights the role of Ca^{2+} in this axis. These results align with previous work by the Warren lab which has shown that piezo1 mediated Ca^{2+} flux drives PKC activation and subsequent localisation of AQPs to the plasma membrane[190]. Here, I specifically show that inhibition of any of these components is sufficient to prevent matrix-dependent remodelling of VSMC morphology. Furthermore, these results show that aquaporin involvement in VSMC stiffening is a regulated process and not simply a consequence of basal water flux. These findings highlight a disconnect between Ca^{2+}/AQP signalling and normal volume regulation on rigid hydrogels that I further explore in chapter 4. The results here are further supported by the apparent lack of involvement of NKCC, demonstrating that VSMC volume homeostasis becomes widely dysregulated as a result of matrix stiffening.

The other major finding of these targeted screens is the involvement of microtubules in the VSMC response to matrix rigidity. Microtubule stabilisation with epothilone B induced a reduction in VSMC area on rigid hydrogels and had no effect on VSMCs on pliable hydrogels. Microtubule destabilisation with nocodazole induced an increase in VSMC area on pliable hydrogels and had no effect on area on rigid hydrogels. These results suggest that microtubules play a dynamic role in VSMC area regulation on pliable and rigid hydrogels. Firstly, the finding that microtubule destabilisation caused an increase in area on pliable hydrogels fits within the previously described tensegrity model, whereby reduced microtubule stability moderates actomyosin force generation and promotes cell spreading. Whereas, on rigid substrates, stabilised microtubules are required to balance excessive actomyosin derived contractility[137]. Furthermore, it is

known that microtubules are involved in focal adhesion dynamics. This suggests that microtubules are tightly integrated into the mechanosensitive machinery[298]. These results are especially interesting considering my findings regarding Ca^{2+} signalling in VSMC mechanosensing. Calcium is a known regulator of microtubule stability[267]. These findings reveal a Ca^{2+}-microtubule signalling axis whereby enhanced matrix rigidity destabilises microtubules and induces increased Ca^{2+} flux across the plasma membrane. This leads to a feedback loop where further microtubule destabilisation is induced, resulting in increased Ca^{2+} flux across the membrane and from intracellular stores. This signalling axis appears to directly induce changes in cell morphology, possibly though increased actomyosin force generation and adhesome remodelling, while also promoting aquaporin-mediated VSMC swelling through PKC activation and subsequent AQP localisation to the membrane[190].

Looking beyond this signalling axis, VSMC response to matrix rigidity appears to have broad pathway dependence. Targeted inhibition of GSK3, Chk2, ATM and PARP-1 all induced concentration dependent reductions in VSMC area on rigid hydrogels. Of this group, GSK3, Chk2 and ATM are all serine-threonine kinases involved in cell transport, proliferation, cell-death, differentiation and DNA repair[208,299,300]. GSK3 is a known regulator of microtubule dynamics, primarily through its interaction with microtubule associated proteins Tau and MACF1[301]. When MACF1 is activated by GSK3 it promotes microtubule-actin interactions which couple the microtubule cytoskeleton to cell-cell junctional complexes[302]. This axis directly links GSK3 activity to the mechanosensitive machinery of VSMCs. Furthermore, work has shown that ATM activation during mechanical stress induces phosphorylation and remodelling of key cytoskeletal and chromatin regulators and that this pathway directly regulates cell stiffness in HeLa cells[303]. My findings here, in conjunction with the literature, suggest that rigid substrates activate not only cytoskeletal and Ca^{2+} regulators, but also nuclear and adhesion associated protein kinases. Finally, the activity of PARP-1 can also be linked to this cytoskeletal and cell-stiffness regulation axis. Work has shown that elevated PARP1 activity disrupts actin organisation in drosophila[304] and that inhibition of PARP1 in monocytes induces reorganisation of the actin cytoskeleton[305].

Taken together these results suggest that VSMC remodelling on rigid matrices is coordinated by a network of complementary signalling pathways including ion and water flux, cytoskeletal dynamics and nuclear kinases. Calcium signalling in particular arose as an important regulator at multiple nodes across these pathways, with links to aquaporins and microtubule dynamics. These findings provided the rational for further investigation into how calcium signalling is differentially regulated on rigid matrices.

6.2 Altered Ca^{2+} flux drives the VSMC response to enhanced matrix rigidity

Given the central role of Ca^{2+} signalling in VSMC physiology and its repeated appearance in the inhibitor screens, I next investigated how Ca^{2+} flux itself is regulated by matrix rigidity. In my drug screens I identified that inhibition of IP_3R, RyR and PKC had matrix-dependent effects. Here, I found that enhanced matrix rigidity induced a significant increase in calcium flux and caused a noticeable difference in Ca^{2+} kinetics. This result, highlighting Ca^{2+} as a core driver of the VSMC matrix rigidity response, potentially explains why inhibition of Ca^{2+} handling pathways, IP_3R, RyR, and PKC, was able to prevent the morphological changes observed in VSMCs on rigid hydrogels.

I next examined the role of microtubule stability in Ca^{2+} flux. During my inhibitor screens, I identified that microtubule destabilisation resulted in an increase in area on pliable hydrogels and had no significant effect on VSMC area on rigid hydrogels. Fascinatingly, these results directly corresponded with my findings in Ca^{2+} flux. Here, microtubule destabilisation resulted in significantly increased Ca^{2+} flux on pliable hydrogels but caused no significant change in Ca^{2+} flux in VSMCs on rigid hydrogels. One interpretation of these results is that microtubules are already maximally destabilised, potentially due to activity of the nuclear kinases discussed above, on rigid hydrogels, and that this drives the substantially increased Ca^{2+} flux observed under these conditions. Whereas on pliable hydrogels, the aberrant, Ca^{2+} driven morphology response to enhanced matrix stiffness can be induced by destabilising microtubules. Furthermore, I found that microtubule stabilisation had no effect on VSMC area on pliable hydrogels and caused a significant reduction in cell area on rigid hydrogels. When assessing Ca^{2+} flux, I found that microtubule stabilisation induced a significant increase in Ca^{2+} flux on pliable hydrogels

and induced a significant reduction of Ca^{2+} flux on rigid hydrogels. These results further support the idea of microtubule stability possessing regulatory capacity over Ca^{2+} flux, whereby microtubule stability prevents the enhanced Ca^{2+} flux usually observed on rigid hydrogels and blocks the aberrant morphological response. Taken together, these results point to a microtubule-Ca^{2+} feedback loop that integrates mechanical signals from the ECM to regulate VSMC morphology in response to matrix stiffening.

Following this, I examined the involvement of upstream components of Ca^{2+} regulation, namely the mechanosensitive ion channel piezo1. Piezo1 has been widely implicated in mechanosensing and force-dependent Ca^{2+} flux in several cell types[306]. Here, I demonstrated that inhibition of piezo1 significantly reduces Ca^{2+} flux on rigid hydrogels. This suggests that the heightened Ca^{2+} flux observed in VSMCs on rigid matrices is driven by the activity of mechanosensitive ion channels at the plasma membrane. Furthermore, I found that activation of piezo1 induced significantly increased Ca^{2+} flux on both pliable and rigid hydrogels. These results suggest that Ca^{2+} influx through piezo1 is one of the key mechanisms by which Ca^{2+} levels are increased in VSMCs during the matrix rigidity response. As previously discussed, the fact that piezo1 activation increased Ca^{2+} flux on rigid hydrogels suggests that piezo1 may only be partially activated by enhanced matrix rigidity, or that piezo1 undergoes differential localisation or off-kinetics between matrices of different stiffnesses. Additionally, the differential response could be explained by downstream effectors of this Ca^{2+} influx. For example, my inhibitor screens revealed that PKC has differential activity on pliable and rigid hydrogels and therefore induces differential downstream effects.

I also examined whether histone deacetylases (HDACs) modulate Ca^{2+} flux in VSMCs. Inhibition of either HDAC1 or HDAC6 had no significant effect on Ca^{2+} flux on either pliable or rigid hydrogels. These results suggest that Ca^{2+} signalling in VSMCs is not broadly HDAC dependent. However, non-statistically significant results suggest that inhibition of HDAC2 and HDAC3 induced increased Ca^{2+} flux on pliable hydrogels, and reduced Ca^{2+} flux on rigid hydrogels. As previously discussed, HDAC3 has been associated with microtubule regulation[281,282], suggesting it may play a role in the microtubule stability-Ca^{2+} axis described above. The possible role of HDAC 2 and 3 in the VSMC response to matrix stiffening may indicate the involvement of other nuclear

signalling pathways. My finding that several nuclear kinases, including GSK3, Chk2 and ATM all reduced VSMC area on rigid hydrogels appears to support this. There is a growing body of published work to suggest that the nucleus is a mechanosensitive organelle, and that this mechanosensitivity derives from crosstalk with mechanosensitive ion channels[307]. These findings suggest a role for the nuclear component in the VSMC response to enhanced matrix rigidity, whether that be through direct regulation of microtubule dynamics, or through nuclear signalling pathways that regulate cytoskeletal organisation and interact with mechanosensitive ion channels.

Taken together these results position Ca^{2+} as a central integrator of the VSMC stiffness response. My findings link mechanosensitive ion channels to microtubule remodelling and nuclear signalling pathways. It appears that these signalling pathways form an interconnected network, suggesting that VSMC stiffness sensing and response is a multifactorial process involving complex interplay between piezo1 mediated Ca^{2+} flux, water flux through aquaporins, microtubule dynamics and nuclear signalling.

6.3 Functional outcomes of VSMC stiffness sensing

In my final results chapter, I examined the downstream consequences of VSMC stiffness sensing pathways by assessing traction stress generation. In my previous chapters I found that key pathways involved in contraction, such as Ca^{2+} signalling, are differentially activated between 12 and 72 kPa hydrogels. As contraction is one of the key mechanisms by which cells exert traction stress on their surrounding matrix, I expected to see increased traction force generation in VSMCs seeded on rigid hydrogels. However, analysis of my data revealed that matrix rigidity is not a key determinant of traction stress generation in VSMCs. One interpretation of this is that on rigid hydrogels, VSMCs undergo phenotypic dedifferentiation into the less contractile, synthetic phenotype, where expression of contractile genes is downregulated. This effect could be further enhanced if the primary cells used in these studies were from aged or diseased individuals, where extracted VSMCs had already undergone this dedifferentiation process. Furthermore, a previous study conducted with rat aortic VSMCs found that differences in traction stress generation were all within margin of error when seeded on moderate rigidity hydrogels (5-

10 kPa)[308]. It is possible that traction stress is differentially regulated by matrix stiffness, but that the range of stiffnesses used in this assay (12 vs 72 kPa), is not wide enough to induce a statistically significant difference. Additionally, previous work has highlighted that mechanosensing is regulated across multiple hierarchical domains, from the whole tissue level, down to the molecular level[309].It is possible that the hierarchical nature of mechanotransduction means that above a certain threshold of pro-contractile stimulus, downstream effectors, such as focal adhesions, dampen force transduction into the extracellular matrix in an effort to maintain homeostasis. Finally, work in VSMCs from mice with Marfan syndrome, which share several of the mechanosensing defects seen in aged VSMCs, have been shown to have reduced traction force generation, even on substrates of enhanced rigidity[310].

Next, I examined the effect of inhibiting GSK3 and HDAC1 on traction stress generation. My previous results showed that GSK3 inhibition reduced VSMC area on rigid hydrogels. Here, I found that GSK3 inhibition had no significant effect on traction stress generation on either pliable or rigid hydrogels. GSK3 is associated with regulation of cytoskeletal dynamics and intracellular transport, but not with direct actomyosin force generation. It is therefore possible that the activity of GSK3 contributes to VSMC stiffening without contributing to enhanced contractility[311]. Furthermore, as previously discussed, VSMCs possess several complementary signalling pathways involved in VSMC mechanotransduction and force generation. These diverse pathways confer redundancy in the contractile machinery and may enable VSMCs to maintain contractile homeostasis on rigid substrates.

Additionally, as previously discussed, my investigation into Ca^{2+} flux and HDAC1 inhibition revealed no statistically significant result, with a trend towards increased Ca^{2+} flux on pliable hydrogels. Here, I also saw no statistically significant change in traction stress generation, however, traction stress did appear to slightly trend upwards when VSMCs were seeded on rigid hydrogels and treated with MS275. While it is hard to draw any strong conclusions from this result, it does highlight the possibility of a decoupling of the normal contractile pathway and HDAC1 signalling on rigid matrices. However, previous work in mouse aortae has found that HDAC1 inhibition causes aortic rings to

relax, possibly due to their inhibitory action on voltage gated Ca^{2+} channels[312]. My result therefore seems to refute the established literature, and further research will be required to validate this finding. It is possible that the HDAC1 effect on contractility is mediated through gene regulation rather than posttranslational modification of proteins such as tubulin. For example, previous work in mice has shown that HDAC1 inhibition though ketogenic diet and β-hydroxybutyrate treatment promotes increased contractility by upregulating expression of contractile markers[313]. It is possible therefore, that the short term Ca^{2+} flux and TFM assays conducted in this thesis were not of a long enough time frame to capture the long-term impacts of HDAC1 inhibition.

I next investigated whether AQP1 regulates traction force generation in VSMCs. My key finding here was that AQP1 blockade did not induce a statistically significant change in traction force generation on either pliable or rigid hydrogels. However, there was a general trend toward reduced traction force generation in both conditions. I have previously shown that AQP1 inhibition significantly reduces cell area of VSMCs seeded on rigid hydrogels. This result suggests that the role of AQP1 in VSMC stiffening involves intrinsic stiffening driven by dysregulated osmotic balance rather than direct involvement in cell contractility pathways. The finding that AQP1 is an effector of upstream signalling pathways, rather than a signalling hub itself is widely supported by the literature[314,315].

Following these findings, I examined the role of piezo1 activation in VSMC traction stress generation. I previously found that activation of piezo1 induced a significant increase in Ca^{2+} flux on both pliable and rigid hydrogels. Here, I found that activation of piezo1 with jedi1 and yoda1 induced a non-significant reduction in traction force generation on pliable hydrogels and had diverse effects on rigid hydrogels. This N = 1 experiment will need further repeats before firm conclusions can be drawn. However, this preliminary result is surprising as Ca^{2+} flux is a key driver of the VSMC contractile machinery. As previously discussed, piezo1 dynamics are complex, with differential localisation, partial activation and regulated off-kinetics all playing roles in Ca^{2+} flux[102]. These complex dynamics may modulate downstream effects of Ca^{2+} flux and explain why the increased Ca^{2+} flux observed when piezo1 is activated did not translate into an observable increase

in contractility. Broadly speaking, these findings support the general finding that VSMC stiffening is driven by complex and integrated signalling pathways and not hypercontractility alone. Further, work will be required to investigate these findings more thoroughly.

Next, I investigated the role of NOX inhibition on VSMCs traction stress generation. The production of reactive oxygen species (ROS) by NOX is a vital signalling axis involved in a range of VSMC processes including phenotypic regulation, immune response, proliferation, migration and apoptosis[316]. ROS are also intrinsically linked with the inflammatory response and have been associated with progression of cardiovascular diseases such as atherosclerosis[317]. Here, I found that inhibition of NOX had no significant effect on traction stress generation. However, there was a general trend towards reduced traction stress on both pliable and rigid hydrogels when treated with NOX inhibitor. Similarly to the HDAC results discussed above, it is possible that the experiments conducted here missed the long-term effects of ROS signalling. ROS signalling typically involves long-term redox modification of proteins through oxidation-reduction reactions or covalent adduct formation[318]. Because NOX-derived ROS can induce irreversible oxidative adducts, it is possible that acute pharmacological inhibition of NOX is not sufficient to reverse the effects of ROS signalling, thus explaining the lack of statistically significant changes in traction stress reported here. Overall, this result suggests that NOX contributes to VSMC stiffening primarily through chronic redox remodelling and phenotypic modulation rather than through acute regulation of traction stress generation.

Finally, I investigated the effect of AQP1 and GSK3 inhibition on VSMC response to mechanical confinement. My key finding from this pilot data was that cell area and volume appear to be reduced under high confinement conditions. This finding is expected, as cells are physically restricted and are unable to spread. Furthermore, previous work has shown that confined VSMCs acquire a highly contractile phenotype *in vitro*[287]. Interestingly, under high confinement conditions AQP1 inhibited cells appeared to have slightly increased volume compared to the control. I have previously shown that inhibition of AQP1 reduces VSMC area on rigid hydrogels and has no significant effect on

pliable hydrogels. It is possible that this result represents a decoupling of normal AQP1 function under conditions of high confinement, possibly driven by altered membrane localisation or channel activity. This result suggests that mechanical confinement represents an additional mechanosensory cue, in addition to matrix rigidity, that influences VSMC morphology.

6.4 Strengths, limitations and future directions

This thesis has a few biological limitations that future work can build on. Firstly, the variability of primary VSMCs used throughout the study is a widespread limitation of research that uses primary cell culture. By their nature, primary cells have different passage history, phenotype and donor history. This is especially important to note in studies such as this where conclusions have been drawn based on comparisons between 'healthy' and 'diseased/aged' conditions. This heterogeneity means that there are possibly pre-existing differences between cells before they are experimentally differentiated. These 'batch effects' are common and may explain a lot of the variability observed in my TFM experiments for example. Furthermore, VSMCs in culture lack the systemic cues, such as endothelial-cross talk, and mechanical cues, such as shear stress, that would normally come from the cell microenvironment *in vivo*.

These limitations open the door for exciting experimental opportunities going forwards. Firstly, utilising animal models, such as mouse, would enable us to examine the role of some of the signalling and mechanistic pathways I have identified *in vivo*. There are several commonly used mouse and rat models of hypertension, such as the spontaneously hypertensive rat (SHR) model and the Angiotensin II model[319]. Utilising these models would allow us to examine the full spectrum of mechanical cues and enable easy comparison between VSMCs from healthy mice and diseased/aged mice. Using models like this would also enable us to explore the temporal dynamics of some of the pathways identified in this thesis such as HDAC and ROX mediated regulation of VSMC stiffening. Utilising these models would also provide us with much greater translational capability in terms of developing pharmacological interventions for VSMC

stiffening in the clinic. In addition to *in vivo* experiments, future work could also involve co-culture systems where VSMCs are cultured alongside endothelial and fibroblast cells. This experimental set-up would facilitate crosstalk between cells, which we know is a key regulator of VSMC behaviour, and enable more accurate simulation of the *in vivo* mechanical environment in culture. Finally, the hydrogel system used here does not accurately model the 3D environment VSMCs exist within *in vivo*. To ameliorate this, future work could utilise 3D organoids to more accurately represent the 3D, multicellular environment of the blood vessel, and enable investigation of VSMC mechanosensing in a more physiologically relevant context. Currently, organoid systems of the vasculature are not widely used, so initial development is likely to be technically challenging, however, they would provide a useful intermediate model between our hydrogel system and animal models.

It is also important to discuss the methodological limitations of this study. Firstly, the experiments here have utilised pharmacological inhibitors to examine the effects of individual pathways on VSMC stiffness response. This approach has several advantages, for example they are easy to use in conjunction with our hydrogel system and are relatively cheap. They also allowed for rapid, parallel testing of many candidate pathways, and for examination of dose responsiveness as shown in chapter 3. Inhibitors also have high clinical relevance as several compounds used here are already used in the clinic. However, pharmacological inhibitors are rarely entirely target-specific and can have off-target effects. For example, Go6983 in particular has been associated with off-target inhibition of a range of kinases including GSK3 and MAPKAP[176]. Additionally, the acute nature of pharmacological inhibition means that long-term transcriptional, epigenetic and ROS-driven effects of target pathways are likely to be missed by the short-term assays conducted here.

Other methodological considerations include the reliance on microscopy techniques. Microscopy techniques are useful as they are comparatively cheap and easy to perform. Additionally, in the context of this study, microscopy techniques allowed for quantitative assessment of variables such as area and volume, which can be easily compared between conditions. Furthermore, live cell imaging allowed for dynamic, real-time

assessment of Ca^{2+} flux and traction force generation which would otherwise be difficult to quantify. This versatility has allowed me to examine the mechanistic linkage between VSMC morphology, Ca^{2+} signalling, and downstream effects using the same microscopy-based approach. However, microscopy techniques also have some drawbacks. For example, microscopy is vulnerable to observer bias and over-simplification in analysis. This is especially true under conditions where variability between cells is high and can be amplified when data sets are small.

In summary this study has several advantages, including the highly tuneable polyacrylamide hydrogel system, the high-throughput use of pharmacological inhibitors and the use of powerful microscopy techniques. Going forward, it would be exciting to conduct work in VSMC co-culture settings, 3D organoid systems and finally in animal models to validate my *in vitro* findings *in vivo*.

6.5 Conclusion: Framing VSMCSS as a whole cell dysfunction

Arterial stiffening plays a key role in vascular ageing and cardiovascular disease progression with stiffening of VSMCs representing a core component of this stiffening axis. VSMCs are highly mechanosensitive cells that integrate cues from their extracellular environment to regulate phenotypic state, gene expression, adhesome and cytoskeletal dynamics, and contractility. We know that VSMCs integrate these cues to modulate their response to enhanced matrix rigidity, however, the mechanisms driving the loss of VSMC compliance in arterial stiffening have yet to be fully elucidated. In this thesis I have utilised a polyacrylamide hydrogel model to mimic the stiffness of healthy and diseased/aged matrix. I use this system in conjunction with a range of microscopy techniques to assess VSMC morphology, Ca^{2+} flux and traction stress generation.

My results highlight that VSMC stiffness sensing is multifactorial, involving several complementary pathways including AQP1-mediated water flux, microtubule dynamics, calcium handling, and nuclear kinases. I further identified Ca^{2+} signalling as a vital integrator of VSMC mechanosensitive pathways and identified a key regulatory role for microtubules dynamics and mechanosensitive ion channels such as piezo1. I also

provided pilot data to suggest that traction forces are not directly increased downstream of the VSMC enhanced matrix rigidity response. This model suggests that VSMCSS is a whole-cell dysfunction, rather than a response driven by hyper-contractility.

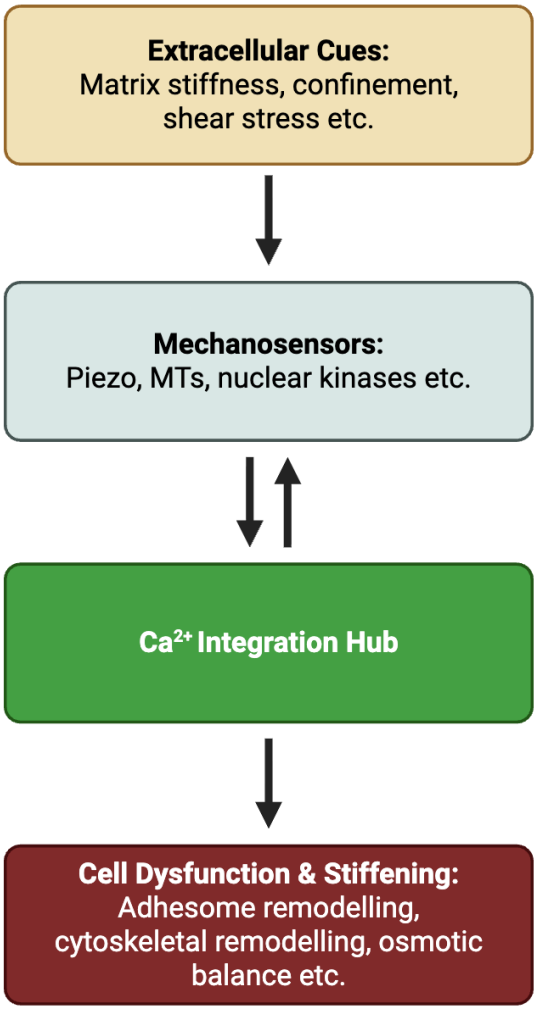

Figure 6.1. Illustration of the hierarchical model of VSMC stiffness sensing and dysfunction in VSMCSS. *Extracellular cues such as ECM stiffness and shear stress are detected by mechanosensitive components such as SACs (piezo1), microtubule stability and nuclear kinases. The downstream signals of these components are integrated by dynamic Ca^{2+} flux. This leads to a feedback loop where increased Ca^{2+} flux leads to further dysregulation of microtubule stability. Aberrantly increased Ca^{2+}flux leads to VSMC dysfunction and stiffening through adhesome and cytoskeletal remodelling, and dysregulated osmotic balance.*

By framing VSMCSS as a whole-cell dysfunction, this work underscores the need to further investigate the role of cytoskeletal regulators, mechanosensitive ion channels and osmotic balance in VSMC stiffening. It will be particularly interesting to further investigate the role Ca^{2+} plays in integrating these signals. The core finding that Ca^{2+} flux is differentially regulated by matrix rigidity is arguably the key finding of this thesis. Ca^{2+} ions are one of the most ubiquitous signalling messengers with roles in nearly every

aspect of cell behaviour. Here, I specifically found that mechanosensitive piezo1-mediated Ca^{2+} entry is essential for the enhanced flux observed on rigid hydrogels and that microtubule stability directly regulates Ca^{2+} handling in a stiffness-dependent manner. These findings position Ca^{2+} flux in the centre of the VSMC mechanosensitive network and may provide a unifying model for how diverse signalling pathways converge to produce whole-cell dysfunction.

References

1. Roth, G. A. *et al.* Global Burden of Cardiovascular Diseases and Risk Factors, 1990–2019: Update From the GBD 2019 Study. *J. Am. Coll. Cardiol.* **76**, 2982 (2020).
2. Luengo-Fernandez, R. *et al.* Economic burden of cardiovascular diseases in the European Union: a population-based cost study. *Eur. Heart J.* **44**, 4752–4767 (2023).
3. Cardiovascular diseases (CVDs). https://www.who.int/news-room/fact-sheets/detail/cardiovascular-diseases-(cvds).
4. Pappano, A. J. , author. http://id. loc. gov/authorities/names/n2006008366. *Cardiovascular Physiology - E-Book*. (Elsevier, 2018).
5. Barros, V. N. The heart cycle: review. *Women's Health* **8**, 66–69 (2019).
6. Stephenson, A., Adams, J. W. & Vaccarezza, M. The vertebrate heart: an evolutionary perspective. *J. Anat.* **231**, 787–797 (2017).
7. Halper, J. Basic Components of Vascular Connective Tissue and Extracellular Matrix. *Adv. Pharmacol.* **81**, 95–127 (2018).
8. Belz, G. G. Elastic properties and Windkessel function of the human aorta. *Cardiovasc. Drugs Ther.* **9**, 73–83 (1995).
9. Gasser, T. C., Ogden, R. W. & Holzapfel, G. A. Hyperelastic modelling of arterial layers with distributed collagen fibre orientations. *J. R. Soc. Interface* **3**, 15 (2005).
10. Kim, H. L. & Kim, S. H. Pulse Wave Velocity in Atherosclerosis. *Front. Cardiovasc. Med.* **6**, 41 (2019).
11. Lacolley, P., Regnault, V. & Laurent, S. Mechanisms of Arterial Stiffening: From Mechanotransduction to Epigenetics. *Arterioscler. Thromb. Vasc. Biol.* **40**, 1055–1062 (2020).
12. Lyle, A. N. & Raaz, U. Killing me un-softly: Causes and mechanisms of arterial stiffness Recent Highlights of ATVB: Early Career Committee Contribution. *Arterioscler. Thromb. Vasc. Biol.* **37**, e1 (2017).
13. Galis, Z. S. & Khatri, J. J. Matrix metalloproteinases in vascular remodeling and atherogenesis: The good, the bad, and the ugly. *Circ. Res.* **90**, 251–262 (2002).
14. Chung, A. W. Y. *et al.* Matrix metalloproteinase-2 and -9 exacerbate arterial stiffening and angiogenesis in diabetes and chronic kidney disease. *Cardiovasc. Res.* **84**, 494–504 (2009).
15. Yasmin *et al.* Matrix metalloproteinase-9 (MMP-9), MMP-2, and serum elastase activity are associated with systolic hypertension and arterial stiffness. *Arterioscler. Thromb. Vasc. Biol.* **25**, 372–378 (2005).
16. Aroor, A. R. *et al.* The Role of Tissue Renin-Angiotensin-Aldosterone System in the Development of Endothelial Dysfunction and Arterial Stiffness. *Front. Endocrinol. (Lausanne).* **4**, 161 (2013).
17. Björkegren, J. L. M. & Lusis, A. J. Atherosclerosis: Recent developments. *Cell* **185**, 1630–1645 (2022).

18. Kent, K. C. Clinical practice. Abdominal aortic aneurysms. *N. Engl. J. Med.* **371**, 2101–8 (2014).

19. Quintana, R. A. & Taylor, W. R. Cellular Mechanisms of Aortic Aneurysm Formation. *Circ. Res.* **124**, 607 (2019).

20. Poulter, N. R., Prabhakaran, D. & Caulfield, M. Hypertension. *The Lancet* **386**, 801–812 (2015).

21. Chen, K., Pittman, R. N. & Popel, A. S. Nitric Oxide in the Vasculature: Where Does It Come From and Where Does It Go? A Quantitative Perspective. *Antioxid. Redox Signal.* **10**, 1185 (2008).

22. Walford, G. & Loscalzo, J. Nitric oxide in vascular biology. *Journal of Thrombosis and Haemostasis* **1**, 2112–2118 (2003).

23. Davenport, A. P. *et al.* Endothelin. *Pharmacol. Rev.* **68**, 357–418 (2016).

24. Ivey, M. E., Osman, N. & Little, P. J. Endothelin-1 signalling in vascular smooth muscle: Pathways controlling cellular functions associated with atherosclerosis. *Atherosclerosis* **199**, 237–247 (2008).

25. Tank, A. W. & Wong, D. L. Peripheral and Central Effects of Circulating Catecholamines. *Compr. Physiol.* **5**, 1–15 (2015).

26. Motiejunaite, J., Amar, L. & Vidal-Petiot, E. Adrenergic receptors and cardiovascular effects of catecholamines. *Ann. Endocrinol. (Paris).* **82**, 193–197 (2021).

27. Paul, M., Mehr, A. P. & Kreutz, R. Physiology of local renin-angiotensin systems. *Physiol. Rev.* **86**, 747–803 (2006).

28. Cat, A. N. D. & Touyz, R. M. Cell signaling of angiotensin II on vascular tone: Novel mechanisms. *Curr. Hypertens. Rep.* **13**, 122–128 (2011).

29. Higuchi, S. *et al.* Angiotensin II signal transduction through the AT1 receptor: novel insights into mechanisms and pathophysiology. *Clin. Sci.* **112**, 417–428 (2007).

30. Majesky, M. W. Developmental basis of vascular smooth muscle diversity. *Arterioscler. Thromb. Vasc. Biol.* **27**, 1248–1258 (2007).

31. Shen, M., Quertermous, T., Fischbein, M. P. & Wu, J. C. Generation of Vascular Smooth Muscle Cells From Induced Pluripotent Stem Cells: Methods, Applications, and Considerations. *Circ. Res.* **128**, 670–686 (2021).

32. Cao, G. *et al.* How vascular smooth muscle cell phenotype switching contributes to vascular disease. *Cell Communication and Signaling 2022 20:1* **20**, 1–22 (2022).

33. Rensen, S. S. M., Doevendans, P. A. F. M. & Van Eys, G. J. J. M. Regulation and characteristics of vascular smooth muscle cell phenotypic diversity. *Netherlands Heart Journal* **15**, 100 (2007).

34. Chen, R., McVey, D. G., Shen, D., Huang, X. & Ye, S. Phenotypic Switching of Vascular Smooth Muscle Cells in Atherosclerosis. *J. Am. Heart Assoc.* **12**, 31121 (2023).

35. Speer, M. Y. *et al.* Smooth Muscle Cells Give Rise to Osteochondrogenic Precursors and Chondrocytes in Calcifying Arteries. *Circ. Res.* **104**, 733 (2009).

36. Durham, A. L., Speer, M. Y., Scatena, M., Giachelli, C. M. & Shanahan, C. M. Role of smooth muscle cells in vascular calcification: implications in atherosclerosis and arterial stiffness. *Cardiovasc. Res.* **114**, 590 (2018).

37. Lin, M. E. *et al.* Runx2 deletion in smooth muscle cells inhibits vascular osteochondrogenesis and calcification but not atherosclerotic lesion formation. *Cardiovasc. Res.* **112**, 606 (2016).

38. Xu, X. *et al.* Sox10 escalates vascular inflammation by mediating vascular smooth muscle cell transdifferentiation and pyroptosis in neointimal hyperplasia. *Cell Rep.* **42**, (2023).

39. Allahverdian, S., Chehroudi, A. C., McManus, B. M., Abraham, T. & Francis, G. A. Contribution of intimal smooth muscle cells to cholesterol accumulation and macrophage-like cells in human atherosclerosis. *Circulation* **129**, 1551–1559 (2014).

40. Zhang, F., Guo, X., Xia, Y. & Mao, L. An update on the phenotypic switching of vascular smooth muscle cells in the pathogenesis of atherosclerosis. *Cell. Mol. Life Sci.* **79**, 6 (2021).

41. Chen, P. Y., Qin, L. & Simons, M. TGFβ signaling pathways in human health and disease. *Front. Mol. Biosci.* **10**, 1113061 (2023).

42. Wang, Z. *et al.* Myocardin and ternary complex factors compete for SRF to control smooth muscle gene expression. *Nature* **428**, 185–189 (2004).

43. Xin, Y. *et al.* Elucidating VSMC phenotypic transition mechanisms to bridge insights into cardiovascular disease implications. *Front. Cardiovasc. Med.* **11**, 1400780 (2024).

44. Guo, X. *et al.* Dedicator of Cytokinesis 2, A Novel Regulator for Smooth Muscle Phenotypic Modulation and Vascular Remodeling. *Circ. Res.* **116**, e71 (2015).

45. Salmon, M., Gomez, D., Greene, E., Shankman, L. & Owens, G. K. Cooperative binding of KLF4, pELK-1, and HDAC2 to a G/C repressor element in the SM22α promoter mediates transcriptional silencing during SMC phenotypic switching in vivo. *Circ. Res.* **111**, 685–696 (2012).

46. Vacante, F., Denby, L., Sluimer, J. C. & Baker, A. H. The function of miR-143, miR-145 and the MiR-143 host gene in cardiovascular development and disease. *Vascul. Pharmacol.* **112**, 24 (2019).

47. Qi, M. & Xin, S. FGF signaling contributes to atherosclerosis by enhancing the inflammatory response in vascular smooth muscle cells. *Mol. Med. Rep.* **20**, 162 (2019).

48. Yuan, X. *et al.* Reversal of Endothelial Extracellular Vesicle-Induced Smooth Muscle Phenotype Transition by Hypercholesterolemia Stimulation: Role of NLRP3 Inflammasome Activation. *Front. Cell Dev. Biol.* **8**, 597423 (2020).

49. Morris, H. E., Neves, K. B., Montezano, A. C., MacLean, M. R. & Touyz, R. M. Notch3 signalling and vascular remodelling in pulmonary arterial hypertension. *Clin. Sci. (Lond).* **133**, 2481 (2019).

50. Domenga, V. *et al.* Notch3 is required for arterial identity and maturation of vascular smooth muscle cells. *Genes Dev.* **18**, 2730 (2004).

51. Ghosh, S. *et al.* Activation dynamics and signaling properties of Notch3 receptor in the developing pulmonary artery. *J. Biol. Chem.* **286**, 22678–22687 (2011).

52. Morrow, D. *et al.* Notch-mediated CBF-1/RBP-J{kappa}-dependent regulation of human vascular smooth muscle cell phenotype in vitro. *Am. J. Physiol. Cell Physiol.* **289**, (2005).

53. Song, Y. *et al.* Activation of Notch3 promotes pulmonary arterial smooth muscle cells proliferation via Hes1/p27Kip1 signaling pathway. *FEBS Open Bio* **5**, 656–660 (2015).

54. Baeten, J. T. & Lilly, B. Differential Regulation of NOTCH2 and NOTCH3 Contribute to Their Unique Functions in Vascular Smooth Muscle Cells. *J. Biol. Chem.* **290**, 16226–16237 (2015).

55. Liu, R. *et al.* Epigenetic Regulation of Vascular Smooth Muscle Cell Phenotype Switching in Atherosclerotic Artery Remodeling: A Mini-Review. *Front. Genet.* **12**, 719456 (2021).

56. Liu, R. *et al.* TET2 is a Master Regulator of Smooth Muscle Cell Plasticity. *Circulation* **128**, 2047 (2013).

57. Greißel, A. *et al.* Histone acetylation and methylation significantly change with severity of atherosclerosis in human carotid plaques. *Cardiovasc. Pathol.* **25**, 79–86 (2016).

58. Harman, J. L. *et al.* Epigenetic Regulation of Vascular Smooth Muscle Cells by Histone H3 Lysine 9 Dimethylation Attenuates Target Gene-Induction by Inflammatory Signaling. *Arterioscler. Thromb. Vasc. Biol.* **39**, 2289–2302 (2019).

59. Liu, M. *et al.* H3K4 di-methylation governs smooth muscle lineage identity and promotes vascular homeostasis by restraining plasticity. *Dev. Cell* **56**, 2765 (2021).

60. Zhang, M. *et al.* HDAC6 Regulates the MRTF-A/SRF Axis and Vascular Smooth Muscle Cell Plasticity. *JACC Basic Transl. Sci.* **3**, 782 (2018).

61. Pipes, G. C. T., Creemers, E. E. & Olson, E. N. The myocardin family of transcriptional coactivators: versatile regulators of cell growth, migration, and myogenesis. *Genes Dev.* **20**, 1545–1556 (2006).

62. Ichii, T. *et al.* Fibrillar collagen specifically regulates human vascular smooth muscle cell genes involved in cellular responses and the pericellular matrix environment. *Circ. Res.* **88**, 460–467 (2001).

63. Wang, L. *et al.* Cartilage oligomeric matrix protein maintains the contractile phenotype of vascular smooth muscle cells by interacting with α7β1 integrin. *Circ. Res.* **106**, 514–525 (2010).

64. Tran, P. K. *et al.* Increased Intimal Hyperplasia and Smooth Muscle Cell Proliferation in Transgenic Mice with Heparan Sulfate-Deficient Perlecan. *Circ. Res.* **94**, 550–558 (2004).

65. Raines, E. W., Koyama, H. & Carragher, N. O. The Extracellular Matrix Dynamically Regulates Smooth Muscle Cell Responsiveness to PDGFa. *Ann. N. Y. Acad. Sci.* **902**, 39–52 (2000).

66. Gilotti, A. C. *et al.* HEPARIN RESPONSES IN VASCULAR SMOOTH MUSCLE CELLS INVOLVE cGMP DEPENDENT PROTEIN KINASE(PKG). *J. Cell. Physiol.* **229**, 2142 (2014).

67. Jain, M. *et al.* Smooth muscle cell–specific fibronectin-EDA mediates phenotypic switching and neointimal hyperplasia. *J. Clin. Invest.* **130**, 295 (2019).

68. Yao, G. *et al.* FBLN7 mediates vascular smooth muscle cell phenotype switching and vascular remodeling in hypertension. *Theranostics* **14**, 7569 (2024).

69. Chiu, J. J. *et al.* Mechanisms of induction of endothelial cell E-selectin expression by smooth muscle cells and its inhibition by shear stress. *Blood* **110**, 519 (2007).

70. Sun, L. *et al.* Shear Stress Induces Phenotypic Modulation of Vascular Smooth Muscle Cells via AMPK/mTOR/ULK1-Mediated Autophagy. *Cell. Mol. Neurobiol.* **38**, 541 (2017).

71. Qi, Y. X. *et al.* PDGF-BB and TGF-β1 on cross-talk between endothelial and smooth muscle cells in vascular remodeling induced by low shear stress. *Proc. Natl. Acad. Sci. U. S. A.* **108**, 1908–1913 (2011).

72. Hsu, S., Chu, J. S., Chen, F. F., Wang, A. & Li, S. Effects of Fluid Shear Stress on a Distinct Population of Vascular Smooth Muscle Cells. *Cell. Mol. Bioeng.* **4**, 627 (2011).

73. Kang, H., Fan, Y. & Deng, X. Vascular smooth muscle cell glycocalyx modulates shear-induced proliferation, migration, and NO production responses. *Am. J. Physiol. Heart Circ. Physiol.* **300**, (2011).

74. Fitzgerald, T. N. *et al.* Laminar shear stress stimulates vascular smooth muscle cell apoptosis via the Akt pathway. *J. Cell. Physiol.* **216**, 389–395 (2008).

75. Lehoux, S., Castier, Y. & Tedgui, A. Molecular mechanisms of the vascular responses to haemodynamic forces. *J. Intern. Med.* **259**, 381–392 (2006).

76. Grote, K. *et al.* Mechanical stretch enhances mRNA expression and proenzyme release of matrix metalloproteinase-2 (MMP-2) via NAD(P)H oxidase-derived reactive oxygen species. *Circ. Res.* **92**, (2003).

77. Lehoux, S., Lemarié, C. A., Esposito, B., Lijnen, H. R. & Tedgui, A. Pressure-induced matrix metalloproteinase-9 contributes to early hypertensive remodeling. *Circulation* **109**, 1041–1047 (2004).

78. Seo, K. W. *et al.* Mechanical Stretch Increases MMP-2 Production in Vascular Smooth Muscle Cells via Activation of PDGFR-β/Akt Signaling Pathway. *PLoS One* **8**, e70437 (2013).

79. Jensen, L. F., Bentzon, J. F. & Albarrán-juárez, J. The Phenotypic Responses of Vascular Smooth Muscle Cells Exposed to Mechanical Cues. *Cells* **10**, 2209 (2021).

80. Hu, B. *et al.* Mechanical Stretch Suppresses microRNA-145 Expression by Activating Extracellular Signal-Regulated Kinase 1/2 and Upregulating Angiotensin-Converting Enzyme to Alter Vascular Smooth Muscle Cell Phenotype. *PLoS One* **9**, e96338 (2014).

81. Wang, Y. *et al.* Arterial Wall Stress Induces Phenotypic Switching of Arterial Smooth Muscle Cells in Vascular Remodeling by Activating the YAP/TAZ Signaling Pathway. *Cell. Physiol. Biochem.* **51**, 842–853 (2018).

82. Kechagia, J. Z., Ivaska, J. & Roca-Cusachs, P. Integrins as biomechanical sensors of the microenvironment. *Nature Reviews Molecular Cell Biology 2019 20:8* **20**, 457–473 (2019).

83. Turlo, K. A. *et al.* An essential requirement for β1 integrin in the assembly of extracellular matrix proteins within the vascular wall. *Dev. Biol.* **365**, 23–35 (2012).

84. Schnapp, L. M. *et al.* The human integrin alpha 8 beta 1 functions as a receptor for tenascin, fibronectin, and vitronectin. *J. Biol. Chem.* **270**, 23196–23202 (1995).

85. Johnson, R. T., Solanki, R. & Warren, D. T. Mechanical programming of arterial smooth muscle cells in health and ageing. *Biophys. Rev.* **13**, (2021).

86. Legate, K. R. & Fässler, R. Mechanisms that regulate adaptor binding to beta-integrin cytoplasmic tails. *J. Cell Sci.* **122**, 187–198 (2009).

87. Sun, Z., Guo, S. S. & Fässler, R. Integrin-mediated mechanotransduction. *J. Cell Biol.* **215**, 445–456 (2016).

88. Austen, K. *et al.* Extracellular rigidity sensing by talin isoform-specific mechanical linkages. *Nat. Cell Biol.* **17**, 1597–1606 (2015).

89. Wrighton, K. H. Cell adhesion: the 'ins' and 'outs' of integrin signalling. *Nat. Rev. Mol. Cell Biol.* **14**, 752–753 (2013).

90. Kim, C., Ye, F. & Ginsberg, M. H. Regulation of integrin activation. *Annu. Rev. Cell Dev. Biol.* **27**, 321–345 (2011).

91. Polacheck, W. J., German, A. E., Mammoto, A., Ingber, D. E. & Kamm, R. D. Mechanotransduction of fluid stresses governs 3D cell migration. *Proc. Natl. Acad. Sci. U. S. A.* **111**, 2447–2452 (2014).

92. Klein, E. A. *et al.* Cell-cycle control by physiological matrix elasticity and in vivo tissue stiffening. *Curr. Biol.* **19**, 1511–1518 (2009).

93. Bae, Y. H. *et al.* A FAK-Cas-Rac-lamellipodin signaling module transduces extracellular matrix stiffness into mechanosensitive cell cycling. *Sci. Signal.* **7**, (2014).

94. Moiseeva, E. P. Adhesion receptors of vascular smooth muscle cells and their functions. *Cardiovasc. Res.* **52**, 372–386 (2001).

95. Dye, W. W., Gleason, R. L., Wilson, E. & Humphrey, J. D. Altered biomechanical properties of carotid arteries in two mouse models of muscular dystrophy. *J. Appl. Physiol.* **103**, 664–672 (2007).

96. Loufrani, L. *et al.* Flow (shear stress)-induced endothelium-dependent dilation is altered in mice lacking the gene encoding for dystrophin. *Circulation* **103**, 864 (2001).

97. Frismantiene, A., Philippova, M., Erne, P. & Resink, T. J. Cadherins in vascular smooth muscle cell (patho)biology: Quid nos scimus? *Cell. Signal.* **45**, 23–42 (2018).

98. Van Roy, F. & Berx, G. The cell-cell adhesion molecule E-cadherin. *Cellular and Molecular Life Sciences* **65**, 3756–3788 (2008).

99. George, S. J. & Beeching, C. A. Cadherin:catenin complex: A novel regulator of vascular smooth muscle cell behaviour. *Atherosclerosis* **188**, 1–11 (2006).

100. Gelfand, B. D. *et al.* Hemodynamic activation of beta-catenin and T-cell-specific transcription factor signaling in vascular endothelium regulates fibronectin expression. *Arterioscler. Thromb. Vasc. Biol.* **31**, 1625–1633 (2011).

101. Tzima, E. *et al.* A mechanosensory complex that mediates the endothelial cell response to fluid shear stress. *Nature* **437**, 426–431 (2005).

102. Fang, X. Z. *et al.* Structure, kinetic properties and biological function of mechanosensitive Piezo channels. *Cell & Bioscience 2021 11:1* **11**, 1–20 (2021).

103. Li, J. *et al.* Piezo1 integration of vascular architecture with physiological force. *Nature* **515**, 279 (2014).

104. Zhang, C. *et al.* Coupling of Integrin α5 to Annexin A2 by Flow Drives Endothelial Activation. *Circ. Res.* **127**, 1074–1090 (2020).

105. Retailleau, K. *et al.* Piezo1 in Smooth Muscle Cells Is Involved in Hypertension-Dependent Arterial Remodeling. *Cell Rep.* **13**, 1161–1171 (2015).

106. Miron, T. R., Flood, E. D., Tykocki, N. R., Thompson, J. M. & Watts, S. W. Identification of Piezo1 channels in perivascular adipose tissue (PVAT) and their potential role in vascular function. *Pharmacol. Res.* **175**, 105995 (2021).

107. Toko, H. *et al.* Angiotensin II Type 1a Receptor Is Involved in Cell Infiltration, Cytokine Production, and Neovascularization in Infarcted Myocardium. *Arterioscler. Thromb. Vasc. Biol.* **24**, 664–670 (2004).

108. Tykocki, N. R., Boerman, E. M. & Jackson, W. F. Smooth Muscle Ion Channels and Regulation of Vascular Tone in Resistance Arteries and Arterioles. *Compr. Physiol.* **7**, 485 (2017).

109. Ahmed, S. & Warren, D. T. Vascular smooth muscle cell contractile function and mechanotransduction. *Vessel Plus* **2**, 36 (2018).

110. Touyz, R. M. *et al.* Vascular smooth muscle contraction in hypertension. *Cardiovasc. Res.* **114**, 529 (2018).

111. Zhang, J., Herrera, A. M., Paré, P. D. & Seow, C. Y. Dense-body aggregates as plastic structures supporting tension in smooth muscle cells. *Am. J. Physiol. Lung Cell. Mol. Physiol.* **299**, 631–638 (2010).

112. Hallmann, R. *et al.* Expression and function of laminins in the embryonic and mature vasculature. *Physiol. Rev.* **85**, 979–1000 (2005).

113. Davis, G. E. & Senger, D. R. Endothelial extracellular matrix: Biosynthesis, remodeling, and functions during vascular morphogenesis and neovessel stabilization. *Circ. Res.* **97**, 1093–1107 (2005).

114. Lin, C. J. *et al.* Heterogeneous Cellular Contributions to Elastic Laminae Formation in Arterial Wall Development. *Circ. Res.* **125**, 1006–1018 (2019).

115. Jana, S., Hu, M., Shen, M. & Kassiri, Z. Extracellular matrix, regional heterogeneity of the aorta, and aortic aneurysm. *Exp. Mol. Med.* **51**, 160 (2019).

116. Kozel, B. A. *et al.* Elastic fiber formation: A dynamic view of extracellular matrix assembly using timer reporters. *J. Cell. Physiol.* **207**, 87–96 (2006).

117. Wagenseil, J. E. & Mecham, R. P. Vascular Extracellular Matrix and Arterial Mechanics. *Physiol. Rev.* **89**, 957 (2009).

118. Rhodes, J. M. & Simons, M. The extracellular matrix and blood vessel formation: not just a scaffold. *J. Cell. Mol. Med.* **11**, 176 (2007).

119. Kohn, J. C., Lampi, M. C. & Reinhart-King, C. A. Age-related vascular stiffening: causes and consequences. *Front. Genet.* **6**, 112 (2015).

120. Greenwald, S. E. Ageing of the conduit arteries. *Journal of Pathology* **211**, 157–172 (2007).

121. Urry, D. W. Neutral Sites for Calcium Ion Binding to Elastin and Collagen: A Charge Neutralization Theory for Calcification and Its Relationship to Atherosclerosis. *Proceedings of the National Academy of Sciences* **68**, 810–814 (1971).

122. Fhayli, W. *et al.* Rise and fall of elastic fibers from development to aging. Consequences on arterial structure-function and therapeutical perspectives. *Matrix Biology* **84**, 41–56 (2019).

123. Paul, R. G. & Bailey, A. J. Glycation of collagen: the basis of its central role in the late complications of ageing and diabetes. *Int. J. Biochem. Cell Biol.* **28**, 1297–1310 (1996).

124. Bansode, S. *et al.* Glycation changes molecular organization and charge distribution in type I collagen fibrils. *Scientific Reports 2020 10:1* **10**, 1–13 (2020).

125. Ribeiro-Silva, J. C., Miyakawa, A. A. & Krieger, J. E. Focal adhesion signaling: vascular smooth muscle cell contractility beyond calcium mechanisms. *Clin. Sci.* **135**, 1189–1207 (2021).

126. Wang, W. Y. *et al.* Extracellular matrix alignment dictates the organization of focal adhesions and directs uniaxial cell migration. *APL Bioeng.* **2**, 046107 (2018).

127. Mohajeri, A. *et al.* Mechanical signaling regulates vascular smooth muscle cell adaptation in aging. *Front. Physiol.* **16**, 1593886 (2025).

128. Sehgel, N. L., Vatner, S. F. & Meininger, G. A. "Smooth Muscle Cell Stiffness Syndrome"—Revisiting the Structural Basis of Arterial Stiffness. *Front. Physiol.* **6**, 335 (2015).

129. Svitkina, T. The Actin Cytoskeleton and Actin-Based Motility. *Cold Spring Harb. Perspect. Biol.* **10**, a018267 (2018).

130. Qiu, H. *et al.* Vascular Smooth Muscle Cell Stiffness as a Mechanism for Increased Aortic Stiffness with Aging. *Circ. Res.* **107**, 615 (2010).

131. Sehgel, N. L. *et al.* Augmented vascular smooth muscle cell stiffness and adhesion when hypertension is superimposed on aging. *Hypertension* **65**, 370–377 (2015).

132. Na, S., Meininger, G. A. & Humphrey, J. D. A Theoretical Model for F-actin Remodeling in Vascular Smooth Muscle Cells Subjected to Cyclic Stretch. *J. Theor. Biol.* **246**, 87 (2006).

133. Cunningham, J. J., Linderman, J. J. & Mooney, D. J. Externally applied cyclic strain regulates localization of focal contact components in cultured smooth muscle cells. *Ann. Biomed. Eng.* **30**, 927–935 (2002).

134. Goodson, H. V. & Jonasson, E. M. Microtubules and microtubule-associated proteins. *Cold Spring Harb. Perspect. Biol.* **10**, (2018).

135. Logan, C. M. & Menko, A. S. Microtubules: Evolving roles and critical cellular interactions. *Exp. Biol. Med.* **244**, 1240 (2019).

136. Ingber, D. E., Wang, N. & Stamenović, D. Tensegrity, cellular biophysics, and the mechanics of living systems. *Rep. Prog. Phys.* **77**, 046603 (2014).

137. Wang, N. *et al.* Mechanical behavior in living cells consistent with the tensegrity model. *Proc. Natl. Acad. Sci. U. S. A.* **98**, 7765 (2001).

138. Sheridan, B. C. *et al.* Microtubules regulate pulmonary vascular smooth muscle contraction. *Journal of Surgical Research* **62**, 284–287 (1996).

139. Platts, S. H., Martinez-Lemus, L. A. & Meininger, G. A. Microtubule-Dependent Regulation of Vasomotor Tone Requires Rho-Kinase. *J. Vasc. Res.* **39**, 173–182 (2002).

140. Ahmed, S. *et al.* Using Polyacrylamide Hydrogels to Model Physiological Aortic Stiffness Reveals that Microtubules Are Critical Regulators of Isolated Smooth Muscle Cell Morphology and Contractility. *Front. Pharmacol.* **13**, (2022).

141. Li, L. & Yang, X. J. Tubulin acetylation: responsible enzymes, biological functions and human diseases. *Cell. Mol. Life Sci.* **72**, 4237 (2015).

142. Akella, J. S. *et al.* MEC-17 is an α-tubulin acetyltransferase. *Nature* **467**, 218 (2010).

143. Kim, G. W., Li, L., Gorbani, M., You, L. & Yang, X. J. Mice Lacking α-Tubulin Acetyltransferase 1 Are Viable but Display α-Tubulin Acetylation Deficiency and Dentate Gyrus Distortion. *J. Biol. Chem.* **288**, 20334 (2013).

144. Matsuyama, A. *et al.* In vivo destabilization of dynamic microtubules by HDAC6-mediated deacetylation. *EMBO J.* **21**, 6820–6831 (2002).

145. Joo, E. E. & Yamada, K. M. MYPT1 regulates contractility and microtubule acetylation to modulate integrin adhesions and matrix assembly. *Nature Communications 2014 5:1* **5**, 1–13 (2014).

146. Hepler, P. K. The Cytoskeleton and Its Regulation by Calcium and Protons. *Plant Physiol.* **170**, 3 (2016).

147. Melander Gradin, H., Marklund, U., Larsson, N., Chatila, T. A. & Gullberg, M. Regulation of Microtubule Dynamics by Ca 2+ /Calmodulin-Dependent Kinase IV/Gr-Dependent Phosphorylation of Oncoprotein 18 . *Mol. Cell. Biol.* **17**, 3459–3467 (1997).

148. Ye, G. J. C., Nesmith, A. P. & Parker, K. K. The role of mechanotransduction on vascular smooth muscle myocytes cytoskeleton and contractile function. *Anat. Rec. (Hoboken)* **297**, 1758 (2014).

149. Hoffmann, E. K., Lambert, I. H. & Pedersen, S. F. Physiology of cell volume regulation in vertebrates. *Physiol. Rev.* **89**, 193–277 (2009).

150. Cacace, V. I. *et al.* Regulatory Volume Increase and Regulatory Volume Decrease Responses in HL-1 Atrial Myocytes. *Cellular Physiology and Biochemistry* **33**, 1745–1757 (2014).

151. Li, C. & Wang, W. Molecular biology of aquaporins. *Adv. Exp. Med. Biol.* **969**, 1–34 (2017).

152. Kruse, E., Uehlein, N. & Kaldenhoff, R. The aquaporins. *Genome Biol.* **7**, 1–6 (2006).

153. Morishita, K., Watanabe, K. & Ichijo, H. Cell volume regulation in cancer cell migration driven by osmotic water flow. *Cancer Sci.* **110**, 2337 (2019).

154. Stroka, K. M. *et al.* Water Permeation Drives Tumor Cell Migration in Confined Microenvironments. *Cell* **157**, 611 (2014).

155. Fels, J., Oberleithner, H. & Kusche-Vihrog, K. Ménage à trois: Aldosterone, sodium and nitric oxide in vascular endothelium. *Biochimica et Biophysica Acta (BBA) - Molecular Basis of Disease* **1802**, 1193–1202 (2010).

156. Connolly, D. L., Shanahan, C. M. & Weissberg, P. L. The aquaporins. A family of water channel proteins. *International Journal of Biochemistry and Cell Biology* **30**, 169–172 (1998).

157. Ataei Ataabadi, E. *et al.* Vascular Ageing Features Caused by Selective DNA Damage in Smooth Muscle Cell. *Oxid. Med. Cell. Longev.* **2021**, 2308317 (2021).

158. Chi, C. *et al.* Vascular smooth muscle cell senescence and age-related diseases: State of the art. *Biochimica et Biophysica Acta (BBA) - Molecular Basis of Disease* **1865**, 1810–1821 (2019).

159. Shah, A. *et al.* Defective base excision repair of oxidative DNA damage in vascular smooth muscle cells promotes atherosclerosis. *Circulation* **138**, 1446–1462 (2018).

160. Gray, K. *et al.* Effects of DNA damage in smooth muscle cells in atherosclerosis. *Circ. Res.* **116**, 816–826 (2015).

161. Sazonova, O. V. *et al.* Extracellular matrix presentation modulates vascular smooth muscle cell mechanotransduction. *Matrix Biology* **41**, 36–43 (2015).

162. Lang, F. Stiff endothelial cell syndrome in vascular inflammation and mineralocorticoid excess. *Hypertension* **57**, 146–147 (2011).

163. Zhu, L. & Chen, L. Progress in research on paclitaxel and tumor immunotherapy. *Cell. Mol. Biol. Lett.* **24**, 40 (2019).

164. Warner, E. F., Li, Y. & Li, X. Targeting Microtubules for the Treatment of Heart Disease. *Circ. Res.* **130**, 1723–1741 (2022).

165. Eckschlager, T., Plch, J., Stiborova, M. & Hrabeta, J. Histone Deacetylase Inhibitors as Anticancer Drugs. *Int. J. Mol. Sci.* **18**, 1414 (2017).

166. Metz, R. P., Patterson, J. L. & Wilson, E. Vascular smooth muscle cells: Isolation, culture, and characterization. *Methods in Molecular Biology* **843**, 169–176 (2012).

167. Sun, C. *et al.* Acutely Inhibiting AQP4 With TGN-020 Improves Functional Outcome by Attenuating Edema and Peri-Infarct Astrogliosis After Cerebral Ischemia. *Front. Immunol.* **13**, 870029 (2022).

168. McMahon, B. A. & Chawla, L. S. The furosemide stress test: current use and future potential. *Ren. Fail.* **43**, 830 (2021).

169. Bozdaganyan, M. *et al.* Exploring tubulin-paclitaxel binding modes through extensive molecular dynamics simulations. *Scientific Reports 2025 15:1* **15**, 8378- (2025).

170. Ravelli, R. B. G. *et al.* Insight into tubulin regulation from a complex with colchicine and a stathmin-like domain. *Nature 2004 428:6979* **428**, 198–202 (2004).

171. Vasquez, R. J., Howell, B., Yvon, A. M. C., Wadsworth, P. & Cassimeris, L. Nanomolar concentrations of nocodazole alter microtubule dynamic instability in vivo and in vitro. *Mol. Biol. Cell* **8**, 973 (1997).

172. Zhao, F., Li, P., Chen, S. R. W., Louis, C. F. & Fruen, B. R. Dantrolene Inhibition of Ryanodine Receptor Ca2+Release Channels. *Journal of Biological Chemistry* **276**, 13810–13816 (2001).

173. Botello-Smith, W. M. *et al.* A mechanism for the activation of the mechanosensitive Piezo1 channel by the small molecule Yoda1. *Nature Communications 2019 10:1* **10**, 4503- (2019).

174. Wang, Y. *et al.* A lever-like transduction pathway for long-distance chemical- and mechano-gating of the mechanosensitive Piezo1 channel. *Nat. Commun.* **9**, 1300 (2018).

175. Suchyna, T. M. *et al.* Bilayer-dependent inhibition of mechanosensitive channels by neuroactive peptide enantiomers. *Nature 2004 430:6996* **430**, 235–240 (2004).

176. Wu-Zhang, A. X. & Newton, A. C. Protein Kinase C Pharmacology: Refining the Toolbox. *Biochem. J.* **452**, 195 (2013).

177. Zabludoff, S. D. *et al.* AZD7762, a novel checkpoint kinase inhibitor, drives checkpoint abrogation and potentiates DNA-targeted therapies. *Mol. Cancer Ther.* **7**, 2955–2966 (2008).

178. Mori, T. *et al.* Chemical library screening for WNK signalling inhibitors using fluorescence correlation spectroscopy. *Biochem. J.* **455**, 339–345 (2013).

179. A 1070722 | GSK-3 Inhibitor | MedChemExpress. https://www.medchemexpress.com/a-1070722.html.

180. Entinostat: A Technical Guide to the Mechanism of Action of a Class I HDAC Inhibitor. (2026).

181. Pavlik, C. M. *et al.* Santacruzamate A, a Potent and Selective Histone Deacetylase (HDAC) Inhibitor from the Panamanian Marine Cyanobacterium cf. Symploca sp. *J. Nat. Prod.* **76**, 10.1021/np400198r (2013).

182. Makgoba, T. B., Kapp, E., Egieyeh, S. & Joubert, J. HDAC3 inhibitors: a patent review of their broad-spectrum applications as therapeutic agents. *Expert Opin. Ther. Pat.* **34**, 273–295 (2024).

183. Shen, S. *et al.* Structural and in Vivo Characterization of Tubastatin A, a Widely Used Histone Deacetylase 6 Inhibitor. *ACS Med. Chem. Lett.* **11**, 706 (2020).

184. Li, W. H. *et al.* PARP-1: a critical regulator in radioprotection and radiotherapy-mechanisms, challenges, and therapeutic opportunities. *Front. Pharmacol.* **14**, 1198948 (2023).

185. Reis, J. *et al.* A closer look into NADPH oxidase inhibitors: Validation and insight into their mechanism of action. *Redox Biol.* **32**, 101466 (2020).

186. Fiji: ImageJ, with 'Batteries Included'. https://fiji.sc/.

187. ImageJ plugins by Qingzong TSENG - PIV (Particle Image Velocimetry) --- ImageJ plugin. https://sites.google.com/site/qingzongtseng/piv.

188. ImageJ plugins by Qingzong TSENG - Traction Force Microscopy. https://sites.google.com/site/qingzongtseng/tfm.

189. Johnson, R. T. *et al.* Piezo1-mediated regulation of smooth muscle cell volume in response to enhanced extracellular matrix rigidity. *Br. J. Pharmacol.* **181**, 1576–1595 (2024).

190. Solanki, R. Unveiling the Mechanisms that Contribute to the Vascular Smooth Muscle Cell Response to Matrix Rigidity. (2024).

191. Mola, M. G. *et al.* The speed of swelling kinetics modulates cell volume regulation and calcium signaling in astrocytes: A different point of view on the role of aquaporins. *Glia* **64**, 139–154 (2016).

192. Verkman, A. S. More than just water channels: unexpected cellular roles of aquaporins. *J. Cell Sci.* **118**, 3225–3232 (2005).

193. Klebe, S. *et al.* Blockade of Aquaporin 1 Inhibits Proliferation, Motility, and Metastatic Potential of Mesothelioma In Vitro but not in an In Vivo Model. *Dis. Markers* **2015**, 286719 (2015).

194. Shabanian, K. *et al.* AQP1 differentially orchestrates endothelial cell senescence. *Redox Biol.* **76**, 103317 (2024).

195. Tie, L., Wang, D., Shi, Y. & Li, X. Aquaporins in Cardiovascular System. *Adv. Exp. Med. Biol.* **969**, 105–113 (2017).

196. Rutkovskiy, A. *et al.* Aquaporin-4 in the heart: Expression, regulation and functional role in ischemia. *Basic Res. Cardiol.* **107**, (2012).

197. Nicosia, M. *et al.* Aquaporin 4 inhibition alters chemokine receptor expression and T cell trafficking. *Sci. Rep.* **9**, 1–11 (2019).

198. Delpire, E. & Gagnon, K. B. Na+-K+-2Cl− Cotransporter (NKCC) Physiological Function in Nonpolarized Cells and Transporting Epithelia. *Compr. Physiol.* **8**, 871–901 (2018).

199. Demian, W. L. *et al.* The Ion Transporter NKCC1 Links Cell Volume to Cell Mass Regulation by Suppressing mTORC1. *Cell Rep.* **27**, 1886-1896.e6 (2019).

200. Rao, K. V. R., Reddy, P. V. B., Curtis, K. M. & Norenberg, M. D. Aquaporin-4 expression in cultured astrocytes after fluid percussion injury. *J. Neurotrauma* **28**, 371–381 (2011).

201. de los Heros, P., Pacheco-Alvarez, D. & Gamba, G. Role of WNK Kinases in the Modulation of Cell Volume. *Curr. Top. Membr.* **81**, 207–235 (2018).

202. Markou, A. *et al.* Molecular mechanisms governing aquaporin relocalisation. *Biochimica et Biophysica Acta (BBA) - Biomembranes* **1864**, 183853 (2022).

203. Peterman, E. E., Taormina, P., Harvey, M. & Young, L. H. Gö 6983 Exerts Cardioprotective Effects in Myocardial Ischemia/Reperfusion. *J. Cardiovasc. Pharmacol.* **43**, 645–656 (2004).

204. Guerrero-Hernández, A., Gómez-Viquez, L., Guerrero-Serna, G. & Rueda, A. Ryanodine receptors in smooth muscle. *Front. Biosci.* **7**, (2002).

205. Nelson, M. T. *et al.* Relaxation of Arterial Smooth Muscle by Calcium Sparks. *Science (1979).* **270**, 633–637 (1995).

206. Villegas, C. *et al.* Epothilones as Natural Compounds for Novel Anticancer Drugs Development. *Int. J. Mol. Sci.* **24**, 6063 (2023).

207. An, W. F. *et al.* Discovery of Potent and Highly Selective Inhibitors of GSK3b. *Probe Reports from the NIH Molecular Libraries Program* https://www.ncbi.nlm.nih.gov/books/NBK133436/ (2014).

208. Zannini, L., Delia, D. & Buscemi, G. CHK2 kinase in the DNA damage response and beyond. *J. Mol. Cell Biol.* **6**, 442 (2014).

209. Espach, Y., Lochner, A., Strijdom, H. & Huisamen, B. ATM Protein Kinase Signaling, Type 2 Diabetes and Cardiovascular Disease. *Cardiovasc. Drugs Ther.* **29**, 51–58 (2015).

210. Mangerich, A. & Bürkle, A. Pleiotropic Cellular Functions of PARP1 in Longevity and Aging: Genome Maintenance Meets Inflammation. *Oxid. Med. Cell. Longev.* **2012**, 321653 (2012).

211. Zhang, C. *et al.* Poly(ADP-ribose) protects vascular smooth muscle cells from oxidative DNA damage. *BMB Rep.* **48**, 354 (2015).

212. Johnson, R. T. *et al.* A microtubule stability switch alters isolated vascular smooth muscle Ca2+ flux in response to matrix rigidity. *J. Cell Sci.* **137**, (2024).

213. Vandebroek, A. & Yasui, M. Regulation of AQP4 in the Central Nervous System. *Int. J. Mol. Sci.* **21**, 1603 (2020).

214. Russell, J. M. Sodium-potassium-chloride cotransport. *Physiol. Rev.* **80**, 211–276 (2000).

215. Orlov, S. N., Pokudin, N. I., Kotelevtsev, Y. V. & Gulak, P. V. Volume-dependent regulation of ion transport and membrane phosphorylation in human and rat erythrocytes. *J. Membr. Biol.* **107**, 105–117 (1989).

216. Adragna, N. C., Di Fulvio, M. & Lauf, P. K. Regulation of K-Cl cotransport: From function to genes. *Journal of Membrane Biology* **201**, 109–137 (2004).

217. Davis, J. P. L., Chipperfield, A. R. & Harper, A. A. Accumulation of intracellular chloride by (Na-K-Cl) co-transport in rat arterial smooth muscle is enhanced in deoxycorticosterone acetate (DOCA)/salt hypertension. *J. Mol. Cell. Cardiol.* **25**, 233–237 (1993).

218. Wilson, F. H. *et al.* Human hypertension caused by mutations in WNK kinases. *Science (1979).* **293**, 1107–1112 (2001).

219. Kim, J. S. & Kehrl, J. H. Inhibition of WNK Kinases in NK Cells Disrupts Cellular Osmoregulation and Control of Tumor Metastasis. *J. Innate Immun.* **16**, 451 (2024).

220. Wang, L., Sadeghnezhad, E., Guan, P. & Gong, P. Review: Microtubules monitor calcium and reactive oxygen species signatures in signal transduction. *Plant Science* **304**, 110589 (2021).

221. Komis, G., Illés, P., Beck, M. & Šamaj, J. Microtubules and mitogen-activated protein kinase signalling. *Curr. Opin. Plant Biol.* **14**, 650–657 (2011).

222. Gundersen, G. G. & Cook, T. A. Microtubules and signal transduction. *Curr. Opin. Cell Biol.* **11**, 81–94 (1999).

223. Ingber, D. E. Tensegrity I. Cell structure and hierarchical systems biology. *J. Cell Sci.* **116**, 1157–1173 (2003).

224. Brown, R. A., Talas, G., Porter, R. A., McGrouther, D. A. & Eastwood, M. Balanced mechanical forces and microtubule contribution to fibroblast contraction. *J. Cell. Physiol.* **169**, 439–447 (1996).

225. Chinnathambi, S. & Desale, S. E. The crosstalk between extracellular matrix proteins and Tau. *Adv. Protein Chem. Struct. Biol.* **141**, 447–466 (2024).

226. Li, Y., Li, Z. X., Jin, T., Wang, Z. Y. & Zhao, P. Tau Pathology Promotes the Reorganization of the Extracellular Matrix and Inhibits the Formation of Perineuronal Nets by Regulating the Expression and the Distribution of Hyaluronic Acid Synthases. *Journal of Alzheimer's Disease* **57**, 395 (2017).

227. Ali, I., Xu, F., Peng, Q. & Qiu, J. The dilemma of nuclear mechanical forces in DNA damage and repair. *Biochem. Biophys. Res. Commun.* **758**, (2025).

228. Sechi, S., Piergentili, R. & Giansanti, M. G. Minor Kinases with Major Roles in Cytokinesis Regulation. *Cells* **11**, 3639 (2022).

229. van der Linden, J. *et al.* Ercc1 DNA repair deficiency results in vascular aging characterized by VSMC phenotype switching, ECM remodeling, and an increased stress response. *Aging Cell* **23**, e14126 (2024).

230. Grootaert, M. O. J., Finigan, A., Figg, N. L., Uryga, A. K. & Bennett, M. R. SIRT6 Protects Smooth Muscle Cells from Senescence and Reduces Atherosclerosis. *Circ. Res.* **128**, 474–491 (2021).

231. Zhang, X. *et al.* DNA damage response, a double-edged sword for vascular aging. *Ageing Res. Rev.* **92**, (2023).

232. Micaroni, M. The Role of Calcium in Intracellular Trafficking. *Curr. Mol. Med.* **10**, 763–773 (2010).

233. Bootman, M. D. & Bultynck, G. Fundamentals of Cellular Calcium Signaling: A Primer. *Cold Spring Harb. Perspect. Biol.* **12**, a038802 (2020).

234. Paupe, V. & Prudent, J. New insights into the role of mitochondrial calcium homeostasis in cell migration. *Biochem. Biophys. Res. Commun.* **500**, 75–86 (2018).

235. Sukumaran, P. *et al.* Calcium signaling regulates autophagy and apoptosis. *Cells* **10**, (2021).

236. Berridge, M. J., Bootman, M. D. & Roderick, H. L. Calcium: Calcium signalling: dynamics, homeostasis and remodelling. *Nat. Rev. Mol. Cell Biol.* **4**, 517 (2003).

237. Woll, K. A. & Van Petegem, F. Calcium-release channels: Structure and function of IP3 receptors and ryanodine receptors. *Physiol. Rev.* **102**, 209–268 (2022).

238. Zhang, Y. *et al.* HDAC-6 interacts with and deacetylates tubulin and microtubules in vivo. *EMBO J.* **22**, 1168 (2003).

239. Wu, Y. X. *et al.* Histone deacetylase 6 as a novel promising target to treat cardiovascular disease. *Cancer Innovation* **3**, e114 (2024).

240. Berridge, M. J. Calcium signalling remodelling and disease. *Biochem. Soc. Trans.* **40**, 297–309 (2012).

241. Lopez-Cavestany, M. *et al.* Matrix stiffness induces epithelial-to-mesenchymal transition via Piezo1-regulated calcium flux in prostate cancer cells. *iScience* **26**, (2023).

242. So, C. L. *et al.* Increased matrix stiffness suppresses ATP-induced sustained Ca2+ influx in MDA-MB-231 breast cancer cells. *Cell Calcium* **104**, 102569 (2022).

243. Gee, K. R. *et al.* Chemical and physiological characterization of fluo-4 Ca2+-indicator dyes. *Cell Calcium* **27**, 97–106 (2000).

244. Kwon, D. H., Ryu, J., Kim, Y. K. & Kook, H. Roles of Histone Acetylation Modifiers and Other Epigenetic Regulators in Vascular Calcification. *Int. J. Mol. Sci.* **21**, 3246 (2020).

245. Kwon, D. H., Kim, Y. K. & Kook, H. New Aspects of Vascular Calcification: Histone Deacetylases and Beyond. *J. Korean Med. Sci.* **32**, 1738–1748 (2017).

246. Rajesth, D., Uribe, V. & Smith, K. A. The open and closed case for Class I HDACs in cardiac development. *Semin. Cell Dev. Biol.* **172**, (2025).

247. Krämer, O. H. HDAC2: a critical factor in health and disease. *Trends Pharmacol. Sci.* **30**, 647–655 (2009).

248. Kook, H. & Kee, H. J. Roles and targets of class I and IIa histone deacetylases in cardiac hypertrophy. *J. Biomed. Biotechnol.* **2011**, (2011).

249. Ferguson, B. S. & McKinsey, T. A. Non-Sirtuin Histone Deacetylases in the Control of Cardiac Aging. *J. Mol. Cell. Cardiol.* **83**, 14 (2015).

250. He, R. *et al.* HDAC3 in action: Expanding roles in inflammation and inflammatory diseases. *Cell Prolif.* **58**, (2025).

251. Watson, N., Kuppuswamy, S., Ledford, W. L. & Sukumari-Ramesh, S. The role of HDAC3 in inflammation: mechanisms and therapeutic implications. *Front. Immunol.* **15**, 1419685 (2024).

252. Seidel, C., Schnekenburger, M., Dicato, M. & Diederich, M. Histone Deacetylase 6 in Health and Disease. *Epigenomics* **7**, 103–118 (2015).

253. Gao, Y. *et al.* Histone Deacetylase 6 Regulates Growth Factor-Induced Actin Remodeling and Endocytosis. *Mol. Cell. Biol.* **27**, 8637 (2007).

254. Bae, C., Sachs, F. & Gottlieb, P. A. The mechanosensitive ion channel Piezo1 is inhibited by the peptide GsMTx4. *Biochemistry* **50**, 6295 (2011).

255. Bowman, C. L., Gottlieb, P. A., Suchyna, T. M., Murphy, Y. K. & Sachs, F. Mechanosensitive Ion Channels and the Peptide Inhibitor GsMTx-4: History, Properties, Mechanisms and Pharmacology. *Toxicon* **49**, 249 (2006).

256. Michelucci, A. & Catacuzzeno, L. Piezo1, the new actor in cell volume regulation. *Pflugers Arch.* **476**, 1023–1039 (2024).

257. Lee, K. M., Tsai, K. Y., Wang, N. & Ingber, D. E. Extracellular matrix and pulmonary hypertension: Control of vascular smooth muscle cell contractility. *Am. J. Physiol. Heart Circ. Physiol.* **274**, (1998).

258. Steucke, K. E., Tracy, P. V., Hald, E. S., Hall, J. L. & Alford, P. W. Vascular smooth muscle cell functional contractility depends on extracellular mechanical properties. *J. Biomech.* **48**, 3044–3051 (2015).

259. An, S. S. *et al.* Cell stiffness, contractile stress and the role of extracellular matrix. *Biochem. Biophys. Res. Commun.* **382**, 697–703 (2009).

260. Wassmann, S. & Nickenig, G. The role of the AT1 receptor in the cardiovascular continuum. *European Heart Journal Supplements* **6**, h3–h9 (2004).

261. Brassard, P., Amiri, F., Thibault, G. & Schiffrin, E. L. Role of angiotensin type-1 and angiotensin type-2 receptors in the expression of vascular integrins in angiotensin II-infused rats. *Hypertension* **47**, 122–127 (2006).

262. Browe, D. M. & Baumgarten, C. M. Angiotensin II (AT1) Receptors and NADPH Oxidase Regulate Cl− Current Elicited by β1 Integrin Stretch in Rabbit Ventricular Myocytes. *Journal of General Physiology* **124**, 273–287 (2004).

263. Moraes, J. A. *et al.* Alpha1beta1 and integrin-linked kinase interact and modulate angiotensin II effects in vascular smooth muscle cells. *Atherosclerosis* **243**, 477–485 (2015).

264. Colchicine: MedlinePlus Drug Information. https://medlineplus.gov/druginfo/meds/a682711.html.

265. Lu, Y., Chen, J., Xiao, M., Li, W. & Miller, D. D. An Overview of Tubulin Inhibitors That Interact with the Colchicine Binding Site. *Pharm. Res.* **29**, 2943 (2012).

266. Hancock, E. N., Palmer, B. M. & Caporizzo, M. A. Microtubule destabilization with colchicine increases the work output of myocardial slices. *Journal of Molecular and Cellular Cardiology Plus* **7**, 100066 (2024).

267. O'Brien, E. T., Salmon, E. D. & Erickson, H. P. How calcium causes microtubule depolymerization. *Cell Motil. Cytoskeleton* **36**, 125–135 (1997).

268. Antony, A., Ng, N., Lauto, A., Coorssen, J. R. & Myers, S. J. Calcium-Mediated Calpain Activation and Microtubule Dissociation in Cell Model of Hereditary Sensory Neuropathy Type-1 Expressing V144D SPTLC1 Mutation. *DNA Cell Biol.* **41**, 225–234 (2022).

269. Song, Y. *et al.* Transglutaminase and Polyamination of Tubulin: Posttranslational Modification for Stabilizing Axonal Microtubules. *Neuron* **78**, 109 (2013).

270. Bar, J., Popp, Y., Koudelka, T., Tholey, A. & Mikhaylova, M. Regulation of microtubule detyrosination by Ca2+ and conventional calpains. *J. Cell Sci.* **135**, (2022).

271. Čermák, V. *et al.* Microtubule-targeting agents and their impact on cancer treatment. *Eur. J. Cell Biol.* **99**, 151075 (2020).

272. Mikesell, A. R. *et al.* Keratinocyte Piezo1 drives paclitaxel-induced mechanical hypersensitivity. *bioRxiv* 2023.12.12.571332 (2023) doi:10.1101/2023.12.12.571332.

273. Roy, A. D., Gonzalez, C. S., Shahid, F., Yadav, E. & Inoue, T. Optogenetically Induced Microtubule Acetylation Unveils the Molecular Dynamics of Actin-Microtubule Crosstalk in Directed Cell Migration. *bioRxiv* 2024.12.01.626286 (2024) doi:10.1101/2024.12.01.626286.

274. Park, S. Y. & Kim, J. S. A short guide to histone deacetylases including recent progress on class II enzymes. *Experimental & Molecular Medicine 2020 52:2* **52**, 204–212 (2020).

275. Backs, J., Song, K., Bezprozvannaya, S., Chang, S. & Olson, E. N. CaM kinase II selectively signals to histone deacetylase 4 during cardiomyocyte hypertrophy. *J. Clin. Invest.* **116**, 1853–1864 (2006).

276. Yan, H. *et al.* Regulation of cardiovascular diseases by histone deacetylases and NADPH oxidases. *Redox Biol.* **77**, 103379 (2024).

277. Pai, P. *et al.* Unlocking cardiac health: exploring the role of class I HDACs in cardiovascular diseases. *Mol. Cell. Biochem.* 1–25 (2025) doi:10.1007/S11010-025-05353-5/METRICS.

278. Du, L. *et al.* MS275 as Class I HDAC inhibitor displayed therapeutic potential on malignant ascites by iTRAQ-based quantitative proteomic analysis. *BMC Gastroenterol.* **22**, 29 (2022).

279. Janke, C. & Montagnac, G. Causes and Consequences of Microtubule Acetylation. *Current Biology* **27**, R1287–R1292 (2017).

280. Donker, L. & Godinho, S. A. Rethinking tubulin acetylation: From regulation to cellular adaptation. *Curr. Opin. Cell Biol.* **94**, 102512 (2025).

281. Bacon, T. *et al.* Histone deacetylase 3 indirectly modulates tubulin acetylation. *Biochemical Journal* **472**, 367 (2015).

282. Li, X. *et al.* HDAC3 promotes meiotic apparatus assembly in mouse oocytes by modulating tubulin acetylation. *Development (Cambridge)* **144**, 3789–3797 (2017).

283. Chen, Y. T. *et al.* Microtubule-associated histone deacetylase 6 supports the calcium store sensor STIM1 in mediating malignant cell behaviors. *Cancer Res.* **73**, 4500–4509 (2013).

284. Gnanasambandam, R. *et al.* GsMTx4: Mechanism of Inhibiting Mechanosensitive Ion Channels. *Biophys. J.* **112**, 31 (2017).

285. Yao, M. *et al.* Force- and cell state–dependent recruitment of Piezo1 drives focal adhesion dynamics and calcium entry. *Sci. Adv.* **8**, eabo1461 (2022).

286. Lekka, M., Gnanachandran, K., Kubiak, A., Zieliński, T. & Zemła, J. Traction force microscopy – Measuring the forces exerted by cells. *Micron* **150**, 103138 (2021).

287. Hemmati, F., Akinpelu, A., Nweze, D. C. & Mistriotis, P. 3D confinement alters smooth muscle cell responses to chemical and mechanical cues. *APL Bioeng.* **8**, 046103 (2024).

288. Static Confiner 6 wells | 4Dcell. https://www.4dcell.com/smartconfinement/static-confiner-6-wells.

289. Burtenshaw, D., Hakimjavadi, R., Redmond, E. M. & Cahill, P. A. Nox, Reactive Oxygen Species and Regulation of Vascular Cell Fate. *Antioxidants* **6**, 90 (2017).

290. Califano, J. P. & Reinhart-King, C. A. Substrate Stiffness and Cell Area Predict Cellular Traction Stresses in Single Cells and Cells in Contact. *Cell. Mol. Bioeng.* **3**, 68 (2010).

291. Liu, F. *et al.* Mechanosignaling through YAP and TAZ drives fibroblast activation and fibrosis. *Am. J. Physiol. Lung Cell. Mol. Physiol.* **308**, L344 (2014).

292. Elmarasi, M. *et al.* Phenotypic switching of vascular smooth muscle cells in atherosclerosis, hypertension, and aortic dissection. *J. Cell. Physiol.* **239**, e31200 (2024).

293. Kim, H. R., Appel, S., Vetterkind, S., Gangopadhyay, S. S. & Morgan, K. G. Smooth muscle signalling pathways in health and disease. *J. Cell. Mol. Med.* **12**, 2165 (2008).

294. Ellefsen, K. L. *et al.* Myosin-II mediated traction forces evoke localized Piezo1-dependent Ca2+ flickers. *Commun. Biol.* **2**, 298 (2019).

295. Atcha, H. *et al.* Mechanically activated ion channel Piezo1 modulates macrophage polarization and stiffness sensing. *Nature Communications 2021 12:1* **12**, 1–14 (2021).

296. Legant, W. R. *et al.* Multidimensional traction force microscopy reveals out-of-plane rotational moments about focal adhesions. *Proc. Natl. Acad. Sci. U. S. A.* **110**, 881–886 (2013).

297. Minaisah, R. M., Cox, S. & Warren, D. T. The Use of Polyacrylamide Hydrogels to Study the Effects of Matrix Stiffness on Nuclear Envelope Properties. *Methods in Molecular Biology* **1411**, 233–239 (2016).

298. Seetharaman, S. & Etienne-Manneville, S. Microtubules at focal adhesions – a double-edged sword. *J. Cell Sci.* **132**, (2019).

299. Beurel, E., Grieco, S. F. & Jope, R. S. Glycogen synthase kinase-3 (GSK3): Regulation, actions, and diseases. *Pharmacol. Ther.* **148**, 114–131 (2015).

300. Lee, J. H. & Paull, T. T. Cellular functions of the protein kinase ATM and their relevance to human disease. *Nat. Rev. Mol. Cell Biol.* **22**, 796–814 (2021).

301. Wu, X. *et al.* Skin Stem Cells Orchestrate Directional Migration By Regulating Microtubule-ACF7 Connections Through GSK3β. *Cell* **144**, 341 (2011).

302. MACF1 microtubule actin crosslinking factor 1 [Homo sapiens (human)] - Gene - NCBI. https://www.ncbi.nlm.nih.gov/gene?Db=gene&Cmd=ShowDetailView&TermToSearch=23499.

303. Bastianello, G. *et al.* Cell stretching activates an ATM mechano-transduction pathway that remodels cytoskeleton and chromatin. *Cell Rep.* **42**, 113555 (2023).

304. Uchida, M. *et al.* Overexpression of Poly(ADP-ribose) Polymerase Disrupts Organization of Cytoskeletal F-actin and Tissue Polarity inDrosophila. *Journal of Biological Chemistry* **277**, 6696–6702 (2002).

305. Rom, S. *et al.* PARP inhibition in leukocytes diminishes inflammation via effects on integrins/cytoskeleton and protects the blood-brain barrier. *J. Neuroinflammation* **13**, 1–16 (2016).

306. Lai, A. *et al.* Mechanosensing by Piezo1 and its implications for physiology and various pathologies. *Biological Reviews* **97**, 604–614 (2022).

307. Mistriotis, P., Wisniewski, E. O., Si, B. R., Kalab, P. & Konstantopoulos, K. Feature Review Coordinated in confined migration: crosstalk between the nucleus and ion channel-mediated mechanosensation Cell Biology. *Trends Cell Biol.* **34**, 809–825 (2024).

308. Huynh, J., Bordeleau, F., Kraning-Rush, C. M. & Reinhart-King, C. A. Substrate Stiffness Regulates PDGF-Induced Circular Dorsal Ruffle Formation Through MLCK. *Cell. Mol. Bioeng.* **6**, 10.1007/s12195-013-0278–7 (2013).

309. Cao, R., Tian, H., Tian, Y. & Fu, X. A Hierarchical Mechanotransduction System: From Macro to Micro. *Advanced Science* **11**, 2302327 (2024).

310. Nolasco, P. *et al.* Impaired vascular smooth muscle cell force-generating capacity and phenotypic deregulation in Marfan Syndrome mice. *Biochimica et Biophysica Acta (BBA) - Molecular Basis of Disease* **1866**, 165587 (2020).

311. Hajka, D. *et al.* GSK3 as a regulator of cytoskeleton architecture: Consequences for health and disease. *Cells* **10**, 2092 (2021).

312. Zheng, C. *et al.* Histone deacetylase inhibitors relax mouse aorta partly through their inhibitory action on L-type Ca2+ channels. *Journal of Pharmacology and Experimental Therapeutics* **363**, 211–220 (2017).

313. Weng, X. *et al.* Ketogenic diet and β-hydroxybutyrate inhibit HDAC1 to preserve vascular smooth muscle cell function in thoracic aortic aneurysm. *J. Adv. Res.* https://doi.org/10.1016/J.JARE.2025.05.035 (2025) doi:10.1016/J.JARE.2025.05.035.

314. Tsunoda, S. P., Wiesner, B., Lorenz, D., Rosenthal, W. & Pohl, P. Aquaporin-1, Nothing but a Water Channel. *Journal of Biological Chemistry* **279**, 11364–11367 (2004).

315. Verkman, A. S. & Mitra, A. K. Structure and function of aquaporin water channels. *Am. J. Physiol. Renal Physiol.* **278**, 13–28 (2000).

316. Clempus, R. E. & Griendling, K. K. Reactive oxygen species signaling in vascular smooth muscle cells. *Cardiovasc. Res.* **71**, 216 (2006).

317. Batty, M., Bennett, M. R. & Yu, E. The Role of Oxidative Stress in Atherosclerosis. *Cells* **11**, 3843 (2022).

318. Forman, H. J., Ursini, F. & Maiorino, M. An overview of mechanisms of redox signaling. *J. Mol. Cell. Cardiol.* **0**, 2 (2014).

319. Jama, H. A. *et al.* Rodent models of hypertension. *Br. J. Pharmacol.* **179**, 918–937 (2022).

Appendix A - Supplementary Tables (Chapter 3)

Table 6.2. Cell density (cells/cm^2) calculated from cell counts per field-of-view in TCAQP1 treated condition. Shows average from N = 3.

	Number of cells (Cells/cm^2)						
Stiffness (kPa)	**10^{-11}**	**10^{-10}**	**10^{-9}**	**10^{-8}**	**10^{-7}**	**10^{-6}**	**10^{-5}**
12	2726.70	3043.75	2219.40	3424.22	3043.75	1395.05	1902.35
72	1225.95	1162.54	1141.41	1183.68	1183.68	1310.51	655.25

Table 6.3. Cell density (cells/cm^2) calculated from cell counts per field-of-view in TGN020 treated condition. Shows average from N = 3.

	Number of cells (Cells/cm^2)						
Stiffness (kPa)	**10^{-11}**	**10^{-10}**	**10^{-9}**	**10^{-8}**	**10^{-7}**	**10^{-6}**	**10^{-5}**
12	1416.19	1120.27	1627.56	1690.97	1331.64	1395.05	908.9
72	1479.60	1289.37	1373.92	1585.29	1162.54	1183.68	1521.88

Table 6.4. Cell density (cells/cm^2) calculated from cell counts per field-of-view in Furosemide treated condition. Shows average from N = 3.

	Number of cells (Cells/cm^2)				
Stiffness (kPa)	**10^{-8}**	**10^{-7}**	**10^{-6}**	**10^{-5}**	**10^{-4}**
72	930.04	866.62	1078.00	930.04	739.80

Table 6.5. Cell density (cells/cm^2) calculated from cell counts per field-of-view in STOCK2S 26 treated condition. Shows average from N = 3.

	Number of cells (Cells/cm^2)				
Stiffness (kPa)	**10^{-8}**	**10^{-7}**	**10^{-6}**	**10^{-5}**	**10^{-4}**
72	824.35	676.39	908.90	549.57	528.43

Table 6.6. Cell density (cells/cm^2) calculated from cell counts per field-of-view in Go6983 26 treated condition. Shows average from N = 3.

	Number of cells (Cells/cm^2)				
Stiffness (kPa)	**10^{-8}**	**10^{-7}**	**10^{-6}**	**10^{-5}**	**10^{-4}**
72	993.45	993.45	676.39	1204.82	1162.54

Table 6.7. Cell density (cells/cm^2) calculated from cell counts per field-of-view in Xestospongin treated condition. Shows average from N = 3.

	Number of cells (Cells/cm^2)				
Stiffness (kPa)	**10^{-9}**	**10^{-8}**	**10^{-7}**	**10^{-6}**	**10^{-5}**
12	1268.23	1099.13	739.80	930.04	1056.86
72	1204.82	1310.51	1521.88	1183.68	1141.41

Table 6.8. Cell density (cells/cm^2) calculated from cell counts per field-of-view in Dantrolene treated condition. Shows average from N = 5.

	Number of cells (Cells/cm^2)				
Stiffness (kPa)	**10^{-12}**	**10^{-11}**	**10^{-10}**	**10^{-9}**	**10^{-8}**
12	951.17	1014.58	1120.27	1373.92	930.04
72	634.12	722.89	355.10	697.53	596.07

Table 6.9. Cell density (cells/cm^2) calculated from cell counts per field-of-view in Epothilone treated condition. Shows average from N = 5.

	Number of cells (Cells/cm^2)				
Stiffness (kPa)	**10^{-12}**	**10^{-11}**	**10^{-10}**	**10^{-9}**	**10^{-8}**
12	621.43	1306.28	1344.32	1166.77	1204.82
72	672.16	1382.37	1471.15	1420.42	1052.63

Table 6.10. Cell density (cells/cm^2) calculated from cell counts per field-of-view in Nocodazole treated condition. Shows average from N = 5.

	Number of cells (Cells/cm^2)				
Stiffness (kPa)	**10^{-12}**	**10^{-11}**	**10^{-10}**	**10^{-9}**	**10^{-8}**
12	1078.00	925.81	1065.31	951.17	1001.90
72	1103.36	963.86	862.40	862.40	735.57

Table 6.11. Cell density (cells/cm^2) calculated from cell counts per field-of-view in A1070722 treated condition. Shows average from N = 4.

	Number of cells (Cells/cm^2)				
Stiffness (kPa)	**10^{-12}**	**10^{-11}**	**10^{-10}**	**10^{-9}**	**10^{-8}**
12	967.03	919.47	824.35	871.91	871.91
72	1373.92	1310.51	1204.82	1521.88	1225.96

Table 6.12. Cell density (cells/cm^2) calculated from cell counts per field-of-view in AZD7762 treated condition. Shows average from N = 4.

	Number of cells (Cells/cm^2)				
Stiffness (kPa)	**10^{-12}**	**10^{-11}**	**10^{-10}**	**10^{-9}**	**10^{-8}**
12	993.45	1352.78	1056.86	993.45	1162.54
72	1247.09	1289.37	1331.64	1479.60	1310.51

Table 6.13. Cell density (cells/cm^2) calculated from cell counts per field-of-view in Ku55933 treated condition. Shows average from N = 3.

	Number of cells (Cells/cm^2)				
Stiffness (kPa)	**10^{-12}**	**10^{-11}**	**10^{-10}**	**10^{-9}**	**10^{-8}**
12	1056.86	1078.00	1331.64	845.49	930.04
72	1204.82	1141.41	655.25	951.17	1289.37

Table 6.14. Cell density (cells/cm^2) calculated from cell counts per field-of-view in EB47 treated condition. Shows average from N = 3.

	Number of cells (Cells/cm^2)				
Stiffness (kPa)	**10^{-12}**	**10^{-11}**	**10^{-10}**	**10^{-9}**	**10^{-8}**
12	1014.58	1035.72	887.76	951.17	634.12
72	1099.13	972.31	782.08	1099.13	1078.00